Liquid Crystalline Oligofluorenes and Their Derivatives: Synthesis, Characterization and Physical Properties

Dissertation

zur Erlangung des Grades
"Doktor der Naturwissenschaften"

dem Fachbereich Chemie und Pharmazie der
Johannes Gutenberg-Universität Mainz
vorgelegt von

Chunyan Chi
geboren in Heilongjiang Province / P. R. China

Mainz, 2004

Tag der mündlichen Prüfung: Nov 15, 2004

Die vorliegende Arbeit wurde in der Zeit von Juni 2001 bis November 2004 im Max-Planck-Institut für Polymerforschung in Mainz unter Anleitung von Herrn Prof. Dr. Wegner ausgeführt.

Abstract

Homo-oligofluorenes (**OFn**), polyfluorenes (**PF2/6**) and oligofluorenes with one fluorenenone group in the center (**OFnK**) were synthesized. They were used as model compounds to understand of the structure-property relationships of polyfluorenes and the origin of the green emission in the photoluminescence (after photooxidation of the PFs) and the electroluminescence (EL) spectra. The electronic, electrochemical properties, thermal behavior, supramolecular self-assembly, and photophysical properties of **OFn**, **PF2/6** and **OFnK** were investigated.

Oligofluorenes with 2-ethylhexyl side chain (**OF2-OF7**) from the dimer up to the heptamer were prepared by a series of stepwise transition metal mediated Suzuki and Yamamoto coupling reactions. Polyfluorene was synthesized by Yamamoto coupling of 2,7-dibromo-9,9-bis(2-ethylhexyl)fluorene. Oligofluorenes with one fluorenone group in the center (**OF3K, OF5K, OF7K**) were prepared by Suzuki coupling between the monoboronic fluorenyl monomer, dimer, trimer and 2, 7-dibromofluorenone.

The electrochemical and electronic properties of homo-oligofluorenes (**OFn**) were systematically studied by several combined techniques such as cyclic voltammetry, differential pulse voltammetry, UV-vis absorption spectroscopy, steady and time-resolved fluorescence spectroscopy. It was found that the oligofluorenes behave like classical conjugated oligomers, i.e., with the increase of the chain-length, the corresponding oxidation potential, the absorption and emission maximum, ionization potential, electron affinity, band gap and the photoluminescence lifetime displayed a very good linear relation with the reciprocal number of the fluorene units (1/n). The extrapolation of these linear relations to infinite chain length predicted the electrochemical and electronic properties of the corresponding polyfluorenes.

The thermal behavior, single-crystal structure and supramolecular packing, alignment properties, and molecular dynamics of the homo-oligofluorenes (**OFn**) up to the polymer were studied using techniques such as TGA, DSC, WAXS, POM and DS. The **OFn** from tetramer to heptamer show a smectic liquid crystalline phase with clearly defined isotropization temperature. The oligomers do show a glass transition which exhibits n^{-1} dependence and allows extrapolation to a hypothetical glass transition of the polymer at around 64 °C. A smectic packing and helix-like conformation for the oligofluorenes from tetramer to heptamer was supported by WAXS experiments, simulation, and single-crystal

structure of some oligofluorene derivatives. Oligofluorenes were aligned more easily than the corresponding polymer, and the alignability increased with the molecular length from tetramer to heptamer. The molecular dynamics in a series of oligofluorenes up to the polymer was studied using dielectric spectroscopy.

The photophysical properties of **OFn** and **PF2/6** were investigated by the steady-state spectra (UV-vis absorption and fluorescence spectra) and time-resolved fluorescence spectra both in solution and thin film. The time-resolved fluorescence spectra of the oligofluorenes were measured by streak camera and gate detection technique. The lifetime of the oligofluorenes decreased with the extension of the chain-length. No green emission was observed in CW, prompt and delayed fluorescence for oligofluorenes in *m*-THF and film at RT and 77K. Phosphorescence was observed for oligofluorenes in frozen dilute *m*-THF solution at 77K and its lifetime increased with length of oligofluorenes. A linear relation was obtained for triplet energy and singlet energy as a function of the reciprocal degree of polymerization, and the singlet-triplet energy gap (S_1-T_1) was found to decrease with the increase of degree of polymerization.

Oligofluorenes with one fluorenone unit at the center were used as model compounds to understand the origin of the low-energy ("green") emission band in the photoluminescence and electroluminescence spectra of polyfluorenes. Their electrochemical properties were investigated by CV, and the ionization potential (I_p) and electron affinity (E_a) were calculated from the onset of oxidation and reduction of **OFnK**. The photophysical properties of **OFnK** were studied in dilute solution and thin film by steady-state spectra and time-resolved fluorescence spectra. A strong green emission accompanied with a weak blue emission were obtained in solution and only green emission was observed on film. The strong green emission of **OFnK** suggested that rapid energy transfer takes place from higher energy sites (fluorene segments) to lower energy sites (fluorenone unit) prior to the radiative decay of the excited species. The fluorescence spectra of **OFnK** also showed solvatochromism. Monoexponential decay behaviour was observed by time-resolved fluorescence measurements. In addition, the site-selective excitation and concentration dependence of the fluorescence spectra were investigated. The ratio of green and blue emission band intensities increases with the increase of the concentration. The observed strong concentration dependence of the green emission band in solution suggests that increased interchain interactions among the fluorenone-containing oligofluorene chain enhanced the emission from the fluorenone defects at higher concentration. On the other

hand, the mono-exponential decay behaviour and power dependence were not influenced significantly by the concentration. We have ruled out the possibility that the green emission band originates from aggregates or excimer formation.

Energy transfer was further investigated using a model system of a polyfluorene doped by **OFnK**. Förster-type energy transfer took place from **PF2/6** to **OFnK**, and the energy transfer efficiency increased with increasing of the concentration of **OFnK**. Efficient funneling of excitation energy from the high-energy fluorene segments to the low-energy fluorenone defects results from energy migration by hopping of excitations along a single polymer chain until they are trapped on the fluorenone defects on that chain or transferred onto neighbouring chains by Förster-type interchain energy transfer process. These results imply that the red-shifted emission in polyfluorenes can originate from (usually undesirable) keto groups at the bridging carbon atoms-especially if the samples have been subject to photo- or electro-oxidation or if fluorenone units are present due to an improper purification of the monomers prior to polymerization.

Table of Contents

1 An Introduction to Conjugated Oligomers

In this chapter, a general review on conjugated oligomers is presented. The motivation and the framework of this thesis are outlined after the review.

1.1 Introduction-why conjugated oligomers

During the past two decades a number of π-conjugated polymers has been investigated as advanced materials for electronic, photonic, and optoelectronic applications and that has caused an ever increasing interest from both academic and industrial research laboratories. [1] The inherent synthetic flexibility, the potential of simple processing, and the possibility of tailoring characteristic properties to accomplish a desired function makes them promising candidates for numerous applications in materials science. Thus, they have been used as laser dyes,[2] scintillators,[2] light-emitting diodes,[3] thin film transistors[4], piezoelectric and pyroelectric materials,[5] photoconductors,[6] and are investigated for optical data storage,[7] optical switching and signal processing,[8] as well as in nonlinear optical application.[9]

The direct analytical characterization and physical studies of extended π-conjugated polymers with high molecular weight are often hampered by low solubility. Structural defects also represent a common obstacle towards obtaining sound physical data. The detailed characterization of precisely defined oligomeric materials is often far easier than characterization of the polydisperse homologs. While polymers are made up of a large number of building blocks linked in a repetitive fashion, the corresponding oligomers constitute their lower homologs with a key feature that increasing the size of an oligomer changes its physical properties-until a convergence limit is reached.

A major motivation of oligomer research is to establish relations between chain length and physical properties. The properties of oligomers are chain-length dependent-until one reaches a borderline length at which further extension will no longer affect their behaviour. This aspect defines clearly the role of conjugated oligomers as models for the related polymers. The heart of oligomer research lies at the extrapolation of physical properties toward infinite chain lengths and the description of a conjugated polymer in its 'ideal' state. Soluble, monodisperse oligomers as finite model systems offer the possibility to attain, by extrapolation, specific information concerning the electronic[10], photonic,[11] thermal, and

morphological properties of their corresponding polydisperse high molecular weight analogues.[12] They also serve as useful models for interpreting structural and conformational properties of a polymer. The "effective conjugation length (ECL)" will be obtained from different measurement methods. Furthermore, the systematic study of oligomers allows direct correlation of physical properties with chemical structures, and enables the generation of useful and predictive structure-property relationship. More recently, monodisperse oligomers have also been shown to be useful as model compounds for elucidating the folding properties of polymers.[13] However, limitations to this "oligomeric approach"[1b] also exist and not all physical or chemical properties of high molecular weight polymers can be modelled with the corresponding smaller oligomers. For instance, macromolecules differ from smaller analogues both in their solution (for example, high viscosity, diffusion behavior) and solid-state properties (for example, amorphous or semicrystalline structures), and such bulk effects are not likely to be reproduced by low molecular counterparts.[14]

If the limit of convergence of a particular physical property is already reached for a rather low oligomer size, and if oligomers have a high degree of structural homogeneity, one may regard oligomers as 'better' materials. Further, the measurement of phenomena such as transport of charge carriers in photoconductivity and of excitons in photoluminescence requires scrupulous purification of samples, since impurities may produce false or at least misleading results. Oligomers are important, therefore, because they can be purified more easily than polymers, whereby quite demanding techniques such as zone melting or vacuum sublimation have been used. Some of their physical properties even surpass those of the polymers. For example, they can be used as defect-free materials for electronic devices such as organic light-emitting diodes (OLEDs),[15] solar cells,[16] and field-effect transistors(FETs)[17]. For oligothiophenes, the mobility of the charge carriers and the transistor characteristics were found to be superior to those of an analogous poly(bithiophene) transistor.[18] Future nanoelectronic or nanophotonic processes will likely require monodisperse materials.

Another interest in monodisperse π-conjugated oligomers of defined length and constitution arises from their potential to act as molecular wires in molecular scale electronics and nanotechnological devices.[4, 12] A variety of spectacular molecular architecture has resulted from the efforts aimed at the construction of such wires. With the progress in synthetic organic methodology and the increasing availability of advanced

analytical methods for the purification and characterization of very large molecules, monodisperse linear π-conjugated oligomers have recently reached the 10 nm length mark,[19] which is about the current resolution limit for microstructure manufacturing by state-of-the-art lithographic techniques.[20] This achievement in organic synthesis has greatly stimulated the interest in the experimental[21] and theoretical[22] study of molecular scale mesoscopic devices.

1.2 Conjugated Oligomers as Model Compounds and Active Semiconductors-A General Review

The general methods of preparation described in this section are applicable to the synthesis of either conjugated or nonconjugated systems. The major obstacle in studying precisely defined oligomers and polymers lies in the difficulty of their isolation in pure form. Early work often focused on fractionation methods for obtaining oligomers or small polymers. One would start with a difunctional monomer and carry out standard polymerisation reactions; however, the reaction times were shortened and the reaction temperatures were lowered to maximize the formation of the lower molecular weight species. The yield of a desired product was often low while separation methods usually proved to be inadequate for the preparative fractionations required. Similarly, one could start with polymeric materials and carry out a degradation process to generate oligomeric compounds. As before, the inadequacy of the requisite fractionation processes can inhibit the utility of this approach.[12a]

New approaches to the preparation of well-defined π-conjugated oligomers have emerged in recent years.[12] The most elegant and efficient way to prepare long-chain oligomers used an iterative divergent/convergent binomial strategy,[23] which is illustrated in Scheme 1 for the synthesis of the 12.8 nm long hexadecameric oligo(p-phenyleneethynylene) rod **1**, reported by Tour and co-workers (Scheme 1).[24] Three attractive features are combined in this approach: 1) two orthogonal protecting groups (SiMe$_3$ and Et$_2$N$_3$) allow the selective deprotection (C≡C−SiMe$_3$ ➤ C≡C−H) or activation (Ar-Et$_2$N$_3$ → Ar-I) in very high yield (steps a and b); 2) the Pd-catalyzed cross-coupling reaction (step c) is selective and high yielding; and 3) the product in this chain elongation step is generally readily separable from by-products and starting materials as a

result of large differences in molecular weight. The same iterative strategy was used for the preparation of oligo(α-thiopheneethynylene) derivatives up to a heptadecamer.[25]

$$1 \quad R = \text{3-ethylheptyl, } n = 4$$
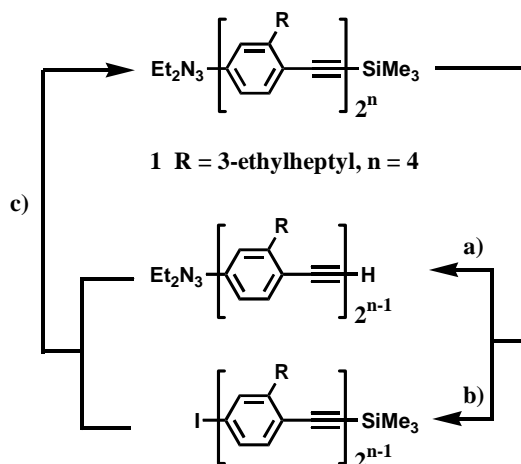
Scheme 1. Iterative binomial synthesis of the 12.8 nm long hexadecameric oligo(p-phenyleneethynylene) **1**: *a)* K_2CO_3, *MeOH or n-Bu$_4$NF, THF; b) MeI, 120°C; c) [Pd(dba)$_2$], CuI, PPh$_3$, HN(iPr$_2$)/THF, (dba = dibenzylideneacetone).*

The binomial strategy for oligomer preparation is also applicable to protocols for solid-phase synthesis.[26] For this purpose, the starting monomer or oligomer is anchored covalently to an insoluble polymer resin such as poly(chloromethylstyrene) (Merrifield's resin). After orthogonal deprotection/activation (Scheme 2, steps a and b) cross-coupling occurs (step c) to yield the extended resin-bound oligomer, which can again be reactivated for the next coupling step. In the last step, low-weight molecules are removed by filtration and washing the resin and the completed oligomers are then cleaved from the polymer support.
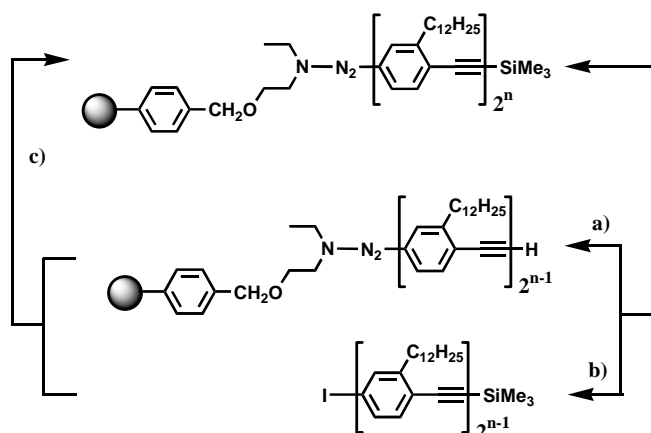
Scheme 2. Binomial oligomer synthesis on a Merrifield's resin: a) n-Bu$_4$NF, THF; b) MeI, 120°C; c) [Pd(dba)$_2$], CuI, PPh$_3$, NEt$_3$.

The second possible strategy is homo- or cross-coupling of a symmetrical or asymmetrical monomer and eventual addition of an end-capping agent to the oligomerization mixture that will irreversibly block the chain ends to prevent any further reaction towards long-chain polymers. This one-pot approach generally lacks control of oligo-selectivity, and such a statistical polymerisation often yields very low amounts of a particular oligomer. Nevertheless, this reaction protocol can be useful if high yielding cross-coupling reactions, which are required in the iterative binomial synthesis, are simply not available or if rapid access to an entire series of monodisperse oligomers is desirable and subsequent chromatographic separations are applicable. Such as strategy has been used in several groups for the synthesis, for example, of monodisperse poly(triacetylene) oligomers,[27] for the synthesis of oligo(pyrrole)s,[28] or for the preparation of linear(1,3-diethynylcyclobutadiene)cyclopentadienylcobalt oligomers.[29]

The practical limit of this method often lies in difficulties encountered during the chromatographic separation such as by size-exclusion chromatography (SEC) of oligomers with relatively low differences in molecular weight. This problem can be alleviated by submitting already higher oligomers ("macro-oligomers") to the endcapping oligomerization reaction, to yield oligomers with large molecular weight differences that are more readily separable.[30]

A general limitation for the construction of larger, well-defined oligomers often arises from the insolubility of π-electron conjugation, which can prevent chromatographic purification and isolation as well as physical characterization. Therefore, the attachment of suitable, solubility-providing side-chains to the repeat units is an essential design criterion in any synthesis planning. Furthermore, appropriate side chains can provide extra stability or modulate the morphological or electronic properties of the targeted oligomers or polymers in a desirable way. A very good example of low side chains can influence the optical properties is provided by poly(alkylthiophene)s. Depending on the number and nature of side chains, the colors of emission in polymer light-emitting devices (LEDs) can be changed from blue to red.[31]

So far, kinds of linear π-conjugated oligomers were reported, herein a summary is given to provide an overview of the recent progress made in the synthesis and characterization of linear well-defined π-conjugated oligomers by looking at some of the most predominant recent systems.

Linear π-conjugated hydrocarbon oligomers constitute a link between classical organic π-systems, such as linear olefins, stilbene, biphenyl or distyrylbenzene and conjugated polymers like polyacetylene, poly(para-phenylene) (PPP) and poly (para-phenylenevinylene) (PPV). They are made from a limited amount of basic building blocks, as there are olefins, acetylenes and aromatic moieties like benzene, naphthalene and anthracene. Within the present oligomeric approach the combination of these structural units leads to the target structures: oligoenes **1**, oligoynes **2**, oligoenynes **3**, oligoarylenes **4**, oligoarylenevinylenes **5**, oligoaryleneethynylenes **6**, oligo[n]acenes **7**, oligorylenes **8** (Chart 1).
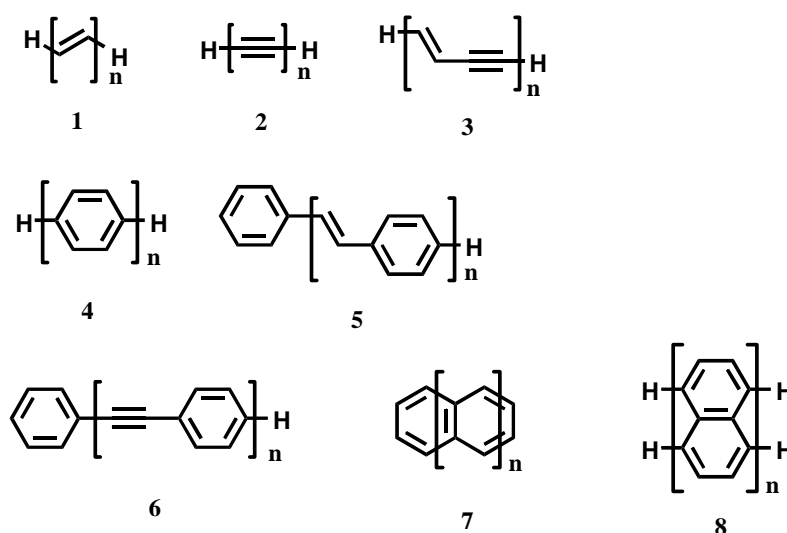
Chart 1. Molecular structures of oligoenes 1, oligoynes 2, oligoenynes 3, oligoarylenes 4, oligoarylenevinylenes 5, oligoaryleneethynylenes 6, oligo[n]acenes 7, oligorylenes 8.

The simplest conjugated oligomer is an oligoene (**1**) chain consisting of an alternating sequence of double and single bonds with the π-π interaction extending over the whole molecule. Linear oligoenes may be viewed as structurally well-defined model compounds for polyacetylene (PA), which has been widely explored over the last years for its interesting material properties, in particular for its high electrical conductivity (up to 10^5 Scm^{-1}) upon doping.[32] Various oligoenes with terminally functionlized donar (D), acceptor (A), or redox-active groups have been synthesized with the aim of investigating their intramolecular energy and electron transfer properties or exploring their use as molecular wires.[33]

The second representatives in the progression of linearly π-conjugated nonaromatic all-carbon backbones are poly(diacetylene)s (PDA). They represent a unique class of conjugated polymers insofar as PDAs can be obtained as perfect macroscopic single crystals by topochemical solid-state polymerization of suitably pre-arranged and substituted buta-1,3-diynes, [34] a requirement, however, which severely limits their accessibility. Oligoenynes have been much less investigated as model compounds for PDA than oligoenes (as models for PA), presumably as a result of the requirement for a topochemically controlled synthesis of the π-conjugated backbone. Other nonaromatic hydrocarbon-consisted linear π-conjugated oligomers including oligoenediynes and oligoynes will not be introduced in detail.

Poly(p-phenylene) (PPP) has found considerable interest over the last years since it acts as an excellent organic conductor upon doping. Whereas in the neutral form PPP is an insulator and displays conductivities down to 10^{-12} Scm^{-1}, doping with I$_2$ or AsF$_5$ raises its conductivity into the metallic region with values around 500 S cm^{-1}.[35] It is therefore not surprising that PPPs have become some of the most widely investigated polymers as documented by several review articles covering all aspects from synthesis to physical properties.[36] A second major interest arises from the fact that polymers with a PPP backbone can be used as the active component in blue light-emitting diode (LEDs).[37]

In the case of PPP, a detailed structure-property analysis has been hampered by its insolubility, and by the fact that most synthetic routes lead only to ill-defined, defect-rich products or to short chain lengths. Many activities have been directed towards soluble, well-defined oligomers that allow optimisation of the polymer-forming reactions and that provide an analysis of physical properties as a function of chain length. The first series of soluble oligo(p-phenylene)s were synthesized by Kern and Wirth[38] and shortly afterwards by Heitz and Ulrich[39] using alkyl substitution in each repeat unit. Oligomers up to the hexamer have been synthesized by stepwise procedures. Using a modular approach, Hensel and Schlüter reported the synthesis of monodisperse oligophenylene rods with up to 16 phenylene rings and with well-defined functional endgroups **9** (Scheme 3).[40] Their synthetic strategy is based on an exponential growth methodology using the Suzuki cross-coupling reaction. While the introduction of alkyl substituents increased the solubility of the oligophenylenes, the electronic properties of the π-system were disturbed by the mutual

distortion of the phenylene units. Great dihedral angles between the plans of neighboring rings and results in a disturbance of the π-orbital overlap along the PPP backbone and a

9
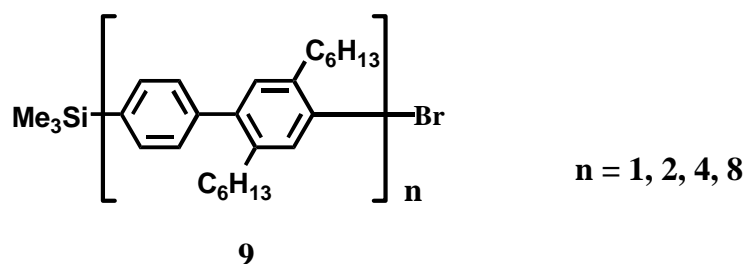
Scheme 3. Molecular structure of soluble oligo(p-phenylene)s.

reduction in the effective conjugation length (ECL). Oligo(p-phenylene)s have played a dominant role as model compounds for PPP in the study of physical mechanisms related to intra- and interchain charge transport or distribution and stabilization of charges and spins on π-conjugated chains.[36f,41]

The planarization of oligo- and poly(p-phenylene)s to maximize the extent of conjugation by enhancing π-orbital overlap has been of notable interest for a number of years. One possible approach in pursuing this objective is the connection of adjacent aryl groups by 1,2-annellation rather than linear 1,4-connection as in the case of classical PPP. The resulting linear [n]acene oligomers **10** (Scheme 4) differ strikingly in their electronic character from PPPs, as a result of the very different connections between individual six-membered rings in the two classes of compounds. Thus, they feature low band gap energies and are inherently sensitive towards oxidation and dimerization.[42] Nevertheless, they represent an interesting class of compounds from both theoretical and experimental viewpoints.[43]

10
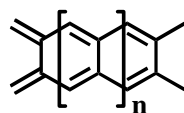
*Scheme 4. Molecular structure of linear acenes **10**.*

Another two strategies for minimizing the mutual distortion of the phenylene rings and to insert solubilizing groups leading to soluble, defect-free oligomers and high molecular weight polymers of the PPP-type have been presented by Müllen and Scherf.[44] In the soluble ladder oligomers **11** (Scheme 5) and the related polymers (LPPP) the complete π-

systems are rendered planar under the influence of the methylene bridges between two adjacent benzene rings. The model oligomers for the ladder poly(p-phenylene) (LPPP) were synthesized by a random approach using the Suzuki coupling as key step. Interestingly, the fluorescence emission spectra of ladder-type oligophenylenes **11** show a very small Stokes shift of a few nanometers resulting from the rigid structure of the planar ribbon polymer.
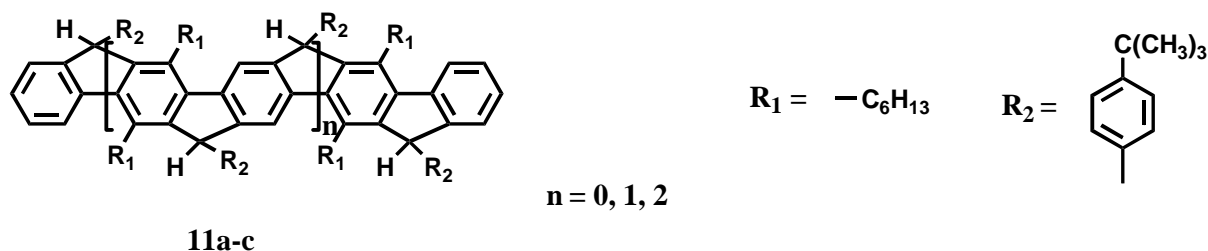
Scheme 5. Molecular structure of the ladder-type oligo (p-phenylene)s.

In the case of the oligo(tetrahydropyrene)s **12**[45] (Scheme 6), the solubilizing alkyl side chain are introduced into the peripheral 4,9-position of the tetrahydropyrene unit so that there is no additional steric hindrance to conjugation between the phenylene units. The oligo(tetrahydropyrene)s **12** represent a soluble structure composed of doubly ethano-bridged biphenyl building blocks. The homologous model oligomers **12** (n = 4, 6, 8, 10, 12) were synthesized by a random approach using the Yamamoto procedure, then isolated from the oligomeric mixture by means of size-exclusion chromatography.

12a-e
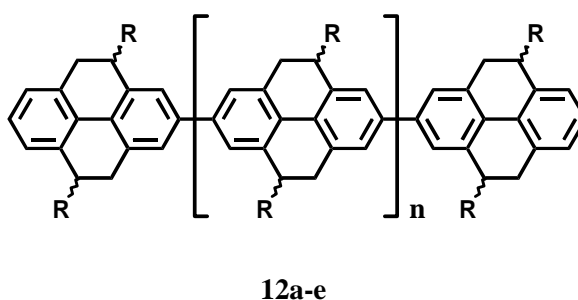
Scheme 6. Molecular structure of oligo-tetrahydropyrenes (n = 4, 6, 8, 10, 12).

Fukuda et al. have reported a simple synthesis of soluble oligofluorenes **14** by the random approach.[46] The oligomerization of 9,9-bis-alkyl-fluorene **13** is based on an oxidative coupling using $FeCl_3$ (Scheme 7). The fluorene moieties were mainly linked in the 2,7'-fashion and the M_n of the oligofluorenes **14** correspond to a number of repeat units of the order of 10. UV-vis absorption and emission spectra in chloroform solution revealed

$\lambda_{max} \approx 380$ nm and $\lambda_{max} \approx 420$ nm, respectively. The synthesis of monodisperse oligofluorenes will be discussed in detailed in this thesis.
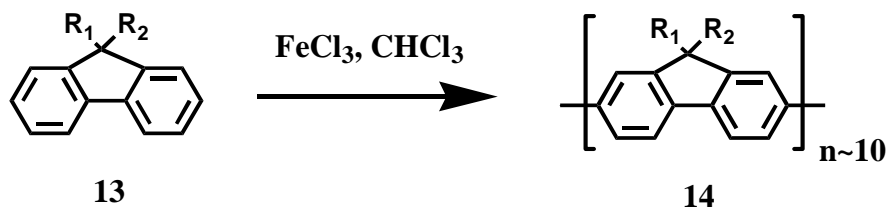
Scheme 7. Oxidative oligomerization of fluorene 13. R_1 = H, n-alkyl; R_2 = n-alkyl.

The report of Friend, Holmes, and co-workers[47] in 1990 that light-emitting device (LEDs) can be constructed from poly(p-phenylenevinylene) (PPV, **15**, Scheme 8) films has provided a highly stimulating impetus to the field of π-conjugated organic molecules, and polymers with the PPV backbone are now among the most extensively studied ones.[48] The physical and electronic properties of PPV and its various, differently substituted derivatives have attracted much attention both from experimental and theoretical scientists.[49] Synthetic chemistry has allowed the controlled manipulation of the HOMO-LUMO (HOMO: the highest occupied molecular orbital; LUMO: the lowest unoccupied molecular orbital) gap energy in PPV based polymers, copolymers, and blends. The manufacture of LEDs,[50] with light emissions covering the whole visible spectrum, and light-emitting electrochemical cells (LECs) has come to reality.[51] The more demanding blue light emitters can also be made from PPV polymers with regions of limited conjugation length or from polymers containing short oligomers of the PPV type as side-chain chromophores.[52] In this respect, oligo(*p*-phenylenevinylene) series such as **16a-c** or **17a-e** (Scheme 8) have helped a great deal in the drive to achieve a basic understanding of the optical properties of PPV polymers.

15 R = H, alkyl, alkoxy, alkylsilyl, ...

16a-c R = H   *n* = 0-2
17a-e R = *t*Bu   *n* = 1-5
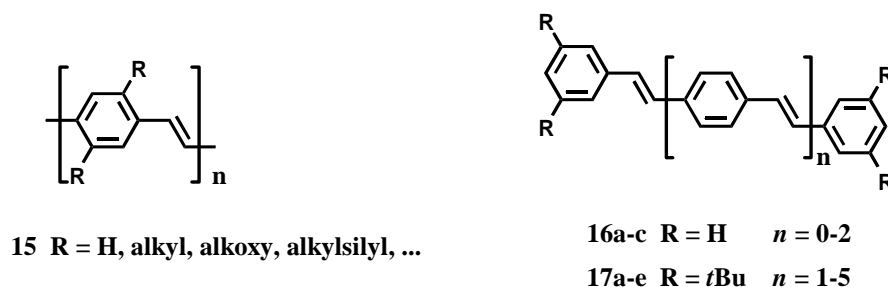
Scheme 8. PPVs and oligomeric model compounds 15, 16 and 17.

The tremendious advances in the chemistry and physics of PPV over recent years have stimulated further interest in related types of structures, such as the poly(*p*-phenyleneethynylene) (PPE) polymers **18**, or the poly(p-phenylenebutadiynylene)s **19** (Scheme 9).[53] PPEs exhibit large photoluminescence efficiencies both in solution and in the solid state as a consequence of their high degree of rigidity, and their extremely stiff, linear backbone enables maximum orientation,[54] which is an important feature for the preparation of oriented films or blends. Their potential as photoluminescence materials in organic polymer-based devices or as fluorescent chemical sensors[55] has already been demonstrated. Additionally, various oligo(*p*-phenyleneethynylene) spacers for the modular construction of organometallic nonlinear optical chromophores[56] or as building blocks for rigid-rod and hyperbranched, dendritic materials have been designed.[57] Oligo(*p*-phenyleneethynylene) series such as **20 a-d** and **21 a-d** (Scheme 9) should become useful to establish structure-property relationships.[58]

18   **19**

20 a-d   n = 1-4   R = H

21 a-d   n = 1-4   R = SiMe₃
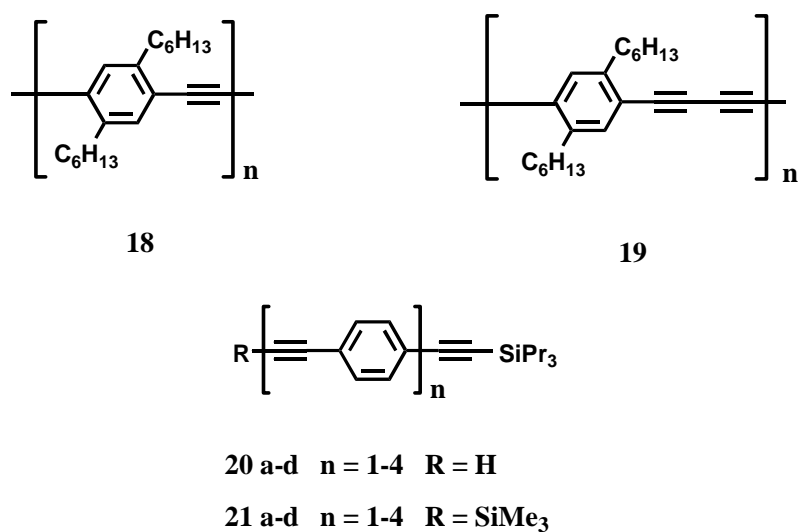
*Scheme 9. Poly(p-phenyleneethynylene)s (PPEs.**18**), poly(p-phenylenebutadiynylene) **19**, and oligomeric model compounds **20, 21** of PPEs.*

Unquestionably, poly- and oligo(α-thiophene)s belong to one of the most carefully studied types of π-conjugated polymers and have received a great deal of attention for both fundamental and practical reasons because conductivity is mostly unaffected by substituents.[59] In addition, both conducting and semiconducting polythiophenes are very stable and readily characterized. Poly- (α-thiophene)s (PT, **22**) (Scheme 10) can generally

be viewed as a *cis*-PA chain in which the structure is stabilized by the bridging sulfur atom.[60] In comparison to PA, this provides several interesting features such as i) higher environmental stability, ii) structural versatility that allows for the modulation of electronic and solubility properties by attaching appropriate side groups to the thiophene monomers, and iii) a nondegenerate ground state related to the non-energetic equivalence of the two limiting mesomeric forms (aromatic and quinoid) of PTs. Poly(α-thiophene)s have excellent semiconducting properties when doped, and oligomers exhibit many of the desirable electronic characteristics that have been evident in the long chain polymer.[61] Oligo(α-thiophenes) in tetrathiafulvalene hybrid systems have also been found to exhibit potent electron donar characteristics, [62] to be attractive building blocks for nonlinear optical materials,[63] and to serve as active components in optical and redox switchable devices.[64] Furthermore, monodisperse oligo(α-thiophene)s and fused derivatives thereof have found growing interest in device applications such as field-effect transistors (FETs),[65] LEDs, [66] photovoltaic cells,[67] and light modulators.[68] The mobility of the charge carriers and the transistor characteristics were found to be superior to those of an analogous poly(bithiophene) transistor and even approach those of transistors based on amorphous silicon. Poly- and oligo(α-thiophenes) can be prepared either by chemical[60] or electrochemical[69] methodologies. The solid-phase synthesis of oligo(α-thiophenes) on a chloromethylated macroporous resin was developed by Malenfant and Fréchet et al..[70] Oligomeric model compounds of PT **23**[71], **24**[72], **25**[73] (Scheme 10) were studied as a function of increasing chain length.

22

23a-g   n = 1-6, 8

24a-f   n = 0-5

25a-d   n = 1-4
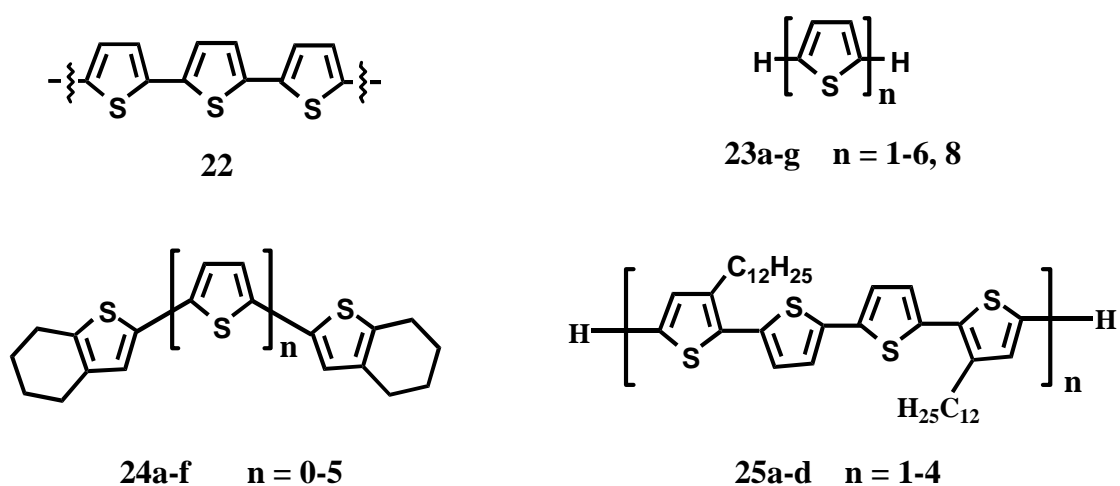
*Scheme 10. Poly(α-thiophene) (**22**) and oligomeric model compounds **23-25**.*

In addition, sulfur-containing oligomers including oligo(α-thiophenevinylene)s and oligo(α-thiopheneethynylene)s, nitrogen-containing oligomers and oligomeric metal complexes were also investigated in many fields.[1] Herein they will be not introduced in detail. Recently, soluble polyfluorene (**PF**) homopolymers have been attracting strong scientific and technological interest as a promising class of conjugated polymers because of their extremely high photoluminescence quantum yields, high thermal and oxidative stability, good solubility in common organic solvents and high processability by facile substitution of the 9-position of fluorene. It is worthwhile to synthesize the corresponding oligofluorenes and investigate their structure-property relationships, a subject of this Ph.D thesis.

1.3 Motivation

Polyfluorenes belong to the class of *rigid-rod* polymers. The monomer unit consists of rigid planar biphenyl units, bridged by a carbon atom in the 9-position, ensuring a high degree of conjugation (**26, PF**, Scheme 11). The carbon-9 atom may also carry additional substituents to modify the polymer processability and the interchain interactions in films, without significantly altering the electronic structure of the individual chains. Suitable substituents enable solubility in common organic solvents as well as the processing of high-quality thin films by spin casting.[74] The thermal stabilities of the homo- and copolymers are excellent with decomposition temperatures exceeding 400 °C. The unique molecular structure and a couple of other attractive properties (e.g., excellent optical and electronic properties) have brought semiconducting polyfluorenes in the focus of current scientific and industrial interest.

26, PF
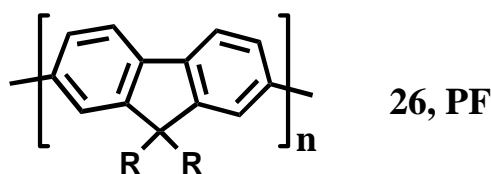
*Scheme 11. Principle chemical structure of substituted polyfluorene (**PF**).*

PFs and their copolymers have evolved as a major class of emitting materials for organic light-emitting diodes (OLEDs).[75] In fact, LEDs fabricated from PF homopolymers exhibit bright blue emission with efficiencies not reached when using other conjugated polymers owing to their pure blue and efficient electroluminescence coupled with a high

charge-carrier mobility and good processability. Another important property of PF homopolymers is their thermotropic liquid crystallinity as first reported by Grell et al. in 1997.[76] They also demonstrated that thin layers of well-aligned PFs can be prepared on a rubbed polyimide (PI) upon annealing in the nematic melts.[77] This was the first report on the alignment of a fully conjugated main-chain liquid-crystalline polymer on an appropriate alignment layer. Other fully conjugated liquid crystalline polymers had been reported previously,[78] but no alignment in the thermotropic phase was mentioned. Lüssem et al. reported the alignment of a segmented poly(aryleneevinylene) on rubbed polyimide, but the oligomeric conjugated liquid crystalline segments in the polymer main chain were separated by aliphatic spacers and the maximum order parameters achieved in aligned layers were below 0.7.[79] Grell et al. [80] reported a dichroic ratio of more than six in absorption spectra and an even larger polarization ratio in photoluminescence spectra of the oriented thin layers of polyfluorenes. Thus, besides the potential of PF homopolymers as emitting materials in blue LEDs, the excellent alignability of the fully conjugated PF polymer backbone opens strategies to construct ultrathin layers with highly anisotropic optical, electrooptical and electric properties. A LED was fabricated using the aligned PF layer and displayed polarized light-emission with a polarization ratio of 15.[79] The alignment of the polymer chains in the liquid-crystalline state also improved the charge-carrier mobility[81] and a field effect transistor with a large in-plane anisotropy of the mobility was reported by Sirringhaus et al.[82]

Polyfluorenes are readily prepared by Ni(0)-mediated coupling (Yamamoto polymerization)[83] of the corresponding dibromo monomers (**27**, Scheme 12). Polymers obtained by this method have weight-averaged molecular weights (M_w) in the order of several hundred thousands with polydispersities (PD) around 3 (according to Gel Permeation Chromatography (GPC) analysis with polystyrene as standard). The large chain-lengths and the polydispersity in chain lengths lead to complex structural characteristics of thin films, raising the difficulty to
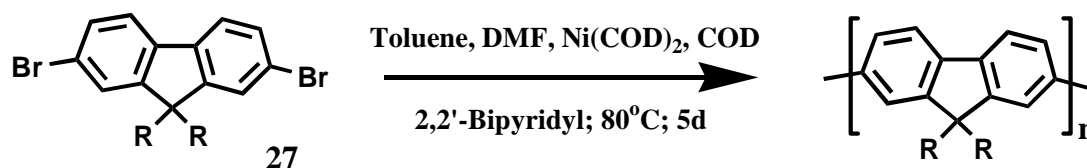
Scheme 12. synthesis of 9,9-dialkyl-PF according to a nickel-mediated Yamamoto coupling reaction (R: -alkyl).

establish a proper structure-property relationship. Moreover, the normal synthetic procedure leads to incorporation of a small amount of chemical defects, which may be responsible for undesirable green-band emission characteristics.[84]

Therefore, for better understanding of the structure-property relationships of PFs, it will be very helpful to study the properties of a series of monodisperse, defect-free oligomers. The absorption spectra of a series of oligomers allow the estimation of the effective conjugation length of the corresponding polymer.[85] In addition, a detailed study of the photoluminescence spectra of pure oligomers may help to solve questions concerning the origin of the green-emission band observed in the photoluminescence and electroluminescence spectra of PF films.[86] Moreover, oligofluorenes may also be used as active materials in organic LEDs and FETs.

Monodisperse dialkyl fluorene oligomers were first reported by Klaerner and Miller.[87] They showed that the Ni(0)-mediated oligomerization of 2,7-dibromo-9,9-bis-(*n*-hexyl)fluorene in the presence of 2-bromofluorene as an end-capping agent gives a mixture of oligomers and low molecular weight polymers that could be fractionated by high pressure liquid chromatography (HPLC). Lee and Tsutsui et al. prepared oligofluorenes up to the tetramer by a repetitive *2n* divergent approach and studied their photophysical properties as a function of the chain-length.[88] The synthesis of longer oligomers of fluorene is a big challenge in synthetic chemistry considering the tedious purification. Herein, the synthesis, structural characterization and physical properties of higher oligofluorenes were presented in this thesis. The work was organized as follows:

m = 1, 2, 3, 4, 5

OFn, n-mer
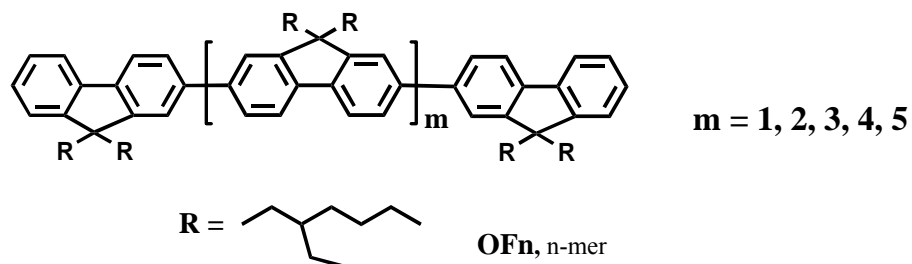
Scheme 13. Oligofluorenes from dimer up to the heptamer

In Chapter 2, the synthesis and structural characterization of oligofluorenes was described in detail. The 9,9-bis(2-ethylhexyl) substituted, monodisperse oligofluorenes from the dimer up to the heptamer (**OFn**, n-mer, Scheme 13) were prepared by repetitive Suzuki and Yamamoto coupling reactions,[89] employing for the first time the Miyaura

reaction for the preparation of the aryl boronates. All compounds were characterized by standard methods such as mass spectroscopy, NMR, and elemental analysis.

In Chapter 3, the chain-length dependence of the electrochemical and electronic properties of the oligofluorenes was studied by cyclic and differential pulse voltammetry (CV), UV-vis absorption and steady-state or transition fluorescence spectroscopy. The relations of ionization potential, electron affinity, oxidation potential, λ_{max}, energy gap, ε_{max}, and fluorescence lifetime with the chain length were concluded. The electronic properties of the corresponding polyfluorenes were predicted by linearly extrapolation of these relationships.

In Chapter 4, thermotropic liquid crystalline properties of higher oligomers of fluorene were observed and characterized by differential scanning calorimetry (DSC), polarizing optical microscopy (POM), electronic diffraction and X-ray diffraction (XRD) techniques. The mono-domain alignment layer of the oligofluorenes on substrates such as rubbed polyimide was achieved and the polarized absorption and emission from the film was studied by UV-vis and fluorescence spctroscopy. In addition, the molecular dynamics of oligofluorenes was also studied by dielectric spectroscopy.

In Chaper 5, transition fluorescence spectroscopy including streak camera and the long-range delayed fluorescence techniques were used to investigate the photophysical properties of the oligofluorenes both in solution and film. The chain-length, concentration, and temperature dependence was discussed in detail.

In order to deeply understand the green emission band of polyfluorenes in film, oligofluorenes (trimer, pentamer, heptamer) with one fluorenone unit in the center as model compounds were synthesized and described in Chapter 6. Similarly, their liquid crystalline behaviors were investigated by DSC, POM, and XRD. Single-crystal structure of pentamer with fluorenone was crystallographically analyzed. Their electrochemistry properties were investigated by cyclic voltammetry.

In Chaper 7 the photophysical properties of oligofluorenes with fluorenone unit were studied by steady-state absorption spectroscopy and time-resolved fluorescence spectroscopy. The chain-length, concentration, and temperature dependence of the fluorescence spectra both in solution and film was discussed. A comparison of the photophysical properties between the oligofluorenes and the oligofluorenes with fluorenone revealed the dramatic changes in the emission spectra due to the existence/ absence of the

fluorenone "defect". Doping of the polyfluorenes with the oligofluorenes with fluorenones was also conducted and followed by the transition spectroscopic measurements.

In the last chapter (Chapter 8), a summary and conclusion of this Ph.D. work was presented.

1.4 References and Notes

[1] (a) *Handbook of Conducting Polymers*; Skotheim, T.A.; Elsenbaumer, R.L.; Reynolds, J. R. Eds. Marcel Dekker, Inc.; New York, **1998**; (b) *Electronic Materials: The Oligomer Approach*; Müllen, K.; Wegner, G. Eds. Weinheim: Wiley-VCH, **1998**;

[2] Meier, H. *Angew.Chem.* **1992**, *104*, 1425-1446; *Angew. Chem. Int. Ed. Engl.* **1992**, *31*, 1399-1420.

[3] Kraft, A.; Grimsdale, A. C.; Holmes, A. B. *Angew.Chem.* **1998**, *110*, 416-443; *Angew. Chem. Int. Ed. Engl.* **1998**, *37*, 403-428.

[4] Horowitz, G. *Adv. Mater.* **1998**, *10*, 365.

[5] Das-Gupta, D. K. in *Introduction to Molecular Electronics* (Eds.: Petty, M. C.; Bryce, M. R.; Bloor, D.), Edward Arnold, London, **1995**, pp.47-71.

[6] Bleier in *Organic Materials for Photonics* (Ed.: G. Zerbi), Elsevier, Amsterdam, **1993**, pp. 77-101; b) Loutfy, R. O.; Hor, A.-M.; Hsiao, C.-K.; Baranyi, G.; Kazmaier, P. *Pure. Appl. Chem.* **1988**, 60, 1047-1054; c) Perlstein, J. H.; Borsenberger, P. M. in *Extended Linear Chain Compounds* (Ed.: Miller, J. S.) Pleenum, New York, **1982**, pp. 339-384.

[7] Feringa, L.; Jager, W. F.; de Lange, B. *Tetrahedron* **1993**, *49*, 8267-8310; b) Kämpf, G. *Ber. Bunsenges. Phys. Chem.* **1985**, *89*, 1179-1190.

[8] (a) Lösch, K. *Macromol. Symp.* **1995**, *100*, 65-69; b) Lehn, J.-M. *Supramolecular Chemistry. Concepts and Perspectives*, Weinheim: Wiley-VCH, **1995**, pp 124-138; (b) Kim, J.-J.; Lee, E.-H. *Mol. Cryst. Liq. Cryst.* **1993**, *227*, 71-84; (c) Dürr, H. *Angew. Chem.* **1989**, *101*, 427-445; *Angew. Chem. Int. Ed. Engl.* **1989**, *28*, 413-431.

[9] Marder, S. R.; Kippelen, B.; Jen, A.K.-Y.; Peyghambarian, N. *Nature* **1997**, *388*, 845-851.

[10] (a) Broszeit, G.; Diepenbrock, F.; Gräf, O. *Liebigs Ann.,* 1997, 2205; (b) Guay, J.; Kasai, P.; Diaz, A.; Wu, R.; Tour, J. M.; Dao, Le H. *Chem. Mater.* **1992**, *4*, 1097-1105.

[11] Beljonne, D.; Cornil, J.; Friend, R. H.; Janssen, R. A. J.; Brédas. J. L. *J. Am. Chem. Soc.* **1996**, *118*, 6453.

[12] (a) Tour, J. M. *Chem. Rev.* **1996**, *96*, 537-553; (b) Müllen, K. *Pure Appl. Chem.* **1993**, *65*, 89-96.

[13] Nelson, J. C.; Saven, J. G.; Moore, J. S.; Wolynes, P. G. *Science* **1997**, *277*, 1793-1796

[14] Scherf, U.; Müllen, K. *Synthesis* **1992**, 23-38

[15] (a) van Hutten, P. F.; Wildeman, J.; Meetsma, A.; Hadziioannou, G. *J. Am. Chem. Soc.* **1999**, *121*, 5910-5918; (b) Goodson, T., III; Li, W.; Gharavi, A.; Yu, L. *Adv. Mater.* **1997**, *9*, 639-643.

[16] (a) Noma, N.; Tsuzuki, T.; Shirota, Y. *Adv. Mater.* **1995**, *7*, 647-648; (b) Eckert, J.-F.; Nicoud, J.-F.; Nierengarten, J.-F.; Liu, S.-G.; Echegoyen, L.; Barigelletti, F.; Armaroli, N.; Ouali, L.; Krasnikov, V.; Hadziioannou, G. *J. Am. Chem. Soc.* **2000**, *122*, 7467-7479.

[17] Schon, J. H.; Dodabalapur, A.; Kloc, C.; Batlogg, B. *Science* **2000**, *290*, 963-965.

[18] a) Garnier, F.; Horowitz, G.; Fichou, D. *Synth. Met.*, **1989**, *28*, C705; b) Garnier, F.; Horowitz, G.; Peng, X.; Fichou, D. *Adv. Mater.*, **1990**, *2*, 592; c) Xu, B.; Fichou, D.; Horowitz, G.; Garnier, F. *Adv. Mater.*, **1991**, *3*, 150; d) Yoshino, K. *Synth. Met.*, **1989**, *28*, C669; e) Fichou, D.; Nunzi, J.-M.; Charra, F.; Pfeffer, N. *Adv. Mater.*, **1992**, *4*, 64.

[19] Pearson, D. L.; Tour, J. M. *J. Org. Chem.* **1997**, *62*, 1376-1387.

[20] MacDonald, S. A.; Willson, C. G.; Fréchet, J. M. J. *Acc. Chem. Res.* **1994**, *27*, 151-158

[21] (a) Muller, C. J.; Vleeming, B. J.; Reed, M. A.; Lamba, J. J. S.; Hara, R.; Jones II, L.; Tour, J. M. *Nanotechnology* **1996**, *7*, 409-411; (b) Bradley, D. D. C. *Chem. Brit.* **1991**, 719-723.

[22] (a) Magoga, M.; Joachim, C.; *Phys. Rev. B* **1997**, *56*, 4722-4729; (b) Brédas, J. L. *Synth. Met.* **1997**, *84*, 3-10; (c) Mujica, V.; Kemp, M.; Roitberg, A.; Ratner, M. *J. Chem. Phys.* **1996**, *104*, 7296-7305.

[23] The iterative doubling approach was first described by Whiting and then later used by Moore to prepare oligo(1,3-phenyleneethynylene)s. see: (a) Igner, E.; Paynter, O. I.; Simmonds, D. J.; Whiting, M. C. *J. Chem. Soc. Perkin Trans. 1,* **1987**, 2447-2454; (b) Bidd, I.; Kelly, D. J.; Ottley, P. M.; Paynter, O. I.; Simmonds, D. J.; Whiting, M. C. *J. Chem. Soc. Perkin Trans. 1* **1983**, 1369-1372; (c) Zhang, J.; Moore, J. S.; Xu, Z.; Aguirre, R. A. *J. Am. Chem. Soc.* **1992**, *114*, 2273-2274; (d) Xu, Z.; Moore, J. S.; *Angew. Chem.* **1993**, *105*, 1394-1396; *Angew. Chem. Int. Ed. Engl.* **1993**, *32*, 1354-1357. For the applications of the binomial strategy to the synthesis of nonconjugated monodisperse molecular rods, see (e) Cai, C.; Vasella, A.; *Helv. Chim. Acta* **1996**, *79*, 255-268; (f) Cai, C.; Vasella, A.; *Helv. Chim. Acta* **1995**, *78*, 732-757.

[24] (a) Schumm, J. S.; Pearson, D. L.; Tour, J. M. *Angew. Chem.* **1994**, *106*, 1445-1448; *Angew. Chem. Int. Ed. Engl.* **1994**, *33*, 1360-1363; (b) Jones II, L.; Schumm, J. S. Tour, J. M. *J. Org. Chem.* **1997**, *62*, 1388-1410.

[25] (a) Pearson, D. L.; Tour, J. M. *J. Org. Chem.* **1997**, *62*, 1376-1387; (b) Pearson, D. L.; Schumm, J. S.; Tour, J. M. *Macromolecules* **1994**, *27*, 2348-2350.

[26] (a) Jones II, L.; Schumm, J. S.; Tour, J. M. *J. Org. Chem.* **1997**, *62*, 1388-1410; (b) Young, J. K.; Nelson, J. C.; Moore, J. S.; *J. Am. Chem. Soc.* **1994**, *116*, 10841-10842; (c) Nelson, J. C.; Young, J. K.; Moore, J. S. *J. Org. Chem.* **1996**, *61*, 8160-8168.

[27] (a) Martin, R. E.; Gubler, U.; Boudon, C.; Gramlich, V.; Bosshard, C.; Gisselbrecht, J.-P.; Günter, P.; Gross, M.; Diederich, F. *Chem. Eur. J.* **1997**, *3*, 1505-1512; (b) Schenning, A. P. H. J.; Martin, R. E.; Ito, M.; Diederich, F.; Boudon, C.; Gisselbrecht, J.-P.; Gross, M. *Chem. Commun.* **1998**, 1013-1014; (c) Anthony, J.; Boudon, C.; Diederich, F.; Gisselbrecht, J.-P.; Gramlich, V.; Gross, M.; Hobi, M.; Seiler, P.

Angew. Chem. **1994**, *106*, 794-798; *Angew. Chem. Int. Ed. Engl.* **1994**, *33*, 763-766; (d) Nierengarten, J.-F.; Guillon, D.; Heinrich, B.; Nicoud, J.-F. *Chem. Commun.* **1997**, 1233-1234.

[28] Groenendaal, L.; Peerlings, H. W. I.; van Dongen, J. L. J.; Havinga, E. E.; Vekemans, J. A. J. M.; Meijer, E. W. *Macromolecules* **1995**, *28*, 116-123.

[29] Altmann, M.; Enkelmann, V.; Beer, F.; Bunz, U. H. F. *Organometallics* **1996**, *15*, 394-399.

[30] Martin, R. E.; Mäder, T.; Diederich, F.; *Angew. Chem.* **1999**, *111*, 834-838; *Angew. Chem. Int. Ed.* **1999**, *38*, 817-821.

[31] Kraft, A.; Grimsdale, A. C.; Holmes, A. B. *Angew. Chem.* **1998**, *110*, 416-443; *Angew. Chem. Int. Ed.* **1998**, *37*, 403-428.

[32] (a) Chiang, C. K.; Ficher, C. R.; Park, Y. W.; Heeger, A. J.; Shirakawa, H.; Louis, E. J.; Gau, S. C.; MacDiarmid, A. G. *Phys. Rev. Lett.* **1977**, *39*, 1098-1101; (b) Handbook of conducting polymers (Eds.: Skotheim, T. A.; Elsenbaumer, R. L.; Reynolds, I. R.), Dekker, New York, **1988**.

[33] (a) Effenberger, F.; Schlosser, H.; Bäuerle, P.; Maier, S.; Port, H.; Wolf, H. C. *Angew. Chem.* **1988**, *100*, 274-277; *Angew. Chem. Int. Ed. Engl.* **1988**, *27*, 281-284; (b) Tolbert, L. M.; Zhao, X.; Ding, Y.; Bottomley, L. A. *J. Am. Chem. Soc.* **1995**, *117*, 12891-12892; (c) Kugimiya, S.; Lazrak, T.; Blanchard-Desce, M.; Lehn, J.-M. *J. Chem. Soc. Chem. Commun.* **1991**, 1179-1182; (d) Duhamel, L.; Duhamel, P.; Plé, G.; Ramondenc, Y. *Tetrahedron Lett.* **1993**, *34*, 7399-7400.

[34] (a) Wenz, G.; Müller, M. A.; Schmidt, M.; Wegner, G. *Macromolecules* **1984**, *17*, 837-850; (b) Campbell, A. J.; Davies, C. K. L. *Polymer* **1994**, *35*, 4787-4793.

[35] (a) Tour, J. M. *Adv. Mater.* **1994**, *6*, 190-198; (b) Kovacic, P.; Jones, M. B. *Chem. Rev.* **1987**, *87*, 357-379.

[36] (a) Feast, W. J.; Tsibouklis, J.; Pouwer, K. L.; Groenendaal, L.; Meijer, E. W. *Polymer* **1996**, *37*, 5017-5047 ; (b) Baughman, R. H.; Brédas, J. L.; Chance, R. R.; Elsenbaumer, R. L.; Shacklette, L. W. *Chem. Rev.* **1982**, *82*, 209-222; (c) Schlüter, A.-D.; Wegner, G. *Acta Polym.* **1993**, *44*, 59-69; (d) Rau, I. U.; Rehahn, M. *Acta Polym.* **1994**, *45*, 3-13; (e) Wittemann, M.; Rehahn, M. *Chem. Commun.* **1998**, 623-624; (f) Novák, P.; Müller, K.; Santhanam, K. S. V.; Hass, O. *Chem. Rev.* **1997**, *97*, 207-281.

[37] (a) Hide, F.; Díaz-García, M. A.; Schwartz, B. J.; Heeger, A. J. *Acc. Chem. Res.* **1997**, *30*, 430-436; (b) Birgerson, J.; Kaeriyama, K.; Barta, P.; Bröms, P.; Fahlman, M.; Granlund, T.; Salaneck, W. R. *Adv. Mater.* **1996**, *8*, 982-985; (c) Baur, J. W.; Kim, S.; Balanda, P. B.; Reynolds, J. R.; Rubner, M. F. *Adv. Mater.* **1998**, *10*, 1452-1455; (d) Grem, G.; Leditzky, G.; Ullrich, B.; Leising, G. *Adv. Mater.* **1992**, *4*, 36-37. (e) Germ, G.; Leditzky, G.; Ullrich, B.; Leising, G. *Synth. Met.* **1992**, *51*, 383-389.

[38] Kern, W.; Seibel, M.; Wirth, H.-O. *Makromol. Chem* **1959**, *29*, 164.

[39] Heitz, W.; Ulrich, R. *Makromol. Chem.* **1966**, *98*, 29.

[40] Liess, P.; Hensel, V.; Schlüter, A. D. *Liebigs Ann.* **1996**, 1037.

[41] (a) Bohnen, A.; Heitz, W.; Müllen, K.; Räder, H.-J.; Schenk, R. *Makromol. Chem.* **1991**, *192*, 1679-1693; (b) Baumgarten, M.; Müllen, K. *Top. Curr. Chem.* **1994**, *169*, 1-103; (c) Baumgarten, M.; Huber, W.; Müllen, K. *Adv. Phys. Org. Chem.* **1993**, *28*, 1-44.

[42] (a) Müllen, K.; Scherf, U. *Makromol. Chem. Macromol. Symp.* **1993**, *69*, 23-33; (b) Horn, T.; Wegener, S.; Müllen, k. *Macromol. Chem. Phys.* **1995**, *196*, 2463-2474; (c) Wegener, S.; Müllen, K.; *Macromolecules* **1993**, *26*, 3037-3040.

[43] Wuckel, L.; Lehmann, G. *Macromol. Chem. Macromol. Symp.* **1990**, *37*, 195-209.

[44] Scherf, U.; Müllen, K. *Makromol. Chem. Rapid Commun.* **1994**, *12*, 489.

[45] Kreyenschmidt, M.; Uckert, F.; Müllen, K. *Macromolecules* **1995**, *28*, 4577.

[46] Fukuda, M.; Sawada, K.; Yoshino, K. *J. Polym. Sci., Polym. Chem.* **1993**, *31*, 2465.

[47] Burroughes, J. H.; Bradley, D. D. C.; Brown, A. R.; Marks, R. N.; Mackay, K.; Friend, R. H.; Burn, P. L.; Holmes, A. B. *Nature* **1990**, *347*, 539-541.

[48] Kraft, A.; Grimsdale, A. C. Holmes, A. B. *Angew. Chem.* **1998**, *110*, 416-443; *Angew. Chem. Int. Ed.* **1998**, *37*, 403-428.

[49] (a) Hwang, D.-H.; Chuah, B. S.; Li, X.-C.; Kim, S. T.; Moratti, S. C.; Holmes, A. B. *Macromol. Symp.* **1997**, *125*, 111-120; (b) Fahlman, M.; Lögdlund, M.; Stafström, S.; Salaneck, W. R.; Friend, R. H.; Burn, P. L.; Holmes, A. B.; Kaeriyama, K.; Sonoda, Y.; Lhost, O.; Meyers, F.; Brédas, J. L. *Macromolecules* **1995**, *28*, 1959-1965; (c) Brédas, J.-L. *Adv. Mater.* **1995**, 7, 263-274.

[50] (a) Burn, P. L.; Holmes, A. B.; Kraft, A.; Bradley, D. D. C.; Brown, A. R.; Friend, R. H.; Gymer, R. W. *Nature* **1992**, *356*, 47-49; (b) Greenham, N. C.; Moratti, S. C.; Bradley, D. D. C.; Friend, R. H.; Holmes, A. B. *Nature* **1993**, *365*, 628-630; (c) Hwang, D.-H.; Kim, S. T.; Shim, H.-K.; Holmes, A. B.; Moratti, S. C.; Friend, R. H. *Chem. Commun.* **1996**, 2241-2242; (d) Burn, P. L.; Kraft, A.; Baigent, D. R.; Bradley, D. D. C.; Brown, A. R.; Friend, R. H.; Gymer, R. W. Holmes, A. B. Jackson, R. W.; *J. Am. Chem. Soc.* **1993**, *115*, 10117-10124; (e) Chung, S.-J.; Jin, J.-I.; Kim, K.-K. *Adv. Mater.* **1997**, *9*, 551-554; (f) Gao, M.; Richter, B.; Kirstein, S.; *Adv. Mater.* **1997**, *9*, 802-805; (g) Tessler, N.; Harrison, N. T.; Friend, R. H. *Adv. Mater.* **1998**, *10*, 64-68.

[51] Yu, G.; Cao, Y.; Andersson, M.; Gao, J.; Heeger, A. J. *Adv. Mater.* **1998**, *10*, 385-388.

[52] (a) Garten, F.; Hilberer, A.; Cacialli, F.; Esselink, E.; van Dam, Y.; Schlatmann, B.; Friend, R. H.; Klapwijk, T. M.; Hadziioannou, G. *Adv. Mater.* **1997**, *9*, 127-131; (b) Lee, J.-K.; Schrock, R. R.; Baigent, D. R.; Friend, R. H. *Macromolecules* **1995**, *28*, 1966-1971.

[53] Mangel, T.; Eberhardt, A.; Scherf, U.; Bunz, U. H. F.; Müllen, K. *Macfromol. Rapid Commun.* **1995**, *16*, 571-580.

[54] (a) Jones II, L.; Schumm, J. S.; Tour, J. M. *J. Org. Chem.* **199**7, *62*, 1388-1410; (b) Weder, C.; Wrighton, M. S.; Spreiter, R.; Bosshard, C.; Günter, P. *J. Phys. Chem.* **1996**, *100*, 18931-18936; (c) Weder, C.; Wrighton, M. S. *Macromolecules* **1996**, *29*, 5157-5165; (d) Ziener, U.; Godt, A.; *J. Org. chem.* **1997**, *62*, 6137-6143; (e) Galda, P.; Rehahn, M. *Synthesis* **1996**, 614-620; (f) Montali, A.;

Bastiaansen, C.; Smith, P.; Weder, C. *Nature* **1998**, *392*, 261-264; (g) Weder, C.; Sarwa, C.; Bastiaansen, C.; Smith, P. *Adv. Mater.* **1997**, *9*, 1035-1039; (h) Schumm, J. S.; Pearson, D. L.; Jones II, L.; Hara, R.; Tour, J. M. *Nanotechnology* **1996**, *7*, 430-433; (i) Tour, J. M.; Jones II, L.; Pearson, D. L.; Lamba, J. J. S.; Burgin, T. P.; Whitesides, G. M.; Allara, D. L.; Parikh, A. N.; Atre, S. V. *J. Am. Chem. Soc.* **1995**, *117*, 9529-9534.

[55] Zhou, Q.; Swager, T. M. *J. Am. Chem. Soc.* **1995**, *117*, 12593-12602.

[56] (a) Polin, J.; Buchmeiser, M.; Nock, H.; Schottenberger, H. *Mol. Cryst. Liq. Cryst.* **1997**, *293*, 287-307; (b) Francke, V.; Mangel, T.; Müllen, K. *Macromolecules* **1998**, *31*, 2447-2453.

[57] Puddephatt, R. J. *Chem. Commun.* **1998**, 1055-1062.

[58] Lavastre, O.; Ollivier, L.; Dixneuf, P. H.; Sibandhit, S. *Tetrahedron* **1996**, *52*, 5495-5504.

[59] Bäuerle, P. *Adv. Mater.*, **1993**, *5*, 879.

[60] Roncali, J. *Chem. Rev.* **1992**, *92*, 711-738.

[61] (a) Tour, J. M.; Wu, R. *Macromolecules* **1992**, *25*, 1901-1907; (b) Casado, J.; Hernández, V.; Hotta, S.; López Navarrete, J. T. *Adv. Mater.* **1998**, *10*, 1458-1461; (c) de Leeuw, D. M. *Synt. Met.* **1993**, *55-57*, 3597-3602.

[62] (a) Roncali, J. *J. Mater. Chem.* **1997**, *7*, 2307-2321; (b) Otsubo, T.; Aso, Y.; Takimiya, K. *Adv. Mater.* **1996**, *8*, 203-211; (c) Bryce, M. R. in *Introduction to Molecular Electronics* (Eds.: Petty, M. C.; Bryce, M. R.; Bloor, D.), Edward Arnold, London, 1995, pp. 168-184; (c) Brisset, H.; Thobie-Gautier, C.; Jubault, M.; Gorgues, A.; Roncali, J. *J. Chem. Soc. Chem. Commun.* **1994**, 1765-1766.

[63] (a) Jen, A. K.-Y.; Cai, Y.; Bedworth, P. V.; Marder, S. R. *Adv. Mater.* **1997**, *9*, 132-135; (b) Shu, C.-F-; Tsai, W. J.; Chen, J.-Y.; Jen, A. K.-Y.; Zhang, Y.; Chen, T.-A. *Chem. Commun.* **1996**, 2279-2280; (c) Jen, A. K.-Y.; Rao, V. P.; Wong, K. Y.; Drost, K. J. *J. Chem. Soc. Chem. Commun.* **1993**, 90-92; (d) Mignani, G.; Leising, F.; Meyrueix, R.; Samson, H.; *Tetrahedron Letters.* **1990**, *31*, 4743-4746; (e) Zhang, J. X.; Dubois, P.; Jérôme, R. *J. Chem. Soc. Perkin Trans. 2* **1997**, 1209-1216.

[64] (a) Tsivgoulis, G. M.; Lehn, J.-M. *Adv. Mater.* **1997**, *9*, 39-41; (b) Tsivgoulis, G. M.; Lehn, J.-M., *Adv. Mater.* **1997**, *9*, 627-630; (c) Kawai, S. H.; Gilat, S. L.; Ponsinet, R.; Lehn, J.-M. *Chem. Eur. J.* **1995**, *1*, 285-293; (d) Gilat, S. L.; Kawai, S. H.; Lehn, J.-M. *Chem. Eur. J.* **1995**, *1*, 275-284; (e) Irie, M.; Sakemura, K.; Okinaka, M., Uchida, K. *J. Org. Chem.* **1995**, *60*, 8305-8309.

[65] (a) Horowitz, *Adv. Mater.* **1998**, *10*, 365-377; (b) Katz, H. E.; Laquindanum, J. G.; Lovinger, A. J.; *Chem. Mater.* **1998**, *10*, 633-638; (c) Siegrist, T.; Kloc, C.; Laudise, R. A.; Katz, H. E.; Haddon, R. C.; *Adv. Mater.* **1998**, *10*, 379-385; (d) Barbarella, G.; Ostoja, P.; Maccagnani, P.; Pudiva, O.; Antolini, L.; Casarini, D.; Bongini, A.; *Chem. Mater.* **1998**, *10*, 3683-3689; (e) Sirringhaus, H.; Friend, R. H.; Li, X. C.; Moratti, S. C.; Holmes, A. B.; Feeder, N. *Appl. Phys. Lett.* **1997**, *71*, 3871-3873; (f) Hajlaoui, R.; Fichou, D.; Horowitz, G.; Nessakh, B.; Constant, M.; Garnier, F. *Adv. Mater.* **1997**, *9*, 557-561; (g) Fichou, D.; Teulade-Fichou, M.-P.; Horowitz, G.; Demanze, F.; *Adv. Mater.* **1997**, *9*, 75-80; (h) Fichou, D.; Bacher, B.; Demanze, F.; Billy, I.; Horowitz, G.; Garnier, F. *Adv. Mater.* **1996**, *8*, 500-504; (i) Horowitz, G.; Peng, X.-Z.; Fichou, D.; Garnier, F. *J. Mol. Electron.* **1991**, *7*, 85-89.

[66] (a) Noda, T.; Ogawa, H.; Noma, N.; Shirota, Y. *Adv. Mater.* **1997**, *9*, 720-722; (b) Geiger, F.; Stoldt, M.; Schweizer, H.; Baüerle, P.; Umbach, E. *Adv. Mater.* **1993**, *5*, 922-925; (c) Noda, T.; Imae, I.; Noma, N.; Shirota, Y. *Adv. Mater.* **1997**, *9*, 239-241.

[67] Noma, N.; Tsuzuki, T.; Schirota, Y. *Adv. Mater.* **1995**, *7*, 647-648.

[68] Fichou, D.; Nunzi, J.-M.; Charra, F.; Pfeffer, N. *Adv. Mater.* **1994**, *6*, 64-67.

[69] McCullough, R. D. *Adv. Mater.* **1998**, *10*, 93-116.

[70] Malenfant, P. R. L.; Fréchet, J. M. *J. Chem. Commun.* **1998,** 2657-2658.

[71] (a) Zhao, M.-T. Singh, B. P.; Prasad, P. N. *J. Chem. Phys.* **1988**, *89*, 5535-5541.

[72] (a) Bäuerle, P.; Segelbacher, U.; Maier, A.; Mehring, M. *J. Am. Chem.Soc.* **1993**, *115*, 10217-10223; (b) Bäuerle, P. *Adv. Mater.* **1992**, *4*, 102-107.

[73] (a) Bäuerle, P.; Fischer, T.; Bidlingmeier, B.; Stabel, A.; Rabe, J. P. *Angew. Chem.* **1995**, *107*, 335-339; *Angew. Chem. Int. Ed.* **1995**, *34*, 303-307; (b) Mustafa, A. H.; Shepherd, M. K.; *Chem. Commun.* **1998**, 2743-2744.

[74] (a) Neher, D. *Macromol. Rapid Commun.* **2001**, *22*, 1365-1385; (b) Scherf, U.; List, E. J. W. *Adv. Mater.* **2002**, *14*, 477-487.

[75] (a) Bernius, M.; Inbasekaran, M.; Woo, E.; Wu, W. S.; Wujkowski, L. *J. Mater. Sci.-Mater. Electron.* **2000**, *11*, 111; (b) Bernius, M. T.; Inbasekaran, M.; O'Brien, J.; Wu, W. S. *Adv. Mater.* **2000**, *12*, 1737; (c) Inbasekaran, M.; Woo, E.; Wu, W. S.; Bernius, M.; Wujkowski, L. *Synth. Met.* **2000**, *111*, 397; d) Bradley, D. D. C.; Grell, M.; Grice, A.; Tajbakhsh, A. R.; O'Brien, D. F.; Bleyer, A. *Opt. Mater.* **1998**, *9*, 1; (e) Gross,M.; Müller, D. D.; Nothofer, H.-G.; Scherf, U.; Neher, D.; Bräuchle, C.; Meerholz, K. *Nature* **2000**, *405*, 661-665; (f) Grice, A. W.; Bradley, D. D. C.; Bernius, M. T.; Inbasekaran, M.; Wu, W. W.; Woo, E. P. *Appl. Phys. Lett.* **1998**, *73*, 629-631; (g) Friend, R. H.; Gymer, R. W.; Holmes, A. B.; Burroughes, J. H.; Marks, R. N.; Taliani, C.; Bradley, D. D. C.; Dos-Santos, D. A.; Brédas, J. L.; Lögdlund, M.; Salaneck, W. R. *Nature* **1999**, *397*, 121-128; (h) Pei, Q. B.; Yang, Y. *J. Am. Chem. Soc.* **1996**, *118*, 7416-7417; (i) Yang, Y.; Pei, Q. *J. App. Phys.* **1997**, *81*, 3294-3298; (j) Lee, S. H.; Jang, B-B.; Tsutsui, T. *Macromolecules*, **2002**, *35*, 1356-1364; (k) Virgili, T.; Lidzey, D. G.; Bradley, D. D. C. *Adv. Mater.* **2000**, *12*, 58-62; (l) Lane, P. A.; Palilis, L. C.; O'Brien, D. F.; Giebeler, C.; Cadby, A. J.; Lidzey, D. G.; Campbell, A. L.; Blau, W.; Bradley, D. D. C. *Phys. Rev. B* **2001**, *63*, 235206.

[76] Grell, M.; Bradley, D. D. C.; Inbasekaran, M.; Woo, E. P. *Adv. Mater.* **1997**, *9*, 798.

[77] (a) Grell, M.; Bradley, D. D. C.; Ungar, G.; Hill, J.; Whitehead, K. S. *Macromolecules.* **1999**, *32*, 5810-5817; (b) Grell, M.; Bradley, D. D. C.; Long, X.; Chamberlain, T.; Inbasekaran, M.; Woo, E. P.; Soliman, M. *Acta Polym.* **1998**, *49*, 439-444; (c) Lieser, G.; Oda, M.; Miteva, T.; Meisel, A.; Nothofer, H. G.; Scherf, U. *Macromolecules* **2000**, *33*, 4490-4495.

[78] Lu, L.; Bao, Z. *Adv. Mater.* **1994**, *6*, 156.

[79] Lüssem, G.; Festag, R.; Greiner, A.; Schmidt, C.; Unterlechner, C.; Heitz, W.; Wendorff, J. H.; hopmeier, M.; Feldmann, J. *Adv. Mater.* **1995**, *7*, 923.

[80] Grell, M.; Knoll, W.; Lupo, D.; Meisel, A.; Miteva, T.; Neher, D.; Nothofer, H. G.; Scherf, U.; Yasuda, A. *Adv. Mater.* **1999**, *11*, 671.

[81] Redecker, M.; Bradley, D. D. C.; Inbasekaran, M.;Wu, W.; Woo, E. P. Grell, M.; Bradley, D. D. C. *Appl. Phys. Lett.* **2000**, *77*, 406.

[82] Sirringhaus, H.; Wilson, R. J.; Friend, R. H.; Inbasekaran, M.; Wu, W.; Woo, E. P.; Grell, M.; Bradley, D. D. C. *Appl. Phys. Lett.* **2000**, *77*, 406.

[83] Yamamoto, T.; Hayashi, Y.; Yamamoto, A. *Bull. Chem. Soc. Jpn.* **1978**, *51*, 209.

[84] a) Lupton, J. M.; Craig, M. R.; Meijer, E. W. *Appl. Phys. Lett*. **2002**, *80*, 4489-4491; b) List, E. J. W.; Güntner, R.; Scandiucci de Freitas, P.; Scherf, U.; *Adv. Mater.* **2002**, *14*, 374;

[85] Martin, R. E.; Diederich, F. *Angew. Chem. Int. Ed*. **1999**, *38*, 1350-1377.

[86] a) Bliznyuk, U. N.; Carter, S. A.; Scott, J. C.; Klaerner, G.; Miller, R. D.; Miller, D. C. *Macromolecules*, **1999**, *32*, 361-369; b)Uckert, F.; Tak, Y. H.; Müllen, K.; Bässler, H. *Adv. Mater.* **2000**, *12*, 905; c) Weinfurtner, K. H.; Fujikawa, H.; Tokito, S.; Taga, Y. *Appl. Phys. Lett.* **2000**, *76*, 2502.

[87] Klaerner, G. Miller, R. D. *Macromolecules* **1998**, *31*, 2007-2009.

[88] Lee, S. H.; Tsutsui, T. *Thin Solid Films* **2000**, *363*, 76-80.

[89] Yamamoto, T.; Morita, A.; Miyazaki, Y.; Maruyama, T.; Wakayama, H.; Zhou, Z.; Nakamura, Y.; Kanbara, T.; Sasaki, S.; Kubota, K. *Macromolecules* **1992**, *25*, 1214-1223.

2 **Synthesis and Structural Characterizations of Oligofluorenes**

The oligofluorenes up to heptamer were synthesized mainly by palladium-catalyzed coupling reactions. Structural proof and purity of the target compounds were defined by standard NMR, mass spectroscopy and elemental analysis.

2.1 Synthesis

The synthesis of the monodisperse oligomers of 9,9-dihexyl fluorene was first reported by Klaerner and Miller et al. according to a statistic oligomerization process.[1] In their method, the polydisperse oligomers (**30**, Scheme 1) of fluorene were obtained by a Ni(0)-mediated oligomerization process of 2,7-dibromo-9,9-bis-(*n*-hexyl)fluorene (**28**) in the presence of 2-bromofluorene (**29**) as an end-capping agent. The crude reaction product was composed of a mixture of oligomers and low molecular weight polymer, as determined by GPC analysis, and then separation of the oligomers from the polymer fraction was achieved by high pressure liquid chromatography (HPLC) on Kromasil C_{18}-10 μm using a gradient elution with acetonitrile/chloroform. Using this technique, oligomers ranging from n = 3 to n = 10 were separated. The chain-length dependence of UV-vis spectroscopy of the oligomers were studied and revealed an effective conjugation length (ECL) of 12 (number of the fluorene units) for the corresponding polyfluorenes.
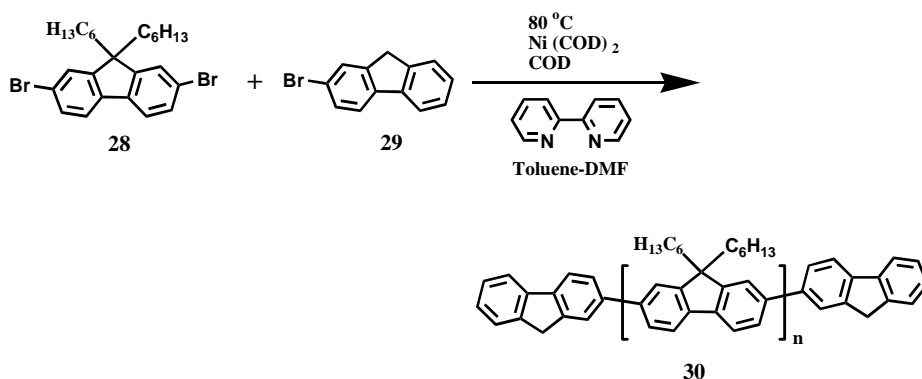
Scheme 1. Statistic preparation of oligomeric poly(9,9-di-n-hexylfluorenes).

Lee and Tsutsui prepared a series of oligofluorenes up to tetramer by a repetitive *2n* divergent approach (Scheme 2) starting from the appropriate 2,7-dibromo-9,9-bis-(*n*-hexyl)fluorene (**28**), followed by the Suzuki coupling with bis-(*n*-hexyl)-fluorene-2-borate (**31**) and subsequent bromination of the coupling product.[2] This *2n* growth approach can connect two units asymmetrically without tedious protection-deprotection steps. All kinds of sequential well-defined monodisperse oligomers can be synthesized easily from monomer (odd unit) and dimer (even unit) containing two reactive functional groups (Scheme 3). The higher oligomers in principle can be synthesized by this strategy, however, hindered by the key step of the bromination. The two-fold bromination of the trimer was found to be much difficult to afford pure α,ω-dibromofluorene of trimer because the bromination also took place in other positions in the fluorenyl ring (Scheme 4). Thus the synthesis of longer oligomers of fluorene remains a big challenge in synthetic chemistry given the tedious purification process.

X, Y = reactive functional groups
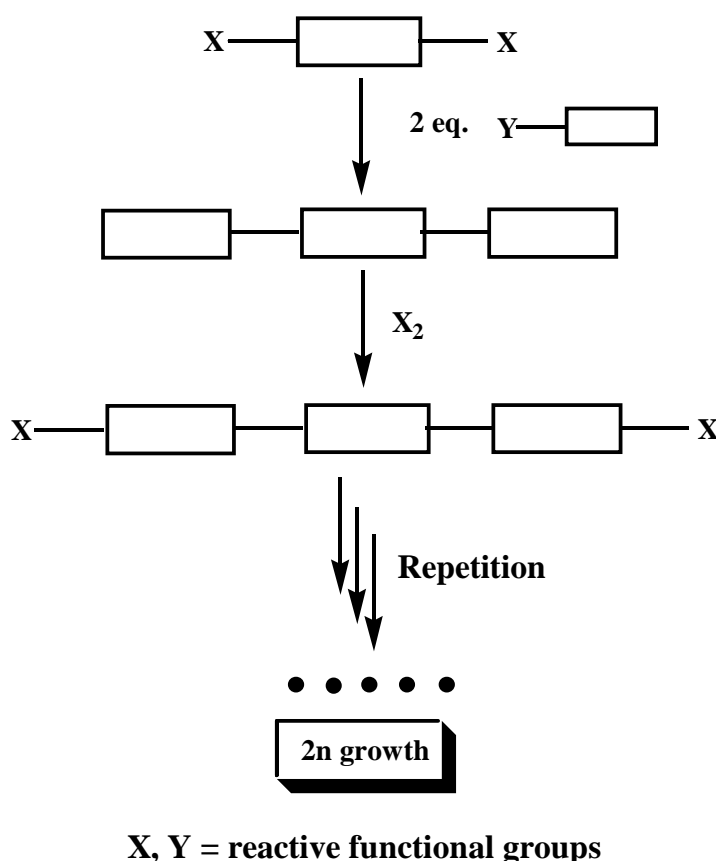
Scheme 2 A repetitive 2n-growth divergent approach to well-defined monodisperse oligomers.

Odd-type oligofluorenes:
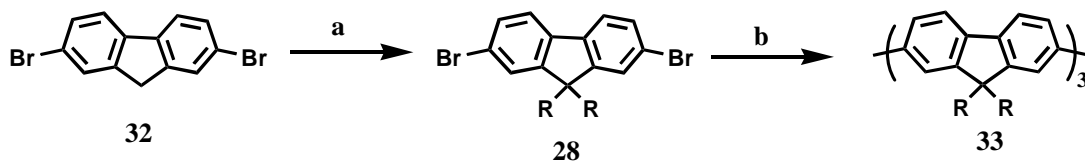
Even-type oligofluorenes:
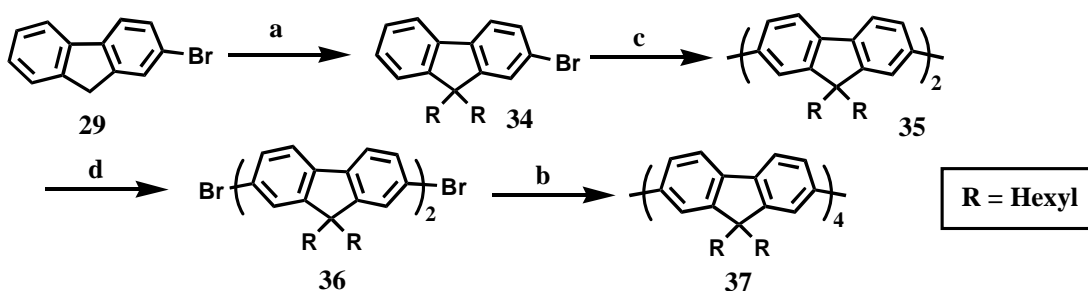
R = Hexyl

Scheme 3. Repetitive stepwise divergent approach to odd/even-type oligo(9,9-bis-n-hexylfluorene-2,7-diyl)s: (a) n-C₆H₁₃Br, 50% aqueous NaOH/DMSO, room temperature; (b) 2-(4,4,5,5-tetramethyl-1,3,2-dioxaborolan-2-yl)-9,9-bis-n-hexylfluorene(31), Pd(PPh₃)₄ (2 mol%), toluene/aqueous Na₂CO₃ (2 M); (c) NiCl₂, PPh₃, Zn, DMF, 50°C; (d) CuBr₂-Al₂O₃, CCl₄, 80°C. DMSO = dimethylsulfoxide, DMF = N,N-dimethylformamide.

n =1, 2, 3......

X = Br, I
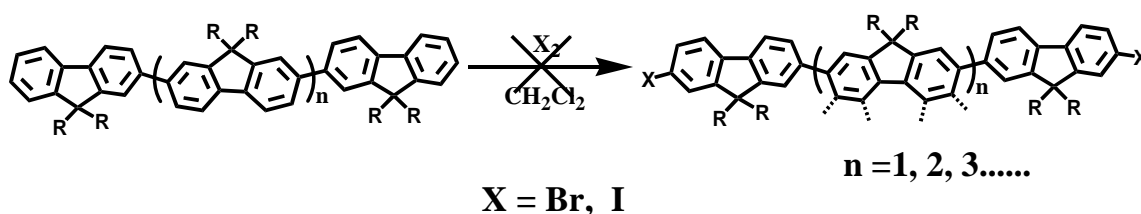
Scheme 4. Unsuccessful two-fold bromination of the higher oligofluorenes.

In this thesis, the facile synthesis of oligofluorenes from the dimer up to the heptamer by a series of stepwise transition metal mediated Suzuki and Yamamoto reactions is presented.[3] 2,7-dibromofluorene and 2-bromofluorene were first alkylated according to the literature[4] with 2-ethylhexyl bromide under basic conditions to give the dibromide and monobromide of fluorene **38** and **39** in 86% and 90% yield, respectively (Scheme 5). The key syntons, the mono- and di-boronate substituted fluorene (**40** and **41**), were reported in literature by bromine-lithium exchange followed by boronation reactions from the

corresponding mono- and dibromofluorenes (**38** and **39** respectively) [4]. However, repeat of this procedure in our work only gave the target compounds in very low yield. Alternatively, palladium-catalyzed Miyaura reaction [5] was used to transform the bromides to the boronates. In these cases the corresponding boronates (**40** and **41**) were obtained in high yields (> 90 %) under mild conditions after standard column chromatography work-up (Scheme 5). Suzuki coupling reactions of the mono-bromofluorene (**39**) with compound **41** and **40** afforded the fluorenyl-dimer **42** (**OF2**) and -trimer **43** (**OF3**), respectively.
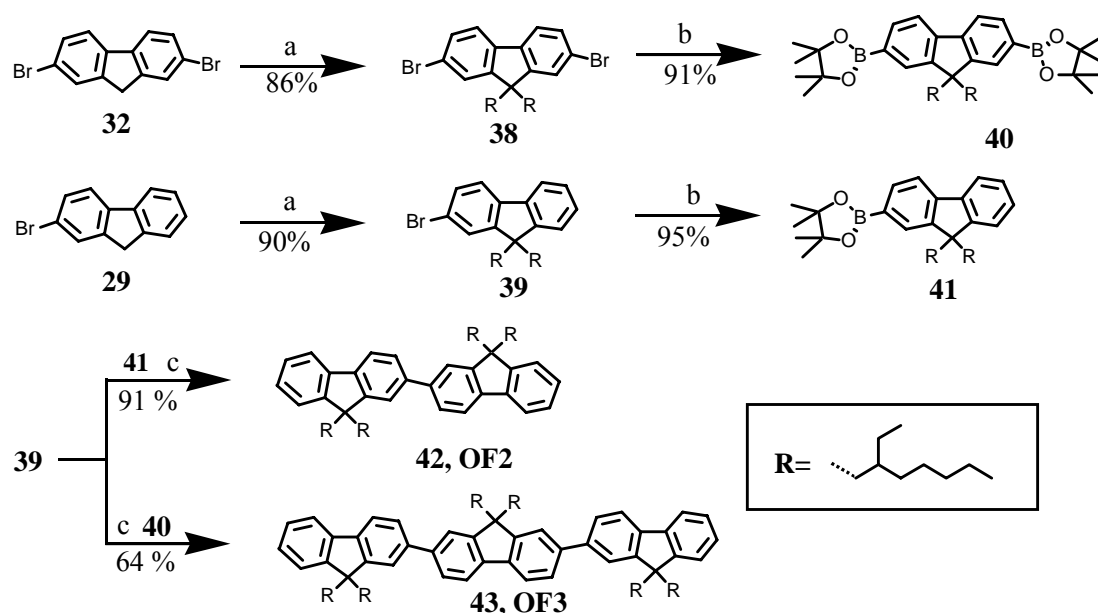
*Scheme 5. Synthesis of fluorenyl-dimer (**42**, **OF2**) and trimer (**43**, **OF3**): (a) $C_8H_{17}Br$, 50%, aqueous NaOH/DMSO, room temperature; (b) bis(pinacolato)diboron, AcOK / DMF, $Pd(dppf)Cl_2$, 60°C; (c) $Pd(PPh_3)_4$, toluene / aqueous Na_2CO_3, reflux. dppf = 1,1'-bis(disphEnylphosphanyl)ferrocene.*

The synthesis of higher fluorenyl oligomers is based on two important syntons, the monobromides of the fluorenyl-dimer (**44**) and trimer (**48**, Scheme 6). The compound **44** and **48** can not be synthesized by simple bromination of compound **42** or **43** with bromine since statistical product mixtures will be obtained which are not separable on large scale. The monobromo-fluorenyl dimer (**44**) was then prepared by Suzuki coupling between **41** and excessive (1.5 equivalent) **38** in 50% yield. Yamamoto homocoupling of **44** gave the fluorenyl-tetramer **45** (**OF4**) in 52 % yield. The fluorenyl-pentamer **46** (**OF5**) was synthesized by Suzuki coupling between **44** with **40** in 47% yield. Contrary to the low yield during the mono-bromination, the two-fold bromination of **42** worked well to provide

dibromo-fluorenyl dimer **47** in 90 % yield.[6] Similarly, the mono-bromo-fluorenyl trimer **48** was synthesized by Suzuki coupling reaction between **41** and excessive **47** in 45% yield. The fluorenyl-hexamer **49** (**OF6**) was then obtained by a Yamamoto homo-coupling of **48** in 52% yield and the fluorenyl-heptamer **50** (**OF7**) was synthesized by Suzuki coupling between the **40** and **48** in 46% yield.
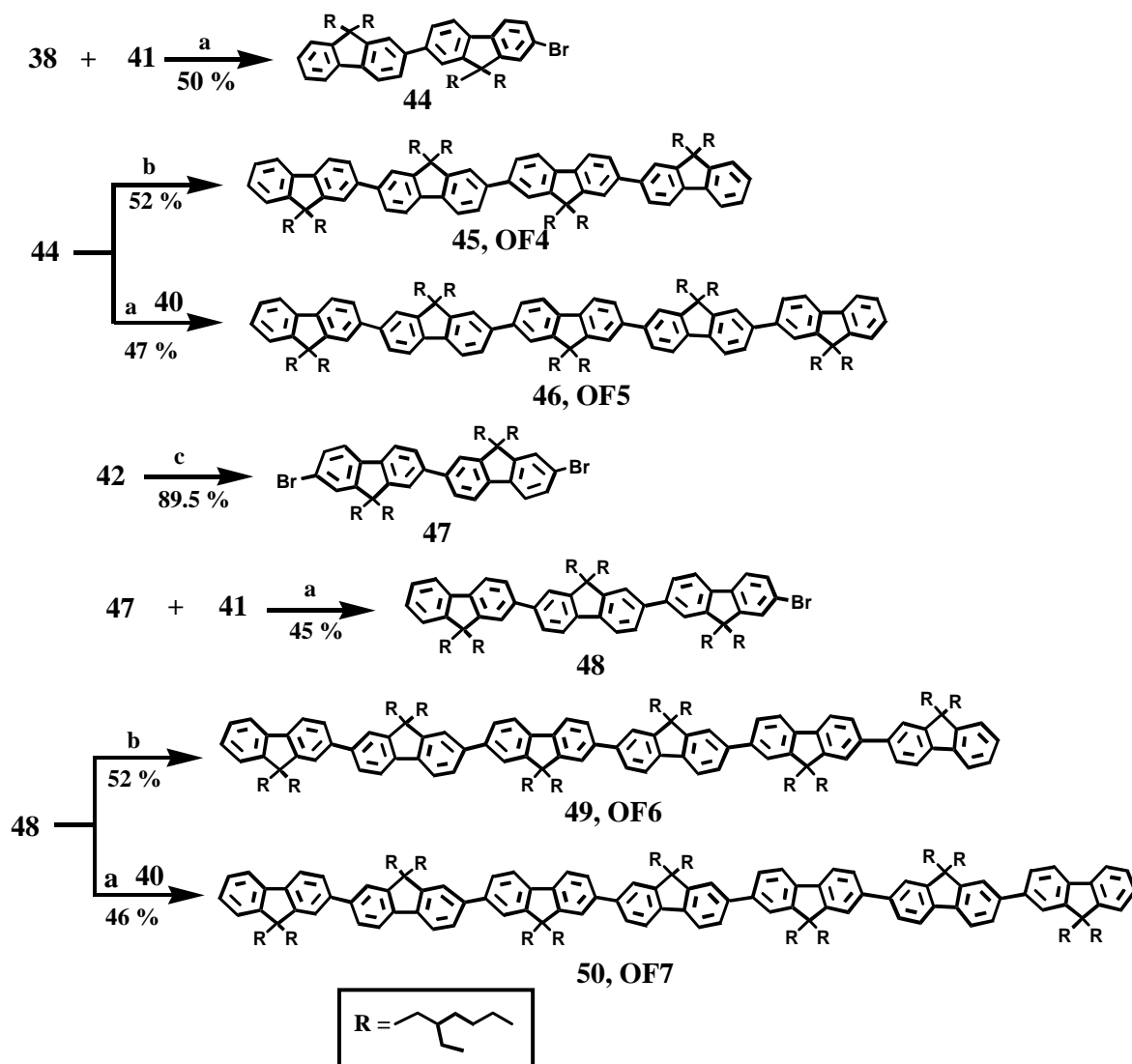
*Scheme 6. The syntheses of the tetramer(**45, OF4**) to heptamer(**50, OF7**) of oligo(9,9-bis-ethylhexylfluorene-2,7-diyl)s: (a) Pd(PPh₃)₄, toluene / aqueous Na₂CO₃, reflux; (b) Ni(COD)₂--COD--Bipy, toluene / DMF, 80°C; (c) Br₂, CH₂Cl₂, reflux. COD = cycloocta-1,5-diene, Bipy = 2,2'-bipyridine.*

For the reason of comparison, the poly(9,9-bis-ethylhexylfluorene-2,7-diyl) **51** (**PF2/6**) was synthesized by Yamamoto coupling reaction of 2,7-dibromo-9,9-bis(2-ethylhexyl)fluorene [7] (Scheme 7) and was purified by repetitive reprecipitation from concentrated chloroform solution to methanol/acetone. The molecular weight of the polymer was determined by GPC using poly(*p*-phenylene) as standard: M_n = 56799 and M_w = 107890 g/mol (P_D = 1.9). (Polystyrene as standard: M_n = 98000 and M_w = 229000 g/mol; P_D = 2.1).
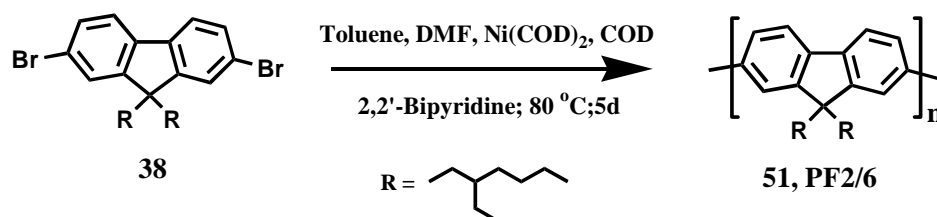
Scheme 7. Synthesis of poly(9,9-bis-ethylhexyl-2,7-diyl)s by Yamamoto coupling.

2.2 Discussion

High-pure oligofluorenes up to heptamer have been synthesized on the hundred milligram scale according to our new route. Such synthetic route can be generalized as a convergent synthetic route (Scheme 8) for many kinds of conjugated oligomers starting from halogen and boronic acid or ester substituted monomers. In this synthetic route, the mono-bromo substituted oligomers were the key syntons, and were obtained by Suzuki coupling between the mono-boronate substituted oligomers and excessive dibromo substituted oligomers. The oligomers with even unit numbers were thus obtained by Yamamoto reaction of the monobromo-substituted oligomers and the oligomers with odd unit number were prepared by Suzuki coupling reaction between an excess of mono-bromo substituted oligomers and the bis-boronate substituted monomers.
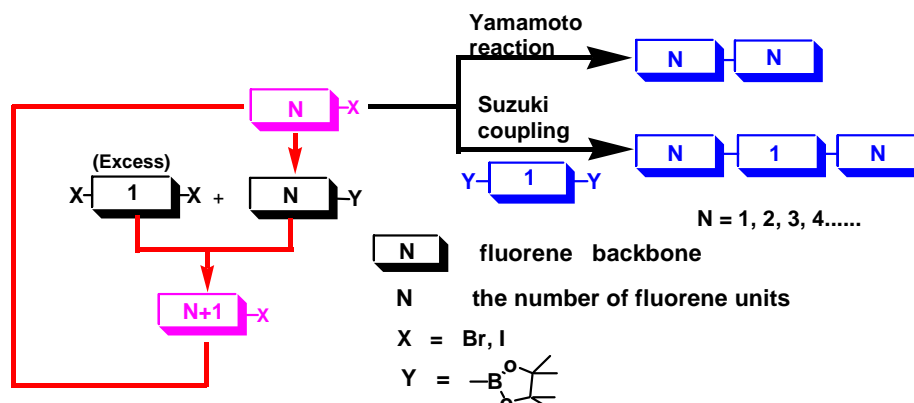
Scheme 8. A schematic convergent synthetic route to conjugated oligofluorenes.

In this synthetic route, the halogenic and boronic monomers (**38~41**) were important starting material. Mono- and dihalogenic fluorene monomers are commercially available, but mono- and diboronic fluorene monomers have to be synthesized. First, the enormous success of the Suzuki reaction[8] in the preparation of oligomers arises from the coupling reaction together with the easy availability of the boronic acids and the boronates.[9] They were prepared by halogen-metal exchange and subsequent trapping of the aryl lithium compound with trialkylborates (Scheme 9).[10] In an alternative method, [11] the dibromide reacted readily with magnesium in tetrahydrofuran (THF) to form a difunctional Grignard reagent and followed by treating with trimethylborate at –78 °C and acidification, affording 9,9-di-2-ethylhexylfluorene-2,7-bis(boronic acid) (**52**). 9,9-Di-2-ethylhexylfluorene-2,7-bis(trimethylene boronate) was then prepared by esterification of the diboronic acid with tetramethylene glycol. The separation and purification of the target compounds was however difficult and the yield was low (around 20%).
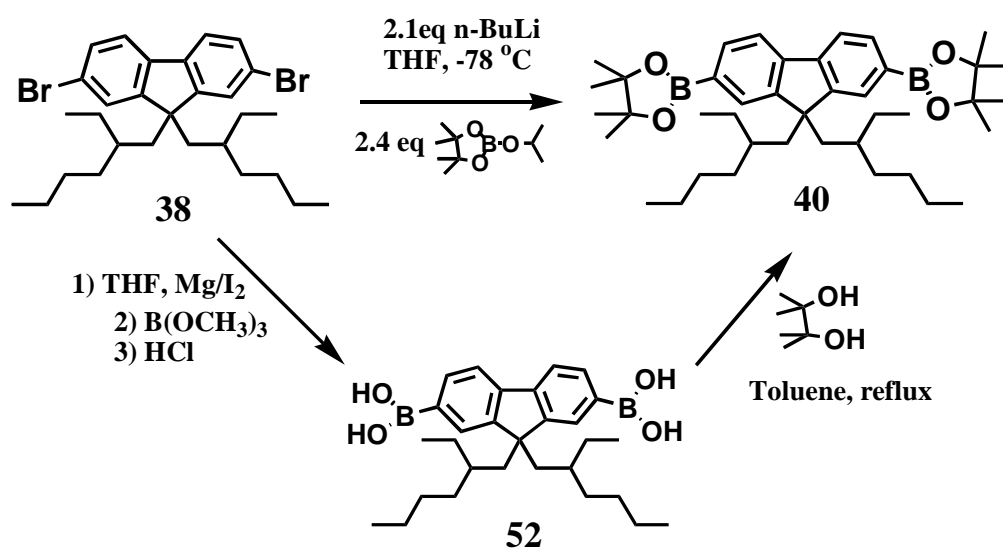
Scheme 9. the synthesis of diboronic fluorene

In this work, aryl boronates were readily available from the aryl halides via Pd(0)-catalyzed reaction with the pinacol ester of diboron (Miyaura reaction) (Scheme 5).[12] This transformation avoids the use of strongly basic organometallic reagents and thus allows the preparation of a wide variety of functionalized aryl boronic esters, moreover, the yield of this reaction is very high (90%), and the purification of target products is also very easy.

2. 3 Structural Characterizations of the Oligofluorenes (OFn)

In the synthesis of the oligofluorenes, all compounds were purified by standard column chromatography and confirmed by field desorption mass spectroscopy (FD-MS) and ^{1}H or ^{13}C-NMR techniques.
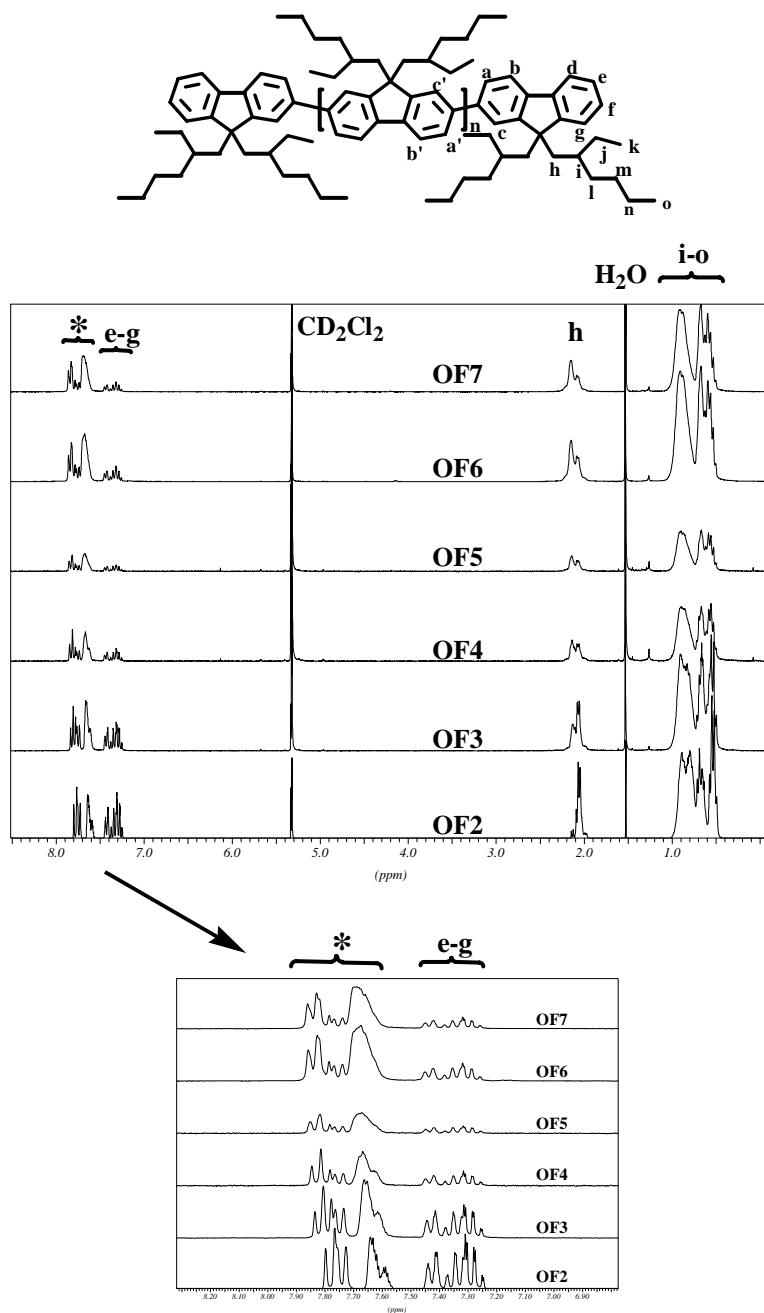
*Figure 2.3.1. Combined ^{1}H NMR spectra of oligofluorenes (**OFn**, n=2~7) in CD$_2$Cl$_2$. (* star respresente the all aromatic hydrogen atoms expect for the **e, f, g** hydrogenic atoms.)*

The combined ^{1}H NMR spectra of all the oligomers are shown in Figure 2.3.1. In the ^{1}H NMR spectra of dimer (Figure 2.3.2), well resolved peaks related to the alkyl and aromatic protons were observed, however the signals became broad due to overlap of the resonances with increasing chain-length, and the peaks assigned to aromatic protons also slightly shift down field. Integration of the resonances in the aromatic and aliphatic regions in the ^{1}H NMR spectra of oligofluorenes was compared with the calculations. The integration ratio of aliphatic/aromatic protons observed for the dimer (**42, OF2**), trimer(**43, OF3**), tetramer (**45, OF4**), pentamer (**46, OF5**), hexamer (**49, OF6**), heptamer (**50, OF7**) are 4.86, 5.14, 5.26, 5.33, 5.36, 5.41, respectively, which are in good agreement with the calculated values: 4.84, 5.10, 5.23, 5,31, 5.36 and 5.41. ^{13}C NMR spectra of the oligomers (Figure 3) were also analyzed and further supported the high purity.

Dimer	Aliphatic Protons/Aromatics Protons
Calculated	68/14 = 4.86
Observed	67.9/14.03 = 4.84
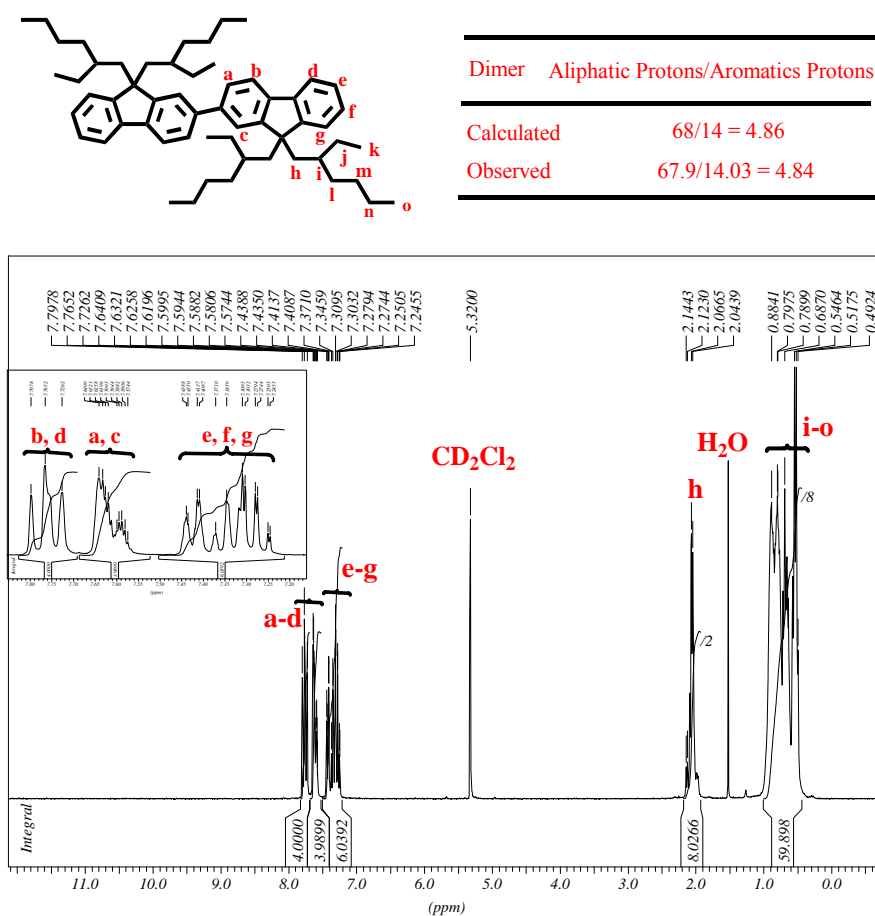
*Figure 2.3.2 Detailed assignment of the ^{1}H NMR spectrum of fluorenyl-dimer (**OF2**).*
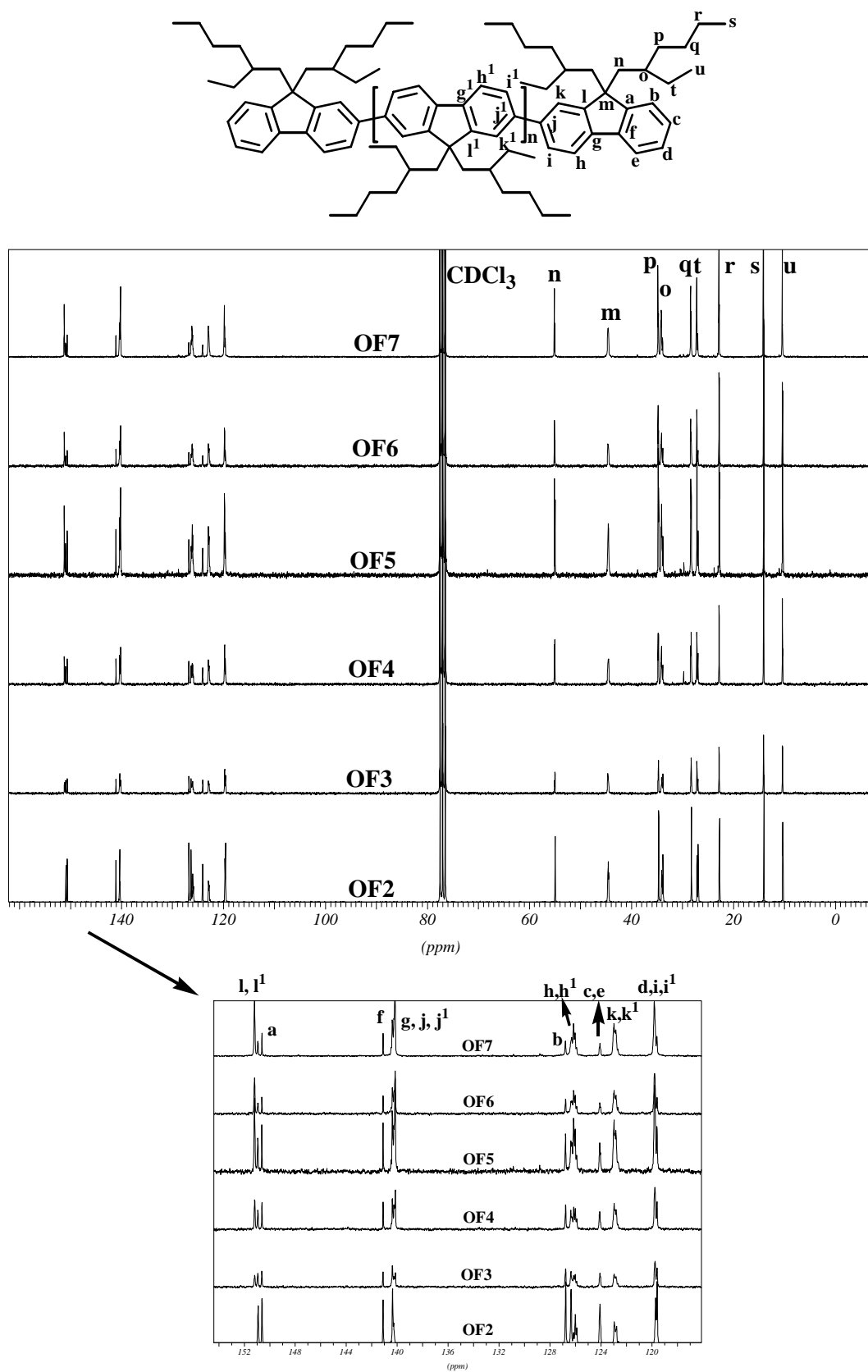
*Figure 3. Combined ^{13}C NMR spectra of the oligofluorenes (**OF2~OF7**).*

Field-desorption mass spectra (FD-MS) of the oligomers are shown in Figure 4a-f. In all case, the molecular ionic peaks correlated to the molecular weight of the oligomers were observed. Some peaks assigned to multi-charged species (M^{2+} and M^{3+}) were also found. For heptamer, the peak at 2724 is assigned to M^+ of heptamer, while the peaks at 1362 and 908.4 are related to the M^{2+} and M^{3+}, respectively. Elemental analysis of the oligomers also fitted well with the calculated value (see experimental part).
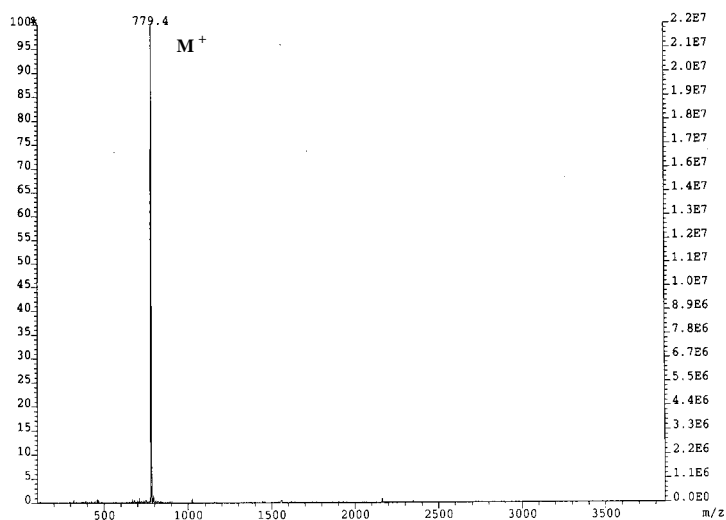
*Figure 4a. FD-MS for the fluorenyl-dimer (**OF2**), m/z=779.4 (M^+).*
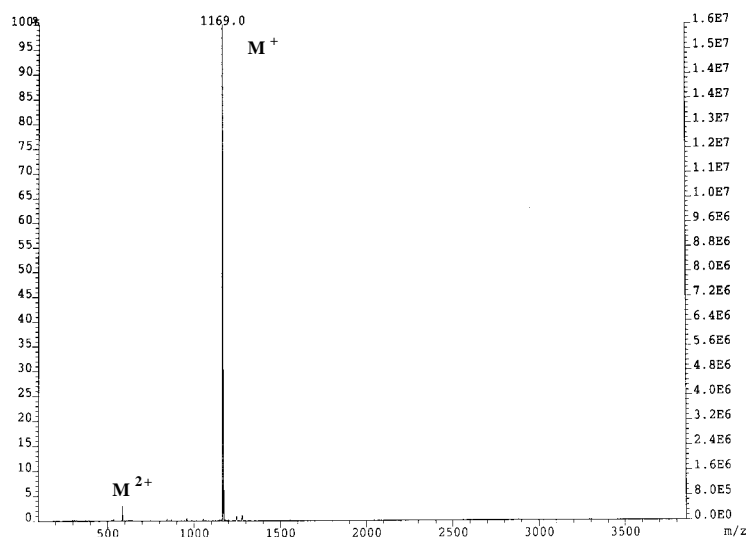
*Figure 4b. FD-MS for the fluorenyl-trimer (**OF3**), m/z=1169.0 (M^+).*
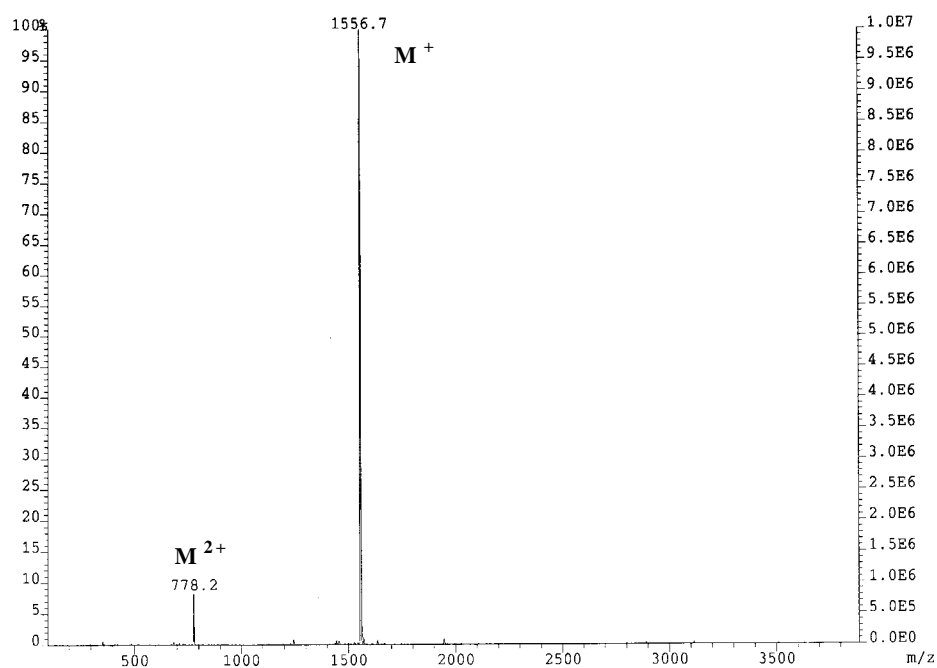
*Figure 4c. FD-MS for the fluorenyl-tetramer (**OF4**), m/z=1556.7 (M$^+$).*
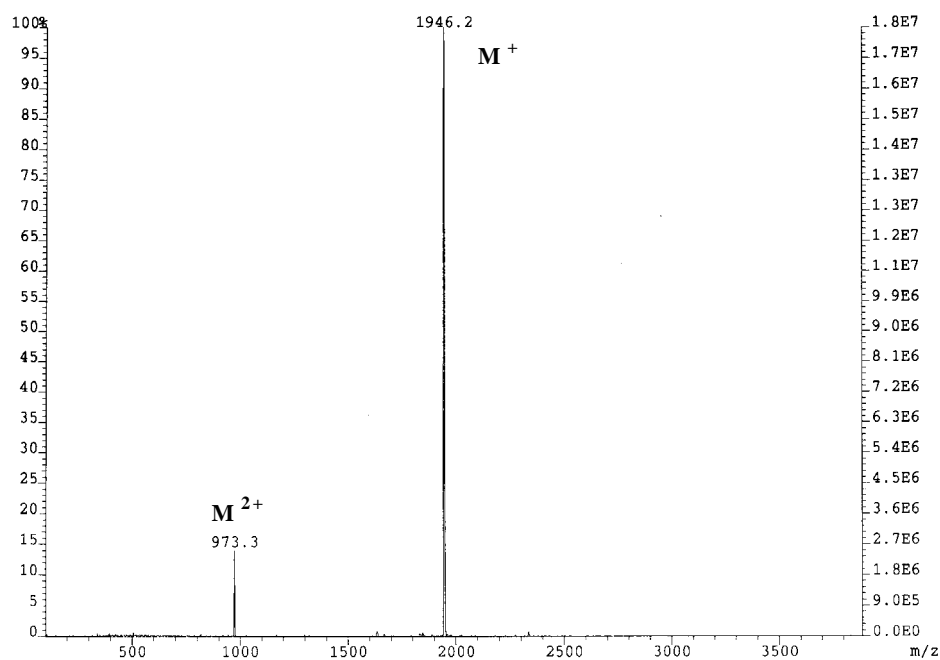
*Figure 4d. FD-MS for the fluorenyl-pentamer (**OF5**), m/z=1946.2 (M$^+$).*
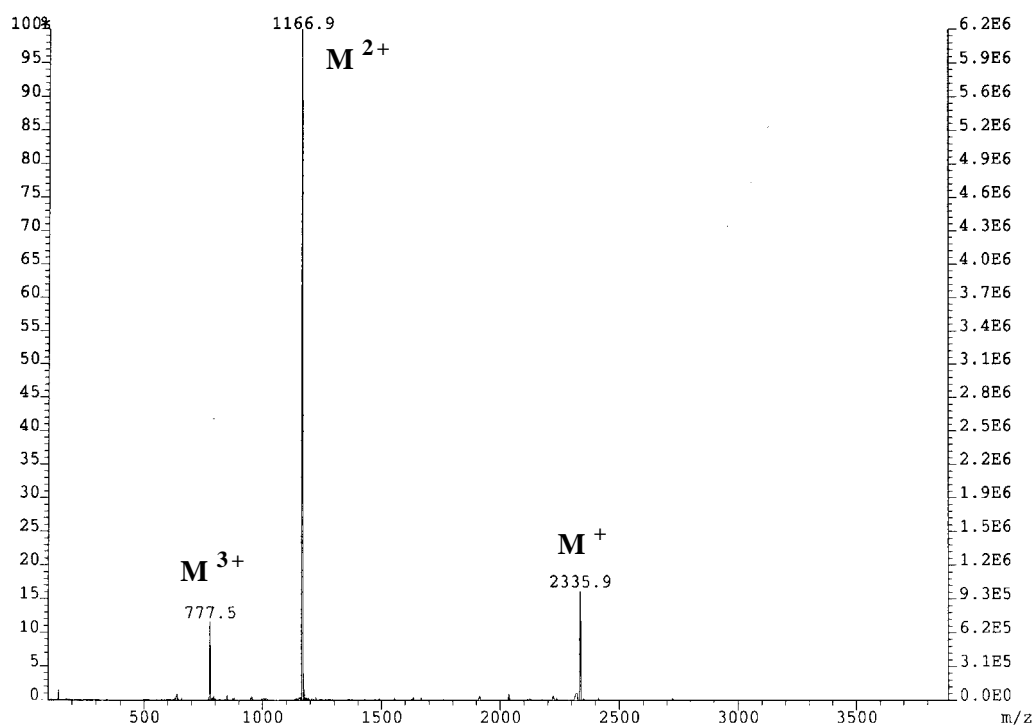
Figure 4e. FD-MS for the fluorenyl-hexamer (OF6), m/z=2335.9 (M⁺).
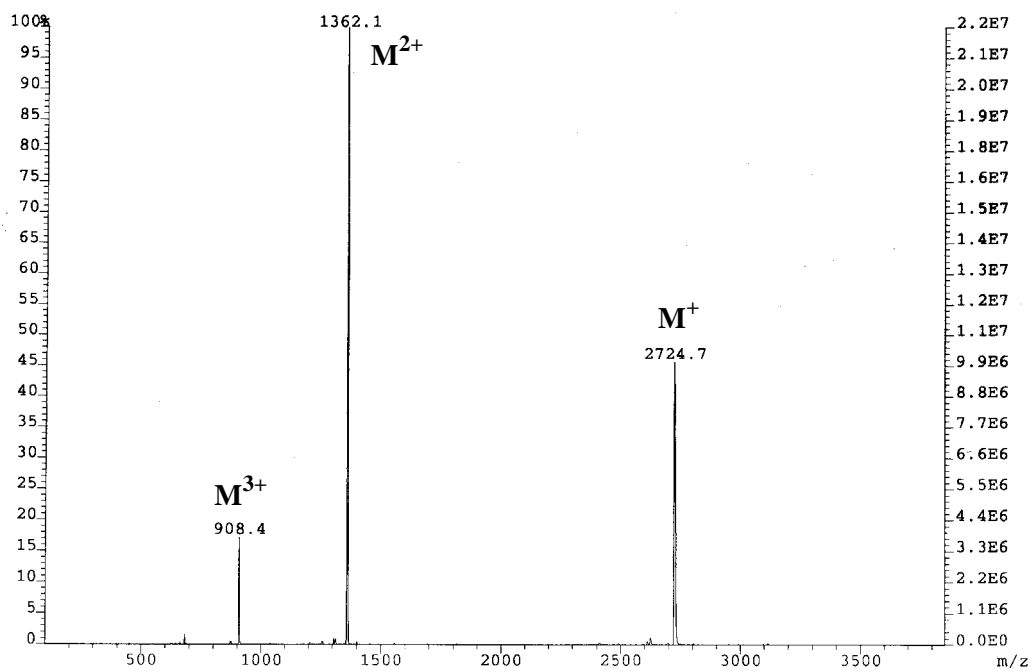
Figure 4f. FD-MS for the fluorenyl-heptamer (OF7), m/z= 2724.7(M⁺).

2.4 Experimental Section

General Remarks.

Reactions requiring an inert gas atmosphere were conducted under argon, and the glassware was oven-dried (140 °C). THF was distilled from potassium prior to use. Commercially available chemicals were used as received. ^{1}H NMR and ^{13}C NMR spectra were recorded on a Bruker DPX 250 spectrometer (250 MHz for ^{1}H, 62.5 MHz for ^{13}C). Chemical shifts are given in ppm, referenced to residual proton resonances of the solvents. Thin-layer chromatography was performed on aluminum plates precoated with Merck 5735 silica gel 60 F$_{254}$. Column chromatography was performed with Merck silica gel 60 (230 ± 400 mesh). Field desorption spectra were recorded on a VG ZAB 2-SE FPD machine. Elemental analysis were performed by the analytical service in University of Mainz.

2,7-Dibromo-9,9-bis(2-ethylhexyl)-fluorene (38): 2-Ethylhexylbromide (38.73 g, 185.18 mmol, 35.74mL) was added to a mixture of 2,7-dibromofluorene (**32**, 25.0 g, 77.16 mmol) and triethylbenzylammonium chloride (0.878 g, 3.86 mmol, 5 mol %) in DMSO (125 mL) and 50% aqueous NaOH (31 mL). The reaction mixture was stirred at room temperature for 5 h. An excess of diethyl ether was added, the organic layer was washed with water, diluted HCl, brine, then dried over MgSO$_4$. The solvent was removed under vacuum and the residue was purified by column chromatography over silica gel with n-hexane as the eluent (R$_f$ = 0.78) and solidified from EtOH at –30 °C to give **38** as a white solid (36.21 g, 85.6 %). m.p. 45 - 54°C; ^{1}H NMR (250 MHz, CD$_2$Cl$_2$): δ = 7.57-7.43 (m, 6 H), 1.94 (d, *J* = 5.35 Hz, 4 H), 0.89-0.68 (m, 22 H), 0.55-0.41 (m, 8 H) ppm; ^{13}C NMR (62.5 MHz, CDCl$_3$) δ = 152.3, 139.1, 130.1, 127.4, 121.0, 55.3, 44.3, 34.6, 33.6, 28.0, 27.1, 22.7, 14.0, 10.3 ppm; MS (FD): *m/z* : 548.2 [M$^+$].

2-Bromo-9,9-bis(2-ethylhexyl)-fluorene (39): Compound **39** was prepared according to the method used for **38** by using 2-ethylhexylbromide (43.3 g, 224.5 mmol, 39.9 mL), 2-bromofluorene (25.0 g, 102.0 mmol), triethylbenzylammonium chloride (1.16 g, 5.10 mmol, 5 mol %), DMSO (165 mL), and 50% aqueous NaOH (41 mL). Purification by column chromatography over silica gel with *n*-hexane as the eluent (R$_f$ = 0.72) gave **39** as a colorless liquid (43.14 g, 90.1 %): ^{1}H NMR (250 MHz, CD$_2$Cl$_2$): δ = 7.70-7.26 (m, 7 H),

1.97 (m, 4 H), 0.90-0.43 (m, 30 H) ppm; ^{13}C NMR (62.5 MHz, CDCl$_3$): δ = 152.8, 150.0, 140.3, 129.8, 127.3, 126.9, 124.0, 120.9, 120.4, 119.6. 55.1, 44.4, 34.6, 33.6, 28.0, 27.0, 22.7, 14.0, 10.4 ppm; MS (FD): *m/z*: 470.2 [M$^+$].

2,7-Bis-(4,4,5,5-tetramethyl[1.3.2]dioxaborolan-2-yl)-9,9-bis(2-ethylhexyl)-fluorene (40): Under an argon atmosphere, **38** (2.43 g, 4.43 mmol), bis(pinacolato)diboron (4.05 g, 15.94 mmol), KOAc (2.60 g, 26.57 mmol) and Pd(dppf)Cl$_2$ (0.226 g, 0.266 mmol) were dissolved in DMF (40 mL) and heated to 60°C overnight. After the reaction mixture was cooled to room temperature, water and diethyl ether were added. The aqueous phase was extracted with diethyl ether and the combined organic layers were dried over MgSO$_4$. The solvent was removed under vacuum and the residue was purified by column chromatography over silica gel with petroleum ether/dichloromethane (3:1) as the eluent (R$_f$ = 0.34) and solidified from EtOH at –30 °C to give **40** as a white solid (2.60 g, 91.5 %): M.p. : 85.5 ~ 87.6 °C; ^{1}H NMR (250 MHz, CD$_2$Cl$_2$): δ = 7.84-7.69 (m, 6 H), 2.00 (d, *J* = 5.3 Hz, 4 H), 1.36 (s, 24 H), 0.86-0.50 (m, 22 H), 0.48-0.45 (m, 8 H) ppm; ^{13}C NMR (62.5 MHz, CDCl$_3$): δ = 150.1, 143.9, 133.5, 130.4, 119.2, 83.5, 54.7, 44.0, 34.6, 33.5, 27.8, 27.2, 24.8, 22.7, 14.1, 10.3 ppm; MS (FD): *m/z*: 643.0 [M$^+$].

2-(4,4,5,5-Tetramethyl[1.3.2]dioxaborolan-2-yl)-9.9-bis(2-ethylhexyl)-fluorene (41): Compound **41** was prepared according to the method used for **40** by using **39** (14.07g, 30.0 mmol), bis(pinacolato)diboron (12.19 g, 48.0 mmol), KOAc (8.82 g, 90.0 mmol) and Pd(dppf)Cl$_2$ (1.23 g, 1.5 mmol) in DMF (300 mL). Column chromatography over silica gel with petroleum ether/dichloromethane (4:1) as the eluent (R$_f$ = 0.59) afforded **4** as an oily product (14.78 g, 95.5 %): ^{1}H NMR (250 MHz, CD$_2$Cl$_2$): δ = 7.82-7.64 (m, 4 H), 7.36-7.21 (m, 3 H), 2.0-1.86 (m, 4 H), 1.34 (s, 12 H), 0.86-0.65 (m, 22 H), 0.50-0.43 (m, 8 H) ppm; ^{13}C NMR (62.5 MHz, CDCl$_3$): δ = 151.0, 149.5, 144.2, 141.1, 133.6, 130.3, 126.6, 124.1, 120.0, 118.8, 83.5, 54.8, 44.5, 44.1, 34.6, 33.5, 28.2, 27.8, 27.3, 26.8, 24.8, 22.7, 14.1, 10.5, 10.1 ppm; MS (FD): *m/z*: 516.7 [M$^+$].

9,9,9´,9´-Tetrakis(2-ethylhexyl)-2.2´-bifluorene (42, OF2): A mixture of **41** (5.17 g, 10.0 mmol) and **39** (4.69 g, 10.0 mmol) in toluene (50 mL) and 2M aqueous Na$_2$CO$_3$ solution (25 mL, 50 mmol) was degassed by pump and freeze cycles (3 ×) and Pd(PPh$_3$)$_4$ (0.577 g, 0.5 mmol) was added under argon. The solution was heated to reflux with vigorous stirring

for 20 h. After the reaction mixture was cooled to room temperature, diethyl ether and water were added. The organic layer was separated and washed with diluted HCl and brine, then dried over $MgSO_4$. The solvent was removed under vacuum and the residue was purified by column chromatograpy over silica gel with petroleum ether as the eluent (R_f = 0.47) to give **52** (7.08 g, 90.8%): ^{1}H NMR (250 MHz, CD_2Cl_2): δ = 7.73-7.80 (m, 4 H), 7.57-7.64 (m, 4 H), 7.25-7.44 (m, 6 H), 2.04-2.14 (m, 8 H), 0.49-0.88 (m, 60 H); ^{13}C NMR (62.5 MHz, $CDCl_3$): δ = 150.9, 150.6, 141.1, 140.4, 126.8, 126.3, 126.0, 124.1, 122.9, 119.6, 54.9, 44.5, 34.6, 33.8, 28.2, 26.9, 22.7, 14.0, 10.3 ppm; MS (FD): m/z: 779.4 [M$^+$]; elemental analysis: calcd for $C_{58}H_{82}$ (779.2): C 89.39, H 10.61; found: C 89.29, H 10.79.

9,9,9´,9´,9´´,9´´-Hexakis(2-ethylhexyl)-2,2´-7´,2´´-terfluorene (43, OF3): Compound **43** was prepared according to the method used for **42** by using **40** (2.0 g, 3.12 mmol), **39** (4.40 g, 9.36 mmol) and Pd(PPh$_3$)$_4$ (0.36 g, 0.31 mmol) in toluene (30 mL) and 2M Na_2CO_3 aqueous solution (15.6 mL, 31.2 mmol) for 27 h. After cooling to room temperature, the mixture was diluted with ethyl acetate and the organic layer was washed with diluted HCl and brine, then dried over $MgSO_4$. The solvent was removed under vacuum and the residue was purified by column chromatography over silica gel with petroleum ether as the eluent (R_f = 0.22) to give **43** as a colorless viscous gum(2.32 g, 63.8 %): ^{1}H NMR (250 MHz, CD_2Cl_2): δ = 7.83-7.73 (m, 6 H), 7.61-7.66 (m, 8 H), 7.44-7.25 (m, 6 H), 2.13-2.05 (m, 12 H), 0.90-0.49 (m, 90 H) ppm; ^{13}C NMR (62.5 MHz, $CDCl_3$): δ = 151.2, 150.9, 150.6, 141.1, 140.4, 140.1, 126.8, 126.3, 126.0, 124.1, 122.9, 119.7, 119.6, 54.9, 44.6, 34.6, 33.8, 28.2, 27.1, 22.8, 14.0, 10.3 ppm; MS (FD): *m/z*: 1168.2 [M$^+$]; elemental analysis: calcd for $C_{87}H_{122}$ (1167.9): C 89.47, H 10.53; found: C 89.26, H 10.42.

7-Bromo-9,9,9´,9´-tetrakis-(2-ethylhexyl)-2,2´-bifluorene (44): Compound **44** was prepared according to the method used for **42** by using **41** (4.13g, 8 mmol), **38** (6.58 g, 12 mmol) and Pd(PPh$_3$)$_4$ (0.28 g, 0.24 mmol) in toluene (40 mL) and 2M aqueous Na_2CO_3 solution (20.0 mL, 40.0 mmol). The reaction took 16 h. After cooling down to room temperature, the mixture was diluted with diethyl ether and the organic layer was washed with diluted HCl and brine, then dried over $MgSO_4$. The solvent was removed under vacuum and the residue was purified by column chromatography over silica gel with petroleum ether as eluent (R_f = 0.49) to give **44** as a colorless oil (3.44 g, 50.2 %): ^{1}H NMR (250 MHz, CD_2Cl_2): δ = 7.80-7.26 (m, 13 H), 2.14-2.04 (m, 8 H), 0.88-0.52 (m, 60 H) ppm;

^{13}C NMR (62.5 MH$_Z$, CDCl$_3$): δ = 153.0, 151.0, 150.6, 141.0, 140.5, 140.1, 139.2, 129.9, 127.4, 126.8, 126.4, 126.0, 124.1, 122.9, 120.9, 120.3, 119.6, 54.9, 44.5, 34.6, 33.8, 28.2, 27.1, 22.7, 14.0, 10.3 ppm; MS (FD): m/z: 857.6 [M$^+$].

9,9,9′,9′,9′′,9′′,9′′′,9′′′-Octakis(2-ethylhexyl)2,2′-7′,2′′-7′′,2′′′-tetrafluorene (45, OF4): A schlenk tube was charged with Ni(COD)$_2$ (101.2 mg, 0.55 mmol), 2,2'-bipyridine (57.5 mg, 0.55 mmol), 1,5-COD (39.8 mg, 0.55 mmol) and DMF (3.0 mL) in a glove box. The mixture was stirred at 80°C for 0.5 h and then **44** (0.32 g, 0.37 mmol) in toluene(11 ml) was added to the blue solution and stirred at 80°C for 8h. After cooling to room temperature, the mixture was diluted with diethyl ether. The organic layer was washed with diluted HCl, brine, and water, then dried over MgSO$_4$. The solvent was removed under vacuum and the residue was purified by column chromatography over silica gel with petroleum ether/dichloromethan (20:1) as the eluent (R$_f$ = 0.61) to afford **45** as a white waxy solid (151 mg, 52.6 %): ^{1}H NMR (250 MHz, CD$_2$Cl$_2$): δ = 7.85-7.75 (m, 8 H), 7.67-7.63 (m, 12 H), 7.45-7.26 (m, 6 H), 2.14-2.06 (m, 16 H), 0.90-0.50 (m, 120 H) ppm; ^{13}C NMR (62.5 MHz, CDCl$_3$): δ = 151.2, 150.9, 150.6, 141.1, 140.36, 140.1, 126.8, 126.4, 126.1, 124.1, 122.9, 119.7, 54.9, 44.4, 34.7, 34.0, 28.2, 27.1, 22.8, 14.0, 10.3 ppm; MS (FD): m/z: 1556.7 [M$^+$], 778.2 [M^{2+}]; elemental analysis: calcd for C$_{116}$H$_{162}$ (1556.6): C 89.51, H 10.49; found: C 89.22, H 10.35.

9,9,9′,9′,9′′,9′′,9′′′,9′′′,9′′′′,9′′′′-Decakis(2-ethylhexyl)-2,2′-7′,2′′-7′′,2′′′-7′′′,2′′′′-pentafluorene (46, OF5): Compound **46** was prepared according to the procedure for **42** by using **40** (124.5 mg, 0.194 mmol), **44** (664.7 mg, 0.776 mmol) and Pd(PPh$_3$)$_4$ (22.4 mg, 0.0194 mmol) in toluene (4 mL) and 1M aqueous Na$_2$CO$_3$ (2.0 mL, 2.0 mmol). The reaction took 16 h. After cooling to room temperature, the mixture was diluted with diethyl ether and the organic layer was washed with diluted HCl and brine, then dried over MgSO$_4$. The solvent was removed under vacuum and the residue was purified by column chromatography over silica gel with petroleum ether/dichloromethan (10:0.8) as the eluent (R$_f$ = 0.31) to afford **46** as a white waxy solid (176.5 mg, 46.8 %): ^{1}H NMR (250 MHz, CD$_2$Cl$_2$): δ = 7.85-7.74 (m, 10 H), 7.67 (br m, 16 H), 7.45-7.26 (m, 6 H), 2.14-2.06 (m, 20 H), 0.92-0.50 (m, 150 H) ppm; ^{13}C NMR (62.5 MHz, CDCl3): δ = 151.2, 150.9, 150.6, 141.1, 140.3, 140.1, 126.8, 126.3, 126.1, 124.1, 123.0, 119.8, 55.1, 44.5, 34.7, 34.0, 28.3,

27.1, 22.7, 14.0, 10.3 ppm; MS (FD): m/z: 1946.2 [M$^+$], 973.3 [M^{2+}]; elemental analysis: calcd for $C_{145}H_{202}$ (1945.2): C 89.53, H 10.47; found : C 89.41, H 10.35.

7,7´-Dibromo-9,9,9´,9´-tetrakis(2-ethylhexyl)-2,2´-bifluorene (47): Br$_2$ (3.15 g, 19.71 mmol) in CH_2Cl_2 (5 mL) was added to a solution of **42** (7.67 g, 9.85 mmol) in CH_2Cl_2 (20 mL) at room temperature. The solution was heated to reflux for 1.5 h. After the reaction mixture was cooled to room temperature, water and diethyl ether was added. The organic layer was washed with $Na_2S_2O_3$ solution, brine and water, then dried over $MgSO_4$. The solvent was removed under vacuum and the residue was recrystallized from ethanol to give **47** as white solid (8.24 g 89.5%): M. p. : 71.5 ~ 72.8 °C; ^{1}H NMR (250 MHz, CD$_2$Cl$_2$): δ = 7.78-7.46 (m, 12 H), 2.08-2.03 (m, 8 H), 0.88-0.55 (m, 60 H) ppm; ^{13}C NMR (62.5 MHz, CDCl$_3$): δ = 153.0, 150.6, 140.6, 140.0, 139.4, 130.0, 127.4, 126.2, 123.0, 121.0, 120.4, 119.9, 55.2, 44.5, 34.7, 33.7, 28.1, 27.1, 22.7, 14.0, 10.3 ppm; MS (FD): m/z: 939.2 [M$^+$]. $C_{58}H_{80}Br_2$ (Mw = 937.1).

7-Bromo-9,9,9´,9´,9´´,9´´-hexakis(2-ethylhexyl)-2,2´-7´,2´´-terfluorene (48):
Compound **48** was prepared according to the method used for **42** by using **47** (4.9 g, 5.24 mmol), **41** (1.69 g, 3.27 mmol) and Pd(PPh$_3$)$_4$ (0.189g, 0.15mmol) in toluene (16 mL) and 2M aqueous Na_2CO_3 (15 mmol, 8.2 ml). The reaction took 16 h. After cooling to room temperature, the mixture was diluted with diethyl ether (200 ml) and the organic layer was washed with diluted HCl, brine, and water, then dried over $MgSO_4$. The solvent was removed under vacuum and the residue was purified by column chromatography over silica gel with hexane/dicloromethane (10:0.5) as the eluent (R$_f$ = 0.42) to give **48** as a sticky colourless oil (1.83g, 45.0 %): ^{1}H NMR (250 MHz, CD$_2$Cl$_2$): δ = 7.84-7.73 (m, 5 H), 7.64-7.57 (m, 10 H), 7.50-7.26 (m, 4 H), 2.12-2.05 (m, 12 H), 0.90-0.53 (br m, 90 H) ppm; ^{13}C NMR (62.5 MHz, CDCl$_3$): δ = 153.0, 151.2, 150.9, 150.6, 141.1, 140.8, 140.3, 140.1, 139.2, 129.9, 127.4, 126.8, 126.4, 126.1, 124.0, 123.0, 120.9, 120.3, 119.8, 55.0, 44.5, 34.7, 33.8, 28.2, 27.1, 22.7, 14.0, 10.3 ppm; MS (FD): m/z: 1248.4 [M$^+$].

9,9,9´,9´,9´´,9´´,9´´´,9´´´,9´´´´,9´´´´,9´´´´´,9´´´´´-Dodecakis (2-ethylhexyl)-2,2´-7´,2´´-7´´,2´´´-7´´´,2´´´´-7´´´´,2´´´´´-hexafluorene (49, OF6): Compound **49** was prepared according to the method used for **45** by using **48** (370.0 mg, 0.300 mmol) in toluene (10 mL) and Ni(COD)$_2$ (82.5 mg, 0.45 mmol), 2,2´-bipyridine (46.8 mg, 0.45 mmol), 1,5-COD

(32.4 mg, 0.45 mmol), and DMF (2.5 mL). After cooling to room temperature, the mixture was diluted with diethyl ether and the organic layer was washed with diluted HCl and brine, then dried over MgSO$_4$. The solvent was removed under vacuum and the residue was purified by column chromatography over silica gel with hexane/dichloromethan (10/0.8) as the eluent (R$_f$ = 0.24) to afford **49** as a white solid (183.0 mg, 52.4 %): ^{1}H NMR (250 MHz, CD$_2$Cl$_2$): δ = 7.86-7.68 (m, 32 H), 7.45-7.26 (m, 6 H), 2.14-2.06 (m, 24 H), 0.90-0.50 (m, 180 H) ppm; ^{13}C NMR (62.5 MHz, CDCl$_3$): δ = 151.2, 150.9, 150.6, 141.1, 140.4, 140.2, 126.8, 126.3, 126.2, 124.1, 122.9, 119.8, 55.1, 44.6, 34.7, 34.0, 28.3, 27.1, 22.8, 14.0, 10.3 ppm; MS (FD): m/z: 2335.9 [M$^+$], 1166.9 [M^{2+}], 777.5 [M^{3+}]; elemental analysis: calcd for C$_{174}$H$_{242}$ (2333.8): C 89.55, H 10.45; found : C 89.32, H 10.36.

9,9,9´,9´,9´´,9´´,9´´´,9´´´,9´´´´,9´´´´,9´´´´´,9´´´´´,9´´´´´´,9´´´´´´-Tetradecakis(2-ethylhexyl)-2,2´-7´,2´´-7´´,2´´´-7´´´,2´´´´-7´´´´,2´´´´´-7´´´´´,2´´´´´´-heptafluorene (50, OF7): compound **50** was prepared according to the method used for **42** by using **48** (650.0 mg, 0.52 mmol), **40** (85.0 mg, 0.13 mmol) and Pd(PPh$_3$)$_4$ (15 mg, 0.013 mmol) in toluene (2.6 mL) and 1 M aqueous K$_2$CO$_3$ (1.3 mL, 1.3 mmol). The reaction took 16 h. After cooling to room temperature, the mixture was diluted with diethyl ether and the organic layer was washed with diluted HCl, brine, and water, then dried over MgSO$_4$. The solvent was removed under vacuum and the residue was purified by column chromatography over silica gel using hexane/dichloromethane (10:0.8) as eluent (R$_f$ = 0.17) to afford **50** as white solid (167.0 mg, 46.4 %): ^{1}H NMR (250 MHz, CD$_2$Cl$_2$) : δ = 7.86-7.69 (m, 38 H), 7.45-7.26 (m, 6 H), 2.15-2.06 (m, 28 H), 0.92-0.50 (m, 210 H) ppm; ^{13}C NMR (62.5 MHz, CDCl$_3$): δ = 151.2, 150.9, 150.6, 141.1, 140.4, 140.2, 126.8, 126.1, 124.1, 123.0, 119.8, 119.6, 55.1, 44.5, 34.7, 34.1, 28.3, 27.1, 22.8, 14.0, 10.4 ppm; MS (FD): m/z: 2724 [M$^+$], 1362 [M^{2+}], 907 [M^{3+}]; elemental analysis: calcd for C$_{203}$H$_{282}$ (2722.5): C 89.56, H 10.44; found: C 89.43, H 10.38.

Poly(9,9-bis(2-ethylhexyl)fluorene-2,7-diyl) (51, PF2/6): A Schlenk tube was placed 2.67 g (14.6 mmol) of bis(1.5-cyclooctadiene)nickel(0), 1.52 g (14.6 mmol) of 2,2'-bipyridine, 1.05 g (14.6 mmol) of 1.5-cyclooctadiene, 8 ml DMF and 20 ml toluene. The mixture was stirred at 80°C for 0.5h (blue solution). The 9,9-bis(2-ethylhexyl)-2,7-dibromofluorene(38, 2g, 3.65 mmol) in 12 ml toluene was added to the blue solution, and the mixture was heated at 80°C for 5 days. After 5 days, 9,9-bis(2-ethylhexyl)-2-bromofluorene was added into the

mixture, and keep at 80°C for 24 h. The mixture was cooled and the poly(2,7-(9,9-bis(2-ethylhexyl)fluorine-2,7-diyl) was precipitated with an equivalent mixture of concentrated hydrochloride acid, methanol, and acetone. The solid was redissolved in chloroform and precipitated from acetone/methanol for several times to give 1.42 g polyfluorenes (71% yield), which has PPP equivalent molecular weights: $M_n = 61000$ and $M_w = 110000$ g/mol; $P_D = 1.79$. (PS as standard $M_n = 98000$ and $M_w = 229000$ g/mol; $P_D = 2.1$).

2.5 Summary

The facile synthesis of oligofluorenes from the dimer up to the heptamer by a series of stepwise transition metal mediated Suzuki and Yamamoto reactions has presented. 2,7-dibromofluorene and 2-bromofluorene were chosen as starting materials, and alkylated with 2-ethylhexyl bromide in 9-position of the fluorenyl ring. Unsymmetrical monobromides of monomer, dimer and trimer of fluorenes were important intermediate compounds for higher oligomers. Oligofluorenes with an odd number of fluorene unit such as trimer, pentamer, heptamer were prepared by Pd-catalyzed Suzuki coupling of excessive monobromides of momomer, dimmer, trimer with 2,7-bis (4,4,5,5-tetramethyl-1,3,2-dioxaborolan-2-yl)-9,9-di-2-ethylhexylfluorene. The oligofluorenes with an even number of fluorene units such as dimer, tetramer, hexamer were synthesized by Yamamoto homocoupling of these monobromides, repectively. Polyfluorenes was synthesized by Yamamoto coupling of 2,7-dibromo-9,9-bis(2-ethylhexyl)fluorene. In this work, aryl boronates were readily available from the aryl halides via Pd(0)-catalyzed reaction with the pinacol ester of diboron (Miyaura reaction). This transformation avoids the use of strongly basic organometallic reagents and thus allows the preparation of a wide variety of functionalized aryl boronic esters, moreover, the yield of this reaction was very high (90%), and the purification of target products was also very easy. In the synthesis of the oligofluorenes, all compounds were purified by standard column chromatography and confirmed by field desorption mass spectroscopy (FD-MS) and ^{1}H or ^{13}C-NMR techniques.

2.6 References

[1] Klaerner ,G.; Miller, R. D. *Macromolecules* **1998**, *31*, 2007-2009.

[2] Lee, S. H.; Tsutsui, T. *Thin Solid Films* **2000**, *363*, 76-80.

[3] Yamamoto, T.; Morita, A.; Miyazaki, Y.; Maruyama, T.; Wakayama, H.; Zhou, Z.; Nakamura, Y.; Kanbara, T.; Sasaki, S.; Kubota, K. *Macromolecules* **1992**, *25*, 1214-1223.

[4] Woo, E. P.; Inbasekaran, M.; Shiang, W.; Roof, G. R. *Int. Pat. Appl. WO 97/05184*, **1997**.

[5] (a) Ishiyama, T.; Murata, M.; Miyaura, N. *J. Org. Chem.* **1995**, *60*, 7508-7510; (b) Read, M. W.; Escobedo, J. O.; Willis, D. M.; Beck, P. A.; Strongin, R. M. *Org. Lett.* **2000**, *2*, 3201-3204; (c) Giroux, A.; Han, Y.; Prasit, P. *Tetrahedron Lett.* **1997**, *38*, 3841-3844.

[6] Kelley, C. J.; Ghiorghis, A.; Qin, Y.; Kauffman, J. M.; Novinski, J. A.; Boyko, W. J. *J. Chem. Res.* **1999**, 401-418.

[7] (a) Yamamoto, T. *Pogr. Polym. Sci.* **1992**, *17*, 1153; (b) Pei, Q.; Yang, Y.; *J. Am. Chem. Soc.* **1996**, *118*, 7416; (c) Grell, M.; Knoll, W.; Lupo, D.; Meisel, A.; Miteva, T.; Neher, D.; Nothofer, H.-G.; Scherf, U.; Yasuda, A. *Adv. Mater.* **1999**, *11*, 671-675.

[8] (a) Miyaura, N.; Suzuki, A. *Chem. Rev.* **1995**, *95,* 2457-2483; (b) Suzuki. A. *J. Organomet. Chem.* **1999**, *576*, 147-168.

[9] Schlüter, A. D. *J. Polym. Sci. Part A: Polym. Chem.* **2001**, *39*, 1533-1556.

[10] (a) Ranger, M.; Leclerc, M. *J. Chem. Soc., Chem. Commun.* **1997**, 1597; (b) Ranger, M.; Rondeau, D.; Leclerc, M. *Macromolecules* **1997**, *30*, 7686-7691.

[11] Zhan, X.; Liu, Y.; Zhu, D.; Huang, W.; Gong, Q. *Chem. Mater.* **2001**, *13*, 1540-1544.

[12] (a) Ishiyama, T.; Murata, T. M.; Miyaura, N. *J. Org. Chem.* **1995**, *60*, 7508-7510; (b) Read, M. W.; Escobedo, J. O.; Willis, D. M.; Beck, P. A.; Strongin, R. M. *Org. Lett.* **2000**, *2*, 3201-3204; (c)Giroux, A.; Han, Y.; Prasit, P. *Tetrahedron Lett.* **1997**, *38*, 3841-3844.

3   Chain-Length Dependence of the Electrochemical and Spectral Properties of Conjugated Oligofluorenes

In this chapter, the electrochemical properties of the oligofluorenes were studied by cyclic and differential pulse voltammetry. The electronic properties were investigated by UV-vis absorption and fluorescence spectroscopy in solution. A series of interesting relations of energy gap, ionization potential, electron affinity, oxidation potential and fluorescence lifetime with the reciprocal number of the fluorene units were found and the linear extrapolation of these relations to infinite polymers predicted the electronic properties of the corresponding polyfluorenes.

3.1 Introduction

Similar to other conjugated oligomers, oligofluorenes **OFn** (Chart 1, n=2~7) serve as model compounds for the analysis of the electronic and electrochemical properties of the corresponding polyfluorenes (**PF2/6**).[1] From a technological viewpoint, the interesting electronic properties of the polyfluorenes[2] suggest that the oligofluorenes could be used as semiconductors in organic electronics and photonics.[3,4] A deep understanding of the electronic and electrochemical properties of the polyfluorenes and oligofluorenes thus is desirable when considering their practical applications in organic devices. Herein, the electronic properties of the monodisperse oligofluorenes **OFn** (n=2~7) (Scheme 3 .1. 1) were thus studied by UV-vis absorption and fluorescence spectroscopy and the electrochemical properties were investigated by cyclic and differential pulse voltammetric techniques. The chain-length dependence of parameters such as band gap (E_g), oxidation potential, ionization potential (I_p), electron affinity (E_a) and fluorescence lifetimes etc. thus can be deduced and extrapolated to the values expected for an idealized infinite polymer.
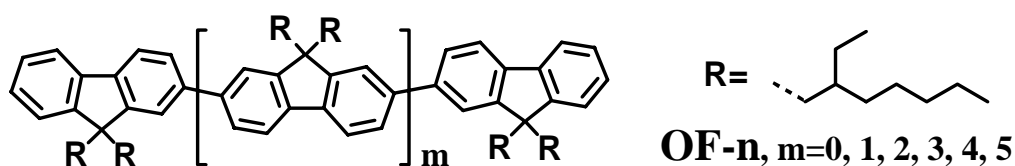
Scheme 3.1.1. *Molecular structures of the oligofluorenes and polyfluorenes,* **OF-n** *represents n-mer.*

3.2 Results and discussion

3.2.1 Electrochemical measurements

The results of the cyclic voltammetry (CV) and differential pulse voltammetry (DPV) measurements in solutions of the oligofluorenes (**OF-n**, n=2~7) are presented in Figure 3 .2. 1 and the data are summarized in Table 3. 2. 1. In all cases, one or multi- reversible oxidation waves were observed. The extension of the chain-length led to an increase of the number of the accessible oxidation states without affecting the reversibility of the oxidation waves. For example, for dimer (**OF2**), two reversible redox waves with $E_{1/2}^1$ and $E_{1/2}^2$ ($E_{1/2}$: half wave potential) at 1.11 and 1.49 V were observed, that correspond to the successive generation of the cation radical and dication. With chain extension to the tetramer (**OF4**), the second redox wave is followed by two one-electron waves corresponding to the successive generation of the trication radical and tetracation ($E_{1/2}^3$ and $E_{1/2}^4$ at 1.47 and 1.67 V, respectively). For the hexamer (**OF6**) and heptamer (**OF7**), four reversible redox waves were observed, indicating that the systems can be charged up to a stable tertcationic state. With the extension of the chain-length, the $E_{1/2}^{1-4}$ for the related oxidation wave displayed a negative shift and a decrease of the $E_{1/2}^2 - E_{1/2}^1$, reflecting the reduction of the on-site Coulombic repulsion between the positive charges in the dicationic state. The difference between the first and the second oxidation waves ($E_{1/2}^2 - E_{1/2}^1$) converged from 0.38 V for dimer to 0.05 V in the heptamer (as clearly distinguished by DPV measurements, Figure 1). The apparent redox potentials ($E_{1/2}^1$ to $E_{1/2}^4$) corresponding to the generation of the various cationic species of **OF-2~OF-7** revealed a linear relation with the reciprocal number of the fluorene units (Figure 3. 2. 2). Extrapolation of the plots of first oxidation $E_{1/2}^1$ *vs* 1/n to 1/n = 0 (Figure 3. 2. 2) gave a value of 0.86V, which is lower than the experimental value of
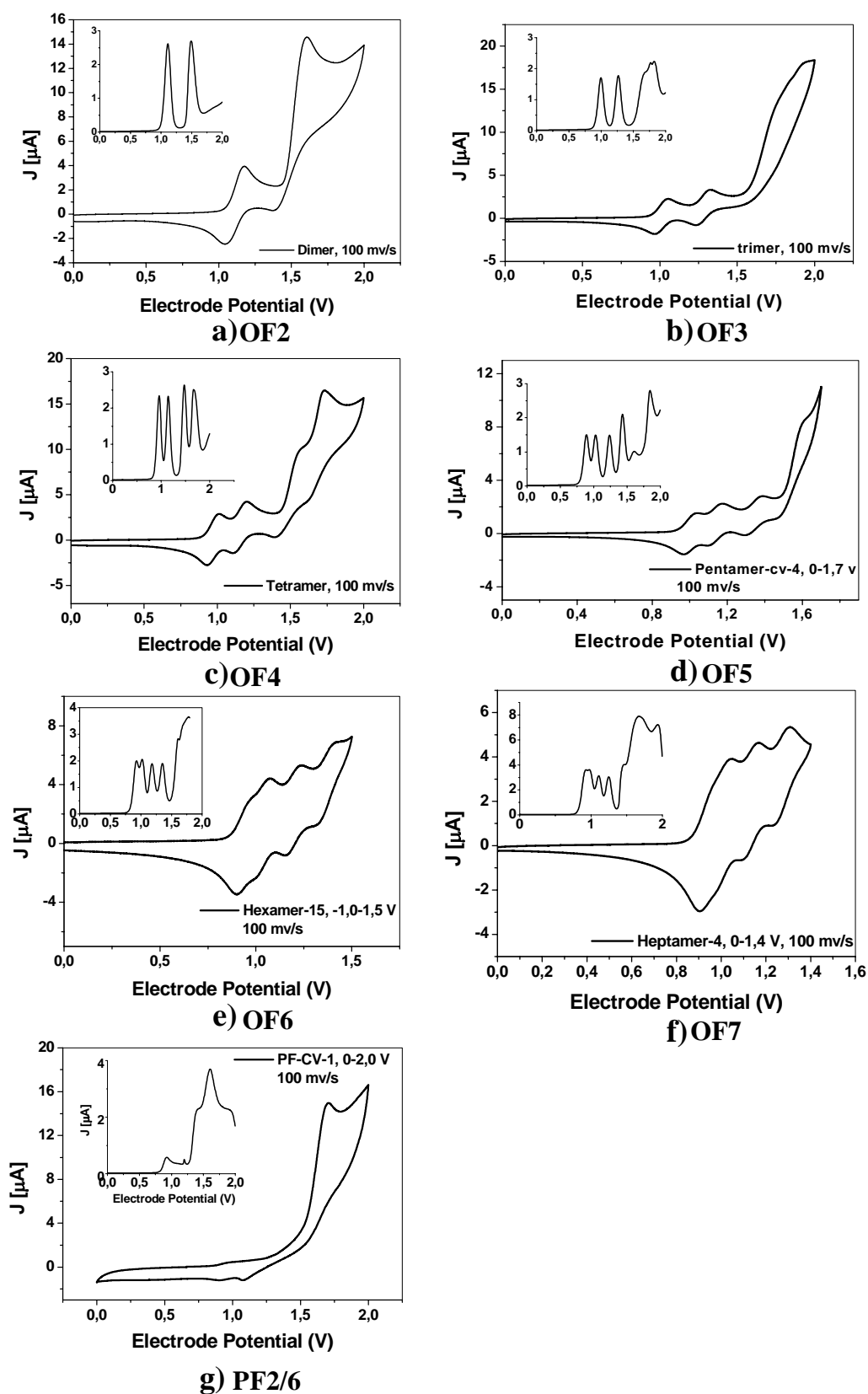
*Figure 3. 2. 1. Cyclic voltammetry and differential pulse voltammetry (inset) waves of oligofluorenes (**OF2** to **OF7**).*

*Table 3. 2. 1. Cyclic voltametric data for **OFn**. [OFn] = 5 × 10^{-4} M, [Bu$_4$NPF$_6$]=10^{-1} M in CH$_2$Cl$_2$, Pt-disc as working electrode, Pt wire as counter electrode. Scan rate =100 mV/s, E$_{1/2}$ (ferrocene) = 0.232 V vs AgNO$_3$/Ag reference electrode.*

Compound	$E_{1/2}^{1}$ (V)	$E_{1/2}^{2}$ (V)	$E_{1/2}^{2}$-$E_{1/2}^{1}$ (V)	$E_{1/2}^{3}$ (V)	$E_{1/2}^{4}$ (V)
OF2	1.11	1.49	0.38		
OF3	1.0	1.27	0.27		
OF4	0.96	1.15	0.19	1.47	1.67
OF5	0.91	1.04	0.13	1.25	1.45
OF6	0.93	1.02	0.09	1.18	1.35
OF7	0.93	0.98	0.05	1.11	1.25

the corresponding polymers (0.93 V from DPV measurements). A convergences to zero of $E_{1/2}^{2}$-$E_{1/2}^{1}$ and $E_{1/2}^{3}$-$E_{1/2}^{1}$ by linear extrapolation were found at about n=13 in the same time, suggesting a coalescence of the three successive one-electron oxidation peaks into a single-step three-electron wave will happen in the 13-mer. Similarly, a convergences to zero of $E_{1/2}^{4}$-$E_{1/2}^{1}$ by linear extrapolation was found at about n=24, that means the all of oxidation waves will be overlap together into a oxidation wave in the 24-mer.

From figure 3. 2. 2, the infinite oxidation half wave potentials 0.84, 0.77, 0.62, 0.70 eV for $E_{1/2}^{1}(\infty)$-$E_{1/2}^{4}(\infty)$, can be obtained respectively by the extrapolation of the linear plot $E_{1/2}^{n}$ ~ 1/n to infinite chain length polymer. The $E_{1/2}^{1}(\infty)$ value is higher than the $E_{1/2}^{2}(\infty)$, $E_{1/2}^{3}(\infty)$, $E_{1/2}^{4}(\infty)$, that indicates the all of oxidation waves will be overlap together into a oxidation wave for the infinite polyfluorene. The slopes of the linear plots are 0.84, 1.45, 3.34, 3.83 respectively for $E_{1/2}^{1}$, $E_{1/2}^{2}$, $E_{1/2}^{3}$, $E_{1/2}^{4}$ *versus* 1/n. From the slope, it is clear that the oxidation wave of higher potential is more sensitive to change in the π-conjugation length than oxidation wave of low potential.
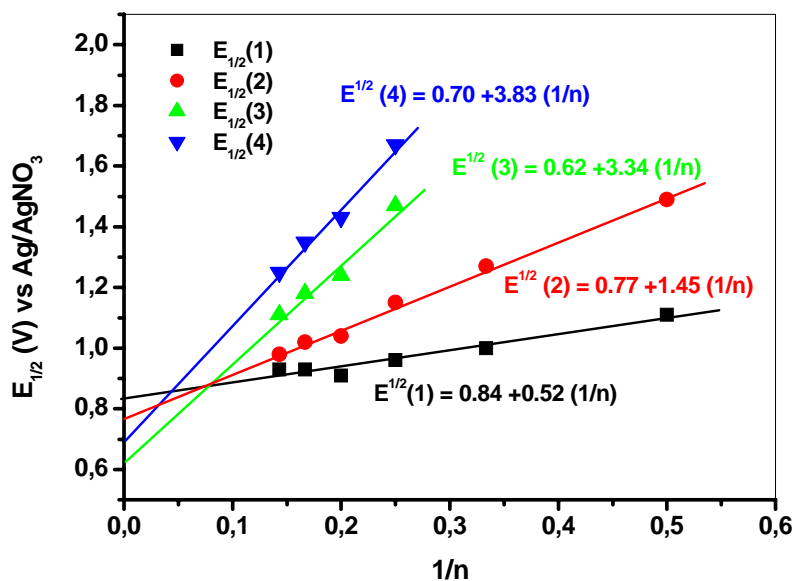
Figure 3. 2. 2. The linear relations between the apparent redox half wave potentials with the reciprocal number of fluorene units (1/n).

As observed above, the oligofluorenes displayed the typical electrochemical behavior of conjugated oligomers such as oligo-α,α'-thiophenes,[5] oligopyrrols[6] and oligothienylenevinylenes[7] etc. From the structural point of view, polyfluorenes can be regarded as a step-bridged polyphenylenes. The electrochemical properties of the oligo-*p*-phenylenes with different substitution modes have been investigated by Müllen et al..[8] While the oligophenylenes with the substitution only in the terminal phenyl rings displayed a two reversible oxidation behavior like normal conjugated oligomers, the substitutions in the middle rings disturb the conjugation and lead to irreversible oxidation states. The steric repulsion between the substituents of the neighboring phenyl rings plays an important role in the electronic decoupling. Herein, the substituents in poly- or oligo-fluorenes are placed in the 9,9'-position of the planar fluorene units and the intrachain steric repulsion between the alkyl-substituents are negligible. Such structural modifications of poly-*para*-phenylenes lead to a more efficient π-conjugation. As a result, the oligofluorenes displayed more accessible, stable cation species and a good relation between the electrochemical properties and the chain-length.

3. 2. 2 Steady-state electronic absorption and fluorescence spectroscopy

The electronic absorption and emission spectra of all the oligomers (**OF2~OF7**) and the polyfluorenes (**PF2/6**) in chloroform solution are presented in Figure 3. 2. 3 and the data are collected in Table 3. 2. 2. As expected, the chain-length extension led to a bathochromic shift of the absorption maximum $\lambda_{max(abs)}$ (correlated to the energy gap E_g) and to a narrowing of the HOMO-LUMO gap (ΔE) estimated from the low-energy absorption edge. The fluorescence spectra of oligofluorenes also display a red-shifted emission with the extension of the chain-length (Figure 3b), from $\lambda_{max(em)}$ = 385 nm for the dimer (**OF2**) to $\lambda_{max(em)}$ = 412 nm for the heptamer (**OF7**). The molar extinction coefficients (ε_{max}) of oligofluorenes at the $\lambda_{max(abs)}$ display in good approximation a linear increase with n (the number of the fluorene units) from dimer to heptamer as seen in Table 2. The increment is 30.3×10^3 L mol^{-1} cm^{-1} per repeat unit, indicating that each repeat unit contributes with the same oscillator strength to the overall absorption, otherwords, ε per repeat unit is independent of chain length. With increasing chain-length, extrapolation of the oligomer to
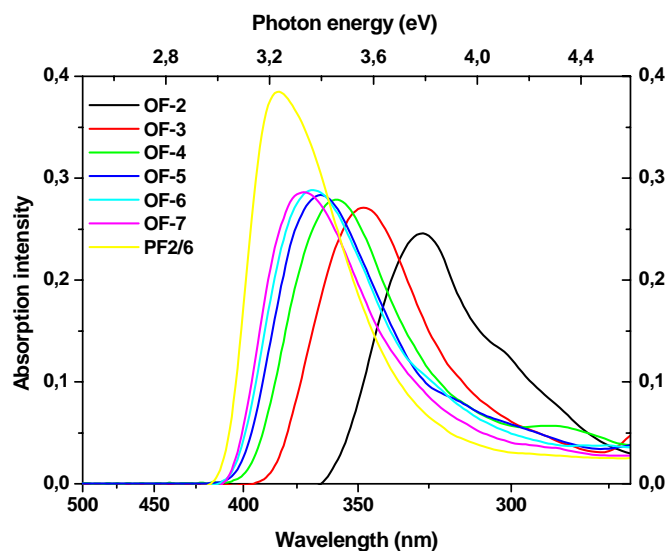
*Figure 3. 2. 3a. UV-Vis absorption of oligofluorenes dimer to heptamer, and polymer in chloroform solution at room temperature. The spectra (**OF2** up to **OF7**, **PF2/6**) were recorded at a concentration of fluorene repeat units of 1.0×10^{-5} molL^{-1}.*
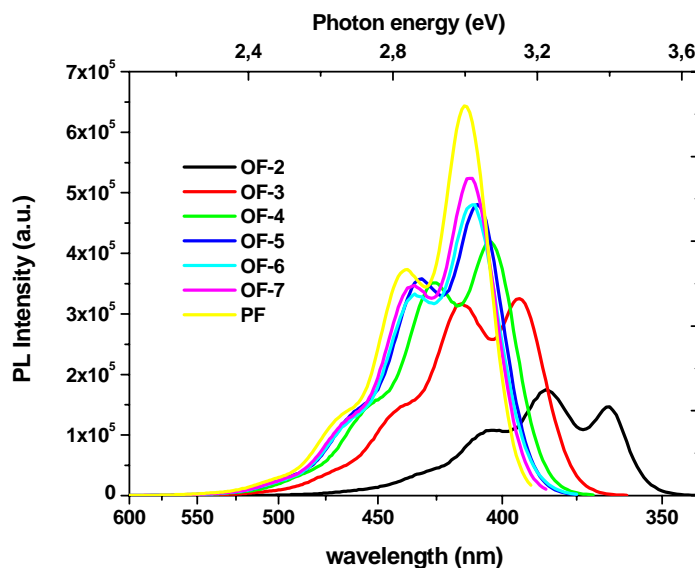
*Figure 3. 2. 3b. Emission spectra of the oligofluorenes and polymer in chloroform solution at room temperature. (The spectra of **OF2** up to **OF7** were recorded at a fixed concentration of fluorene repeat units of 1.0 × 10⁻⁶ molL⁻¹, emission spectra of **PF2/6** was recorded at a fixed concentration of fluorene repeat units of 2.5 × 10⁻⁷ molL⁻¹).*
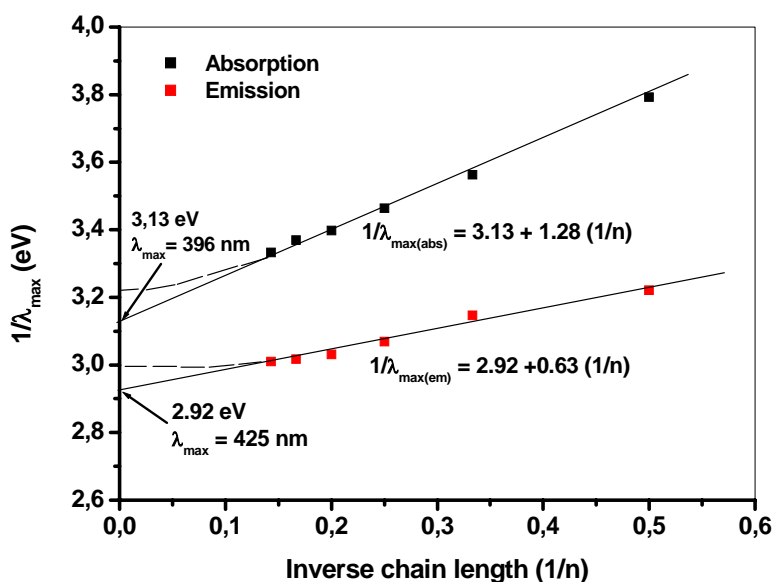
Figure 3. 2. 4. Linear relations of the absorption and emission maxima of oligofluorenes with the inverse number of fluorene units(1/n). The absorption maximum for poly-[9,9-bis-(2-ethylhexyl)fluorene-2,7-diyl] is 383nm(3.24 eV), The effective conjugation length (n = 14) can be obtained from the absorption linear fit. The emission maximum for poly-[9,9-

bis-(2-ethylhexyl)fluorene-2,7-diyl] is 414nm(3.00 eV), The effective conjugation length (n = 8) can be obtained from the emission linear fit.

Table 3. 2. 2. *Data for the spectral properties of the oligofluorenes (**OFn**) and polyfluorenes. $\lambda_{max(abs)}$, ε_{max}, ΔE is obtained from electronic absorption spectra; $\lambda_{max(PL)}$ is obtained from emission spectra ; E_{ox}' relative to AgNO$_3$/Ag reference electrode is obtained from cyclic voltammetry. I_p and E_a value relative to the vacuum level. ^{a}Data for the hypothetical 'ideal' polymer PF(∞) obtained from extrapolation. ^{b} ΔE is calculated from the low-energy absorption edge.*

Sample	$\lambda_{max(abs)}$		ε_{max}	$\lambda_{max(PL)}$				ΔE^b	I_p	E_a	E_{ox}'
	nm	eV	(Lmol^{-1}cm^{-1})	nm	eV	nm	eV	(eV)	(eV)	(eV)	(eV)
OF-2	327	3.79	49170	365	3.40	385	3.22	3.46	5.66	2.20	1.06
OF-3	348	3.56	81330	394	3.15	415	2.99	3.22	5.55	2.33	0.95
OF-4	358	3.46	111500	404	3.07	426	2.91	3.14	5.51	2.37	0.91
OF-5	365	3.40	141700	409	3.03	432	2.87	3.10	5.50	2.40	0.89
OF-6	368	3.37	173000	411	3.02	434	2.86	3.08	5.48	2.40	0.88
OF-7	372	3.33	200300	412	3.01	434	2.86	3.06	5.47	2.41	0.87
PF2/6	383	3.24	-	414	3.00	437	2.84	3.04	5.45	2.41	0.85
PF(∞)^a	396	3.13	-	425	2.92	-	-	2.88	5.39	2.51	-

data to 'infinite' chain length is appropriate in order to predict the properties of an 'ideal' polymer. Thus in our case, a linear relation between the wavenumber of absorption and emission maximum ($\nu_{max\,(abs)}$ and $\nu_{max\,(emi.)}$)and the reciprocal number of the fluorene units (1/n) was observed in Figure 3. 2. 4. A linear extrapolation of the plot to regular infinite chains (1/n = 0) in solution exhibit an absorption maximum at λ_{max}(abs) = 396 nm (3.13 eV) and a maximum emission at λ_{max}(emi) = 425 nm (2.92 eV). These hypothetical energies expectedly lie lower than those experimentally found for polyfluorenes solution (λ_{max}(abs) = 383 nm (3.24 eV) and λ_{max}(emi) = 414 nm (3.00 eV) as a result of saturation. From the maximum absorption and emission of experimental polymer, we can estimate an effective conjugation length (ECL) of 14-repeat units from the absorption plot, and 8-repeat units from the emission plot in Figure 3. 2. 4. Practically, the $\nu_{max\,(abs)}$ and $\nu_{max\,(emi.)}$ tend to saturate to a constant value with increasing the chain length. Fluorescence, however, saturates faster than absorption because the relaxed exciton compromises only part of the

oligomer while the hot exciton is delocalized along the whole chain.[9] This can be observed with slope 1.28 related to absorption plot and 0.63 related to fluorescence linear plot from Figure 3. 2. 4. The plot of ΔE *vs* 1/n is shown in Figure 3. 2. 5, extrapolation of the HOMO-LUMO gap (ΔE) data to an infinite chain length leads to a predicted gap value, 2.88 eV for infinite defect-free polyfluorenes smaller than the present experimental value for PFs, suggesting that the synthesis of longer OF-n may allow further band-gap reduction.

For a given chain length, oligofluorenes with 2-ethylhexyl group side chain absorb at shorter wavelengths than those of series oligofluorenes with hexyl group and 2s-methylbutyl group,[10] these differences reflect the effect of the larger number of alkyl substitutents on the electronic density of the π-conjugated system. Apart from these modest differences, the spectra of oligomers of the different side chain are very similar in shape both in absorption and emission and exhibit a structured fluorescence band.

As shown in Table 3. 2. 2, the longest oligomer **OF7** shows HOMO-LUMO gap (*ΔE*) around 3.06 eV. The ΔE value is close to that of polyfluorenes (ΔE = 3.04 eV) with the same side-chain and is smaller than the band gap of poly(*p*-phenylene)(PPP) (3.6 eV)[11] due to the fluorenyl structure possessing a more efficient π-conjugation. The effective conjugation and HOMO-LUMO gap of linear π-conjugated systems are related to the average delocalization (or confinement) length of π-electrons.[12] Whereas, for polyenes, this parameter depends essentially on the degree of bond length alternation, in polyaromatic system, other factors such as planarity and aromatic resonance energy plays also a determining role.[13] The smaller HOMO-LUMO gap of oligofluorens compared to oligo(*p*-phenylene) reflects the higher planarity.

3.2.3 Determination of ionization potential (I$_p$) and electron affinity (E$_a$)

The ionization potential (I$_p$) and electron affinity (E$_a$) of conjugated oligomers and polymers are important parameters when applying them as semi-conducting materials in devices. To transpose the measured redox behavior into estimates for the ionization potential I$_p$ and electron affinity E$_a$, it is necessary to relate the electrochemical potentials to the vacuum level relative to which I$_p$ and E$_a$ are defined. An empirical relationship has been proposed by Brédas *et al.*[14] on the basis of a detailed comparison between valence effective

Hamiltonian calculations and experimental electrochemical measurements. The expectation is that:

$$Ip = (E'_{ox} + 4.4) \text{ eV and}$$

$$Ea = (E'_{red} + 4.4) \text{ eV,}$$

where E'_{ox} and E'_{red} are, respectively, the onset potentials for oxidation and reduction relative to Ag/AgCl reference electrode. The I_p and E_a values of poly(9,9-dioctylfluorene) have been electrochemically determined according to this method by S. Janietz and D. D. C. Bradley *et al.*[15] They used a three electrode configuration undivided cell: the working electrode was glassy carbon, the counter electrode was a platinum mesh and the reference electrode was Ag/AgCl (3M NaCl and saturated Ag/Cl) which was separated by a diaphragm. For this arrangement the ferrocene half wave potential was estimated to be 435 mV against Ag/AgCl.

In our experiment, the redox potentials in all the measurements were internally calibrated by adding ferrocene(Fc) during the measurements and in the case of using $AgNO_3/Ag$ as reference electrode the $E_{1/2}(Fc^+/Fc) = 0.232$ V. The calculation for I_p and E_a relative to the vacuum level thus can be written by

$$Ip = (E_{ox} + 4.4 + 0.435 - 0.232) \text{ eV}$$

$$Ea = (E_{red} + 4.4 + 0.435 - 0.232) \text{ eV}$$

where E_{ox} and E_{red} are, respectively, the onset potentials for oxidation and reduction relative to $AgNO_3/Ag$ reference electrode. Herein, the oxidation onset E_{ox} can be easily drawn out from the CV curves, listed in table 3. 2. 2, however E_{red} can not be directly obtained from the CV measurements because the stable anionic state is not experimentally accessible. Alternative, the E_a were estimated by equation *Ea = Ip-ΔE*, where the *ΔE* is the HOMO-LUMO gap. With the extension of the chain-length, the I_p values (table 3. 2. 2) decreased from 5.66 eV for dimer down to 5.37 eV for heptamer, and at the mean time, the E_a values increased gradually, resulting in a convergence of the HOMO-LUMO gap. The I_p and E_a were plotted *vs* the reciprocal number of the fluorene units (1/n), and approximately linear relations were observed (Figure 3. 2. 5).

A theoretical evaluation of the I_p and E_a of conjugated polyacetylene, polyphenylene, polythiophene and polypyrrol has been done by Brėdas et al. by the valence effective Hamiltonian (VEH) technique,[14] and in all cases the values are in good agreement with the experimental results. The approximately linear relationship between the I_p or E_a with the

1/n was also predicted and proved. Here, such a relation was observed again for the conjugated oligofluorenes.
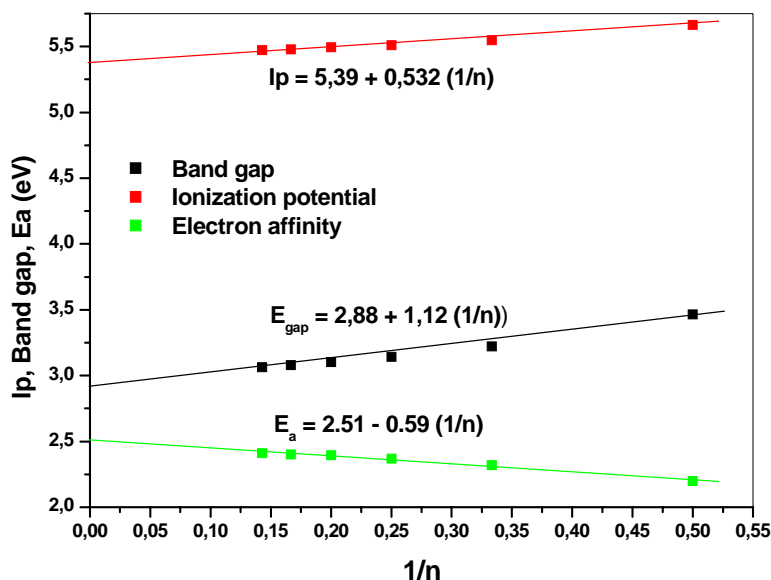
Figure 3. 2. 5. Linear relations of the energy gaps (ΔE), ionization potentials (Ip) and electron affinities (Ea) with the reciprocal number of fluorene units (1/n).

Extrapolation of quantities such as ionization potential, electron affinity, oxidation potential, λ_{max} and ΔE, determined on short-chain oligomers, has been widely used to analyze the chain length dependence of the electronic properties of π-conjugated oligomers and to predict the properties of an infinite defect-free polymer chain. For oligofluorenes, the effective conjugation length can be obtained from extrapolation of I_p, E_a, $E_{1/2}$[1], ΔE $\lambda_{max\,(Flu)}$ *versus* 1/n (n is the number of fluorene units) is around 6-8 repeat units, which is different with the value 14 obtained from $\lambda_{max\,(Abs)}$. That means the **ECL** is dependent on measurement method. As recently discussed by Meier et al., the existence of a finite ECL in linear π-conjugated systems implies the convergence of the above parameters towards a limiting value for a certain chain length.[16] Indeed, such a saturation limit has been observed for all series of oligomers investigated so far.[3]

For oligofluorenes, a similar analysis done using literature[7a] gives a slope of 1.12 for energy band plot (Figure 3. 2. 5). The lower slope found for **OFns** indicates that a similar increment in the number of fluorene unit in the conjugated chain is smaller effective in term

of increase of effective conjugation length and gap reduction for the **OFns** than for the other oligomers such as thienylenevinylene oligomers. Interestingly, the slope of $E_{1/2}^1 \sim 1/n$ (0.52) in Figure 3. 2. 2 is about twice smaller than that of Figure 3. 2. 5. Since $E_{1/2}^1$ is related to the **HOMO** energy level, the twice smaller slope indicates that the gap reduction resulting from chain extension involves symmetrical changes of the **HOMO** and **LUMO** energies with respect to mid-gap.

3.2.4 Transition fluorescence spectroscopy

The transition fluorescence spectra of the oligofluorenes in *m*-THF solution were recorded by Streak camera techniques.[17] The lifetimes (τ) were determined by analysis of the Streak camera photos (Figure 3. 2. 6a). In all the cases, mono-exponential fluorescence decay curves were observed and the lifetimes of the oligomers were in the subnanosecond range (Figure 3. 2. 6b). Interestingly, the lifetimes of the oligomers displayed a linear relation with the reciprocal number of the fluorene units (1/n) as described in Figure 3. 2. 6c. According to literature, such strong decrease of the lifetime can be explained by the enhanced transition dipolar coupling interactions with the increased unit numbers,[9c] and detailed discussion will be given in Chapter 5. 5. 1. An extrapolation to the infinite polymers gave a value of τ= 386 ps, which is very close to the determined value of 397 ps for the corresponding polymers **PF2/6**. Detailed studies of the transition fluorescence spectra of the oligofluorenes with the concentration, temperature and solvents will be presented in Chapter 5.

<div align="center">(a)</div>

<div align="center">(b)</div>

<div align="center">(c)</div>
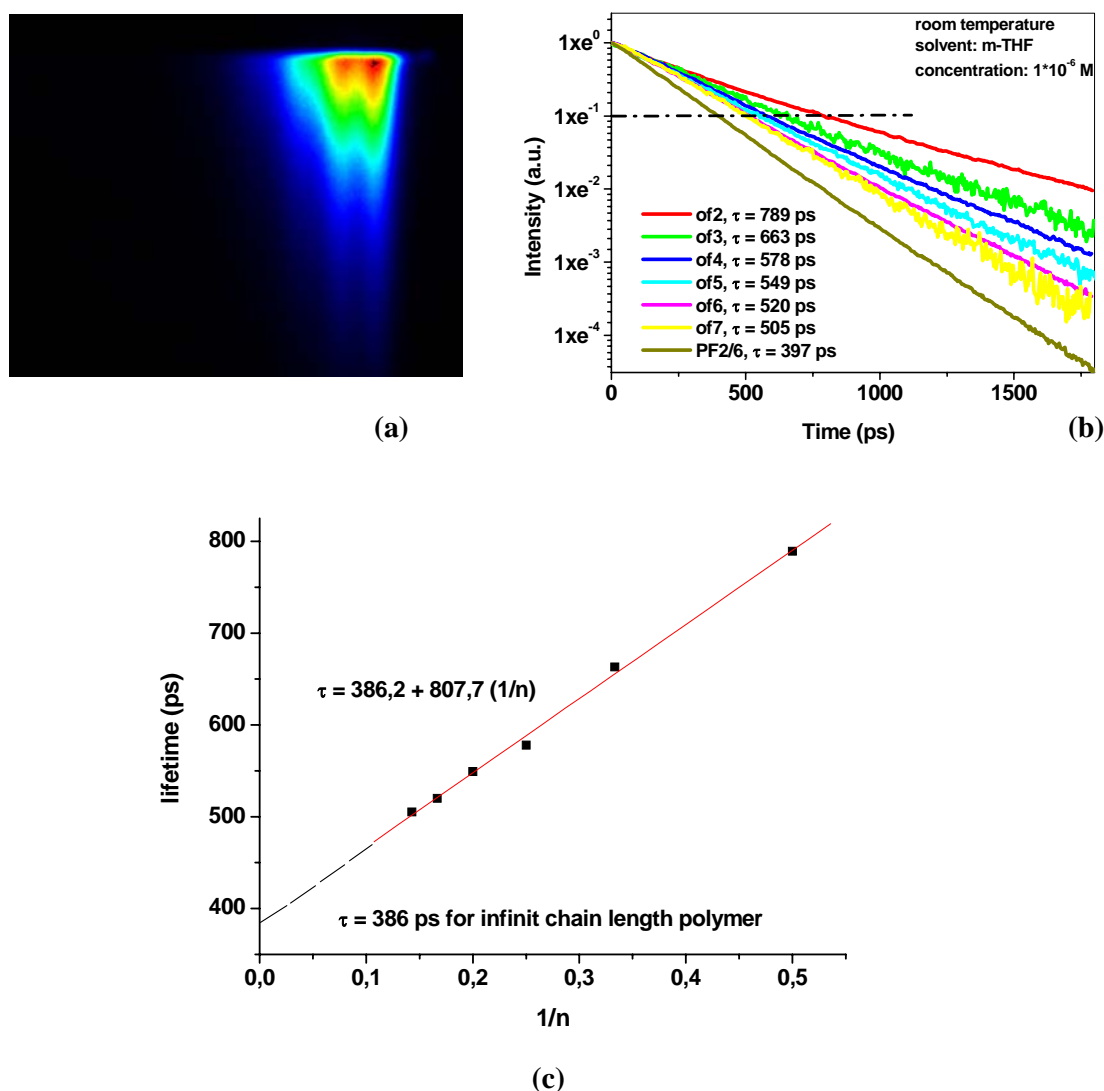
*Figure 3. 2. 6. (a) The fluorescence spectra of OF6 recorded from m-THF solution at room temperature by Streak camera; (b) The mono-exponential fluorescence decay plots of the oligofluorenes(OF2 up to **OF7**) and Polyfluorenes (**PF2/6**); (c) Linear relation of the fluorescence lifetimes with the reciprocal number of the fluorene units(1/n).*

3. 3 Conclusion

In conclusion, the electrochemical and electronic properties of oligofluorenes were systematically studied by several combined techniques such as cylic voltammetry, differential pulse voltammetry, UV-vis absorption spectroscopy, steady- and transition state fluorescence spectroscopy. It was found that the oligofluorenes behave like classical conjugated oligomers, i.e., with the increase of the chain-length, the band gap, the first

oxidation potential, the accessible oxidation states, the emission maximum and the photoluminescence lifetime displayed a very good linear relation with the 1/n. The ionization potential and electron affinity of the oligomers also showed interesting relations to the chain-length. The extrapolation of the linear part of the curves to infinite polymers also gave good agreements with experimental values.

3.4 Experimental Section

The electrochemical measurements of oligofluorenes **OF2~OF7** and the polyfluorenes (**PF2/6**, 5.0×10^{-4}M in dry dichloromethane) were performed in a standard three-electrode cell, a platinum wire sealed in insulated rubber as working electrode, a $AgNO_3$/Ag non-aqueous electrode as reference electrode and a platinum wire as counter electrode. Tetrabutylammonium hexafluorophosphorate (TBAPF$_6$, 0.1M) was used as supporting electrolyte. The electrochemical potentials were calibrated by an internal reference couple ferrocene/ferrocium (Fc/Fc$^+$) in each measurements and in all case $E_{1/2}$ (Fc/Fc$^+$) = 0.232 V.

UV-vis absorption spectra were recorded with chloroform solution of oligomers and polymer (fluorene unit concentration 1×10^{-5} M) at room temperature on a Perkin-Elmer Lambda 9 UV/Vis/NIR spectrophotometer. The fluorescence spectra were obtained by excitation of the solutions at the absorption maximums on a Spex Fluorolog II (212). The time resolved fluorescence was measured using a Hamamatsu C4742 Streak camera and a frequency-doubled mode-locked titanium-sapphire laser.

3.5 References

[1] (a) Martin, R. E.; Diederich, F. *Angew. Chem. Int. Ed.* **1999**, *38*, 1350; (b) *Electronic Materials: The Oligomer Approach*; Müllen, K. and Wegner, G., Eds; Weinheim: Wiley-VCH, **1998**.

[2] (a) Ohmori, Y.; Uchida, M.; Morishima, C.; Fujii, A.; Yoshino, K. *Jpn. J. Appl. Phys.* **1993**, *32*, 1663; (b) Pei, Q.; Yang, Y. *J. Am. Chem. Soc.* **1996**, *118*, 7416; (c) Klärner, G.; Lee, J.-K.; Davey, M. H.; Miller, R. D. *Adv. Mater.* **1999**, *11*, 115; (d) Virgili, T.; Lidzey, D. G.; Bradley, D. D. C. *Adv. Mater.* **2000**, *12*, 58; (e) Scherf, U.; List, J. W.; *Adv. Mater.* **2002**, *14*, 477; (f) Neher, D. *Macromol. Rapid Commun.* **2001**, *22*, 1365.

[3] *Semiconducting Polymers: Chemistry, Physics and Enginerring;* Hadziioannou, G.; van Hutten, P. F., Eds; Weinheim: Wiley-VCH, **2000**.

[4] (a) Tasaka, S.; Katz, H. E.; Hutton, R. S.; Orenstein, J.; Frederickson, G. H.; Wang, T. T. *Synth. Met.* **1986**, *16*, 17; (b) Fichou, D.; Nishikitani, Y.; Horowitz, G.; Roncali, J.; Garnier, F. *Synth.Met.* **1989**, *28*, C729; (c) Garnier, F.; Yassar, A.; Hajlaoui, R.; Horowitz, G.; Deloffre, F.; Servet, B.; Ries, S.; Alnot, P. *J. Am. Chem. Soc.* **1993**, *115*, 8716; (d) Katz, H. E.; Dodabalapur, A.; Torsi, L.; Elder, D. *Chem. Mater.* **1995**, *7*, 2238; (e) Katz, H. E.; *J. Mater. Chem.* **1997**, *7*, 369; (f) Geiger, F.; Stoldt, M.; Schweizer, R.; Bäuerle, P.; Umbach, E. *Adv. Mater.* **1993**, *5*, 922; (g) Caspar, J. V.; Ramamurthy, V.; Corbin, D. R.; *J. Am. Chem. Soc.* **1991**, *113*, 600; (h) ten Hoeve, W.; Wynberg, H.; Havinga, E. E.; Meijer, E. W. *J. Am. Chem. Soc.* **1991**, *113*, 5887; (i)Bäuerle, P. *Adv. Mater.* **1992**, *4*, 102; (j) Guay, J.; Kasai, P.; Diaz, A.; Wu, R.; Tour, J. M.; Dao, L. H. *Chem. Mater.* **1992**, *4*, 1097.

[5] (a) Bäuerle, P. *Adv. Mater.* **1992**, *4*, 102-106; (b) Guay, J., Kassai, P.; Diaz, A.; Wu, R.; Tour, M. *Chem. Mater.* **1992**, *4*, 1097-1105.

[6] (a) Geissler, U.; Hallensleben, M.; Toppare, L. *Synth. Met.,* **1993**, *55*, 1662; (b) Zotti, G.; Martina, S.; Wegner, G.; Schlüter, A. D. *Adv. Mater.*, **1992**, *4*, 798; (c) Martina, S.; Enkelmann, V.; Schlüter, A. D.; Wegner, G.; Zotti, G.; Zerbi, G. *Synth. Met.*, **1992**, *55*, 1096; (d) van Haare, J. A. E. H.; Groenendaal, L.; Havinga, E. E.; Janssen, R. A.; Mejer, E. W. *Angew. Chem.*, **1996**, *108*, 696; *Angew. Chem. Int. Ed.*, **1996**, *35*, 638; (e) Rohde, N.; Eh, M.; Geissler, U.; Hallensleben, M. L.; Voigt, B.; voigt, M. *Adv. Mater.*, **1995**, *7*, 401; (f) Andrieux, C. P.; Hapiot, P.; Audebert, P. Guyard, L.; Nguyen Dinh An, M.; Groenendaal, L.; Meijer, E. W. *Chem. Mater.* **1997**, *9*, 723-729.

[7] (a) Elandaloussi, E. H.; Frère, P.; Richomme, P.; Orduna, J.; Garin, J.; Roncali, J. *J. Am. Chem. Soc.* **1997**, *119*, 10774-10784; (b) Jestin, I. ; Frère, P.; Mercier, N.; Levillain, E. ; Stievenard, D. ; Roncali, J. *J. Am. Chem. Soc.* **1998**, *120*, 8150-8158; (c) Apperloo, J. J.; Raimundo, J.-M; Frère, P.; Roncali, J.; Janssen, R. A. *Chem. Eur. J.* **2000**, *6*, 1698-1707.

[8] Bohnen, A.; Heitz, W.; Müllen, K.; Räder, H.-J.; Schenk, R. *Makromol. Chem.* **1991**, *192*, 1679-1693.

[9] Franco, I.; Tretiak, S. Chem. Phys. Lett. 2003, 372, 403-408.

[10] (a) Lee, S. H.; Tsutsui, T. *Thin Solid Film* **2000**, *363*, 76-80; (b) Geng, Y.; Trajkovska, A.; katsis, D.; Ou, J. J. ; Culligan, S. W. ; Chen, S. H. *J. Am. Chem. Soc.* **2002**, *124*, 8337-8347; (c) Anèmian, R.; Mulatier, J.-C.; Andraud, C.; Stèphan, O.; Vial, J.-C. *Chem. Commun.* **2002**, 1608-1609.

[11] Brédas, J. L.; Silbey, R.; Boudreaux, D. S. ; Chance, R. R. *J. Am. Chem. Soc.* **1983**, *105*, 6555-6559.

[12] Hernandez, V.; Castiglioni, C.; Del Zopo, M.; Zerbi, G. *Phys. Rev. B* **1994**, *50*, 9815.

[13] Roncali, J. *Chem. Rev.* **1997**, *97*, 173.

[14] Brédas, J. L.; Silbey, R.; Boudreaux, D. S. ; Chance, R. R. *J. Am. Chem. Soc.* **1983**, *105*, 6555-6559.

[15] Janietz, S.; Bradley, D. D. C.; Greil, M.; Giebeler, C.; Inbasekaran, M.; Woo, E. P. *App. Phys. Lett.* **1998**, *73*, 2453-2455.

[16] Meier, H.; Stalmach, U.; Kolshorn, H. *Acta. Polym.* **1997**, *48*, 379.

[17] (a) Kobayashi, T. *J. Phys. Chem.* **1978**, *82*, 2277-2281; (b) Ishlkawa, M.; Watanabe, M.; Hayakawa, T.; Koishi, M. *Anal. Chem.* **1995**, *67*, 511-518.; (c) Kusumi, A.; Tsuji, A.; Murata, M.; Sako, Y.; Yoshizawa, A. C.; Kagiwada, S.; Hayakawa, T.; Ohnishi, S. *Biochemistry* **1991**, , 6517-6527.

4 **Liquid crystalline properties**

In this chapter, the thermal behavior, supramolecular packing, alignment properties and molecular dynamics of the monodisperse oligofluorenes were investigated to understand the basic structure-property relationships for oligo- and polyfluorenes. Linear relationship between the phase transition temperatures, e.g., isotropic transition (T_{iso}) or glass transition(T_g), and the reciprocal number of the fluorenyl units were observed. The higher oligomers (tetramer to heptamer) adopt a smectic liquid crystalline phase as evidenced by 2D wide-angle X-ray scattering measurements and single-crystal structure analysis. The oligofluorenes can be easily aligned on a rubbed polyimide substrate and give an over areas monodomain alignment layer which shows polarized optical absorption and emission.

4. 1 Introduction

Polyfluorenes belong to the class of worm-like polymers. The monomer unit consists of rigid planar biphenyl units, bridged by a methylene unit at 9-position, ensuring a high degree of conjugation. The carbon-9 atom may also carry additional substituents to modify the polymer processability and the interchain interactions in films. The structure of the alkyl side-chains in the 9-position of the fluorene moieties strongly influences the solid-state packing of the polymers. The thermal stabilities of the homo- and copolymers are excellent with decomposition temperatures exceeding 400°C.[1]

As we mentioned in previous chapters, polyfluorenes (PFs) are an important organic material for light emitting diodes (LEDs), exhibiting bright blue emission with efficiencies not reached when using other conjugated polymers. Beside this excellent emission properties, PFs were found to exhibit a thermotropic nematic liquid crystalline phase as first reported by Grell et al. in 1997.[2] These authors also demonstrated that thin layers of well-aligned PFs can be prepared on rubbed polyimide. This was the first report on the alignment of a fully conjugated main-chain liquid-crystalline polymer in thin layers on an appropriate alignment substrate. A dichroic absorption ratio of more than six and an even larger photoluminescence ratio as a fuction of polarization were reported on aligned PF layers. Thus the excellent alignability of the fully conjugated PFs polymer backbone opens strategies to construct ultrathin layers with highly anisotropic optical, electrooptical and

electric properties. A LED was fabricated based on an aligned PF emission layer displaying polarized light-emission with a polarization ratio of 15 at a reasonable brightness.[3] It was further disclosed that the alignment of the polymer chains in the liquid-crystalline state improved the charge-carrier mobility[4] and a field-effect transistor with a large in-plane anisotropy of the mobility was reported by Sirringhaus et al.[5]

Monodomain alignment of PFO on top of PI was induced by heating to 200°C followed by either slow cooling or quenching to room temperature. In both cases the dichroic ratio was ca. 6.5. The layers exhibit polarized photoluminescence with a polarization ratio of ca. 10.[2]

Later, alignment layers of PFs with various kinds of side chains (Scheme 4. 1. 1) were investigated by Neher et al.. The dichroic ratios are 16, 13, 12, 9 and 3 for PF2/6, PF8/1/1C2/6, PF3/5, PFO and PF4/12, respectively.[6] The largest dichroic ratio was found in PF2/6. Depending on the thermal process, dichroic ratios reach up to 16 at $\lambda = 380$ nm. The differential scanning calorimetric (DSC) curves of PF2/6 are shown in Figure 4. 1. 1. They reveal a phase transition to a birefringent LC phase at $T_{LC} = 167$°C upon heating, and a reverse transition at 132°C upon cooling.[7] The transitions are well resolved in the DSC scan. The dichroic ratio decreased when using symmetric, branched substituents such as **PF3/5** ($T_{LC} = 200$ °C). For an alignment layer of **PFO** which shows a transition temperature at $T_{LC} = 175$°C, the dichroic ratio at maximum absorption is only 9, in agreement with results by Grell et al.. Further evidence that the attachment of linear alkyl chains reduces the degree of alignment comes from a comparison of **PFO** and poly(didecylfluorene-co-dibutyl-fluorene) (**PF4C12**). For the latter case, the dichroic ratio is three only. There is a clear correlation between the degree of anisotropy and the shape of the absorption spectra. Most importantly, an additional shoulder appears at the long-wavelength side of the absorption band, which is most prominent in the spectra of **PF4C12**.

Grell et al. have intensively studied the spectral properties of PFO with respect to the correlation between sample treatment, chain geometry and optical properties.[8] In particular, a well-resolved peak at 436 nm appeared when solid PFO samples were cooled to 77K and reheated to room temperature. While the peak had first been interpreted as an interchain excitation (aggregates), detailed investigations revealed that the peak is most likely related to the absorption of highly ordered PF chains with more extended conjugation, thus being an intrachain property. Based on X-ray scattering results, a planar zigzag conformation, being identical to a 2/1 helix, has been proposed[8] (Figure 4. 1. 2).
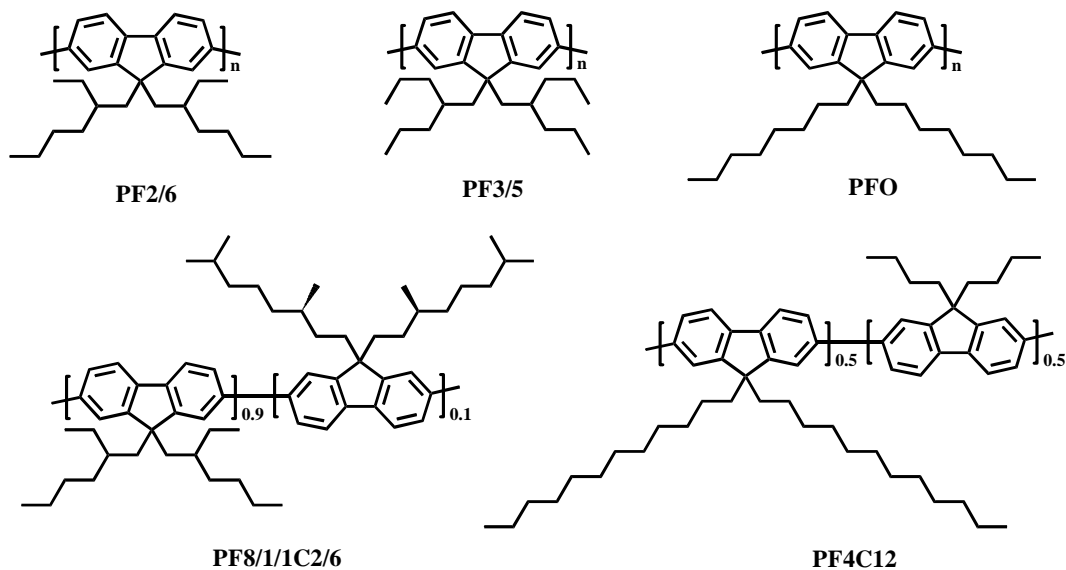
Scheme 4. 1. 1. Chemical structure of poly(9,9-bis(2-ethylhexyl)fluorene-2,7-diyl) (PF2/6), poly(9,9-bis(2-propylpentyl)fluorene) (PF3/5), poly(9,9-bis(2-octyl)fluorene (PFO), poly(2,7-(9,9-bis(2-ethylhexyl))co-(9,9-bis((3S)-3,7-dimethyloctyl))fluorene) (PF8/1/1C2/6), and poly(2,7-(9,9-bis(2-butyl)co-(9,9-bis(dodecyl))fluorene) (PF4C12),.
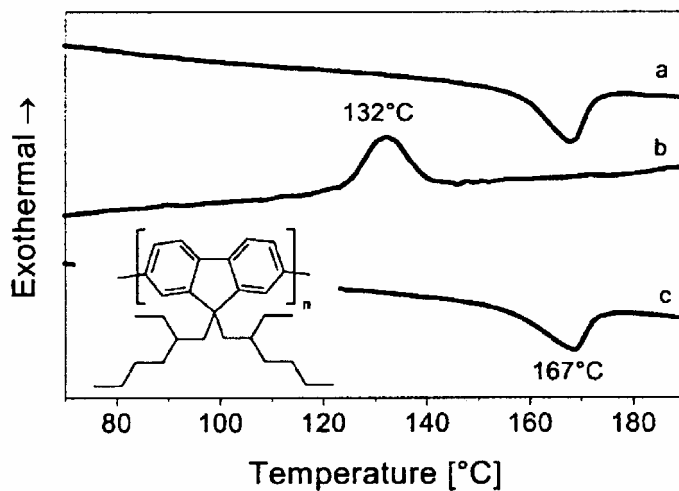
Figure 4. 1. 1. DSC scan of PF2/6: (a) heating at 10 K/min of a toluene-cast sample, (b) cooling scan of the same sample at 10 K/min, (c) heating scan for a sample quenched from 200 °C.
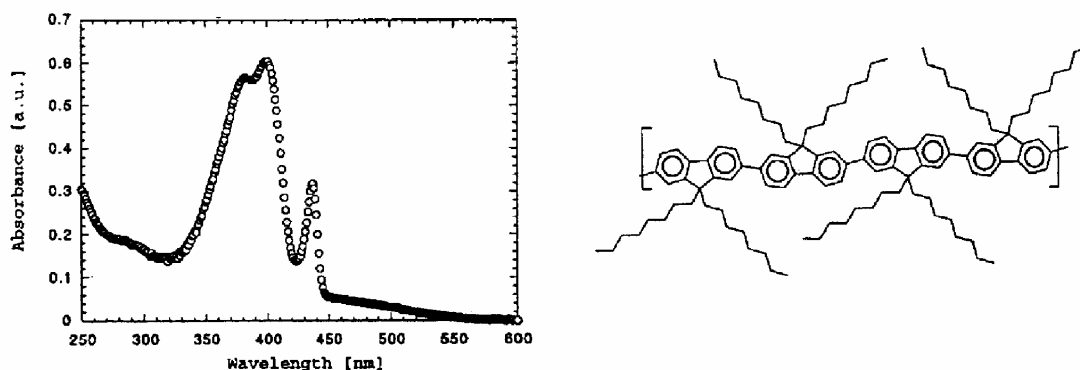
Figure 4. 1. 2. The UV-vis absorption spectrum of a solid layer of PFO after cooling to 77K and re-heating to r.t. The sharp absorption features have been assigned to planar chains with extended conjugation as shown on the right side[8]. (A fully extended PFO chain segment, adopting the "planar zigzag" or 2_1 helix conformation).

In contrast to PFO, UV-vis absorption spectra of PFs with branched side chains do not reveal a pronounced shift in absorption even after extended annealing. Thin layers as well as drawn fibers of PF2/6 have been studied by means of electron microscopy and X-ray scattering by Lieser et al.[9] Figure 4. 1. 3 shows a comparison of the electron diffraction pattern of PF2/6 film oriented on the top of a rubbed polyimide substrate (annealed at 175°C for 2h in an inert atmosphere) with the X-ray diffraction pattern of a fiber drawn from the same polymer and annealed subsequently at 170°C for 4h. Both show a similar diffraction pattern. Based on the diffraction experiments, a packing of the annealed chains in a trigonal lattice a = b = 1.67 nm, c = 4.04 nm, $\alpha = \beta = 90°$, $\gamma = 120°$ was suggested.

(A)

(B)
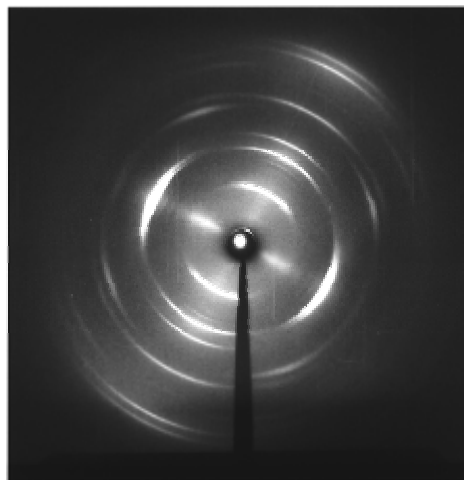
Figure 4. 1. 3[9] (A) Electron diffraction pattern of an oriented PF2/6 film (30 nm)on top of a 20 nm polyimide alignment layer from a circular area of 2.7 ㎛ in diameter (meridian in direction SW-NE). The sample has been annealed at 175 °C for 2h in an inert atmosphere to induce alignment of the polymer chains. (B) X-ray diffraction pattern of a fiber drawn from the same polymer and annealed subsequently at 170 °C for 4 h.

Most importantly, the experimental results suggest a 5/q helical conformation of the polymer. From accessible diffraction data alone, the prima-facie choice of parameter q of the 5/q helix would be $q = 1$. However, molecular orbital (MO) calculations and molecular modelling performed to yield information on the geometry of the PF repeating unit, chain conformation and the S_0-S_1 transition energy are more in favour of $q = 2$. Figure 4. 1. 4 shows the molecular modelling results of 5/q helices of PF with $q = 1, 2$, based on RHF/6-31 G calculations of bi-and terfluorene.[9] The projected monomer lengths resulted to be 8.09 Å for $q = 1$ and 8.38 Å for $q = 2$, which were both in accordance with the length of the *c*-axis of the unit cell divided by 5. But, in contrast to the 'helical' shape of the 5/1 helix, the 5/2 helix has a more 'linear' shape in which the orientation of the individual monomer units deviates only slightly from the main trajectory of the backbone. Further support for the 5/2 helix structure came from the torsional angle dependence of the electronic transition energy. The torsional angle between neighboring monomers is about 72° in the case of a 5/1 helix, compared to about 144° in the case of a 5/2 helix. Therefore, the rather extended conjugation in PF2/6 as evidenced by the absorption and emission properties is in favour of a 5/2 helix.

Figure 4. 1. 4. Molecular Modeling of oligo(25)-fluorene with 5/q helix: (a) q = 1; (b) q = 2. Structures are based on RHF/6-31G calculations of bi- and terfluorene. Ethylhexyl side chains were replaced by hydrogen[9].

The very large dichroic ratio of the orientated **PF2/6** layers in the UV-vis absorption spectra and the large polarization ratio in photoluminescence and electroluminescence spectra can thus be well understood from the rather low viscosity of the metrically hexagonally packed cylindrically shaped polymers in conjunction with the almost linear structure of the proposed 5/2 helix. On the other hand, **PFO** with linear side chains might just present a mixed character in which the bent monomer unit in conjunction with the rotational potential of the backbone favours a cylindrical helical conformation while the linear side chains induce a planar zigzag backbone conformation with higher viscosity. These mixed characteristics could explain the lower degree of orientation of **PFO** and, particularly, of **PF4C12** on alignment PI layers, compared to **PF2/6** or **PF3/5**.

The thermal properties, supramolecular packing, alignment of polyfluorenes with various kinds of side chains were investigated widely, but the structure-properties relationship has not yet been deeply understood. Therefore, the chain-length dependence of the thermal behavior, supramolecular packing and molecular dynamics of monodisperse oligofluorenes as model compounds for polyfluorenes were investigated.

4. 2 Phase Transition Characteristics of Oligofluorenes

Thermal gravimetric analysis (TGA) measurements of all of the oligomers (OF2-OF7) and the polymer (PF2/6) were conducted under a nitrogen atmosphere at 10 K/min heating rate, and the curves are shown in Figure 4. 2. 1. It clearly shows that the fluorenyl dimer start to decompose at about 250°C, while the trimer up to heptamer and polymer decompose above 370 °C.
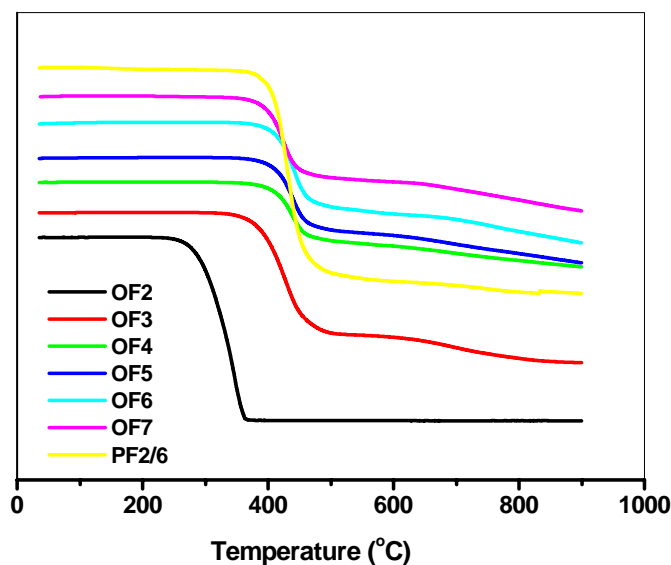
Figure 4. 2. 1. TGA traces of OF2-OF7, and PF measured in a nitrogen atmosphere (heating at 10 K/min).

Differential scanning calorimetry (DSC) measurements were done on a Mettler DSC 30 with a heating and cooling rate of 10 K min^{-1}. The curves of the oligofluorenes and polyfluorenes during the second heating scan are shown in Figure 4. 2. 2 and the transition temperatures are listed in Table 4. 2. 1. From the DSC traces, the glass transitions (T_g) in the low temperature range for all of the oligomers were observed, and followed by an endothermic transition for the tetramer (**45**), the pentamer (**46**), the hexamer (**49**), and the heptamer (**50**) as the temperature was increased. The latter transition with the very small enthalpy (see Table 4. 2. 1) was identified as the transition of the liquid crystalline phase into the isotropic phase (T_{iso}) from the polarized optical microscopic (**POM**) study. The liquid crystalline phase width between glass transition and isotropic transition increased from tetramer to heptamer. PF2/6 exhibits a well-known 'melting' point[10] at about 160 $^{\circ}$C ($\Delta H = -$ 4.77 Jg^{-1}) upon heating, and above this temperature, exhibits a nematic liquid crystalline phase.[7]
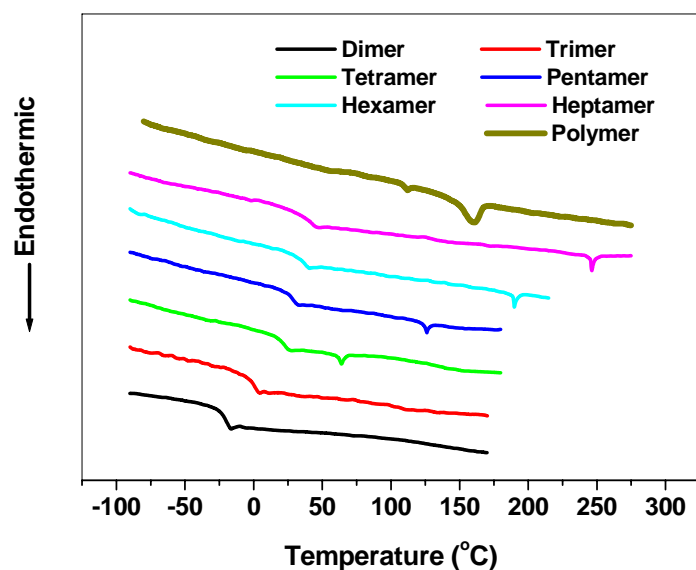
Figure 4. 2. 2. DSC traces (the second heating scan at 10 K/min) of fluorenyl dimer up to heptamer and polymer under a nitrogen atmosphere. In all the oligomers, a glass transition is evident but not in the polymer. Notice also the sharp endothermic peaks in the tetramer, pentamer, hexamer and heptamer due to the LC-to-isotropic transition.

Table 4. 2. 1 Compilation of glass transition temperature (T_g), isotropization temperature (T_{iso}), and enthalpy of isotropization (ΔH_{iso}) for the oligofluorenes.

Sample	T_g (K)	T_{iso} (K)	ΔH_{iso} (Jg^{-1})
Dimer (5)	252		
Trimer (6)	274		
Tetramer (13)	295	337	0.50
Pentamer (14)	301	399	0.47
Hexamer (15)	307	463	0.71
Heptamer (17)	315	519	0.74

A typical Schlieren texture was observed by POM from tetramer to heptamer in the liquid crystalline phase (Figure 4. 2. 3), indicating the liquid crystalline structure to be probably of nematic character, and a further study will be presented in the following part.
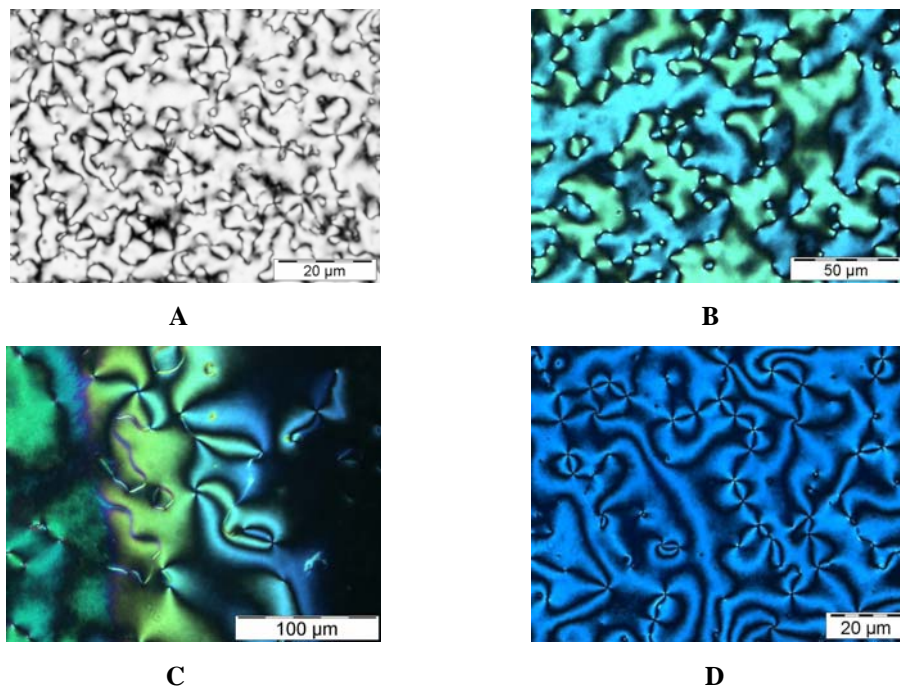
Figure 4. 2. 3. Typical Schlieren textures obtained for tetramer to heptamer during slow cooling (5 K/min) from isotropic phase between two crossed polarizers. (A) tetramer at 40 °C; (B) pentamer at 85 °C; (C) hexamer at 185 °C; (D) heptamer at 100 °C.

A linear relation was obtained between the isotropization point (T_{iso}) and the molar fraction of end groups (X_E) (Figure 4. 2. 4), and a linear fit yielded an equation:

$$T_{iso} = 748.7 - 1679.7 \ (1/n) \tag{4.1}$$

The temperature T_{iso} of the liquid crystalline to isotropic phase transition was extrapolated to a hypothetical T_{iso} ('ideal' polymer) for n→∞ if plotted in the coordinates $T_{iso} = T_{iso}$ (n→∞) (1-K(1/n)) where 1/n is the reciprocal of the number of fluorene units and K is an empirical constant. A T_{iso}(n→∞) = 748.7 K (475.5 ^{o}C) was obtained for infinite polymer and is much above the decomposition range of the high polymer. In this regard, it is important to note that the polymer exhibits a well-known "melting" transition around 160 °C. Above 160° C the polymer exists in a nematic liquid crystal phase; below that temperature another solid phase is formed, the true nature of which is not yet understood. It may be of higher order Smectic type but of such a rigidity of the packing that a transition to a glassy state is suppressed. Whether this substantial difference in the phase structure and nature of transitions has consequences for the electrooptical properties of these materials

needs further studies. Most importantly, the oligofluorenes do not show the same high-order phase the polymer exhibits below the melting temperature of ca. 160 °C.
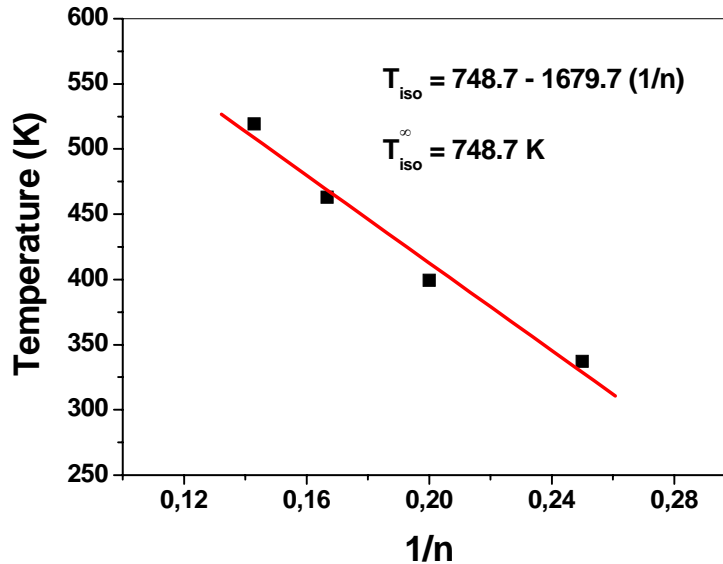
Figure 4. 2. 4. Plot of melting point (T_{iso}) versus the reciprocal of the number of fluorene units (1/n), T_{iso}^{∞} can be obtained from the linear fit. (T_{iso}^{∞} = 748.7 K).

The glass transition temperatures, listed in Table 4. 2. 1, tend to level off as the chain length increases, exhibiting n^{-1} dependence:

$$T_g = 337.0 - 174.7 n^{-1}.$$
(4. 2)

Therefore, the extrapolated T_g for the polymer is estimated to be ca. 337.0 K (64 °C). The occurrence of this glass transition is difficult to see in the DSC curves for the polymer (see Figure 4. 2. 5). The similar extrapolated T_g at 332±2 K for polymer is also obtained from dielectric spectroscopy investigation.
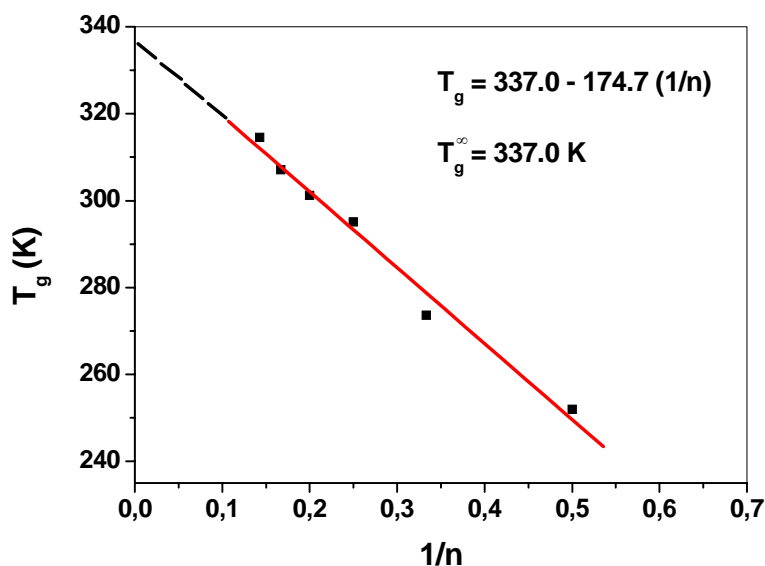
Figure 4. 2. 5. Plot of glass transition (T_g) versus the 1/n (n is the number of fluorenyl units), T_g^{∞} can be obtained from the linear extrapolation. (T_g^{∞} = 337.0 K)

4. 3 Molecular structure and supramolecular packing

To study further the structure and supramolecular packing of the oligofluorenes, wide angle X-ray scattering (WAXS) was performed of powder and aligned fibers. Moreover the single-crystal structures of several oligofluorene derivatives were also obtained to support and supplement further the results.

4. 3. 1 The powder X-ray diffraction

A Debye camera was used to record the powder X-ray diffraction pattern. Only one reflection (d = 8.05 Å) and a halo were observed for the higher oligomers (OF4-OF7). The reflection is correlated to the length of a fluorenyl unit. The powder X-ray diffraction patterns of the tetramer up to heptamer using a Kiessig camera are shown in Figure 4. 3. 1; the data are compiled in Table 4. 3. 1. The diffraction patterns are similar for all of oligomers (OF4-OF7) beside the little differences in orientational order (Figure 4. 3. 1a) and show two distinct reflections and a halo. The outer diffraction circle (d = 8.05 Å) is

correlated to the monomer length, and the inner diffraction circle (d = 14.7 Å) is correlated to the intermolecular distance (Figure 4. 3. 1b). The reflection is inhomogeneous for short chain oligomers, such as tetramer. The outer reflection shows some sampling in meridional direction and the innermost reflection in equatorial direction. This indicates the tetramer

Tetramer - RT   **Pentamer - RT**   **Hexamer - RT**

Annealed from 60 ºC to

40 ºC for 70 h

Heptamer - RT   **Heptamer annealed from 60 °C to**

40 °C for 70 h

Figure 4. 3. 1a. Powder X-ray diffraction of tetramer up to heptamer by Kiessig camera.

Figure 4. 3. 1b. The analysis of the powder X-ray diffraction pattern.

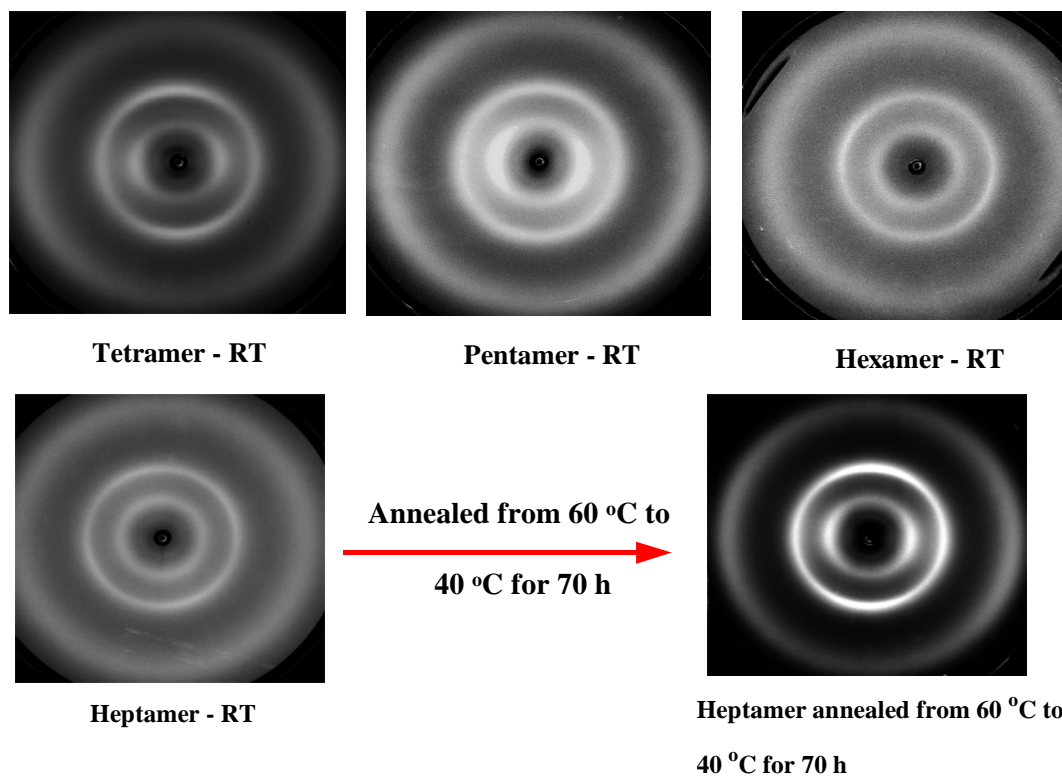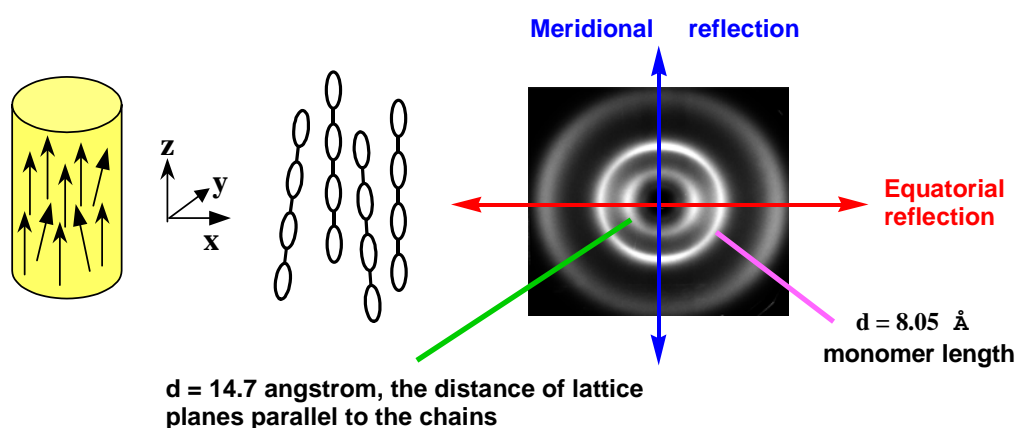molecules to be oriented slightly according to a distinct direction in the capillary under gravity (gravitational force) because the liquid crystalline phase exists at room temperature due to its low glass transition. With the extension of the molecular chain-length to hexamer and heptamer, the inhomogeneous diffraction circles change gradually to homogeneous, indicating a lack of orientation. When the heptamer was heated to 60 $^{\circ}$C into the liquid crystalline phase, and then annealed from 60 $^{\circ}$C to 40 $^{\circ}$C, inside the capillary the sample was preferentially oriented.

Powder X-ray diffraction patterns of the oligomers were also recorded on flat film in liquid crystalline phase (Table 4. 3. 1). Similarly two diffraction circles were observed, and the d-value was slightly smaller than that at room temperature. The d-value 8.05 or 8.02 Å is probably a superposition of a meridional reflection and a packing reflection as is seen in the fiber patterns. Therefore the change to 7.8 Å as a function of temperature is a superposition and does not tell anything about a change of the meridional reflection

Table 4. 3. 1 The data of powder X-ray diffraction patterns from tetramer up to heptamer.

	RT, Debye （Å）	RT, 100mm Kiessig Kamera（Å）	T>RT, Flat film （Å）
Tetramer	d = 8.05 Å	8.02, 14.7	7.8, 13.7
Pentamer	8.05	8.02, 14.7	7.8, 13.7
Hexamer	8.05	8.02, 14.7	7.8, 13.7
Heptamer	8.05	8.02, 14.7	7.8, 13.7

4. 3. 2 The 2D WAXS of extruded fibers

The fibers of the series of oligomers were mechanically extruded by a mini-extruder in the liquid crystalline phase. Polymer fiber was drawn above the "melting point" of 170°C. The incident X-ray beam was perpendicular to the fiber axis and a two-dimensional scattering pattern was then recorded in a Kiessig camera.
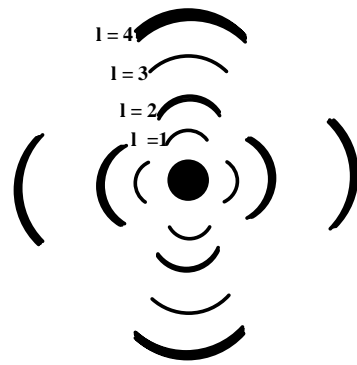
(a) Tetramer fiber (extruded at 40 ^{o}C)
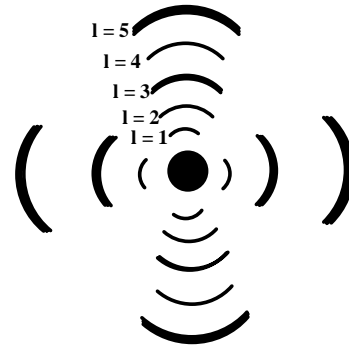
(b) Pentamer fiber (extruded at 70 ^{o}C)
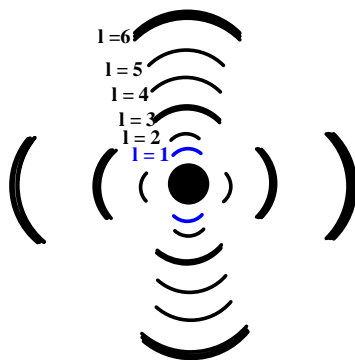
(c) Hexamer fiber (extruded at 75 ^{o}C)
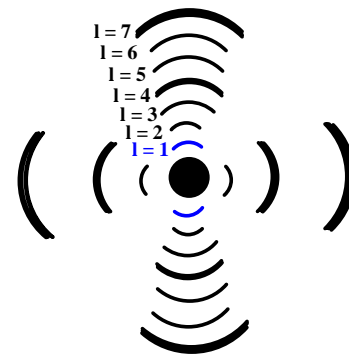
(d) Heptamer fiber (extruded at 85 ^{o}C)
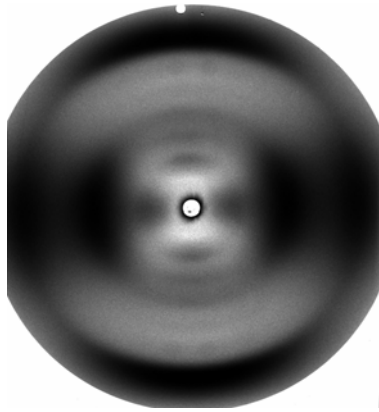
(e) The experimental X-ray diffraction
pattern for the heptamer.
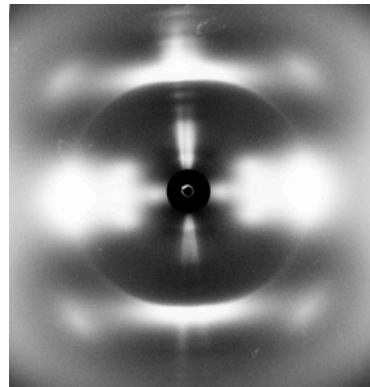
(f) The experimental X-ray diffraction
pattern for PF2/6

*Figure 4. 3. 2. 2D sketches of X-ray diffraction patterns of tetramer to heptamer and Kiessig diffraction patterns for heptamer and **PF2/6**.*

The 2D X-ray scattering patterns for tetramer up to heptamer and PF2 /6 are shown in figure 4. 3. 2. and their d-value were compiled in table 4. 3. 2. Some reflections in the meridional direction were weak, so the patterns from figure 4. 3. 2 a-d were drawn from Chemdraw according to the experimental patterns, and a real experimental pattern of the heptamer is shown in figure 4. 3. 2e for the comparison with the drawn pattern.

Table 4. 3. 2. The d-value of 2D X-ray diffraction of tetramer up to heptamer and polymer.

Tetramer (Å)	Pentamer (Å)	Hexamer (Å)	Heptamer (Å)	Polymer (Å)	
28.07	39.22[a]	49.02[a]	56.85[a]	11.6	
15.87	30.86	25.73	28.45	10.2	
10.71	19.32	16.28	19.04	9.2	
8.02	14.40	12.05	14.4	8.02	Sequence of
	10.11	9.70	11.50	7.04	(weak)
	8.07	8.02	9.8	6.44	meridional
			8.02	5.97	reflections
				5.52	
				4.64	
				4.24	
				4.05	
30.86[b]	30.86[b]	30.86[b]	30.86[b]		Sequence
14.40	14.40	14.40	14.40	14.34	of
8.31	8.31	8.31	8.31	8.33	equatorial
halo:	halo:	halo:	halo:	4.17	reflections
$(2\theta = 20.56^{o})$	$(2\theta = 20.56^{o})$	$(2\theta = 20.56^{o})$	$(2\theta = 20.56^{o})$		
				5.86	Off meridional reflection on the 5 th layer line

[a]: the value was obtained from Figure 4. 3. 3. by linear extrapolation; [b]: the d-value of 30.86 Å was obtained from the same diffraction d= 14.40 Å with the X-ray tube run at higher voltage to decide whether the intensity arises from the peak in the Brems-spectrum.

From all of fiber X-ray diffraction patterns for tetramer up to heptamer similar reflections were observed on the equator, and based on the relation of the d-values ($1:\sqrt{3}$), a hexagonally ordered packing can be assumed. For the meridional reflection, the fourth, fifth, sixth, seventh-order reflections can be observed as strong reflection for tetramer, pentamer, hexamer, and heptamer respectively, and the d-values of these reflections were compiled in Table 4. 3. 2. The strongest meridional reflection is for all oligomers OFn, the reflection the d-value of which corresponds to the length of a fluorene moiety, i.e. 8.05 Å. It is, however, the reflection of n-th order for OFn (see Fig 4. 3. 3). For both the hexamer and heptamer the 1st order cannot be detected over the background. From the plot in fig 4. 3. 3, its position can be estimated. The d-value of the first order in every meridional reflection pattern was related to the whole molecular length, and other d-values of the reflections are approximately the 1/2, 1/3 ⋯⋯ 1/n of the whole molecular length.
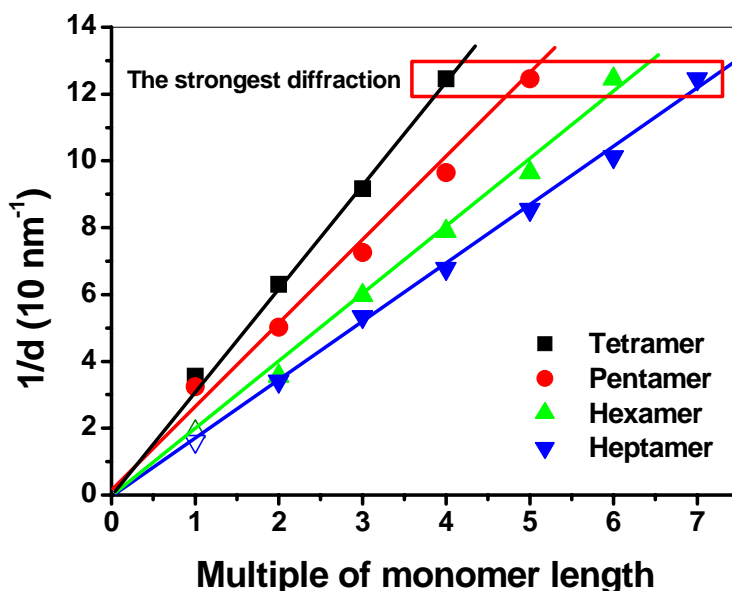
Figure 4. 3. 3. The position of meridional reflections of the oligofluorenes. The strongest meridional reflection is the 4th, 5th, 6th, 7th orders of a basic reflection for tetramer to heptamer, respectively.

The conclusions which can be drawn : 1) the chains are packed in lamellar ≡ smectic B or higher order; 2) no axial shift disorder exists because no continuous layer lines; 3) side chains are not ordered ⇒ no additional reflection due to alkane packing (high background due to scattering of amorphous material).

Based on above X-ray diffraction patterns, a smectic packing model (Figure 4. 3. 4a) was proposed and a simulation of X-ray diffraction pattern was conducted by Cerius2 software based on this model for tetramer up to heptamer (Figure 4. 3. 4b). For example, for heptamer, a hexagonal packing was built in the a, b-plane, and a layer-like packing model was built along "c" axis, i.e., that is along the molecular axis. A unit cell with a = b = 16.7 Å, c= 56.85 Å (related to the molecular length), $\alpha = \beta = 90^o$, $\gamma = 120^o$ was then figured out. The molecular conformation of the heptamer was first optimised by energy minimization, and the helix-like conformation is shown in Figure 4. 3. 5. The calculated length of the molecule based on molecular models was 59.2 Å, a value significantly larger than that obtained from the fiber X-ray diffraction pattern. This discrepancy could be reconciled by assuming that the backbone packs at an offset angle of roughly 15° with respect to the layer normal. The simulated X-ray diffraction pattern shows a similar reflection pattern to that obtained by the experiments with more resolved reflections, and especially the meridional reflections are very similar to the experimental values (Figure 4. 3. 4b): the 7th order is strongest, and the 1st order is too weak to be observed.
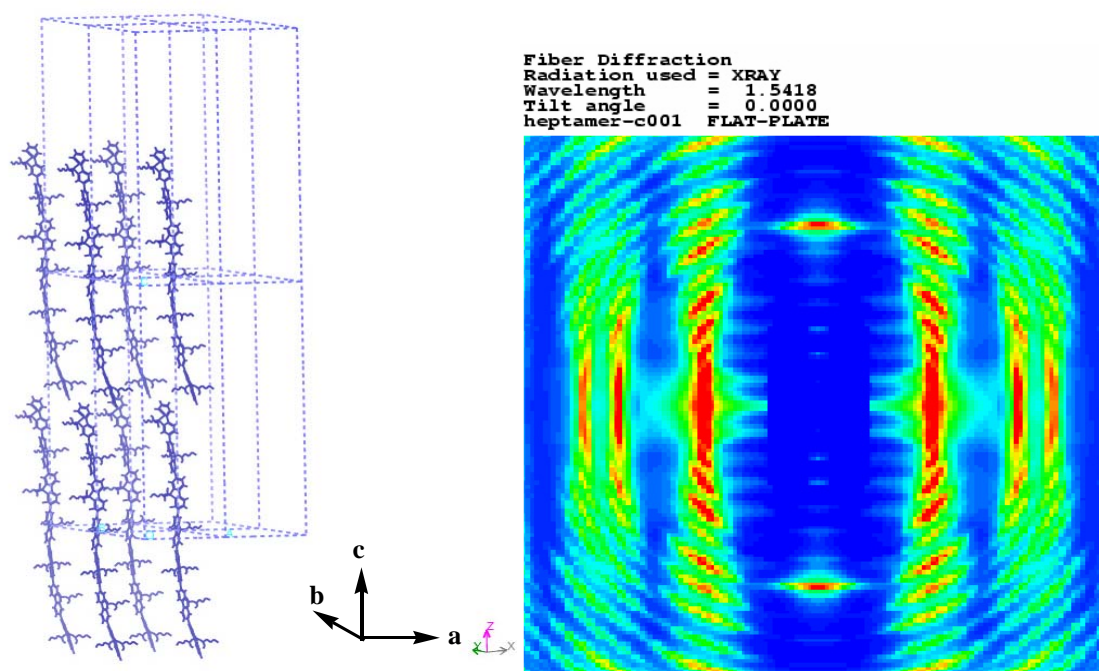
Figure 4. 3. 4 a) a smectic model for heptamer; b) the simulated 2D X-ray diffraction pattern by Cerius2 software.
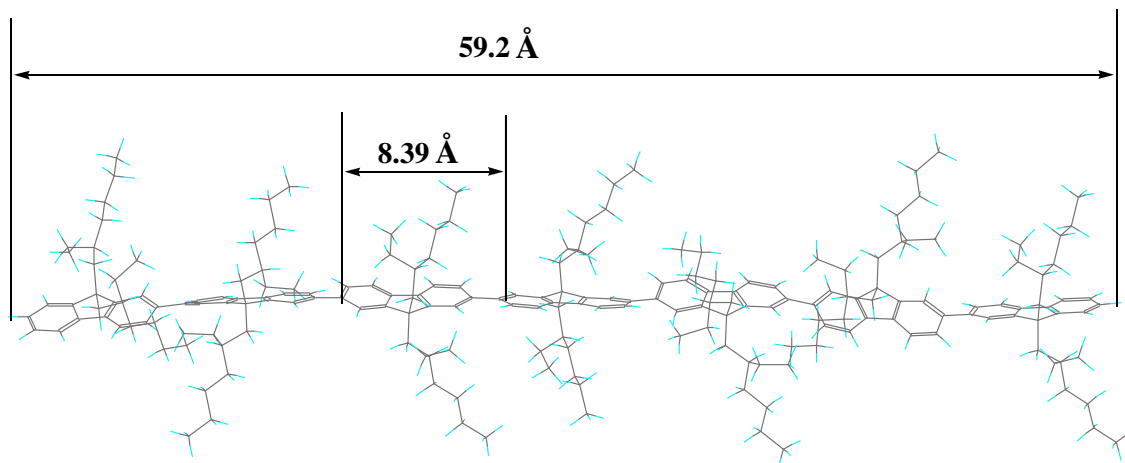
Figure 4. 3. 5 the optimized helix-like conformation for OF7 by energy minimization, and the torsional angle between neighboring monomers has no big difference with the result from single crystal structure which will be shown in next part of this chapter.

Figure 4. 3. 4a shows one molecule in the unit cell. With the molecular mass of 2722 g/mol and Z = 1 a crystallographic density of $\rho = 0.33$ g/cm^3 was calculated. For organic small molecules and polymers, the crystallographic density is usually around 1 g/cm$^{3, 11}$. The observation that a fiber or film from tetramer up to heptamer sink down in 2-propanol at room temperature ($\rho = 0.979$ g/cm^3) determines a lower limit for the density. The crystallographic density would be 0.99 g/cm^{-1} if we put three molecules into the unit cell (Z = 3), without change of the simulated diffraction pattern like Figure 4. 3. 4b except for the change of the intensity. The most probable choice in view of the limited number of data is therefore a unit cell of the trigonal crystal system with space group *P3*.

To the tetramer, pentamer, hexamer, the same helix-like conformation was obtained by optimising with energy minimization and the same unit cells with Z = 3 were built with the c-parameter adapted to the molecular chain length. The molecular conformation and their packing structures are further supported by the single-crystal structures of the oligofluorene derivatives as shown in the following part.

4. 3. 3 The single-crystal structures

The growth of single crystals of homo-oligofluorenes with 2-ethylhexyl side chain was found to be very difficult after attempts by various methods due to inherent disorder. However, single crystals of their derivatives such as diboronic fluorene, dibromo fluorenyl dimer and fluorenyl pentamer with one fluorenone unit could be obtained, and some helpful information for homo-oligomers can be deduced by the single-crystal structural analysis of these oligofluorene derivatives.

4. 3. 3. 1 Diboronic fluorene monomer

Single crystal of the diboronic monomer (Scheme 4. 3. 1.) was obtained by slow evaporation of a solution of a mixture of ethanol and a small amount of dichloromethane. Suitable single crystals were mounted into glass capillaries. The data collection was carried out at 120 K. Pertinent crystallographic data are summarized in Table 4. 3. 3. The single-crystal structures were solved by direct methods using the program Shelx91. The projection of the fluorene backbones is shown in figure 4. 3. 6.

40
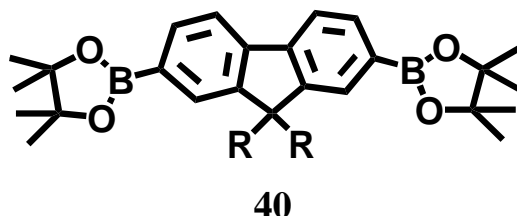
Scheme 4. 3. 1.The molecular structure of diboronic fluorene monomer

In the process of producing models for the refinement it turned out that the ethylhexyl side groups are disordered. This is a natural consequence of the fact that this group is chiral, but had been used as a racemic mixture in the chemical synthesis. This is why the exact coordination of atoms in the side groups could not be obtained in some cases.

As shown in the figure 4. 3. 6a, the fluorene moiety is nearly planar and the substitute at the 9-position extend above and below that plane and away from the fluorene group. One aliphatic chain is ordered, and another one is disordered (see figure 4. 3. 6b). For the disordered side chain, the ratio of R, S, is 50% respectively, and the same atom was used

for the two conformations of 2-ethylhexyl side-chains (Figure 4. 3. 7). The three-dimensional packing structure is shown in figure 4. 3. 6c. We can see that two molecules form a face-to-face packed dimer structure with a *van der Waals* distance of 3.4-3.6 Å. Preliminary data for the triclinic unit cell (P$_1$) of molecule **40** are summarized in Table 4. 3. 3. The unit cell parameters are : a = 12.5Å, b = 13.1 Å, c = 13.17 Å; α = 108.2°, β = 92.6°, γ = 102.3°, and there are two molecules in one unit cell (Z = 2).
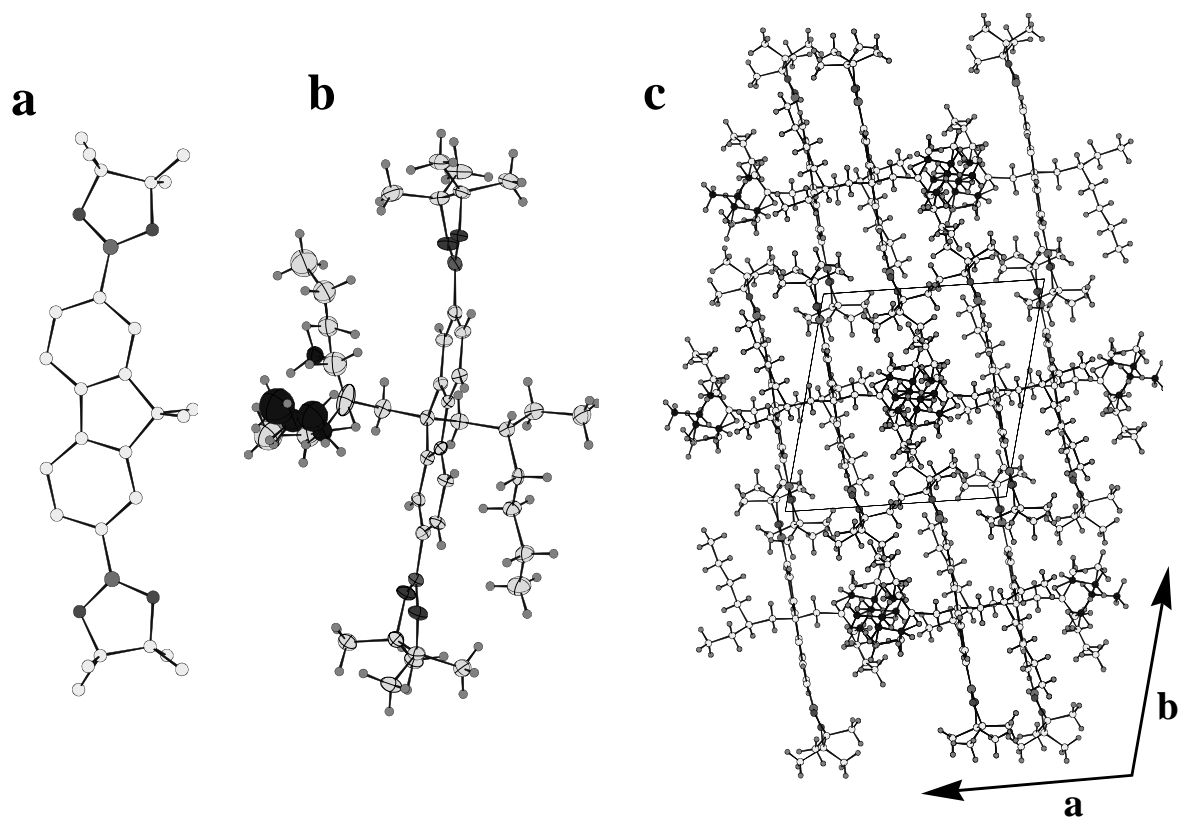
Figure 4. 3. 6. The molecular conformation of diboronic fluorene monomer. a) shown without the aliphatic side-chains; b) shown with the aliphatic side chains and c) the 3D packing structure.
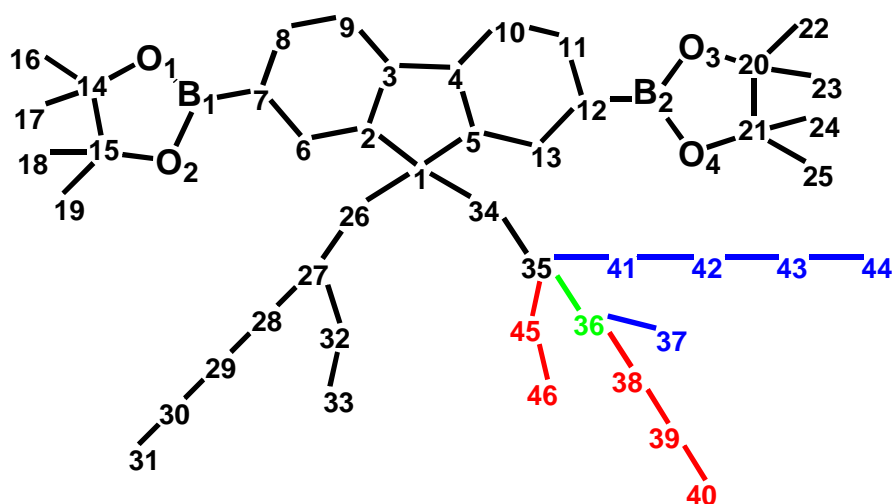
Figure 4. 3. 7. The structure of diboronic fluorene (40). One aliphatic chain is ordered, and another one is disordered. For the disordered side chain, the ratio of R, S, is 50%, respectively, and the same atom (36) was used for the two conformation of 2-ethylhexyl side chain.

Table 4. 3. 3. Summary of the pertinent crystallographic data of the compounds 40, 47, 53

	Bisboronic monomer (**40**)	Dibromo dimer (**47**)	Pentamer with one fluorenone unit (**53**)
a (Å)	12.5327 (5)	13.0864 (6)	23.3964 (8)
b (Å)	13.1166 (5)	13.8647 (6)	19.0660 (7)
c (Å)	13.1714 (6)	15.0723 (7)	24.3245 (8)
α (°)	108.1961 (13)	85.6071 (12)	90
β (°)	92.6247 (12)	71.6985 (13)	94.8980 (15)
γ (°)	102.3195 (13)	83.8922 (12)	90
V (Å^3)	1994.8 (3)	2578 (1)	10810.9 (11)
Z	2	2	4
D$_x$ g/cm^3	1.058	1.02	1.15
Unique reflections	9022	8793	14832
Observed reflections	2238	1934	1247
Space group	P-1	P-1	P2$_1$/c
Temperature (K)	120	120	150

4. 3. 3. 2 Dibromo fluorenyl dimer

A single crystal of the dibromo dimer (**47**, Scheme 4. 3. 2) was obtained by slow evaporation from a solvent mixture of hexane and dichloromethane. Suitable single crystals were mounted in glass capillaries. The data collection was carried out at 120 K. Pertinent crystallographic data are summarized in Table 4. 3. 3 and the crystal structure is shown in figure 4. 3. 8.

47
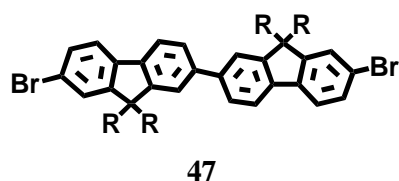
*Scheme 4. 3. 2.The molecular structure of dibromo dimer (**47**).*
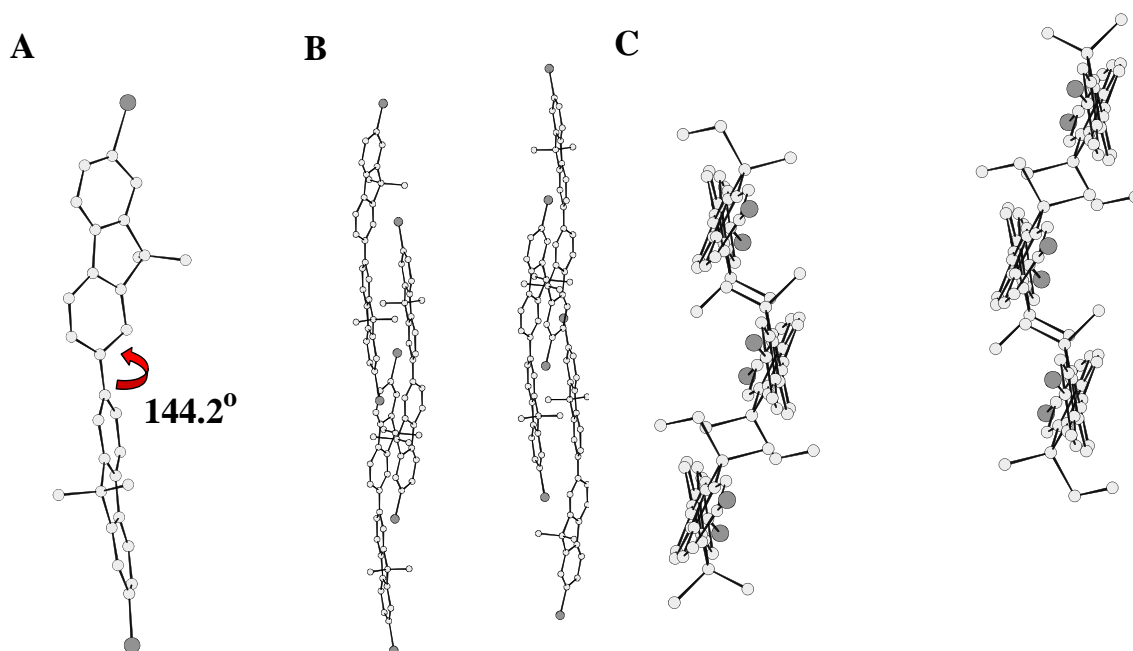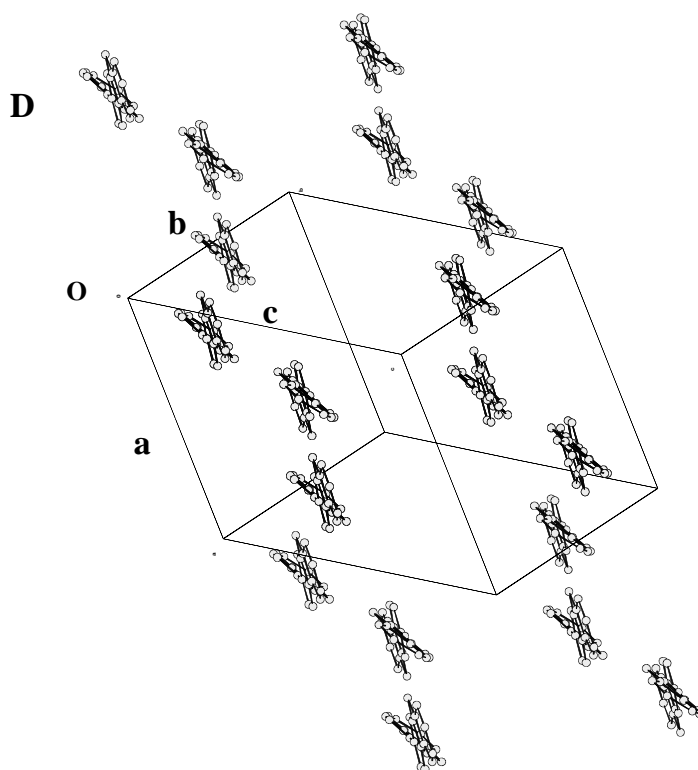
*Figure 4. 3. 8. The single-crystal structure of dibromo fluorenyl dimer (**47**). A) shown without the aliphatic side-chains; B) the 3D packing structure; C) the 3D packing structure projected along the molecular axis; D) the 3D packing as related to the unit cell.*

As mentioned above, the exact coordinates of atoms in the disordered side groups could not be obtained. So, we analyzed the single-crystal structure of the dibromo dimer without considering the side-chains.

For the dibromo dimer, the twist angle between two fluorene units is 144.2° (Figure 4. 3. 8A). This is a very important information for homo- oligofluorenes, and is in agreement with the torsional angle between neighboring monomers for polyfluorenes, which is about 144° in the case of a 5/2 helix[9]. The molecules show the layer-like packing structure (Figure 4. 3. 8B-D), and in each layer, the molecules are packed by head-to-tail mode and the side chains tend to pack together in the space between the layers. The distance between the two layers is approximate 13.9 Å, and in each layer, the two molecules pack with a *van der Waals* distance of 3.4-3.6 Å. Figure 4. 3. 8C, D show the three-dimensional packing structure which was observed along the molecular axis.

The space group for the molecule is triclinic, and the preliminary data for the unit cell are: a = 13.09 Å, b = 13.86 Å, c = 15.07 Å; α = 85.61°, β = 71.70°, γ = 83.89°, with two molecules in the unit cell (Z = 2).

4. 3. 3. 2 Pentamer with one fluorenone group

Single crystal of the pentamer with one fluorenone unit was obtained from a dichloromethane solution by slow diffusion of ethanol. Suitable crystals were mounted in glass capillaries. The data collection was carried out at 150 K. Pertinent crystallographic data are summarized in Table 4. 3. 3.

In the pentamer the disorder of side chain led to the fact that the ratio of observed to possible reflections is very low (approx 10%), so only the structure of the backbone will be discussed. The structure of the backbone is shown in Figure 4. 3. 9A. It can be seen that here also a helix-like conformation is observed with rotation angles near 140°. However, this conformation is disrupted in the vicinity of the fluorenone group. Here, between the ring 3 and ring 4 the rotation is reversed. One reason may be the polarity of the fluorenone group. Also, it is known that polyfluorenes with non-branched side chains adopt an almost planar zig-zag conformation[8]. As to the two fluorene rings of the end group, i.e. the first and fifth unit, they have similar twist angles of +141.7° and +144° around the second and fourth fluorene units, respectively. This twist angles are also similar with those in the dibromo dimer, further supporting that the twist angle is approximately 144° in homogeneous oligofluorenes.
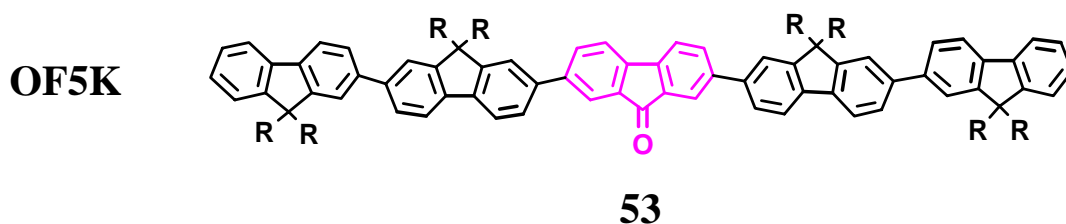
*Scheme 4. 3. 3. The molecular structure of pentamer with one fluorenone unit (**OF5K**).*
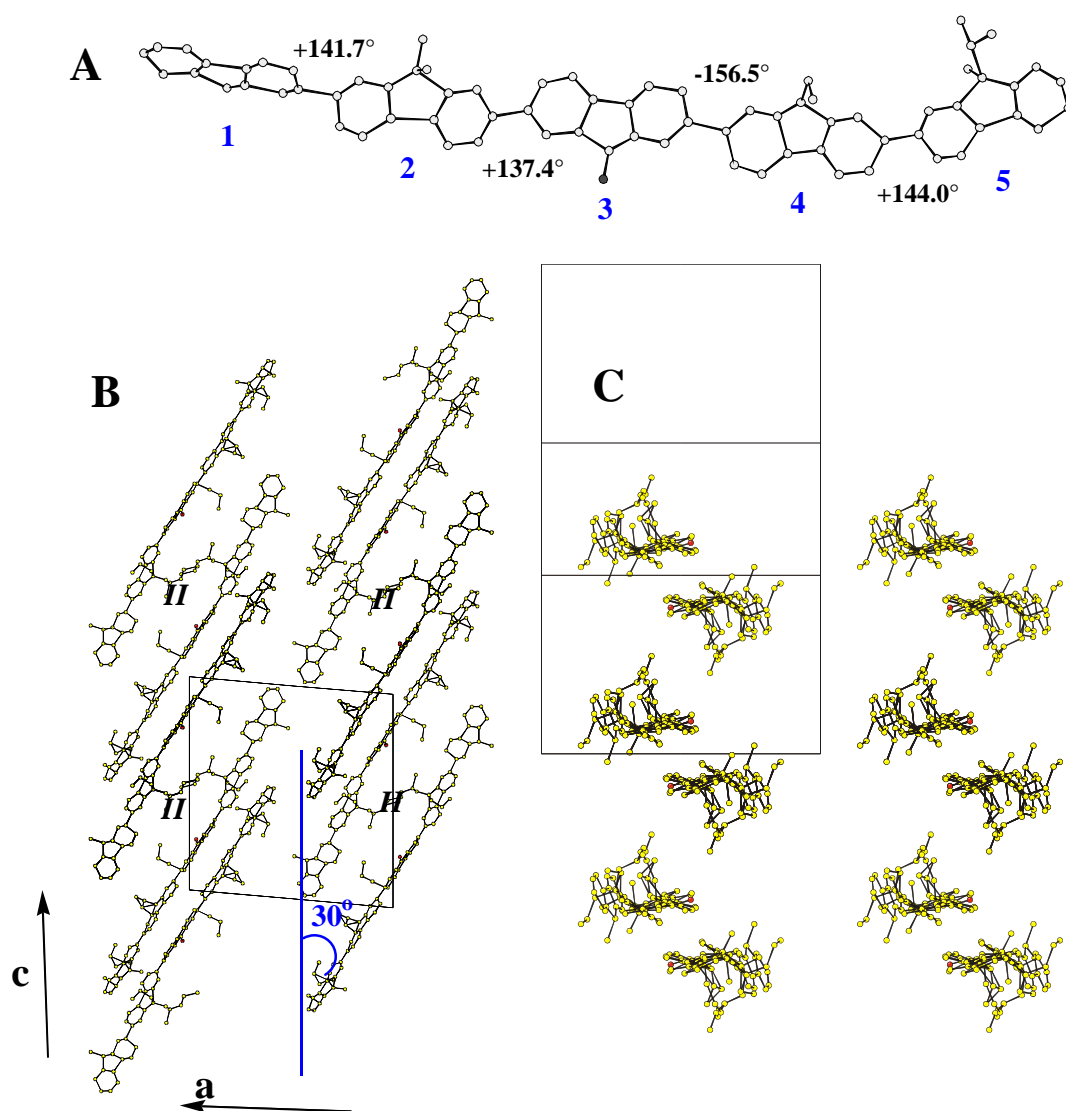
Figure 4. 3. 9. The single-crystal structure of pentamer with one fluorenone group. A) shown without the aliphatic side-chains; B) the 3D packing structure; C) the 3D packing structure projected along the molecular axis.

The three-dimensional packing mode is shown in figure 4. 3. 9B, C. For OF5K, a layer-like smectic packing mode was obtained. In each layer, the angle of inclination of the molecules is 30° with regard to the c-axis. Two molecules form a centra-symmetric structure due to the interchain dipolar-dipolar coupling interaction with a *van der Waals distance* of 3.5-3.6Å. Most of the aliphatic chains tend to pack in the space (symbol "II" area in Figure 4. 3. 9B) between the two symmetry related molecules. The 3D packing

mode of OF5K further supports that the higher homo-oligofluorenes are likely packed according to a similar smectic model.

Preliminary data for the monoclinic unit cell ($P2_1$/c) of molecule **53** are: (Table 4. 3. 3): a = 23.40 Å, b = 19.07 Å, c = 24.32 Å; α = 90°, β = 94.90°, γ = 90°, Z = 4. The crystallographic density is ρ = 1.15 g/cm^3.

The X-ray fiber diffraction pattern of OF5K is shown in Figure 4. 3. 10, and the d-values are compiled in Table 4. 3. 4. The five meridional reflections and two equatorial reflections are observed. Similarly to homo-oligofluorenes, the 41.14 Å is correlated to the molecular length, and the 8.04 Å is correlated the monomer length. The molecular conformation was optimised by energy minimization. (Figure 4. 3. 11), and that is very similar with the result from single crystal analysis.

Similar reflections are observed on the equator, and based on the relation of the d-value ($1:\sqrt{3}$), a hexagonal type packing can be concluded. If a smectic type packing and a unit cell is built like Figure 4. 3. 5a except for c = 41.14 Å (the molecular length), that means the lamellar thickness is almost equal to the molecular length, but the *d*-value for 2nd layer line should be c/2 = 20.6 Å. It is unreasonable to get this value at d = 26.85 Å. Therefore, a unit cell with a = b = 16.7 Å, c= 82.28 Å (related to the two molecular lengths), α = β = 90°, γ = 120° was then figured out. For this structure consisting of bilayers the meridional reflection can be indexed as 41.14 (00.2), 26.85 (00.3), 14.70 (00.6), 10.04 (00.8), 8.04 (00.10). The molecules are oriented along the "c" axis of the unit cell (Figure 4. 3. 12). The direction of the red arrows represents the vector direction of the dipole moment in each layer, and the vector direction is reverse for the two single layers in each double layer, so the repeat double layers are stabilized by dipolar-dipolar interaction between neighboring two single layers. The blue and pink arrows represent the direction around which the repeat units rotate with regard to the neighboring unit (Figure 4. 3. 12). The values for these rotations are taken from the single crystal structure analysis of OF5K (Figure 4. 3. 9A). Here the fluorenone group in the center of the molecules causes a disruption of the helix-like conformation. If one assumes a head-to-head or tail-to tail arrangement in the double layer the distance of this perturbation of the conformation is approximately 1/3 of the total layers thickness. This explains the observation of the 00.3 reflection. The calculated length of the molecule based on molecular models is 42.3 Å, a value slightly larger than that obtained from the fiber x-ray diffraction pattern. This discrepancy can be reconciled by

assuming that the backbone packs at an offset angle of roughly 14° with the respect to the layer normal.
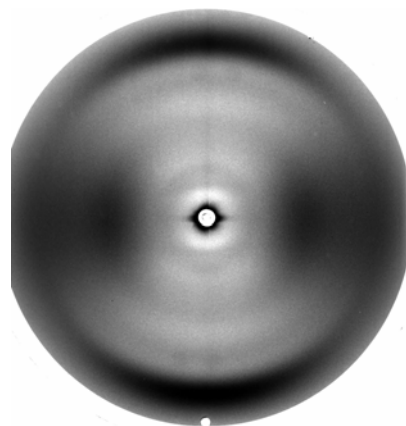
*Figure 4. 3. 10. The X-ray diffraction pattern for pentamer with one fluorenone group (**OF5K**).*
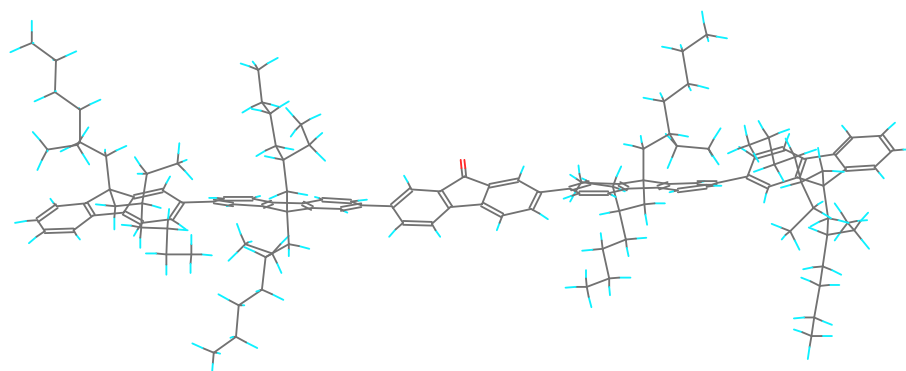
*Figure 4. 3. 11. The optimised helix-like conformation for **OF5K** by energy minimization*

*Table 4. 3. 4 The d-values derived from 2D X-ray diffraction patterns of the pentamer with one fluorenone group (**OF5K**).*

Sequence of equatorial reflections (Å)	Sequence of meridional reflections (Å)[a]
14.07	41.14 (00.2)
8.04	26.85 (00.3)
	14.70 (00.6)
	10.04 (00.8)
	8.04 (00.10)

[a]*: For the meridional reflections: 41.14 Å is related to molecular length.*

The analysis of the fiber X-ray diffraction pattern for OF5K shows that the supramolecular packing in the extruded fiber is different from the single crystal structure of crystals obtained from solution.
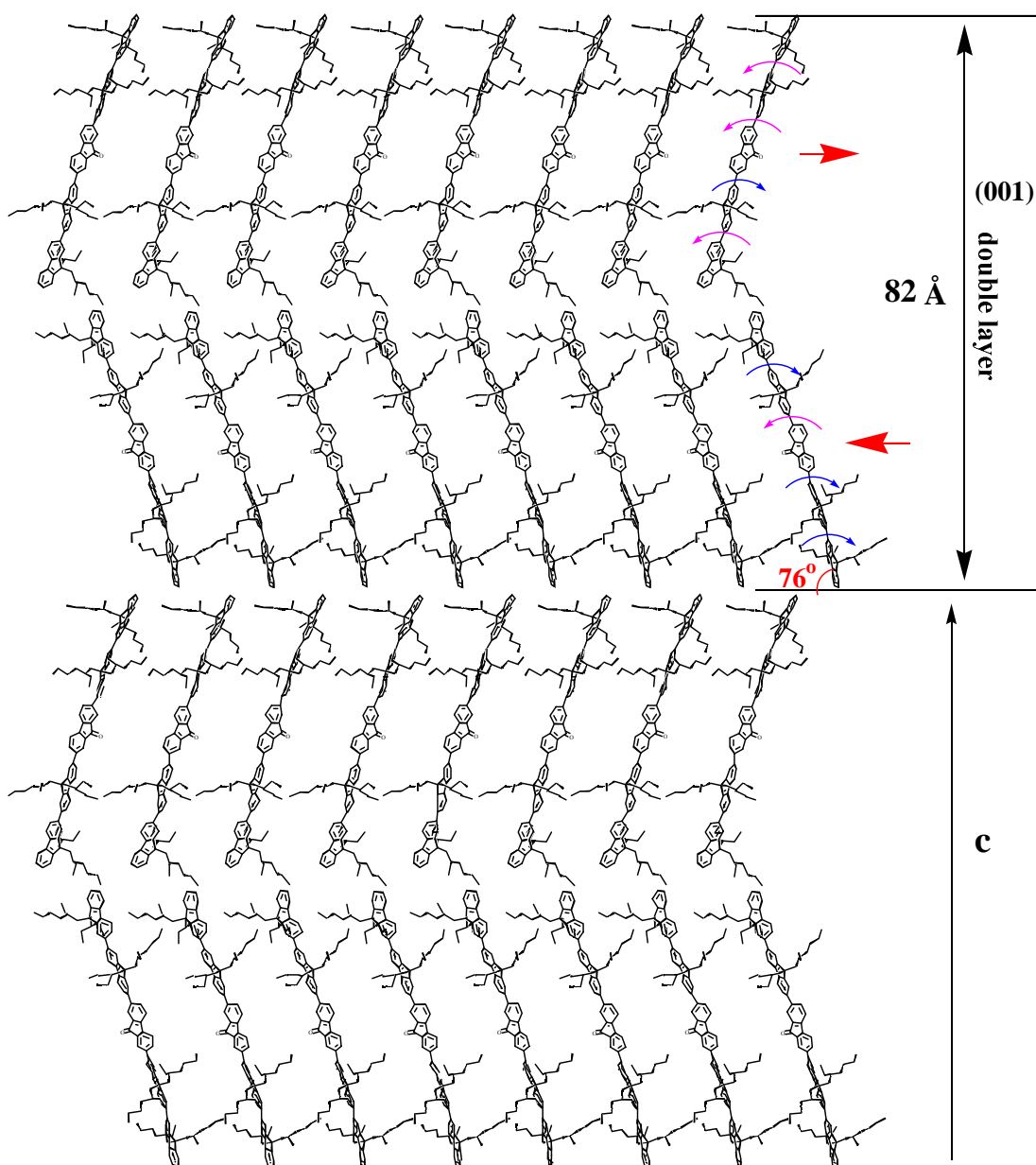
*Figure 4. 3. 12. Schematic diagram of the packing of **OF5K** drawn into fibers; the direction of the red arrows represent the vector direction of the dipole moment in each layer. The blue and pink arrows represent the directions around which the repeat units rotate with regard to the neighboring unit.*

4.4 Alignment on a rubbed polyimide (PI) substrate

The application of organic material as active materials in backlights for LCDs requires high degree of polarization of the emitted light which is achieved by a high degree of molecular alignment of the chromophores. There are numerous methods to achieve such orientation, and in the following part, a general introduction to the formation of alignment layers will be first described.

4. 4. 1 A general introduction to the formation of alignment layers

4. 4. 1. 1 Quantitative description of molecular orientation-order parameter, polarization ratio and dichroic ratio

The degree of molecular orientation is commonly quantified by means of the orientational order parameter S, a single scalar quantity describing the spread of a molecular axis about the director (overall axis of preferential orientation), with a large value of S implying a small spread. Properly speaking, this term-originating from Landau's theory of phase transitions[12]- should be applied only to anisotropic systems that are in the thermodynamic equilibrium, but it is used in the literature for any aligned state of anisotropic molecules. Marrucci *et al*. reduced the three-dimensional problem[13] to its two-dimensional analogue and defined the order parameter in two dimensions by:[14]

$$\text{S} \equiv 2 < \cos^2\theta > -1 = <\cos 2\theta> = \int_0^\pi f(\theta)\cos 2\theta\, d\theta \qquad (4.3)$$

Where $f(\theta)$ is the normalized distribution function of the main chain orientation, i.e. the probability of a molecule being oriented with an angle θ to the director ($f(\theta)$) is large around $\theta = 0$ or π but is small for $\theta \approx \pi/2$). This definition ensures the order parameter becomes zero in the isotropic case and unity in the fully aligned case.

By means of the order parameter of the emitters, an upper limit of the achievable polarization ratio P can be estimated using the following relation:

$$P \leq \frac{1+S}{1-S} \qquad \text{or} \qquad S \geq \frac{P-1}{P+1} \qquad (4.4)$$

where the polarization ratio is defined as the ratio of the emitted light intensity parallel (I_{pl}) and perpendicular (I_{pp}) to the molecular alignment:

$$P = \frac{I_{pl}}{I_{pp}} \qquad (4.5)$$

These inequalities are also valid when replacing the polarization ratio *P* by the *dichroic ratio D* yielding:

$$D \leq \frac{1+S}{1-S} \qquad \text{or} \qquad S \geq \frac{D-1}{D+1} \qquad (4.6)$$

where the dichroic ratio is the ratio of the absorbance parallel (A_{pl}) and perpendicular (A_{pp}) to the molecular orientation:

$$D = \frac{A_{pl}}{A_{pp}} \qquad (4.7)$$

From relation (4.4) one can estimate that for a polarization ratio of P = 20 an order parameter of at least S = 0.9 is required, stressing the need for high degree of orientation.

An exact calculation of the order parameter using the measurable polarization (dichroic) ratio R is only possible with the knowledge of the angle α between the emission (absorption) dipole and the molecular symmetry axis, using the relation:[15]

$$S = \frac{R-1}{R+1}(1-2\cos^2\alpha) \qquad (4.8)$$

Furthermore, for an accurate calculation, anisotropic internal fields should be considered as well as surface reflection due to birefringence of the light entering or leaving the film.[16] This difficulty is often ignored, and in order to be more exact in the following, the degree of molecular orientation will be described only in terms of the dichroic ratio D (in the case of absorption) and the polarization ratio P (in the case of emission).

4. 4. 1. 2 Alignment methods

Efforts focused on the development of polarized EL emission devices have used stretch-aligned, [17] rubbing-aligned, [18] and Langmuir-Blodgett (LB) [19] deposited polymers, or specifically synthesized liquid crystalline (LC) polymers.[20]

Polymers can be aligned by means of a number of mechanical methods, the first of which is orientation by *stretching*. Polarized electroluminescence realized by this technique was first reported by Dyreklev *et al.*, who obtained a polarization ratio of about 2 from stretch-orientated conjugated polythiophenes. [21] Although in photoluminescence, much higher polarization ratios have been reported, for example from stretch-oriented MEH-PPV (poly(2-methoxy-5-[2'-ethylhexyloxy]-*p*-phenylene-vinylene)), [22] the method of stretch orientation has severe drawbacks. Soft materials are required for elongation but they tend to relax back into an unoriented equilibrium state. This problem may be circumvented by quenching into a glassy or crystalline state after stretching from the soft state (melt or solution),[23] or by drawing a precursor during conversion.[24] For stretch alignment there is a severe difficulty in preparing well oriented films of thickness $\leq 1\mu$m that retain structural integrity. Fibrillation usually occurs at high draw ratios[25] and even at 1μm thickness, and power efficiency is problematic due to the high voltage required in OLED application. Additionally, transferring the film onto a substrate to fabricate a robust device is not straightforward.[15]

A second method of mechanical alignment is the rubbing of conjugated polymer films-a procedure known for two decades from the preparation of alignment layers for liquid crystals-in order to directly obtain polarized emission from the aligned chains without the need for additional alignment layers. To date, the best performance of a device with a directly rubbed polymer emissive layer was achieved with a precursor PPV aligned by rubbing during conversion.[26] A polarization ratio of 12 in electroluminescence was reported. However, due to mechanical damage of the films, controlling the uniformity of film thickness and preventing erosion of the polymer from the substrate is difficult, especially when $\approx$ 100 nm thickness films are used to ensure low voltage drive requirements. The stability and lifetime of such devices is problematic.

LB deposition is well suited to fabrication of very thin films with a well-defined number of molecular layers, and orientation can be achieved by anisotropic compression of the Langmuir layer during the dipping process.[17] There are, however, problems arising from the difficulty in scaling up and speeding up the LB deposition process.

Alignment on particular substrates such as poly(tetrafluoroethylene) (PTFE) was also reported by means of friction transfer technique in 1991.[27] Usually, such an alignment layers is fabricated by squeezing and shearing a PTFE rod on a surface, yielding a molecularly oriented ultra-thin PTFE film with the direction of orientation of the PTFE main chains matching the friction direction. Layers of friction-transferred poly(p-phenylene) (PPP) have also been used for alignment of epitaxially grown thiophene/phenylene co-oligomers for example, and polarization ratios of up to ~100 have been obtained in photoluminescence.[28] The friction transfer is a multipurpose technique, because it allows the alignment of small molecules, conventional polymers and conjugated polymers-regardless whether they are liquid crystalline or not,[24,25,29] but, due to the insulating nature of PTFE, the fabrication of electroluminescence devices is very difficult.

Finally, the alignment method which will be introduced herein is that liquid crystalline polymers (LCPs) can be aliged on top of an alignment layer. The liquid crystalline polymers have low viscosity in the liquid crystalline state and the tendency to align with the long axis of their rod-like molecules along a preferred direction, which is known as the director. However, the size of such aligned domains in LCPs is much too small (only a few micrometers – on the average the directors are oriented randomly) to produce polarized light from suitable electroluminescence LCPs, unless macroscopic alignment is imposed by external action. The conventional method to achieve the required monodomains of uniform homogeneous molecular alignment in thin films is the use of additional alignment layers upon which the LCPs align when they are brought into the mesogenic –low viscous – state. The alignment of the LC molecules is preserved into the crystalline state by cooling down slowly, or into the glassy (frozen) LC state by cooling down quickly (quenching). The most common alignment layer consists of polyimide[13], because polyimide has excellent alignment ability as well as thermal and chemical stability.[30] Furthermore, it is transparent for visible light and therefore fulfills another fundamental requirement for incorporation into an LED structure. Polyimide can be aligned by rubbing with a cloth[2] or by irradiation with UV-light.[31]

So far the most common procedure for obtaining highly aligned samples of low-molecular weight or polymer thermotropic liquid crystals (LCs) is the use of polyimide which has been uni-directionally rubbed by a cloth as an alignment layer. Subsequently, the polymer is deposited by spincoating. Afterwards, the alignment of the LCs into monodomains is accomplished by heating them into the LC phase, followed by rapid

cooling for preservation of the emerging order. This technique does not only result in high degrees of anisotropy, but it is also suitable for mass production and for large area treatment. The first example of monodomain alignment of fully conjugated LCPs by means of rubbing-aligned polyimide was the orientation of a poly(9,9-dioctylfluorene) (PF8) by Grell *et al.*[2]

In the following section we will show that highly ordered monodomain alignment layers of oligofluorenes can be achieved on the rubbed polyimide substrate. The films of highly oriented oligofluorenes were investigated by means of optical microscopy, DSC, transmission electron microscopy (TEM) and electron diffraction.

4. 4. 2 Preparation of alignment film

The primary requirements for the alignment in liquid crystalline state are (i) low viscosity in the mesophase and (ii) low transition temperatures below any transition temperature in the alignment layer. Thermotropic liquid crystalline oligofluorenes fulfill excellently the required conditions. To achieve a high degree of uniaxial orientation the oligomers were thermally aligned on rubbed polyimide layers. Details on thermal alignment conditions for the series oligomers is similar with the polyflourenes, and can be found in the reports of Grell et al.[3] The preparation of the alignment layer of oligofluorenes will be described in detail in the experimental part.

4. 4. 3 The morphology of alignment films

The morphology of aligned oligofluorenes films (**OF-4**, **OF-5**, **OF-6**, **OF-7**) was first investigated by POM techniques. The high alignability was confirmed when viewing samples of oriented oligofluorenes under an optical microscope between crossed polarizers. As an example the texture for heptamer is shown in Figure 4. 4. 1, and the alignment films of other oligomers (**OF-4**, **OF-5**, and **OF-7**) are similar to heptamer. A large monodomain birefringence was observed, suggesting an uniaxial alignment of the molecules. A complete extinction of the whole sample area was observed during every 90° stage rotation, when the direction of rubbing was exactly parallel or perpendicular to one of the polarizers. When the light vibrates under an angle of 45° from the rubbing direction, the field of view looks bright and indicates that the molecules are aligned with the molecular long axis along the

rubbing direction. Apart from high orientation, these observations reveal a high degree of homogeneity and confirm a large monodomain texture of the oligofluorenes.

A
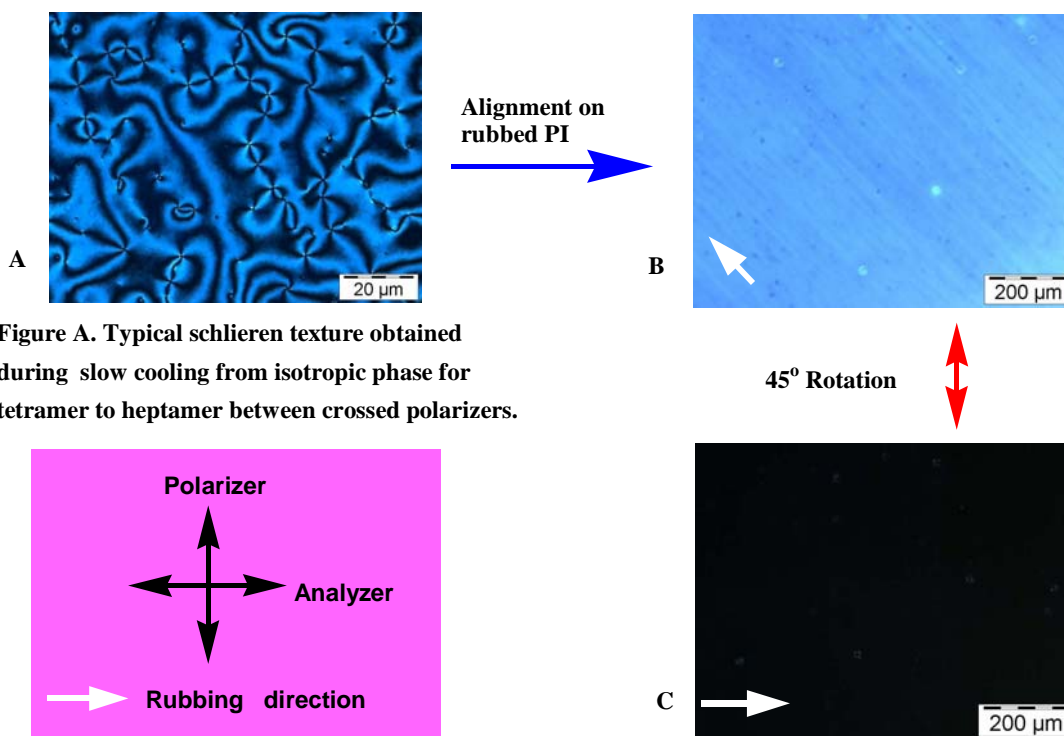
Figure A. Typical schlieren texture obtained during slow cooling from isotropic phase for tetramer to heptamer between crossed polarizers.

Alignment on rubbed PI

B

45° Rotation

C

the white arrows in these pictures correspond to the rubbing direction

Figure B and C. A film of tetramer to heptamer of oligofluorenes, which was aligned on top of the rubbed polyimide, viewed in a polarization microscope (crossed polarizers).

Figure 4. 4. 1 The polarized optical microscopy of the aligned and unaligned film.

For the tetramer, a partial orientation was observed during every 90°stage rotation from a partial extinction of birefrengence in large area after spin-coating onto the rubbed polyimide *without annealing*. That means that an aligned film can be obtained from the tetramer without annealing due to its low glass transition temperature (22°C) and because the liquid crystalline phase exists at room temperature. A *complete extinction* was observed during every 90°stage rotation after annealing in liquid crystalline phase (40°C) for 30 min. This means the alignment degree is improved by annealing. For pentamer up to heptamer, the large domain alignment layers can be achieved only after annealing in the liquid crystalline phase.

The DSC curves of the oriented heptamer film are shown in figure 4. 4. 2, An endothermic peak ($\Delta H = -2.74 \ Jg^{-1}$) was observed in the first heating run, and it is

significantly different from the second heating trace, where a typical glass transition was observed with the $\Delta C_p = 0.19$ Jg^{-1}K^{-1}. This means the oligomeric molecules form a higher ordered (packing) phase in the oriented film instead of the glassy state in the bulk sample, while the higher ordered solid phase is not a crystalline phase due to the small enthalpy change, but the endothermic peak in the first heating run maybe related to the same phase transition with the endothermic peak of PF2/6 (Figure 4. 2. 2).
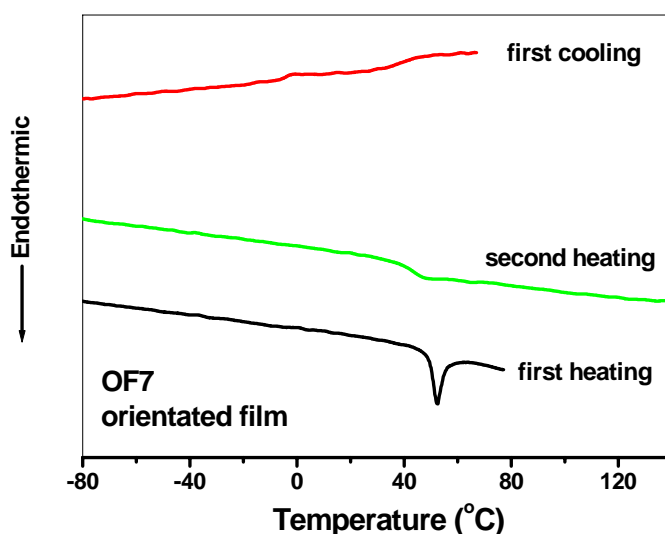
Figure 4. 4. 2. The DSC curves of oriented heptamer alignment film (heating or cooling rate: 10 K/min)

Oligofluorene with fluoreneone units such as OF5K was also aligned on the rubbed polyimide surface with annealing in its liquid crystalline phase. A complete extinction over the film was also observed at every 90° of stage rotation when the direction of rubbing was exactly parallel to one of the polarizers, indicating a monodomain alignment layer.

Electron diffraction was carried out on the alignment films to further understand and the molecular order in the thin film. For example, the electron diffraction pattern of the alignment layer of the OF7 (left) and OF5K (right) is shown in Figure 4. 4. 3. A similar diffraction pattern to that of the fiber X-ray diffraction was obtained. This means that the molecules tend to pack as lamellae i.e. with a smectic order in the alignment layer along the rubbing direction.

(OF7)   **(OF5K)**
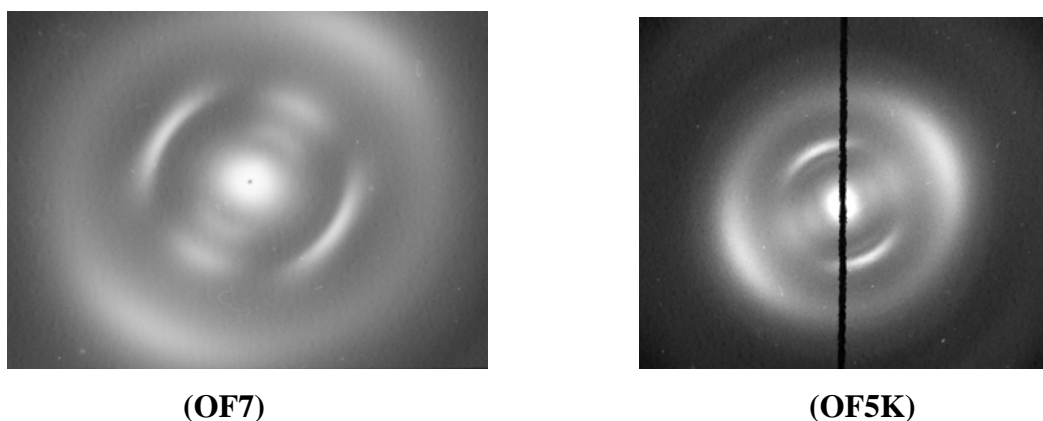
Figure 4. 4. 3. Electron diffraction pattern of alignment film: OF7 at -130 ^{o}C (left); OF5K at room temperature (right).

4. 4. 4 Polarized absorption and emission from the alignment layers of the oligofluorenes

As mentioned above, high degrees of macroscopic order are observed in the oriented films of oligofluorenes on the top of rubbed polyimide alignment layers. Moreover, the alignability of the oligomers can be quantitatively analyzed by polarized absorption and fluorescence spectra taken parallel and perpendicular to the rubbing direction of the alignment layer. As shown in figure 4. 4. 3, typical dichroic ratios (D) at the absorption maximum peak are 5, 10, 16, 23 from tetramer up to heptamer, and polarization ratio (P) at emission maximum are 5, 35, 37, 41 for tetramer up to heptamer, respectively (see Table 4. 4. 1). The large difference between the absorption parallel and perpendicular to the rubbing direction points to a narrow orientational distribution and high degree of molecular alignment along this director. At the same time, the alignability increases with the extension of chain-length of oligomers.

The very large dichroic ratio (23) and polarization ratio (41) was obtained for heptamer, and this value is much larger than that of PF2/6.[6] This means the monodisperse oligofluorenes are more likely to align on the top of the rubbed PI surface than polyfluorenes. This is further confirmed by our experiment: the PF2/6 sample (M_w = 2.3 × 10^5 g/mol, PS standard) was spin-cast onto the same PI substrate from same concentration solution, i.e. under the same conditions as the oligofluorenes; the film were annealed in

liquid crystalline phase (180 °C) for 2h and a *imcomplete extinction* was observed over every 90°stage rotation in POM, suggesting the existence of order defects in the alignment films.
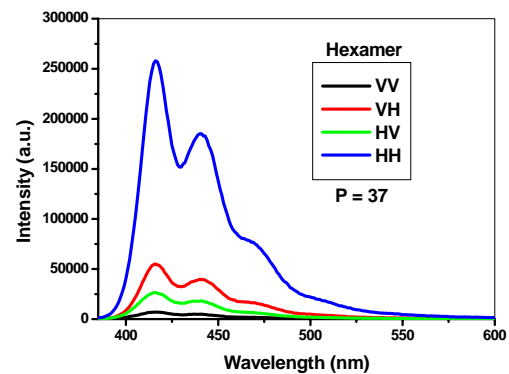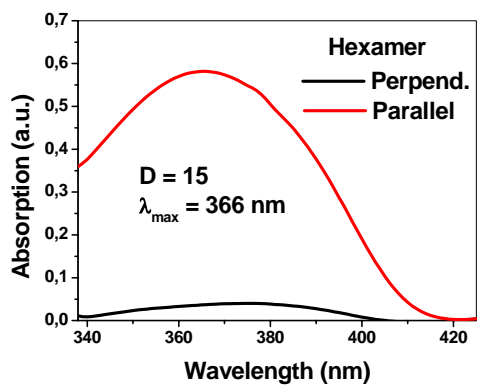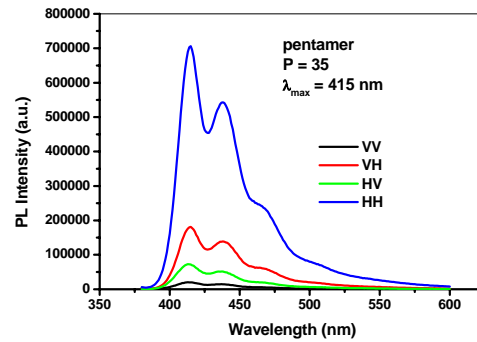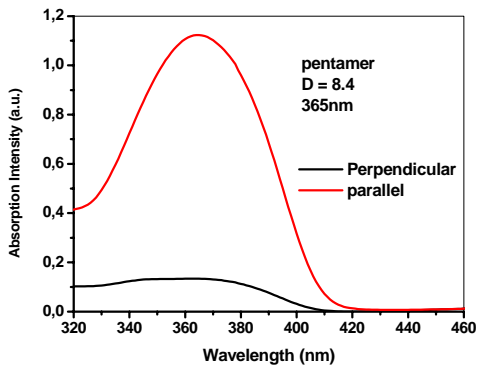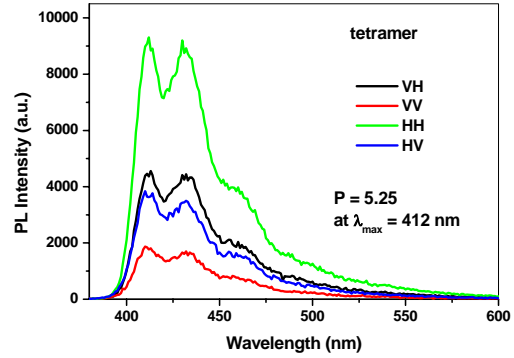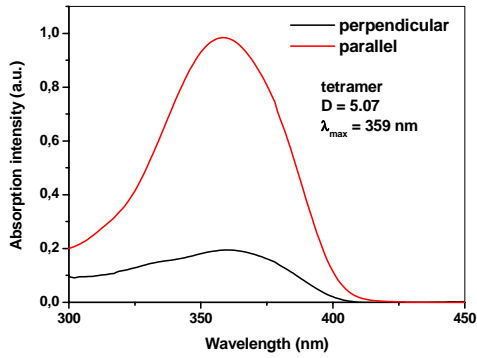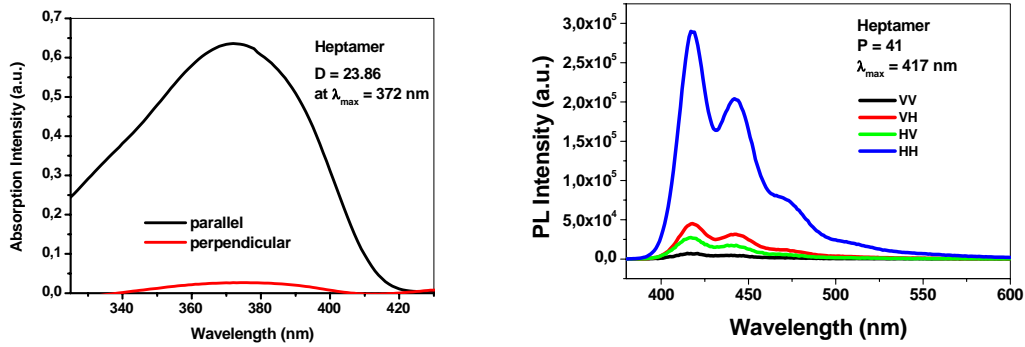
Figure 4. 4. 3. Polarized UV-vis absorption and photoluminesence spectra of the aligned films of fluorenyl tetramer to heptamer on a rubbed polyimide substtrate.

Table 4. 4. 1. The dichroic ratio (D) and polarization ratio (P) of the aligned film from tetramer up to heptamer.

	OF4	OF5	OF6	OF7
D	5	10	16	23
P	5	35	37	41

The polarized absorption and fluorescence spectra for OF5K are shown in Figure 4. 4. 4 and a dichroic ratio $D = 8$ and polarization ratio $P = 9.3$ were obtained. These values are lower than the corresponding values of OF5, indicating that the incorporation of fluorenenone group in oligofluorenes decreases the alignability.
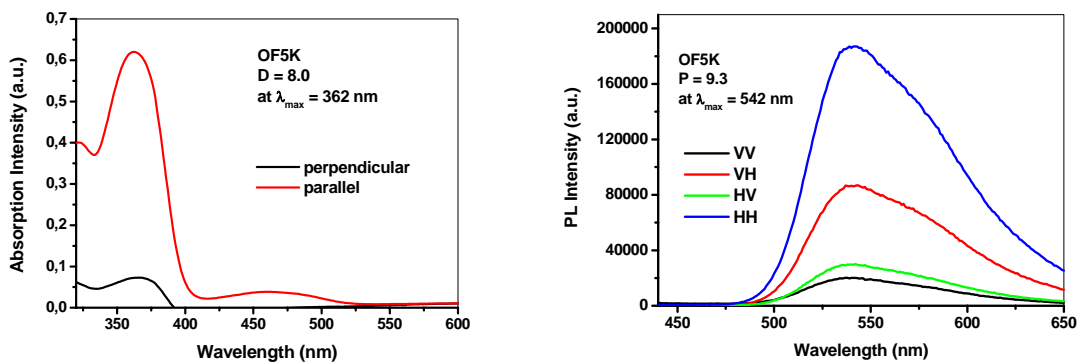
Figure 4. 4. 4. Polarized UV-vis absorption and photoluminescence spectra of the aligned film of OF5K on a rubbed polyimide substrate.

4. 5. A dielectric spectroscopy investigation

This section of the work has jointly carried out with Prof. G. Floudas and has published in *J. Chem. Phys.* **2004**, *120*, 2368-2374

The purpose of the study is to investigate the molecular dynamics of the oligofluorenes as a function of chain-length from the dimer up to heptamer and the polymer. Despite numerous efforts in establishing reliable structure-property relationships in polyfluorenes, the underlying molecular dynamics, with impact on carrier mobility, remain, totally unexplored. We are interested in the role of intra- versus intermolecular interactions, the origin of the glass transition and its molecular weight dependence, and finally the detection and role of keto defects on the dynamics. For this purpose a pentamer with a fluorenone group was also investigated; the large dipole associated with the keto group acts as a probe of chain defects. The results from the labeled pentamer were contrasted with the homo-oligofluorenes and the polymer. Furthermore we provide the (weak) intrinsic dipole moment associated with the glass transition process and index of refraction.

4. 5. 1 Basics of dielectric spectroscopy

The complex dielectric permittivity $\varepsilon^* = \varepsilon' - i\varepsilon''$, where ε' is the real and ε'' is the imaginary part, is a function of frequency ω, temperature T and pressure P, $\varepsilon^* = \varepsilon^*(\omega, T, P)$.[32] In Figure 4. 5. 1, some representative dielectric loss spectra are shown for the dimer
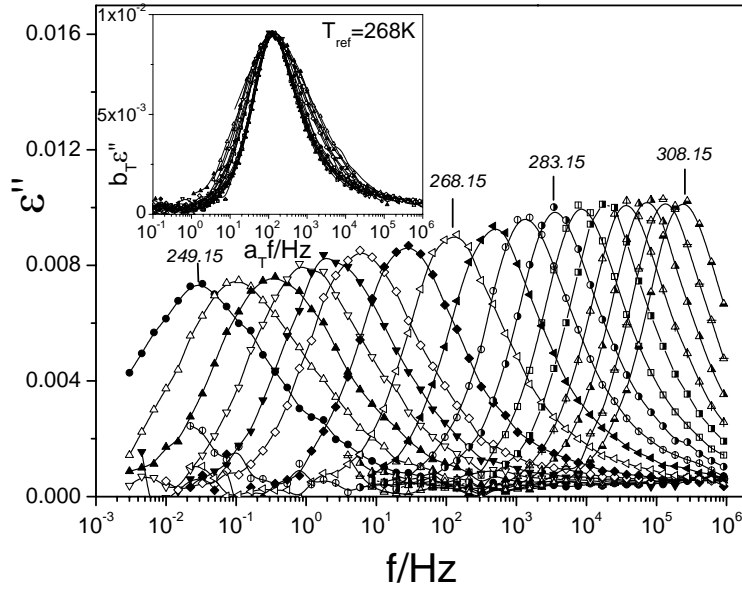
Figure 4.5. 1. Dielectric loss spectra for the dimer, at atmospheric pressure, for different temperatures in the range from 249.15 to 308.15 K. Notice the broadening of the loss curves with decreasing temperature. The normalized spectra, at a reference temperature of T_{ref}=268 K, are shown in the inset.

at different temperatures within the range 249.15<T<308.15 K. Notice that the curves progressively broaden with decreasing temperature. In the inset, the same data are shifted to the corresponding data at a reference temperature (T_{ref}=268.15 K) exhibiting spectral broadening beyond a simple Debye function. In the analysis of the DS spectra we have used the empirical equation of Havriliak and Negami (HN)[33]:

$$\frac{\varepsilon^*(T,P,\omega) - \varepsilon_\infty(T,P)}{\Delta\varepsilon(T,P)} = \frac{1}{\left[1 + \left(i\omega\tau_{HN}(T,P)\right)^\alpha\right]^\gamma} \qquad (4.9)$$

where $\tau_{HN}(T,P)$ is the characteristic relaxation time in this equation, $\Delta\varepsilon(T,P)=\varepsilon_0(T,P)-\varepsilon_\infty(T,P)$ is the relaxation strength of the process under investigation and α, γ (with limits o<α, $\alpha\gamma\leq$1) describe, respectively, the symmetrical and asymmetrical broadening of the distribution of relaxation times. In the fitting procedure we have used the ε" values at every temperature and in some cases the ε' data were also used as a consistency check. The linear

rise of the ε" at lower frequencies is caused by the conductivity ($\varepsilon"\sim(\sigma_o/\varepsilon_f)\omega^{-1}$, where σ_o is the dc-conductivity and ε_f is the permittivity of free space) which has been included in the fitting procedure. From τ_{HN}, the relaxation time at maximum loss, τ_{max}, is obtained analytically following

$$\tau_{max} = \tau_{HN} \left[\frac{sin\left(\dfrac{\pi\alpha}{2+2\gamma}\right)}{sin\left(\dfrac{\pi\alpha\gamma}{2+2\gamma}\right)} \right]^{-1/\alpha} \tag{4. 10}$$

4. 5. 2 Results and discussion

The dielectric loss data of the dimer, as well as of the remaining oligofluorenes (and the polymer), exhibit a non-Debye main relaxation (called α-process) at temperatures above the calorimetric T_g. Moreover, the dielectric loss spectra of all samples exhibit a temperature-dependent broadening that is increasing by lowering temperature. This is depicted in Figure 4. 5.1. for the dimer. Notice, that a single (α-) process affects the dynamics above T_g. For the trimer, however, a very weak slower process than the α-process exists freezing at the same temperature (T_g). The origin of this process is not clear at present but it could originate from the slight curvature of the backbone resulting in an uncompensated weak dipole along the chain.

To quantify the effect of temperature on the broadening of the relaxation time spectra related with the α-process, we plot in Figure 4. 5. 2, the HN shape parameters α and αγ as a function of reduced temperature.
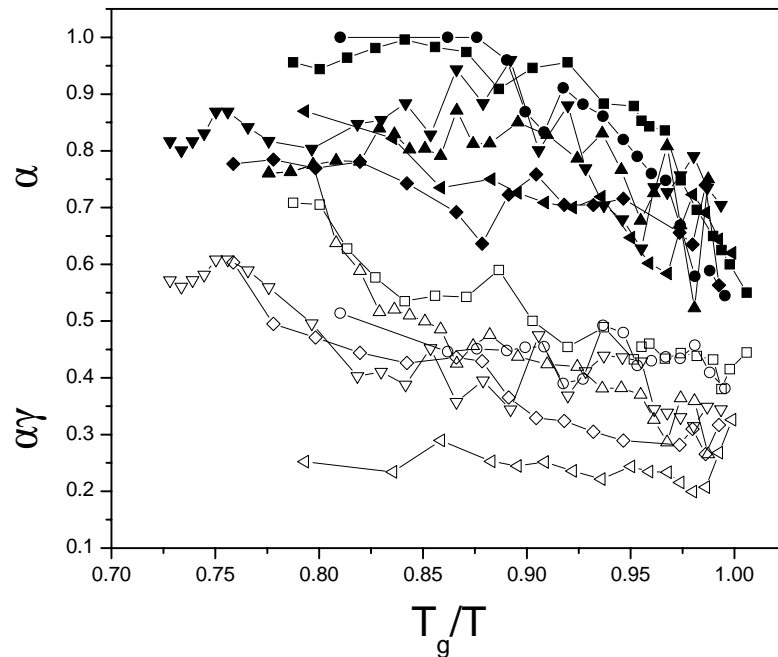
Figure 4. 5. 2. Temperature dependence of the Havriliak-Negami shape parameters α (filled symbols) and αγ (open symbols) plotted as a function of reduced temperature for the different oligofluorenes; (squares): dimer, (circles): trimer, (up triangles): tetramer, (down triangles): pentamer, (rhombus): hexamer and (left triangle): heptamer. Notice that the spectral broadening starts at $T_g/T=0.9$ in all samples.

Notice that up to the highest temperature investigated the spectra deviate from a simple Debye process (with $\alpha=\gamma=1$). Although the low frequency slope of the relaxation spectrum (α) approaches one for the dimer and trimer at high temperatures, the high frequency slope (αγ) is much less than one, indicating an asymmetric broadening of the loss curves towards higher frequencies. At $T_g/T<0.9$, all spectra broaden from the low frequency side as well. Furthermore, there is progressive broadening with increasing degree of polymerization, n, at a given reduced temperature. This is better illustrated in Figure 4. 5. 3, where the normalized loss spectra of the oligofluorenes are compared under similar ΔT (=$T-T_g$) conditions.
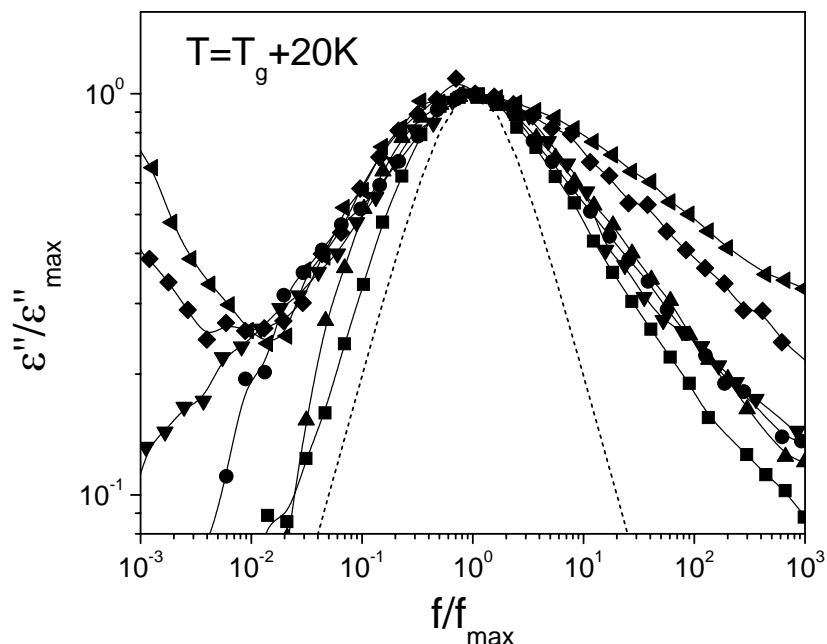
Figure 4. 5. 3. Normalized dielectric loss spectra for the oligofluorenes compared at a temperature of about T_g+20 K. The symbols are as follows; (squares): dimer, (circles): trimer, (up triangles): tetramer, (down triangles): pentamer, (rhombus): hexamer, (left triangle): heptamer. The dashed line gives the Debye function. Because of the slight temperature miss-match, the frequency axis is also normalized.

Notice the strong deviations from the Debye function for all oligomers that become more pronounced with increasing n. In order to quantify the role of intramolecular vs intermolecular correlations on the broadening of the distribution of relaxation times, a toluene solution was prepared with dimer concentration of 40% and measured with DS. Should the distribution of relaxation times originate from intermolecular correlations, the inter-chain dilution should result in a narrower distribution, that, in the limit of infinite dilution would result in a Debye function. The α-process (not shown here) showed similar broadening in the solution beyond a Debye function suggesting that the distribution of relaxation times is largely of intramolecular origin. A second experiment aiming in extracting the influence of inter- and intra-molecular correlations was made on a heptamer fiber sample prepared by a laboratory microextruder. This particular sample preparation results in a uniform macroscopic orientation giving rise to intense wide-angle X-ray scattering peaks. Intramolecular degrees of freedom are expected to be suppressed in this

macroscopically aligned state. The thermal properties were subsequently examined with DSC (not shown here) and still exhibited a step at the glass transition however with reduced amplitude (Δc_p=0.12 J/Kg, i.e., half the value from the unaligned sample) suggesting the suppression of the intramolecular degrees of freedom by chain orientation. It is interesting that even at this highly oriented state, intramolecular correlations associated with the α-process are still present, and give rise to the glass transition.

The T-dependence of the relaxation times at maximum loss for the oligofluorenes and the polymer are shown in Figure 4. 5. 4 as a function of temperature. The solid lines are fits to the well-known Vogel-Fulcher-Tammann (VFT) equation:
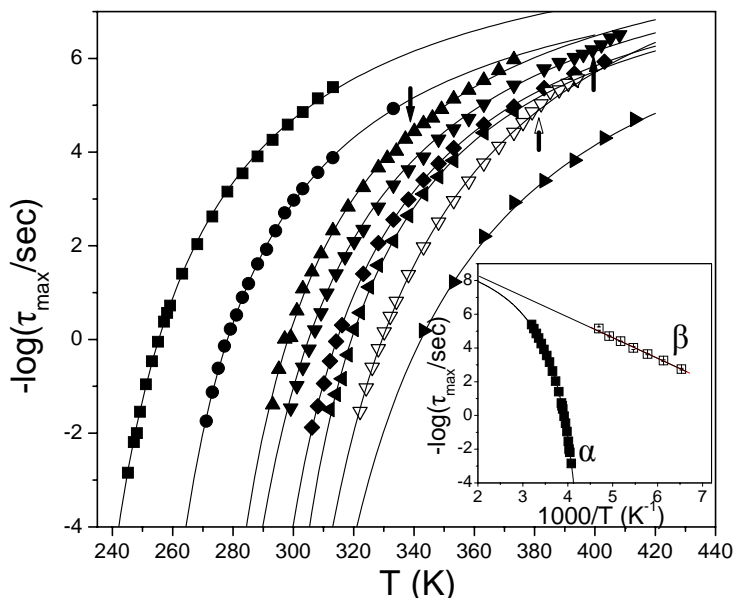
Figure 4. 5. 4. Temperature dependence of the relaxation times at maximum loss for the different oligofluorenes ((squares): dimer, (circles): trimer, (up triangles): tetramer, (down triangles): pentamer, (rhombus): hexamer, (left triangle): heptamer, the polymer (right triangle) and the pentamer with fluorenone sample (open triangles)). The lines are fits to the VFT equation (see text). The arrows for the tetramer, the pentamer and the pentamer with the fluorenone group indicate the respective melting temperatures. Notice the slight up-ward deviation of the α- relaxation times from the VFT dependence. In the inset, the α- (filled squares) and β- (open squares) processes of the dimer are plotted in the usual Arrhenius representation. The lines are fits to the VFT and Arrhenius dependencies. Notice that the two processes do not merge.

Table I. Vogel-Fulcher-Tammann (VFT) parameters of the oligofluorenes, the polymer and the pentamer with fluorenone.

Sample	$-\log(\tau_0/s)$	B (K)	T_0 (K)
Dimer	9.4±0.1	970±32	211±1
Trimer	8.9±0.1	903±39	234±1
Tetramer	9.4±0.2	1004±76	252±2
Pentamer	9.4±0.1	1110±48	255±2
Hexamer	9.1±0.05	1006±24	266±1
Heptamer	8.9±0.2	920±64	274±2
Polymer	9.2±0.2	1470±230	272±7
Pentamer with fluorenone	10.5±0.2	1440±76	270±2

$$\tau_{max} = \tau_0 \, exp\left(\frac{B}{T-T_0}\right)$$
(4. 11)

where B is an activation parameter, T_0 is the "ideal" glass temperature located near but below the T_g ($T_0 = T_g - c_2^g$ and c_2^g is a constant) and τ_0 is the high temperature intercept. The above parameters are summarized for the different samples in Table I. In Figure 4. 5. 4 the $\tau(T)$ dependence for the pentamer with the fluorenone unit (open triangles) is also included and shows distinctly different behavior from the pentamer without the fluorenone group (filled down triangle). The different $\tau(T)$ dependence results in an increased T_0 (Table I) by as much as 15 K, that can be interpreted as reflecting a change of the backbone rotational angles by the incorporation of the fluorenone group. Furthermore, the intensity of the α-process (T∆ε~120 K) was found to be about ten times higher in the pentamer with the fluorenone unit and, in addition, very sensitive to sample preparation/orientation effects. Dielectric spectroscopy is very sensitive to the presence of the carbonyl group (keto defects) due to the large dipole moment. Keto defects can be accidentally incorporated on the backbone during synthesis as a result of photo- or electro- oxidation. The much lower dielectric strength of the α-process in the unsubstituted oligomers and the polymer confirm the absence of such defects from the present system.

The VFT equation adequately describes the dynamics over the whole T-range investigated except for the tetramer and pentamer samples above their melting temperatures. For these samples a slight decrease of the α-relaxation times is obtained above T_m (arrows in Figure 4. 5. 4). This effect is also seen in polymer liquid crystals on the length scale of the δ-process.[34] There are two additional points that need attention with respect to the τ(T). First, the values of the high temperature intercept, $-\log(\tau_0/s)$, are low; τ_0 is associated with the frequency of attempts to cross a barrier or with the time required to move in free space and is expected to have a phonon-like time scale, i.e., $\tau_0 \sim 10^{-14}$s.[35] The slower relaxation times suggest the absence from contributions of the high-frequency tail of the α-process at phonon-like times. This could be important in investigating the vibrational spectra by i.e., Raman spectroscopy.[36] Second, there is a variation in the fragility or steepness index, defined from the initial slope $m = d\log(<\tau>/s)/d(T_g/T)$ of the normalized relaxation times (not shown here). The slope varies systematically from 80 (dimer) to about 100 (heptamer) in qualitative agreement with the proposed correlation[37] between non-exponentiality of the structural response and fragility, i.e., $m = m_0 - s \bullet \beta_{KWW}$, where m_0 and s are constants and β_{KWW} is the Kohlrausch-Williams-Watts exponent of the stretched-exponential function. For example, for the dimer (with m=80) the α and γ values "correspond" to a β_{KWW} of 0.36 whereas for the heptamer (with m=100) to β_{KWW} of 0.26 at T_g (in reality a one-to-one correspondence is not possibly since in the HN function there are two parameters characterizing the shape whereas in the KWW function only one).

In the inset to Figure 4. 5. 4 an Arrhenius diagram of the relaxation times for the dimer is shown. Apart from the α-process, it includes a faster process (called β-process), found in all oligofluorenes, with the following intensity and shape characteristics: Δε~0.004 within the T-range: 163<T<223 K, α=0.4±0.1, γ=1.0, with an Arrhenius temperature dependence of relaxation times:

$$\tau_{max} = \tau_0^* \; exp\left(\frac{E}{RT}\right) \qquad\qquad (4.\ 12)$$

where τ_0^* is the high temperature intercept ($-\log\tau_0^* = 12.3 \pm 0.7$) and E is the apparent activation energy (E=28.1 kJ/mol in all samples). The intensity associated with the β-process is a small fraction of the intensity of the α-process (typically $(T\Delta\varepsilon)_\beta/(T\Delta\varepsilon)_\alpha \sim 0.1$) suggesting either a (heterogeneous) relaxation of a reduced number of dipoles or a

(homogeneous) relaxation of dipoles with a smaller angle of dipolar reorientation. Notice that the τ_0^* for the β-process is systematically shorter than the τ_0 of the α-process (Table I) revealing that the two processes approach each other with increasing temperature but never merge. In this respect, measurements at higher frequencies could be helpful but the low loss (Figure. 4. 5. 1) of these materials and lower sensitivity of the high-frequency set-up precludes such an investigation.

Returning to the α-process, a more critical test of the ability of the VFT equation to describe the experimentally obtained relaxation times is through the temperature derivative method.[38] This method focuses on the first (and second) derivatives of $-\log\tau_{max}$ as a function of T or T^{-1} and practically reduces the number of parameters by linearizing certain model functions. The VFT dependence, for example, is linearized by the first derivative method as:

$$\left[\frac{-d\,log\,\tau_{max}}{dT}\right]^{-1/2} = (T - T_0)B^{-1/2} \qquad (4.\ 13)$$

Notice that the case $T_0=0$ reduces to an Arrhenius T-dependence. The result of the first derivative of the relaxation times with T is shown in Figure 4. 5. 5. From this representation it immediately follows that $\tau_{max}(T)$ for all oligofluorenes (below T_m) exhibit a VFT dependence with a good accuracy. Furthermore, all data sets have similar slopes suggesting only small variations of the apparent activation energies (Table I). For the polymer sample, the smaller temperature range investigated (because of the higher conductivity) precludes a similar analysis and conclusion.

Based on the VFT T-dependence we can define an operational glass temperature from DS as the temperature with a corresponding relaxation time at maximum loss of 10^2 s. The thus obtained T_g is plotted in Figure 4. 5. 6 as a function of the degree of polymerization (n) for the oligofluorenes and the polymer (the M_n value was used) together with the DSC T_g. Notice the good agreement between the DSC (rate 10 K/min) and DS ($\tau\sim10^2$s) T_g. The line in Figure 4. 5. 6 is a fit to the Fox-Flory equation:
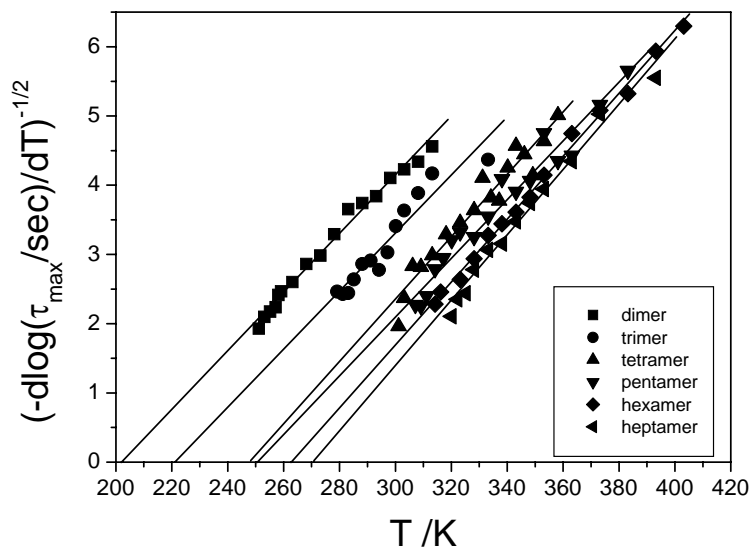
Figure 4. 5. 5. Temperature dependence of the dynamics in the oligofluorenes in a [-dlog(τ_{max}/dT]$^{-1/2}$ vs T representation. The lines are fits to the VFT behavior (see text).
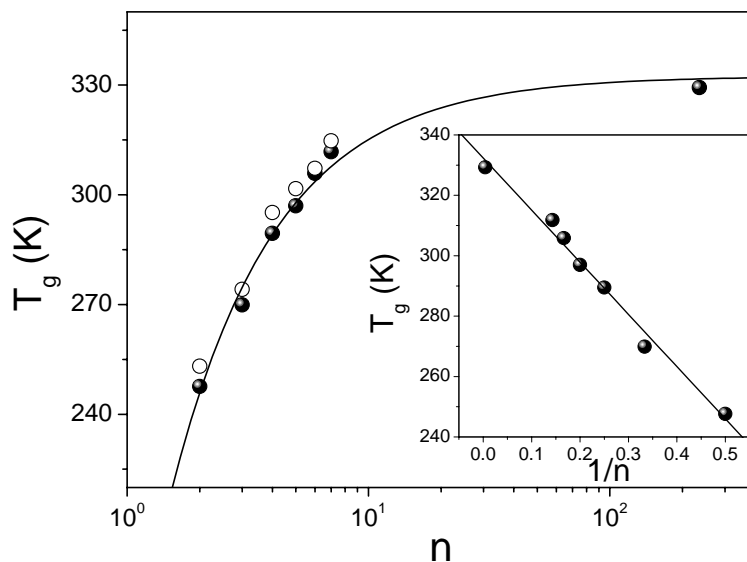
Figure 4. 5. 6. Dependence of the glass temperature on the degree of polymerization: (open symbols): from DSC, (filled symbols): from DS (in DS the T_g is defined as the temperature corresponding to a relaxation time of 100 s). In the inset the DS values are plotted as a function of n^{-1} and the line is the result of the linear fit according to the Fox-Flory equation. The polymer T_g is at 332±2 K.

$$T_g = T_g^{\infty} - \frac{K}{n} \qquad\qquad (4.\ 14)$$

where T_g^{∞}=332.4±2 is the glass transition at practically infinite molecular weight and K=173±9. Therefore the actual glass temperature for polyfluorene is at 332 K that is difficult to obtain from DSC alone. In the inset, the DS values are plotted as a function of n^{-1} and display a good linearity, according to eq 6, implying the contribution from chain-end effects as with amorphous polymers.

From the dielectric strength of the α-process and the permittivity at high (ε_{∞}) and low (ε_0) frequencies we can estimate the effective dipole moment associated with this relaxation from the Fröhlich equation for spherical molecules[39]

$$\Delta\varepsilon = \frac{4\pi N_0 g \mu^2}{3 k_B T} \left(\frac{\varepsilon_{\infty} + 2}{3} \right)^2 \frac{3\varepsilon_0}{2\varepsilon_0 + \varepsilon_{\infty}} \qquad\qquad (4.\ 15)$$

where N_0 is the number of dipoles per unit volume ($N_0 = N\rho/M_0$, where ρ is the density, M_0 is the monomer molecular weight and N is the Avogadro number), μ is the dipole moment averaged over all possible configurations and g is a measure of the orientational pair correlations (g=1+z<cosγ>, where z is the average number of nearest neighbors and γ is the angle between neighbors). The effective dipole moment, μ_{eff}=(gμ)$^{1/2}$, is plotted in Figure 4. 5. 7 as a function of temperature for the oligofluorenes. In the dipole moment calculation a macroscopic density of 1 g/cm³ was assumed.
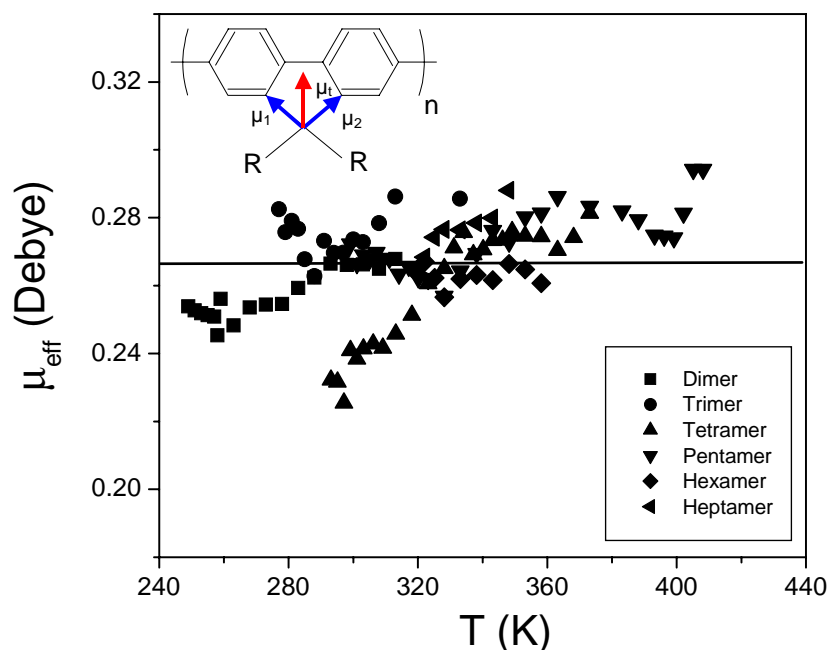
Figure 4. 5. 7. Temperature dependence of the normalized effective dipole moment for the α-process in the oligofluorenes; (squares): dimer, (circles): trimer, (up triangles): tetramer, (down triangles): pentamer, (rhombus): hexamer, (left triangle): heptamer. The solid line results in an average value from the different samples ($<\mu>=0.27\pm0.03$ D).

Notice that the effective dipole moment with a direction perpendicular to the backbone, is 0.27 ± 0.03 Debye, independent of chain length for all oligomers suggesting local rotational motions as responsible for the α-process. This again emphasizes the role of intramolecular correlations in setting not only the time-scale but also the intensity of the α-process. In addition, from the ε_0 (=2.9) value in the glassy state (T=250 K, dimer) we obtain a refractive index of 1.7, a value well within the reported frequency dependence of n.[40]

4. 6 Conclusion

The thermal behaviors, structural and supramolecular packing, alignment properties, and molecular dynamics of a series of oligofluorenes up to the polymer were studied using techniques such as TGA, DSC, WAXS, POM and DS.

The oligomers from tetramer to heptamer show a smectic liquid crystalline phase with clearly defined isotropization temperatures; and this allows extrapolation to the expected isotropization temperature of the polymer at around 475 °C, well above the thermal decomposition temperature. Most importantly, the oligofluorenes do not show the same high-order phase that the polymer exhibits below the melting temperature of approximately 160 °C. However, unlike the polymer, the oligomers do show a glass transition which exhibits n^{-1} dependence and allows extrapolation to a hypothetical glass transition of the polymer at around 64 °C. As this glass transition refers to a freezing of a liquid-crystal phase not seen for the polymer, it is not too surprising that this phenomenon cannot be detected for the polymer.

A smectic packing and helix-like conformation for the oligofluorenes from tetramer to heptamer was supported by WAXD experiment, simulation, and single-crystal structure of some oligofluorene derivatives. The twist angle between the two neighboring fluorene units was approximately 144 °, and was in agreement with the torsional angle between neighboring monomers for polyfluorenes in the case of a 5/2 helix.

Oligofluorenes were aligned more easily than the corresponding polymer, and the alignability increased with the molecular length from tetramer to heptamer.

The molecular dynamics in a series of oligofluorenes up to the polymer was studied using dielectric spectroscopy. Two dielectrically active processes were found, one below T_g (β-process) and one above (α-process) associated with the DSC T_g. The latter bears many polymeric features: a) The relaxation times at maximum loss display a strong T-dependence following the VFT equation up to the melting temperature. However, the high temperature intercept was much slower than the expected phonon-like time scale. b) A distribution of relaxation times beyond a simple Debye process was found for all oligomers and at all temperatures investigated (up to $T_g/T\sim0.73$). c) Spectral broadening exists at a fixed molecular weight by decreasing temperature, and at a fixed temperature by increasing molecular weight. Dilution experiments proved that spectral broadening is caused largely by intramolecular interactions. Based on the intensity associated with the α-process the effective monomer dipole moment is 0.27±0.03 D. d) The glass transition exhibits a strong molecular weight dependence according to the Fox-Flory equation and the polymer T_g is obtained at 332 K by DS. e) Dielectric spectroscopy is very sensitive to the presence of keto defects that drastically influence the optical and electronic properties. This work confirmed the absence of such defects from the present oligomers and the polymer. On the

other hand, the investigation of a labeled pentamer with a fluorenone group (i.e., a keto defect) revealed that the effect on the molecular dynamics is mainly to stiffen the backbone and increase the T_g by about 15 K.

4. 7 Experimental

Thermal gravimetric analysis (TGA) and Differential Scanning Calorimetry (DSC) was measured on a Mettler DSC 30 with heating or cooling rate of 10 K min^{-1}. Polarization microscopy was performed on a Zeiss Axiophot with a nitrogen flushed Linkam THM 600 hot stage. The film thickness was measured by a Tencor α-step profiler.

The series of oligomers were extruded in liquid crystalline phase. The fiber was drawn from a liquid crystalline PF2/6 melt around 170 °C. Wide angle X-ray powder and fiber diagrams were recorded in a vacuum Kiessig film camera (Huber, Germany)

Single crystal experiment

Crystals of the diboronic monomer were obtained by slow evaporation from a mixture of ethanol and a small amount of dichloromethane; the dibromo-dimer was also crystallized by slow evapovation from a mixture of hexane and dichloromethane; the pentamer with one fluorenone group was crystallized from a dichloromethane solution by slow diffusion of ethanol. Suitable crystals were mounted in glass capillaries. The data collection was carried out at 120 K or 150 K on a Nonius KappaCCD diffractometer with graphite monochromated Mo Kα radiation for the monomers and dimer and Cu Kα radiation for the pentamer. The crystal structures were solved by direct methods using the program Shelx91.

Alignment film

The rubbed PI substrat were commercially available from the E.H.C. Co., Ltd., Japan, and used as received. Films of oligofluorenes were spin cast from 10 mg/mL in the chloroform solution at 1600 rpm for 40s onto rubbed polyimide alignment layers. These films was annealed at a nitrogen atmosphere at their corresponding liquid crystalline phase, which are 40 °C, 60 °C, 80 °C, 100 °C for tetramer up to heptamer, respectively for 30 min, and finally by 'freezing' the alignment into the crystalline or glassy state by slow cooling. The

final film thickness of the layers was 20 nm for polyimide and 30 nm for oligofluorenes, respectively.

Dielectric spectroscopy

The sample cell consisted of two electrodes with 20 mm in diameter and the sample with a thickness of 50 or 20 μm. The dielectric measurements were made at different temperature in the range 123-453 K, at atmospheric pressure, and for frequencies in the range from 3×10^{-3} to 1×10^{6} Hz using a Novocontrol BDS system composed from a frequency response analyzer (Solartron Schlumberger FRA 1260) and a broad dielectric converter.

4. 8 References and Notes

[1] Teetsov, J.; Fox, M. A. *J. Mater. Chem.,* **1999**, *9*, 2117-2122.

[2] Grell, M.; Bradley, D. D. C.; Inbasekaran, M.; Woo, E. P.; *Adv. Mater.* **1997**, *9*, 798.

[3] Grell, M.; Knoll, W.; Lupo, D.; Meisel, A.; Miteva, T.; Neher, D. Nothofer, H. G.; Scherf, U.; Yasuda, A. *Adv. Mater.* **1999**, *11*, 671.

[4] Redecker, M.; Bradley, D. D. C.; Inbasekaran, M.; Woo, E. P. *Appl. Phys. Lett.* **1999**, *74*, 1400

[5] Sirringhaus, H.; Wilson, R. J.; Friend, R. H.; Inbasekaran, M.; Wu, W.; Woo, E. P.; Grell, M.; Bradley, D. D. C. *Appl. Phys. Lett.* 2000, *77*, 406.

[6] a) Meisel A. 'Alignment, Characterization and Application of Polyfluorene in Polarized Light-Emitting Devices'. Ph. D. Dissertation Thesis, Johann Wolfgang Goethe-Universität Frankfurt **2001**; b) Neher, D. *Macromol. Rapid Commun.* **2001**, *22*, 1365-1385.

[7] Nothofer, H.-G.; Meisel, A.; Miteva, T.; Neher, D.; Forster, M.; Oda, M.; Lieser, G.; Sainova, D.; Yasuda, A.; Lupo, D.; Knoll, W.; Scherf, U. *Macromol. Symp.* **2000**, *154*, 139-148.

[8] a) Grell, M.; Bradley, D. D. C.; Ungar, G.; Hill, J.; Whitehead, K. S. Macromolecules 1999, 32, 5810; b) Grell, M.; Bradley, D. D. C.; Long, X.; Chamberlain, T.; Inbasekaran, M.; Woo, E. P.; Soliman, M. *Acta Polym.* **1998**, *49*, 439.

[9] Lieser, G.; Oda, M.; Miteva, T.; Meisel, A.; Nothofer, H. G.; Scherf, U.; Neher, D. *Macromolecules* **2000**, *33*, 4490.

[10] Grell, M.; Knoll, W.; Lupo, D.; Meisel, A.; Miteva, T.; Neher, D.; Nothofer, H.-G.; Scherf, U.; Yasuda, A. *Adv. Mater.* **1999**, *11*, 671-675.

[11] Müllen, K.; Wegner, G. 'Electronic Materials: The Oligomer Approach' Eds. Weinheim: Wiley-VCH, **1998,** chapter 5, 295-328.

[12] Landau, L. M.; Lifshitz, E. M.; Pitaevskii, L. P.; *Statitstical Physics, part 1,* 3rd ed., Pergamon, Oxford **1980**.

[13] Doi, M. *J. Polym. Sci., Polym. Phys. Ed.* **1981**, *19*, 229.

[14] a) Marrucci, G.; Maffettone, P. L. 'Description of the Liquid-Crystalline Phase of Rodlike Polymers at High Shear Rates'. *Macromolecules* **1989**, *22*, 4076; b) Tsvetkov, V. N. *Acta Physicochim.* USSR **1942**, *16*, 132.

[15] Sauer, T.; Arndt, T.; Batchelder, D. N.; Kalachev, A. A.; Wegner, G. 'The Structure of Langmuir-Blodgett Films from Substituted Phthalocyaninato-Polysiloxanes'. *Thin Solid Films* **1990**, *187*, 357.

[16] Grell, M.; Bradley, D. D. C. 'Polarized luminescence from oriented molecular materials'. *Advanced Materials.* **1999**, *11(11)*, 895.

[17] a) Dyreklev, P.; Berggren, M.; Inganäs, O.; Andersson, M. R.; Wennerström, O.; Hjertberg, T. *Adv. Mater.* **1995**, *7*, 43; b) Lemmer, U.; Vacar, D.; Moses, D.; Heeger, A. J.; Ohnishi, T.; Noguchi, T. *Appl. Phys. Lett.* **1996**, *68*, 21.

[18] Hamaguchi, M.; Yoshino, K. *Appl. Phys. Lett.* **1995**, *67*, 23

[19] Cimrova, V.; Remmers, M.; Neher, D.; Wegner, G. *Adv. Mater.* **1996**, *8*, 146.

[20] a) Lüssem, G.; Festag, R.; Greiner, A.; Schmidt, C.; Unterlechner, C.; Heitz, W.; Wendorff, J. H.; Hopmeier, M.; Feldmann, J. *Adv. Mater.* **1995**, *7*, 923. b) Lüssem, G.; Geffarth, F.; Greiner, A.; Heitz, W.; Hopmeier, M.; Oberski, M.; Unterlechner, C.; Wendorff, J. H.; *Liq. Cryst.* **1996**, *21*, 903.

[21] Dyreklev, P.; Berggren, M.; Inganas, O.; Andersson, M. R.; Wennerstrom, O.; Hjertberg, T. *Advanced Materials.* **1995**, *7(1)*, 43.

[22] Hagler, T. W.; Pakbaz, K.; Voss, K. F.; Heeger, A. J. *Phys. Rev. B* **1991**, *44*, 8652.

[23] Smith, P.; Lemstra, P. J. *J. Mater. Sci.* **1980**, *15*, 505.

[24] a) Bradley, D. D. C.; Friend, R. H.; Lindenberger, H.; Roth, S. *Polymer* **1986**, *27*, 1709; b) Lemmer, U.; Vacar, D.; Moses, D.; Heeger, A. J.; Ohnishi, T.; Noguchi, T. *Appl. Phys. Lett.* **1996**, *68*, 3007.

[25] Bradley, D. D. C. *J. Phys. D: Appl. Phys.* **1987**, *20*, 1389.

[26] Jandke, M.; Strohriegl, P.; Gmeiner, J.; Brütting, W.; Schwoerer, M. *Synthetic Metals* **2000**, *111*, 177.

[27] Wittmann, J. C.;Smith, P. *Nature* **1991**, *352*, 414.

[28] Yoshida, Y.; Tanigaki,N.; Yase, K.; Hotta, S. *Adv. Mater.* **2000**, *12(21)* 1587.

[29] a) Pichler, K.; Friend, R. H.; Burn, P. L. Holmes, A. B. *Synth. Met.* **1993**, *55*, 454; b) Winkler, B.; Tasch, S.; Zojer, E.; Ungerank, M.; Leising, G.; stelzer, F. *Synth. Met.* **1996**, *83*, 177.

[30] Stroog, C. E. *J. Polym. Sci.* **1976**, *11*, 161.

[31] a) O'Neill, M.; Kelly, S. M. *J. Phys. D: Appl. Phys.* **2000**, *33*, R67; b) Gibbons, W. M.; Shannon, P. J.; Sun, S. T. Swetlin, B. J. *Nature* **1991**, *351*, 49; c) Kim, J.-H.; Kumar, S.; Lee, S.-D. *Phys. Rev. E* **1998**, *57(5)*, 5644; d) Hasegawa, M.; Taira, Y. *J. Photopoly. Sci. Technol.* **1995**, *8*, 241; e) Kim, J.-H.; Acharya, B. R.; Kumar, S.; Ha, K. R. *Appl. Phys. Lett.* **1998**, *73*, 3372.

[32] Floudas, G. in *Broadband Dielectric Spectroscopy*, edited by Kremer, F. and Schönhals, A. (Springer, New York; **2002**), Ch. 8.

[33] Havriliak, S. and Negami, S. *Polymer* **1967**, *9*, 161.

[34] Floudas, G.; Mierzwa, M. and Schoenhals, A. *Phys. Rev. E* **2003**, *67*, 31705.

[35] Angell, C.A. *Polymer* **1997**, *38*, 6261.

[36] Ariu, M.; Lidzey, D. G.; Laurentieu, M.; Bradley, D. D. C.; Jandke, M.; Strohriegl, P. *Synthetic Metals* **2001**, *116*, 217.

[37] Böhmer, R.; Ngai, K. L.; Angell, C. A.; Plazek, D. J. *J. Chem. Phys* **1993**, *99*, 4201.

[38] Stickel, F.; Fischer, E. W.; Richert, R. *J. Chem. Phys.* **1996**, *104*, 2043.

[39] McCrum, B. G.; Read, B. E.; Williams, G. In *Anelastic and Dielectric effects in Polymeic Solids*; Dover Publ. Inc. New York, **1991**.

[40] Geng, Y.; Culligan, S. W.; Trajkouska, A.; Wallace, J. U.; Chen, S. H. *Chem. Mater.* **2003**, *15*, 542.

5 Photophysical properties of oligofluorenes

*The steady state spectra (UV-vis absorption and fluorescence spectra) of oligofluorenes (**OF-n**) and polyfluorenes (**PF2/6**) both in solution and film are presented in this chapter. The transient photoluminescence properties of the oligofluorenes in m-THF and thin-film were investigated by ultra fast photoluminescence using a streak camera and conventional time-resolved photoluminescence technique at both room temperature and 77K. Concentration and laser excitation intensity dependences of PL spectra of the oligofluorenes are also discussed. Phosphorescence was observed for oligofluorenes in frozen matrix of m-THF solution at 77K. Its lifetime increases with increasing of molecular length. Finally, the nature of the photophysical processes is explained by the energy level diagram involving singlet and triplet states of oligofluorenes.*

5. 1 Introduction

Photophysical properties of polyfluorenes and corresponding oligofluorenes in solution and as thin-films are the basic issues when considering their applications in electroluminescence devices. The knowledge of the relationship between photophysical properties and chain-length, environment (for example, temperature and solvents) allows an accurate tuning of the electro-optic properties in LEDs.

The photophysical properties of oligofluorenes[1] and polyfluorenes[2] have been studied, particularly the excited-state dynamics of singlet and triplet states which are closely connected with the luminescence quantum efficiency. The energy of the lowest singlet and triplet state of poly- and oligo-fluorenes were recently investigated[3], but so far the chain-length dependence of their photophysical properties has not been fully reported and discussed. In this chapter the photophysical properties of oligofluorenes (**OFn**) with 2-ethylhexyl side chains are investigated by steady-state and time-resolved fluorescence spectroscopy. The chain-length dependence, concentration dependence, laser excitation power dependence of the photophysical properties are discussed and explained by energy-level diagrams of the excited singlet and triplet states.

5. 2 Basic theory and method

5. 2. 1 Radiative and non-radiative transitions between electronic states

The energy level diagram of organic π-conjugated molecules is very important to explain the mechanism of their complex photophysical properties. The general energy level diagram, so-called Perrin-Jablonski diagram, (Figure 5. 2. 1) is convenient for visualizing in a simple way several possible photophysical processes[4]: photon absorption, internal conversion, fluorescence, intersystem crossing, phosphorescence, delayed fluorescence and triplet-triplet transition. The singlet electronic states are denoted S_0 (ground electronic state), S_1, S_2... and the triplet states, T_1, T_2, ... Vibrational levels are associated with each electronic state. It is important to note that absorption is very fast ($\approx 10^{-15}$ s) with respect to
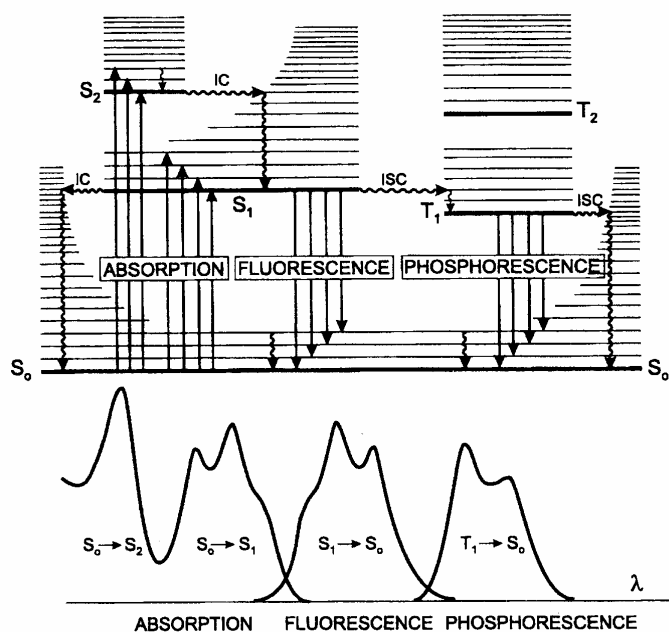
CHARACTERISTIC TIMES
absorption 10^{-15} s
vibrational relaxation 10^{-12}-10^{-10} s
lifetime of the excited state S_1 10^{-10}-10^{-7} s → fluorescence
intersystem crossing 10^{-10}-10^{-8} s
internal conversion 10^{-11}-10^{-9} s
lifetime of the excited state T_1 10^{-6}-1s →phosphorescence

Figure 5. 2. 1. Perrin-Jablonski diagram and illustration of the relative positions of absorption, fluorescence and phosphorescence spectra[4]. The arrows with full line:

absorption and emission of light; wavy lines: radiationless transitions (IC: internal conversion, ISC: intersystem crossing).

all other processes so that there is no concomitant displacement of the nuclei according to the Franck-Condon principle[4]; The vertical arrows corresponding to absorption start from the 0 (lowest) vibrational energy level of S_0 because the majority of molecules are in this level at room temperature, as shown in Figure 5. 2. 2[4]. Absorption of a photon can bring a molecule to one of the vibrational levels of S_1, S_2,....
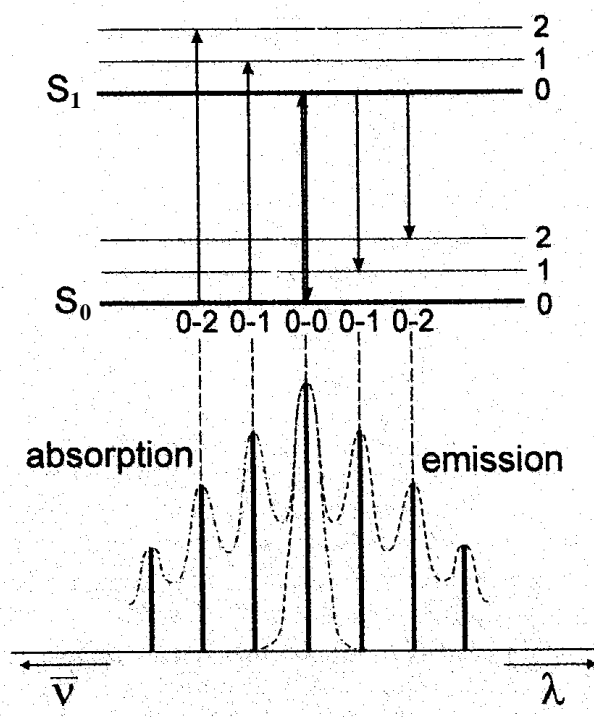
Figure 5. 2. 2. Illustration of the vibrational bands in the absorption and fluorescence spectra of aromatic hydrocarbons[4].

Once a molecule is excited by absorption of a photon, it can return to the ground state with emission of fluorescence, but many other pathways for de-excitation are also possible (Figure 5. 2. 3)[4]: internal conversion (i.e. direct return to the ground state without emission of fluorescence), intersystem crossing (possible followed by emission of phosphorescence), intramolecular charge transfer and conformational change. Interactions in the excited state with other molecules may also compete with de-excitation: electron transfer, proton transfer, energy transfer, excimer or exciplex formation.

Delayed fluorescence (DF) and phosphorescence (Ph) are ubiquitous features of molecular solids.[5] The triplet state, which is usually populated by intersystem crossing (ISC) from optically excited singlet states, can either decay monomolecularly or bimolecularly. In the case of monomolecular decay, long-lived phosphorescence is emitted, whereas the bimolecular reaction leads to generation of an excited singlet state and a singlet ground state, respectively. The excited singlet state then leads to delayed fluorescence.
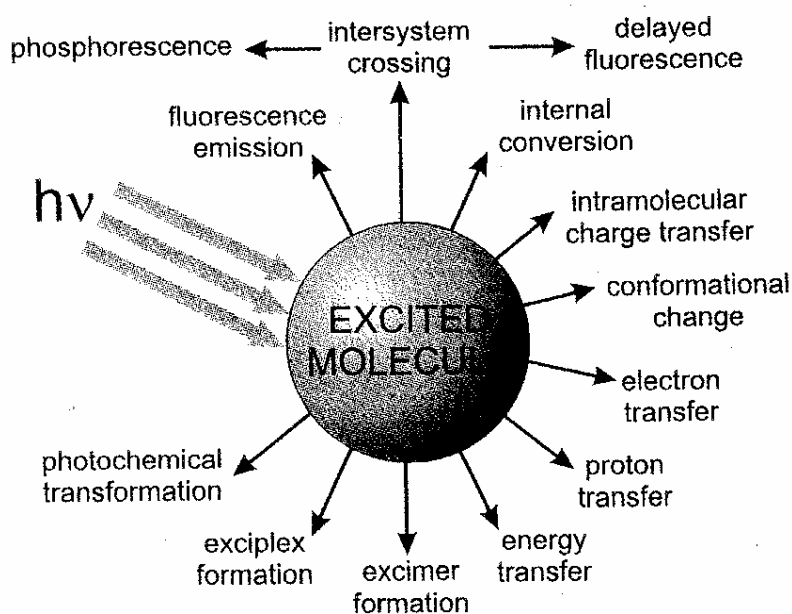
Figure 5. 2. 3. Possible de-excitation pathways of excited molecules[4].

5. 2. 2 The Boltzmann Law

For some aromatic hydrocarbons such as naphthalene, anthracene and perylene, the absorption and fluorescence spectra exhibit vibrational bands. The energy spacing between the vibrational levels and the Franck-Condon factors that determine the relative intensities of the vibronic bands are similar in S_0 and S_1. As a result, the emission spectrum often appears to be symmetrical to the absorption spectrum ('mirror image' rule), as illustrated in Figure 5. 2. 2.

The ratio of the numbers of molecules N_1 and N_0 in the 1 and 0 vibrational levels of energy E_1 and E_0, respectively, is given by the Boltzmann Law:

$$N_1/N_0 = \exp[-(E_1-E_0)/kT] \tag{5. 2. 1}$$

where k is the Boltzmann constant ($k = 1.3807 \times 10^{-23}$ JK^{-1}) and T is the absolute temperature. For example, the absorption and emission spectra of anthracene show a wavenumber spacing of about 1400 cm^{-1}, i.e. an energy spacing of 2.8×10^{-20} J, between the 0 and 1 vibrational levels. In this case, the ratio N_1/N_0 at room temperature (298 K) is about 0.001. However, it should be noted that most fluorescent molecules exhibit broad and structureless absorption and emission bands, which means that each electronic state consists of an almost continuous manifold of vibrational levels. If the energy difference between the 0 and 1 vibrational levels of S_0 (and S_1) is, for instance, only about 500 cm^{-1}, the ratio N_1/N_0 becomes about 0.09. Consequently, excitation can then occur from a vibrationally excited level of the S_0 state. This explains why the absorption spectrum can partially overlap the fluorescence spectrum. On the other hand, the energy gap between S_0 and S_1 is of course much large than between the vibrational levels, so the probability of finding a molecule in S_1 at room temperature as a result of thermal energy is nearly zero (E_{s1}-$E_{s0} \approx 4 \times 10^{-19}$ J, compared with kT $\approx 4 \times 10^{-21}$ J).

5. 3 Materials and methods

All of materials studied in this chapter were oligofluorenes with 2-ethylhexyl side chains (**OFn**) from dimer to heptamer and the corresponding polyfluorenes (**PF2/6**) (see Scheme 3. 1. 1), and their synthesis was described in Chapter 2.

5. 3. 1 Steady state absorption and emission methods

UV-vis spectra were recorded at room temperature with a Perkin-Elmer Lambda 9 UV/Vis/NIR spectrophotometer. Photoluminescence spectra were obtained on a Spex Fluorolog II (212). Thin films of all materials were prepared by spin-coating of a solution in chloroform onto quartz substrates. The thickness of all of the films is approximately 50 nm, as was estimated by Tencor P-10 Surface Profiler.

5. 3. 2 Time-resolved fluorescence method 5. 3. 2. 1 Streak camera technology (ultra-fast-time-resolved spectrophotometry)
5. 3. 2. 1. 1 What is a streak camera

The streak camera technique is also called "fast time-resolved photoluminescence measurement" It is a device to measure ultra-fast light phenomena and can deliver intensity *vs.* time or *vs.* position (or wavelength) information. Its name dates back to the early days of the high speed rotating drum cameras. These cameras would "streak" reflected light onto film. No other instruments which directly detect ultra-fast light phenomena have better temporal resolution than the streak camera.

Since the streak camera is a two dimensional device, it can be used to detect several tens of different light channels simultaneously. For example, when it is used in combination with a spectroscope, time variation of the incident light intensity with respect to wavelength can be measured (time-resolved spectroscopy). Used in combination with proper optics, it is possible to measure time variation of the incident light with respect to position (time and space-resolved measurement).

5. 3. 2. 1. 2 Operating principle

Figure 5. 3. 1 shows the operating principle of the streak camera. The light being measured passes through a slit and is formed by the optics into a slit image on the photocathode of the streak tube. At this point, let us assume that we have four optical pulses which vary slightly in terms of both time and space, and which have different optical intensities, are coming through the slit and arrive at the photocathode.
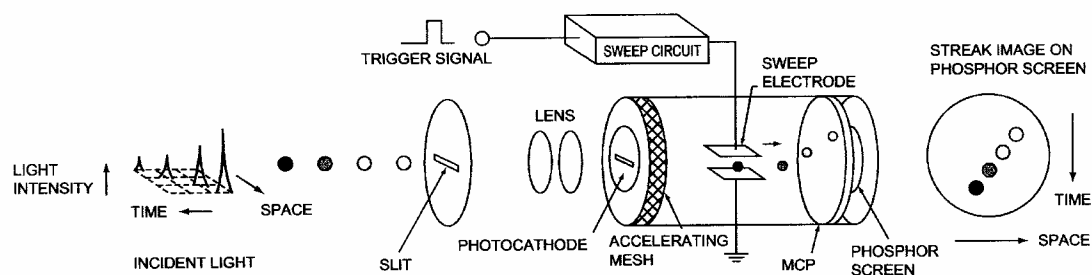
Figure 5. 3. 1. Operating principle of the streak tube.

The incident light on the photocathode is converted into a number of electrons proportional to the intensity of the light, so that these four optical pulses are converted

sequentially into electrons. These then pass through a pair of accelerating electrodes, where they are accelerated and bombarded against a phosphor screen.

As the electrons produced from the four optical pulses pass between a pair of sweep electrodes, high voltage is applied to the sweep electrodes at a timing synchronized to the incident light (see Figure 5. 3. 2). This initiates a high-speed sweep (the electrons are swept from top to bottom). During the high-speed sweep, the electrons, which arrive at slightly different times, are deflected in slightly different angles in the vertical direction, and enter the MCP (micro-channel plate). As the electrons pass the MCP, they are multiplied several thousands of time, after which they impact against the phosphor screen, where they are converted again into light.
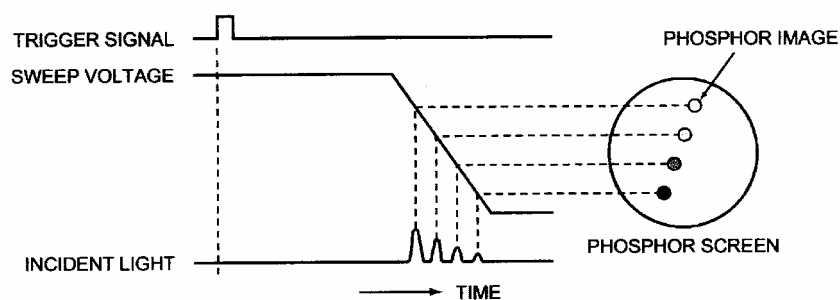
Figure 5. 3. 2. Operation timing (at time of sweep).

On the phosphor screen, the phosphor image corresponding to the optical pulse which was the earliest to arrive is placed in the uppermost position, with the other images being arranged in sequential order from top to bottom; in other words, the vertical direction on the phosphor screen serves as the time axis. Also, the brightness of the various phosphor images is proportional to the intensity of the respective incident optical pulses. The position in the horizontal direction of the phosphor image corresponds to the horizontal location of the incident light.

In this way, the streak camera can be used to convert changes in the temporal and spatial light intensity of the light being measured into an image showing the brightness distribution on the phosphor screen. We can thus find the optical intensity from the phosphor image, and the time and incident light position from the location of the phosphor image.

5. 3. 2. 1. 3 System configuration

In order to measure ultra-high speed optical phenomena using a streak camera, a trigger section and a readout section are required. The basic configuration of this system is shown below (Figure 5. 3. 3).

The trigger section controls the timing of the streak sweep. This section has to be adjusted so that a streak sweep is initiated when the light being measured arrives at the streak camera. For this purpose, we use a delay unit, which controls how long the trigger signal which initiates the streak sweep is delayed, and a frequency divider, which divides the frequency of the external trigger signal, if the repetition frequency of the trigger signal is too high. Also, in cases where the trigger signal cannot be produced from the devices such as a laser, it has to be produced from the light being measured itself, and this requires a PIN photodiode.
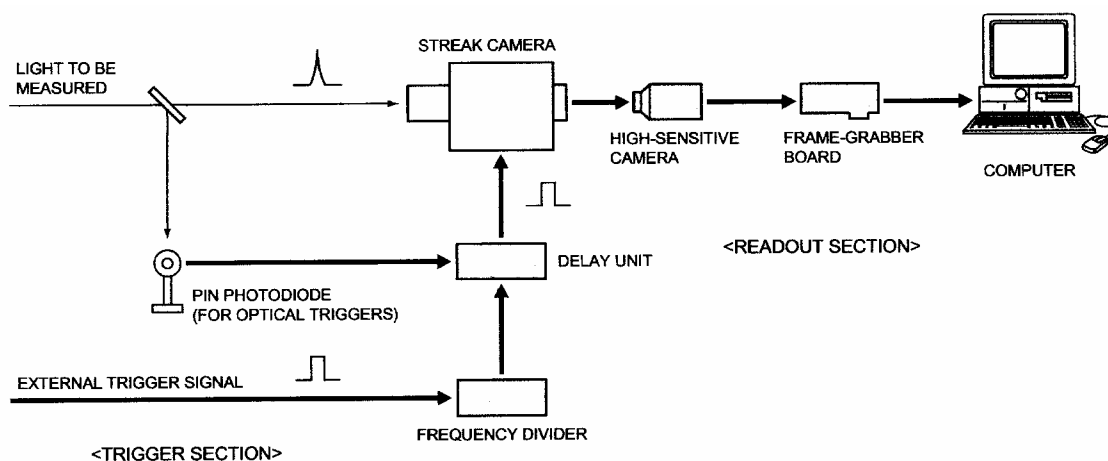
Figure 5. 3. 3. Basic System Configuration of Streak Camera.

The readout section reads and analyzes streak images produced on the phosphor screen which is on the output side of the streak camera. Because the streak image is faint and disappears in an instant, a high-sensitivity camera is used. Analysis of streak images is done by transferring the images through a frame grabber board to a computer. The color of the streak images represents the PL intensity. The spectra of PL intensity *vs.* wavelength and PL Intensity *vs.* time are obtained from the analysis of streak camera images (Figure 5. 3. 4).

In addition to the units which make up this basic configuration, there are spectroscopes, optics, and other peripheral equipments which can be used depending on each applications.
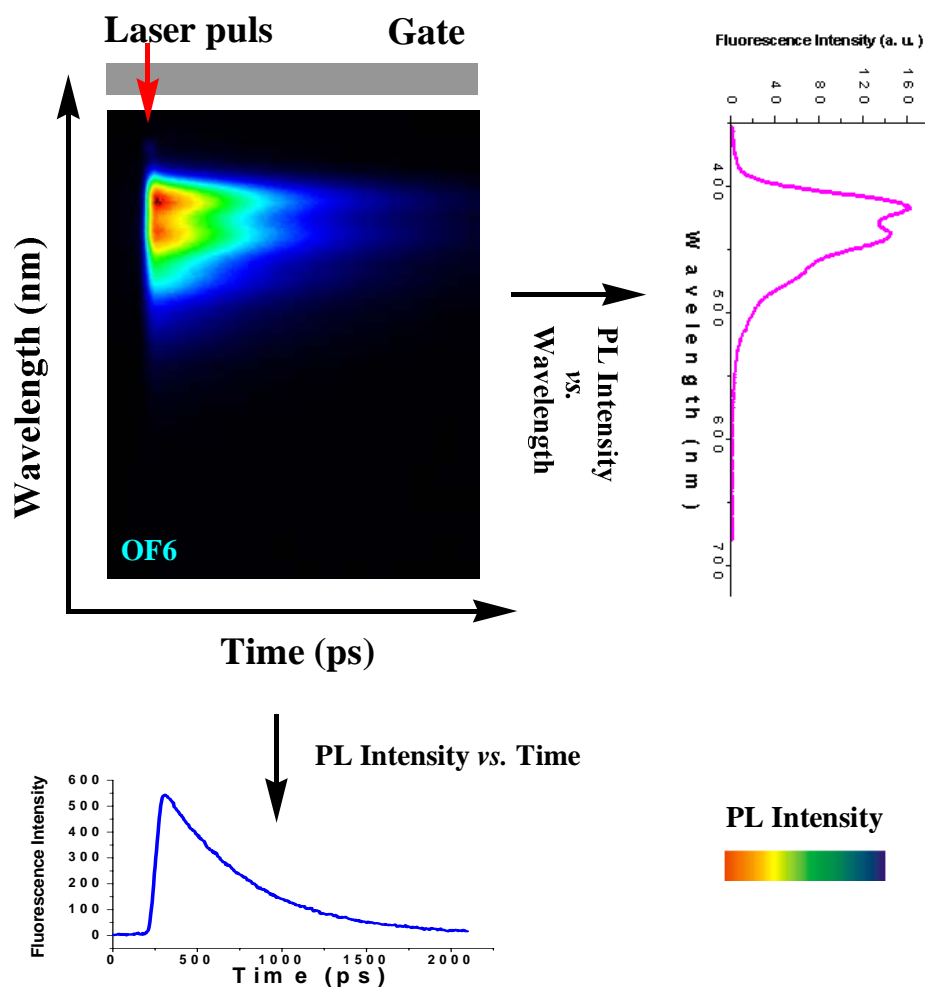
Figure 5. 3. 4. The spectra of PL intensity vs. wavelength and PL Intensity vs. time are obtained from the analysis of streak camera records.

5. 3. 2. 2 Gate detection technique

The long-range delay fluorescence measurements can be done by gate detection technique. Gate detection technique is an interesting alternative to the single-photon timing technique (SPT).[6] The intensity decays were measured using stroboscopic or pulse sampling methods. The basic idea is to sample the intensity decay following pulsed excitation (Figure 5. 3. 5). The detection gate is displaced across the intensity decay until the entire decay is measured. In fact, the first time-domain (TD) lifetime instruments used gated detection to sample the intensity decay.[7]

Gate detection can be accomplished in two ways. One method is to turn on or gate the gain of the detector for a short period during the intensity decay.[8] Surprisingly, this can be accomplished on a timescale adequate for measurement of nanosecond lifetimes. Alternatively, the detector can be on during the entire decay, and the electrical pulse measured with a sampling oscilloscope.[9] Such devices can sample electrical signals with a resolution of tens of picoseconds. In recent years there has been a reintroduction of gated detection methods.[10]

The sample is excited by a train of light pulses delivered by a flash lamp or a pulsed lasers. A computer-controlled digital delay unit is used to gate (or 'strobe') the photomultiplier by a voltage pulse (whose width defines a time window) at a time accurately delayed with respect to the light pulse. Synchronization with the laser pulse is achieved by a master clock or electric triggering. By this procedure, only photons emitted from the sample that arrive at the photocathode of the photomultiplier during the gate time will be detected. The fluorescence intensity as a function of time can be constructed by moving the time window after each pulse from before the pulse light to any suitable end time (e.g. ten times the excited-state lifetime). The principle of the gate detection technique is shown in Figure 5. 3. 5.[6b] and Figure 5. 3. 6[4].

The gate detection technique offers some advantages. It can detect many photons per pulse, which should provide improved statistics. It does not require expensive electronics. High-frequency light sources are unnecessary because the intensity of the signal is directly proportional to the intensity of the light pulse, in contrast to the single-photon timing technique. High-intensity picosecond lasers operating at low repetition rate can be used, with the advantage of lower cost than cavity dumped, mode-locked picosecond laser. A disadvantage of this method is the lack of knowledge of the noise level for each data point, so that one needs to estimate the experimental uncertainties during data analysis, and lifetime measurements with samples of low fluorescence intensity are more difficult.
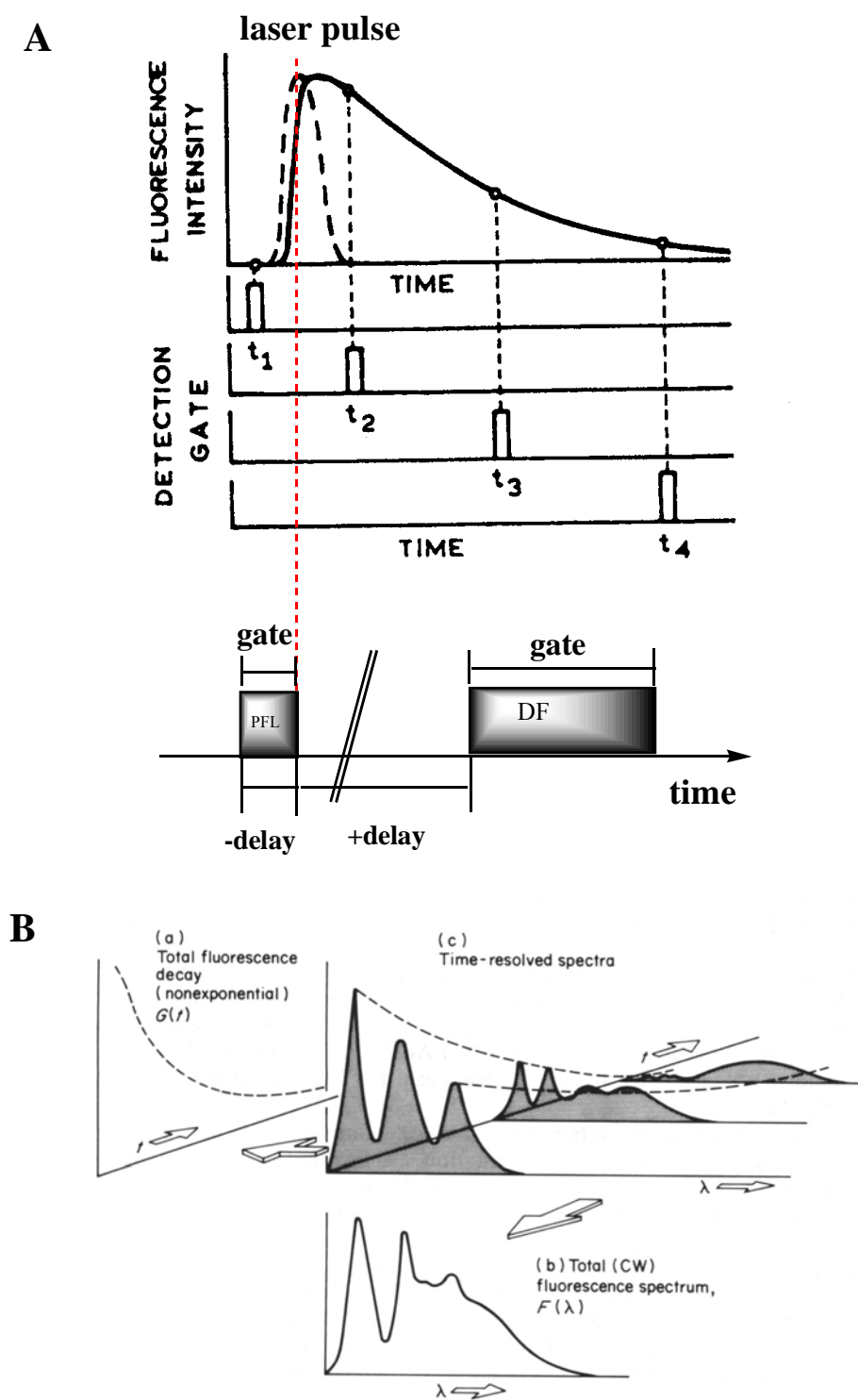
Figure 5. 3. 5. A: Principle of the gate detection technique[6b]; B: Relation between CW and TR-PL. (PFL: prompt fluorescence; DF: delayed fluorescence).
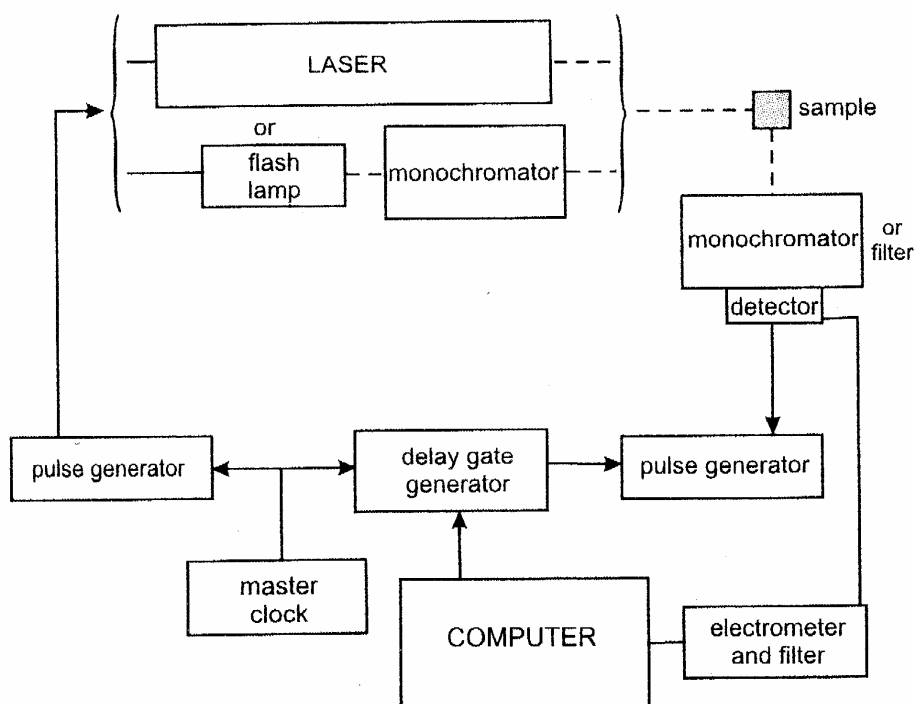
Figure 5. 3. 6. Basic System Configuration of Delayed photoluminescence measuremente[4].

5.4 Steady-state spectra

Electronic absorption spectra of monodisperse oligo(9.9-bis(2-ethylhexyl)fluorene-2.7-diyl)s **OF2-OF7** in diluted chloroform solution with the same fluorene unit concentration of 1.0×10^{-5} M are shown in Figure 5. 4. 1a and the data are collected in Table5. 4. 1.

The oligofluorenes exhibit unstructured absorption bands, as is also seen for polyfluorenes.[11] The absorption maximum is red-shifted with increasing number (*n*) of fluorene units. Absorption energies decrease with n (the number of fluorene unit in oligofluorene) following the quantum-mechanical law eqn. (5. 4. 1) of Davidov based on monomer interactions in oligomers:

$$\Delta E = \text{A-}2|M|\left|\cos\frac{\pi}{n+1}\right| \qquad (5.4.1)$$

Where A is a constant related to the monomer absorption energy, and *M* is the matrix element of the interaction between neighboring fluorene unit, a constant independent of *n*.[12]

The molar extinction coefficient (ε) and effective conjugation length of the oligofluorenes in chloroform solution have been discussed in chapter 3. The UV-vis

absorption spectra of thin films of the oligofluorenes and polyfluorene on quartz substrates (Figure 5. 4. 1b) are practically similar to the solution data except for slight red-shifts in absorption maxima, as listed in Table 5. 4. 1. In some cases, the absorption spectra in solid state are generally slightly broadened by 100-250 meV as result of small local variations of the π-overlap due to some conformational disorder of the oligomer and polymer chains in the solid state.

Figure 5. 4. 1c showes the photoluminescence (PL) spectra of dimer (**42, OF-2)** to heptamer (**50, OF-7**) in chloroform with the same concentration of fluorene units (1.0 x 10^{-6} M), excited at the corresponding energy of maximum absorption. In contrast to the absorption, the emission spectra exhibit a well – resolved vibronic structure, similar to polyfluorenes, assigned to the π←π* 0-0, 0-1 and 0-2 intrachain singlet transitions,[13] The well-resolved vibronic progression with an energetic spacing of approximate 160 m eV is observed, which is related to the stretching mode of C=C-C=C substructures of the oligomer or polymer backbone.[14] The spectral position and the intensity of the PL maximum changes with the number of fluorene units *n*. This is explained by the increase of effective conjugation from dimer to heptamer. Notably, the relative intensity ratio of the three emission bands also changes with *n*. The relative component part of the 0-0 transition increases, while that of the 0-1 transition decreases with *n*. This may be related to the increase of the intrachain coupling interaction with the molecular length.

The fluorescence spectra were also measured for **OF7** in different solvents, which are the *m*-cyclohexane, *m*-THF, toluene, chloroform (Figure 5. 4. 2). The spectra in *m*-cyclohexane were slightly blue shifted by 4-5 nm compared with the spectra in chloroform due to the high polarity of chloroform, but the solvatochromic effect was very weak due to low polarity of homo-oligofluorenes; thus the shift is only several nanometers from polar solvent to nonpolar solvent.

Normalized solid-state PL spectra of oligofluorenes (**42**, **43**, **45**, **46**, **49** and **50**) from spin-coat thin films on a quartz plate excited at the absorption maxima are shown in Figure 5. 4. 1d, and the key data are also listed in Table 5. 4. 1. The films typically display solid-state emission spectrum which are similar in shape and position to the spectrum in dilute solution, slight red-shifts in the emission maximum are observed and relative intensities of the 0-1 intrachain singlet transition increase in all cases. Most importantly, the green-band emission usually seen for the polymer[15] is absent for all of the oligomers, as seen in Figure

5. 4. 1d. Even upon high temperature annealing (180 °C) in air, this green emission is still negligible for the oligomers. This results casts doubt on the widely discussed hypothesis that the "green" emission seen with variable intensity in polymer samples (see Figure 5. 4. 3)[16] originates from excimer formation by inter-chain interaction or chemical defects in the polymer backbone. It is difficult to see why such interchain interactions are suppressed in the case of oligomers if explanation of excimer formation is true.
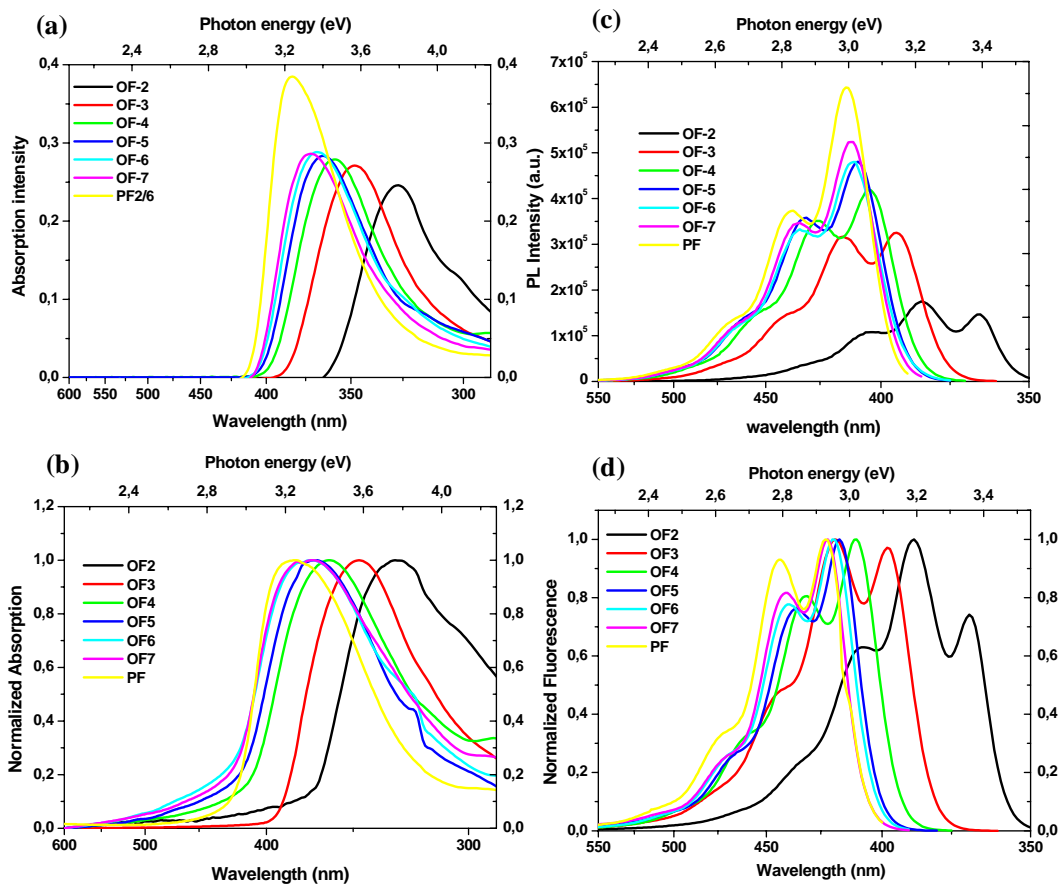
*Figure 5. 4. 1. a)UV-Vis absorption of oligofluorenes dimer to heptamer, and polymer in chloroform solution at room temperature. The spectra (**OF2** up to **OF7**, **PF2/6**) were recorded at a fixed concentration of fluorene repeat units of 1.0×10^{-5} molL^{-1}; b) UV-Vis absorption of oligofluorenes dimer to heptamer film (thickness: around 50 nm) on quartz; c) emission spectra of the oligofluorenes and polymer in chloroform solution at room temperature; the spectra of **OF2** up to **OF7** were recorded at a fixed concentration of fluorene repeat units of 1.0×10^{-6} molL^{-1}, emission spectra of **PF2/6** was recorded at a*

fixed concentration of fluorene repeat units of 2.5×10^{-7} $molL^{-1}$; d) emission spectra of oligofluorenes dimer to heptamer film on quartz;

Table 5. 4. 1. Summary of UV-Vis absorption $\lambda_{max(abs)}$(or $\nu_{max(abs)}$) and photoluminescence $\lambda_{max(PL)}$ (or $\nu_{max(PL)}$) spectra of fluorene oligomers and polymer, from chloroform solutions and solid films.

Sample	Solution						Film					
	$\lambda_{max(abs)}$		$\lambda_{max(PL)}$[a]				$\lambda_{max(abs)}$		$\lambda_{max(PL)}$[a]			
	nm	(eV)[b]	nm	(eV)	nm	(eV)[b]	nm	(eV)[b]	nm	(eV)[b]	nm	(eV)[b]
OF-2	327	(3.79)	365	(3.40)	385	(3.22)	329	(3.77)	369	(3.36)	388	(3.20)
OF-3	348	(3.56)	394	(3.15)	415	(2.99)	349	(3.55)	398	(3.12)	419	(2.96)
OF-4	358	(3.46)	404	(3.07)	426	(2.91)	363	(3.42)	410	(3.02)	431	(2.88)
OF-5	365	(3.40)	409	(3.03)	432	(2.87)	370	(3.35)	417	(2.97)	436	(2.84)
OF-6	368	(3.37)	411	(3.02)	434	(2.86)	372	(3.33)	420	(2.95)	439	(2.82)
OF-7	372	(3.33)	412	(3.01)	434	(2.86)	373	(3.32)	422	(2.94)	440	(2.82)
PF2/6	383	(3.24)	414	(3.00)	437	(2.84)	383	(3.24)	422	(2.94)	443	(2.80)

[a]*Since the resolution of the low energy peak was too low at the temperature where the data have been recorded only λ_{max} of the two high energy component are given;* [b] $\nu_{max(abs)}$ *and* $\nu_{max(abs)}$ *in unit of eV*
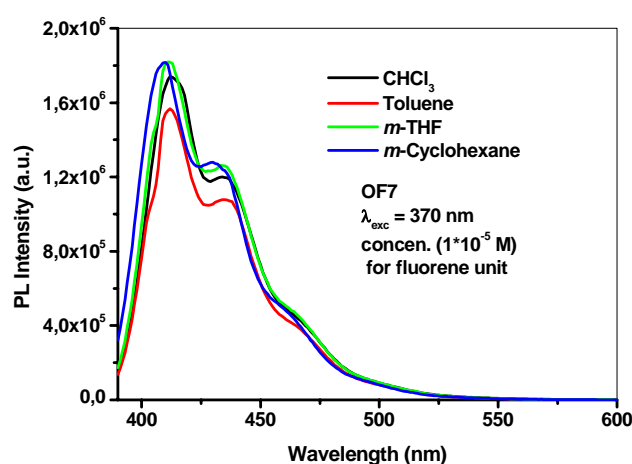
*Figure 5. 4. 2. The steady state fluorescence spectra of **OF7** in different solvents.*
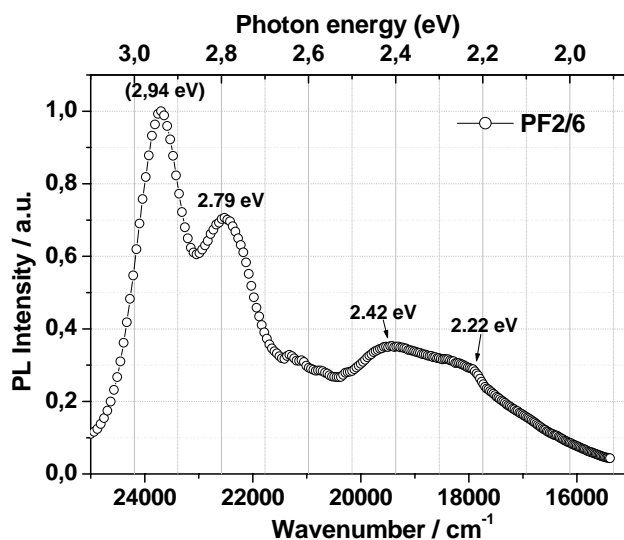
*Figure 5. 4. 3 Fluorescence spectra of thin films of the **PF2/6** obtained for a sample annealed at 180 °C for 1 hr in air.*

5. 5 Fast time-resolved fluorescence

5. 5. 1 The spectra and decay of fluorescence

The time-resolved fluorescence spectra of the oligofluorenes and corresponding polymer in *m*-THF recorded by Streak camera techniques were shown in Chapter 3. 2. 4. In all the cases, mono-exponential fluorescence decay curves were observed and the lifetimes of the oligomers were in the subnanosecond range (Figure 3. 2. 6). The lifetimes (τ) of the oligomers displayed a linear relation with the reciprocal number of the fluorene units (1/n) with the equation:

$$\tau = 386 + 808 \, (1/n) \tag{5. 5. 1}$$

in which τ is in the unit of *ps*. The decrease of lifetimes with the extension of the chain–length (Table 5. 5. 1) can be explained by the enhanced transition dipolar coupling interactions with the increased unit numbers.[17]

Table 5. 5. 1. The lifetimes of oligofluorenes and polyfluorenes, which were measured by streak camera technique with m-THF solution (1 × 10^{-6} M) at room temperature.

	OF2	OF3	OF4	OF5	OF6	OF7	PF2/6
τ (ps)	789	663	578	549	520	505	397
μ_n (D)[a]	6.8	9.3	11.5	13.0	14.4	14.97	-

[a] μ_n was derived from absorption spectra and in the units of Debye (10^{-18} esu.cm).

First, transition dipolar moments of the oligomers can be calculated from eqn. 5. 5. 2, which represents the relation between oscillator strength f and transition dipole moment (for diluted solution)[18]

$$f = \frac{8\pi^2 m_0 \nu}{3he^2}\left|\left\langle\overrightarrow{M_{ul}}\right\rangle\right|^2 = 4.702\times10^{-7}\tilde{\nu}\left|\left\langle\overrightarrow{M_{ul}}\right\rangle\right|^2 \tag{5. 5. 2}$$

In the equation, f is the oscillator strength, m_0 is the electron mass, e is the electron charge, ν is the frequency, $\tilde{\nu}$ is the wavenumber, h is Plank's constant($h = 6.6256 \times 10^{-27}$ erg s), and $\overrightarrow{M_{ul}}$ is the transition dipole moment between state l and u.

The oscillator strength is related to the spectrum of the molar decadic extinction coefficient $\varepsilon(\tilde{\nu})$. Integration over the absorption band gives the osillator strength defined by eqn. 5. 5. 3[18]:

$$f = \frac{2303m_0 c^2}{\pi n_0 Ne^2}\int_{band}\varepsilon(\tilde{\nu})d\tilde{\nu} = \frac{4.319\times10^{-9}}{n_0}\int_{band}\varepsilon(\tilde{\nu})d\tilde{\nu} \tag{5. 5. 3}$$

in which n_0 is the refractive index. For small organic molecules, n_0 is approximated as 1.4. If f in eqn. 5. 5. 2 is replaced by eqn. 5. 5. 3, eqn. 5. 5. 4 can be deduced:

$$\left|\left\langle\overset{\rho}{M}_{ul}\right\rangle\right|^2 = \frac{9.185\times10^{-3}}{n_0\tilde{\nu}}\int_{band}\varepsilon(\tilde{\nu})d\tilde{\nu} \tag{5. 5. 4}$$

in which $\tilde{\nu}$ is the absorption maximum wavenumber (cm^{-1}) and $\overrightarrow{M_{ul}}$ is in the units of Debye (10^{-18} esu.cm). Based on eqn. 5. 5. 4, the transition dipole moment can be calculated, if the absorption spectrum $\varepsilon(\tilde{\nu})$ is measured.

The absorption spectra of all of oligofluorenes (OF-n) in dilute chloroform solution in Figure 5. 4. 1(a) can be addressed in terms of ε(Lmol^{-1}cm^{-1})$\sim \tilde{\nu}$ (cm^{-1}). The transition dipole moments between ground state S_0 and excited state S_1 were then calculated according to eqn. 5. 5. 4 and listed in Table 5. 5. 1. Herein the "μ_n" represents the transition dipole

moment of the corresponding **OF-n**. As shown in Figure 5. 5. 1 a linear relation between the transition dipole moment μ and the number of fluorene units n is obtained in a double logarithmic scale. That is, with the extension of chain length, the values of μ_n increase as:

$$\log(\mu) = 0.6 + 0.6\log(n) \tag{5.5.5}$$

obtained by linear fitting (Figure 5. 5. 1). This is obviously only valid as long as n$<<$ n$^\infty$ where n$^\infty$ is the number of unit defining the conjugation length.
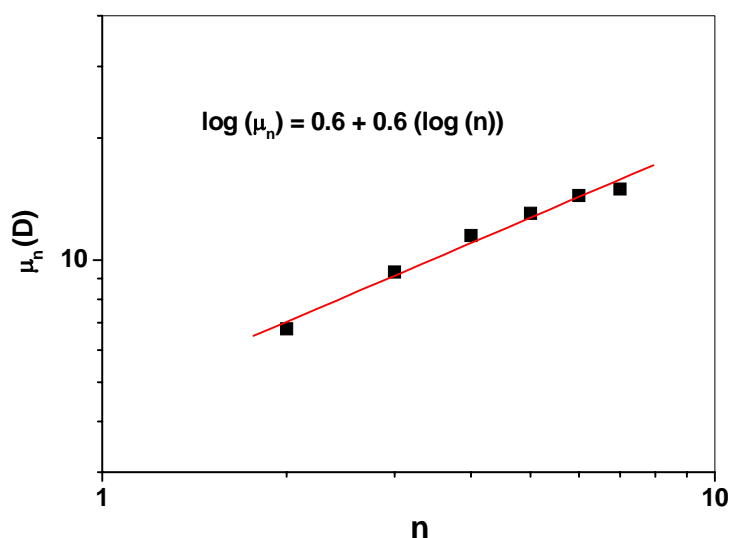
Figure 5. 5. 1. The dependence of transition dipole moment (μ_n) on the degree of polymerization of oligofluorenes.

Generally, an exponential dependence holds for μ_n as function of n (5. 5. 6)[17]

$$\mu_n = n^\alpha \mu_1 \tag{5.5.6}$$

In which μ_1 is the transition dipole moment of the monomer unit. Combined with eqn. 5. 5. 5 and eqn. 5. 5. 6, the parameter μ_1 with 0.6 D and α with 0.6 are obtained. The value of α is in excellent correlation with the Kasha aggregate model ($\alpha = 0.5$).[19]

In addition, photoluminescence intensities were found to decay exponentially due to the well-defined structure of polyfluorenes with very short lifetime in the sub-nanosecond range. The high luminescence quantum efficiency QE of oligofluorenes ranging from 0.9 to 1,[17] measured by means of an etalon, allows the approximation eqn. (5. 5. 7)

$$QE = W_r/(W_r + W_{nr}) \approx 1 \tag{5.5.7}$$

and leads to a direct relation between their fast decay times τ and the radiative rate W_r according to eqn. (5. 5. 8)

$$\tau = 1/ (W_r + W_{nr}) \propto \frac{1}{W_r} = \frac{3\varepsilon_0 hc^3}{\omega^3 (\mu_n)^2} \tag{5. 5. 8}$$

in which ϖ is the emission frequency. It is noteworthy that the nonradiative rate W_{nr} was neglected. Given the small bathochromic (i.e., small change of ϖ), eqn. (5. 5. 9) can be inferred from eqn. (5. 5. 6) and (5. 5. 8), and an approximately linear relationship between τ and *1/n* can be obtained according to Kasha aggregate model with α = 0.5 and K as a constant. Thus our experimental results (Figure 3. 2. 6 (c)) can be explained by eqn. (5. 5. 9)

$$\tau \propto \frac{3\varepsilon_0 hc^3}{\varpi^3 (\mu_n)^2} \propto K \frac{1}{n} \tag{5. 5. 9}$$

Bright sky-blue photoluminescence can be observed for all of oligofluorenes and polyfluorenes. Similar to steady-state fluorescence spectra, the emission of all of compounds in solution or film displayed well-resolved band structures, assigned to the 0-0, 0-1 and 0-2 intrachain singlet transitions. No green emission bands (500-600 nm) were observed in all of oligomers in CW and prompt fluorescence.

Figure 5. 5. 2 shows fluorescene spectra and decay of emission for **OF5** and **PF2/6** both in solution and thin film at room temperature (RT) and 77K. The peaks of the spectra are sharper at 77K compared to RT, and the position of the peaks are slight red-shifted (1-2 nm) comparing to the spectra in solution (*m*-THF) (Figure 5. 5. 2 (a) and (c)).

The decay of fluorescence is faster for the films than in *m*-THF solution (τ = 549 ps) for **OF5**, and become faster with increasing temperature, for example, the lifetimes were longer at 77K (τ = 390 ps) than at room temperature (τ = 343 ps) for **OF5** film. Similar phenomena were also observed for **PF2/6** (Figure 5. 5. 2 (d)). This can be explained by temperature dependent exciton mobility. For example, the exciton concentration is higher in solid films than in dilute solution so that the fluorescence is quenched easier by exciton-exciton collision. The high exciton mobility and high exciton concentration provide the sufficient number of collision during the excited-state lifetime, so that the trapping in defect site results in the decrease of the lifetime of fluorescence.

(A)   (B)

(C)   (D)
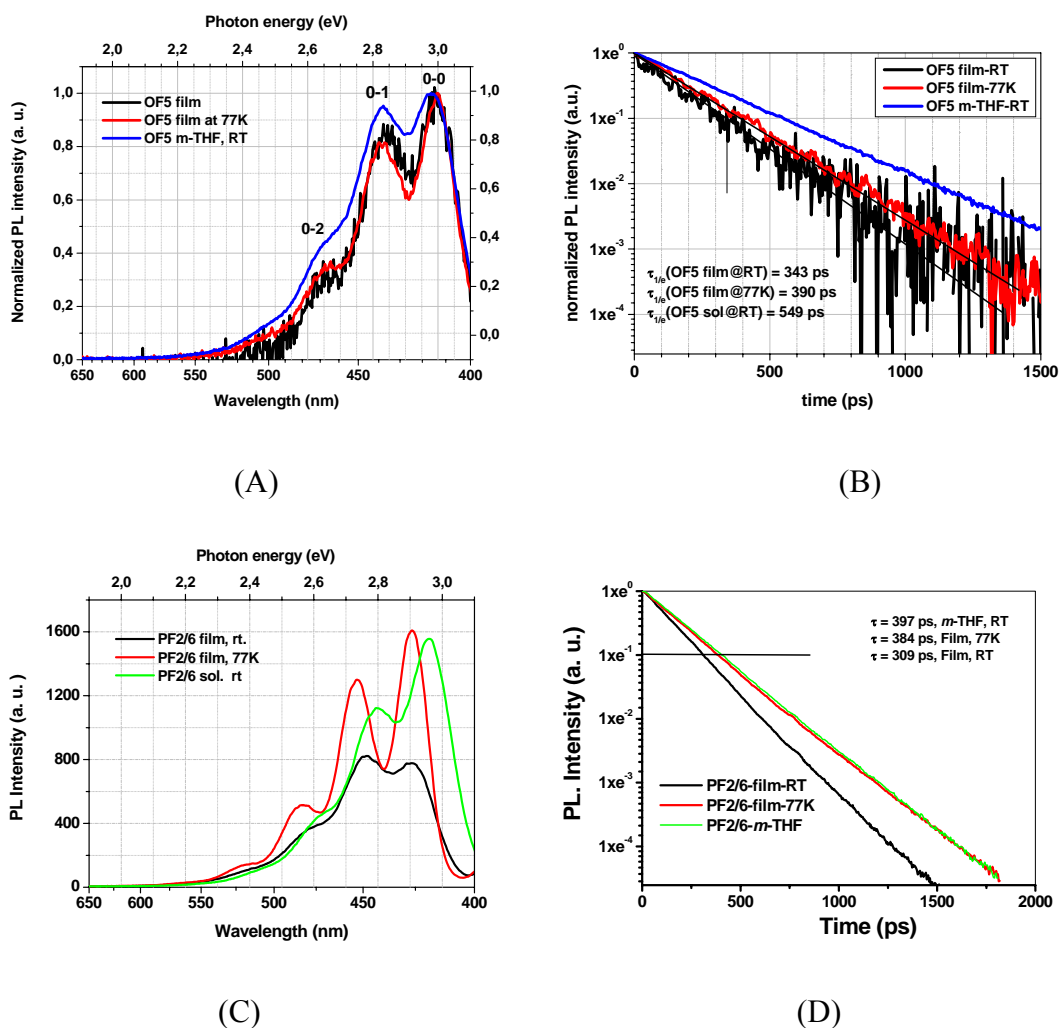
*Figure 5. 5. 2.The time-resolved fluorescence spectra for **OF5** and **PF2/6** both in solution and in film. (A) the fluorescence spectra of **OF5** in both solution and film at room temperature and 77K. (**OF5** in m-THF was excited at 370 nm); (B) the decay of emission of **OF5**; (C) the fluorescence spectra of **PF2/6** in both solution (m-THF) and film at room temperature and 77K ; (D) the decay of emission of **PF2/6**.*

The delayed fluorescence spectra of **PF2/6** (left) and **OF5** (right) are shown in Figure 5. 5. 3. Green light emission was not observed for **PF2/6** solution at room temperature and fresh film at 77K. Green emission bands[20] (500-600 nm) were not observed for all of oligomers in the delayed fluorescence spectra at RT and 77K
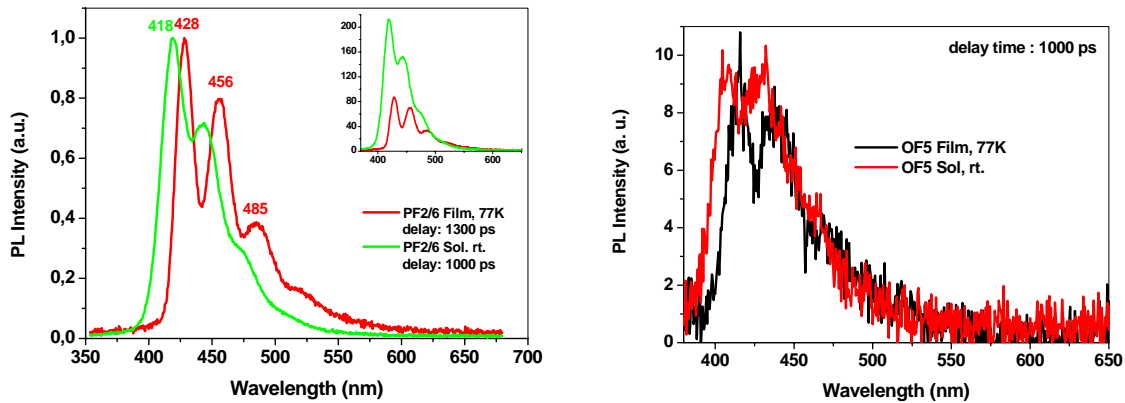
*Figure 5. 5. 3. The delayed fluorescence spectra of **PF2/6** (left) and **OF5** (right) both in solution and film at room temperature and 77K.*

5. 5. 2 Concentration dependence

Concentration dependence was studied with the heptamer (**OF7**) at RT by the Streak camera technique. (Figure 5. 5. 4). No changes were observed in the shape and position of fluorescence spectra, but the fluorescence intensity increased with the concentration from 10^{-7} M to 10^{-4} M. Almost the same PL emission intensity was observed with the concentration from 10^{-4} to 10^{-3} M (Figure 5. 5. 4 (A) and (B)). This means that the fluorescence intensity becomes saturated when the concentration increases to 10^{-4}M.

(A)   (B)

(C)   (D)
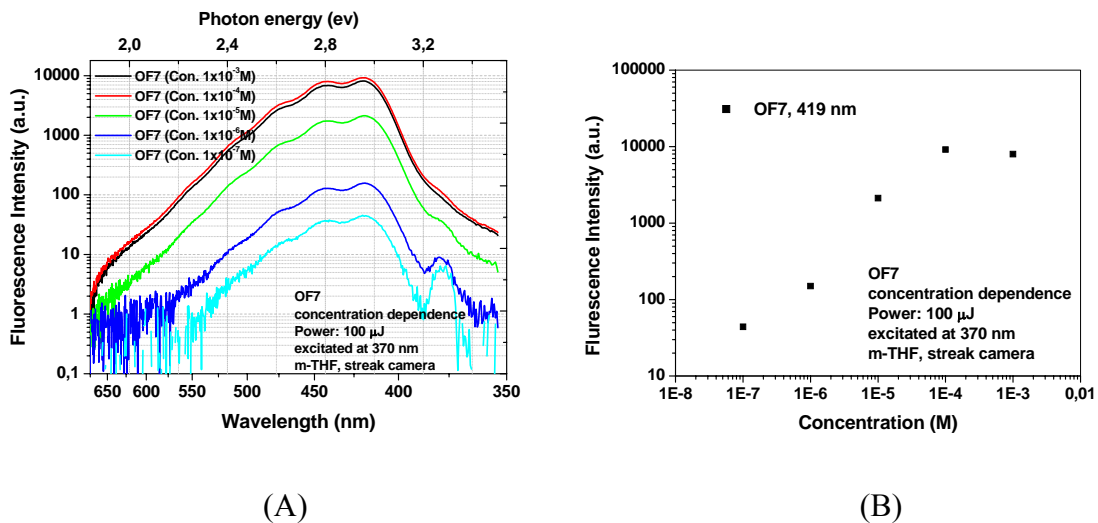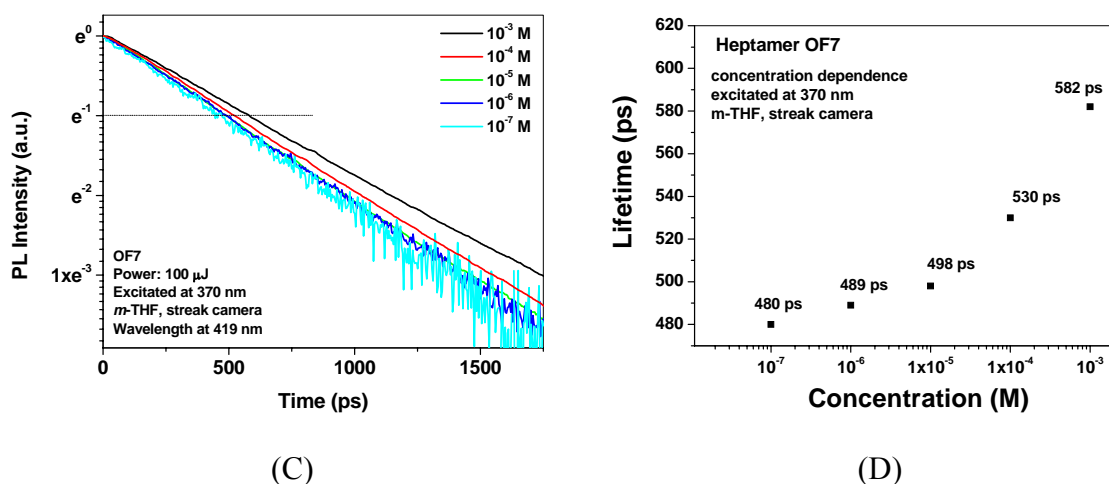
Figure 5. 5. 4. Concentration dependence of the fluorescence spectra of the heptamer at RT. (A) the fluorescence spectra at different concentration in m-THF; (B) the dependence of the fluorescence intensity on the concentration probed at 419 nm; (C) the decay of fluorescence at different concentration in m-THF probed at 419 nm; (D) the dependence of lifetime (1/e) on the concentration probed at 419 nm.

The decay of fluorescence displayed the same monoexponential behaviour under different concentration, and a lifetime increase at increasing concentration (Figure 5. 5. 4 (C) and (D)). The monoexponential decay behaviour of **OF7** at different concentrations means that aggregates and excimer formation are not exist in high concentration solution. The obvious concentration dependence of the lifetime could be related to the solvent-molecules and molecules-molecules interchain interactions.

5. 5. 3 Power intensity dependence

Figure 5. 5. 5 (A) shows the fluorescence spectra of heptamer (**OF7**) at different power of the exciting light (the excitation wavelength is 370 nm). The shape and position of the spectra are almost the same at the different laser excitation intensities.

In Figure 5. 5. 5 (B) the dependence of fluorescence intensity upon laser excitation intensity for the solution of **OF7** at RT is depicted. The fluorescence intensity varies approximately linear with the laser excitation intensity. The data points are not enough to give accurate fitting in Figure 5. 5. 5(B), the dependence of fluorescence intensity on the laser excitation intensity of **OF-n** will be discussed in more detail in Chaper 5. 6.

(A)   (B)
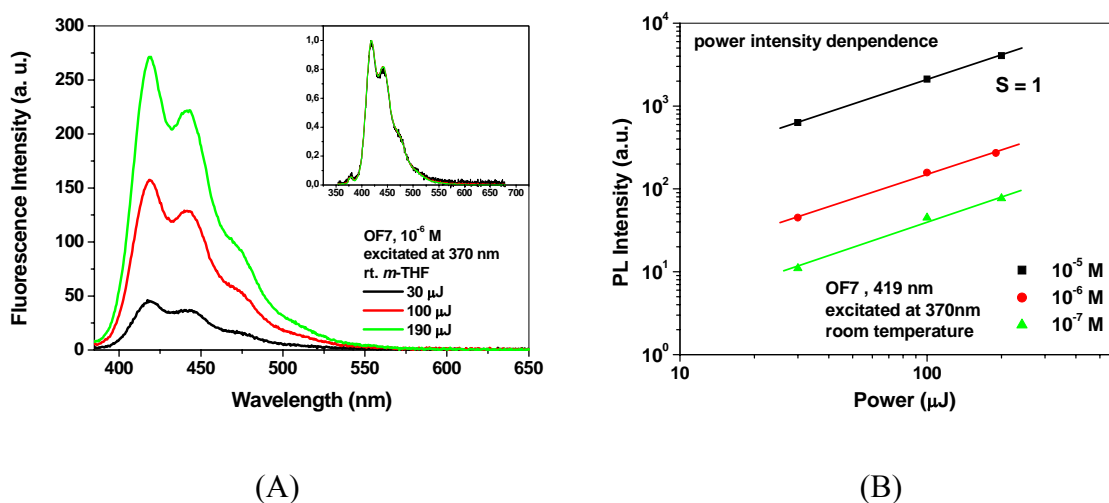
*Figure 5. 5. 5. (A) The fluorescence spectra of **OF7** at different power of the exciting light; the inserted picture: the normalized fluorescence spectra of OF7 at different power;(B) the dependence of the fluorescence intensity on the laser excitation intensity.*

5. 6 Long range delayed fluorescence

The long range delayed fluorescence measurements for **OF5** were done in *m*-THF solution both at RT and 77K. The CW and delayed fluorescence spectra did not change with power intensity except for the increasing of fluorescence intensity (Figure 5. 6. 1 (a) and (b)). The shape of the fluorescence spectra was sharper at 77K compared to those at room temperature (Figure 5. 6. 1 (c)). The fluorescence spectra at different excitation wavelength from 345-405 nm are shown in Figure 5. 6. 1(d), and the wavelength of emission maximum did only slightly shift (2-3 nm).

In Figure 5. 6. 2 the dependence of fluorescence or DF intensity on the laser excitation intensity is depicted for a dilute *m*-THF solution of **OF5** at room temperature and 77K. Delayed emission was recorded with a time delay of 10 ns after excitation at 365 nm. The fluorescence, and the DF intensity varies approximately linear with the laser excitation intensity with the slope S= 1.

(a)

(b)

(c)

(d)
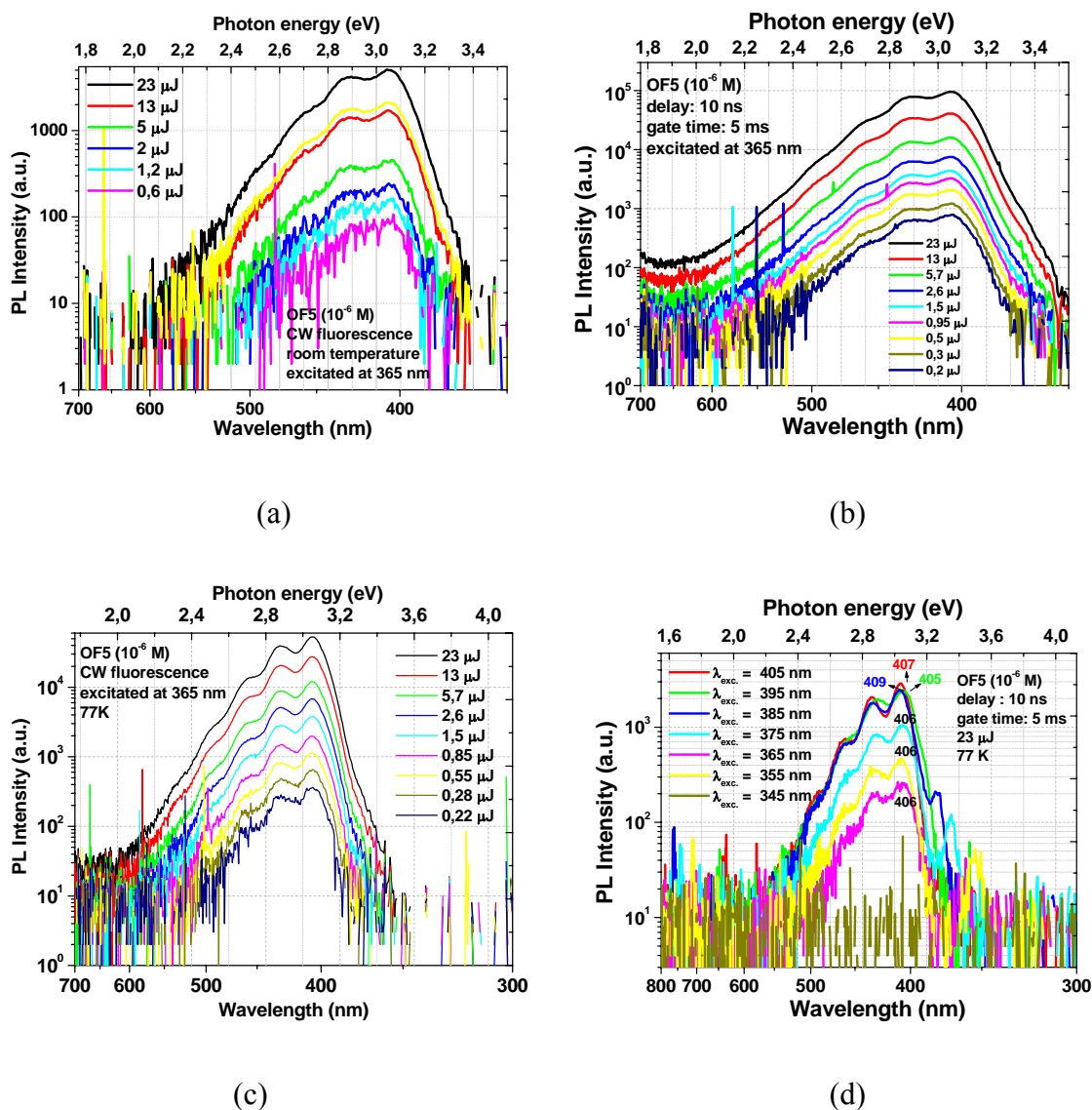
*Figure 5. 6. 1. The fluorescence spectra of **OF5** in m-THF. a) CW fluorescence at room temperature at different intensities; b) the delayed fluorescence at room temperature at different intensities, delay time: 10 ns, gate time: 5 ms; c) CW fluorescence in 77K at different intensities; d) the delayed fluorescence at different wavelength of excitation. For (a), (b), (c) the excitation wavelength is 365 nm; for (d) the delay time of measurement of DF is 10 ns.*
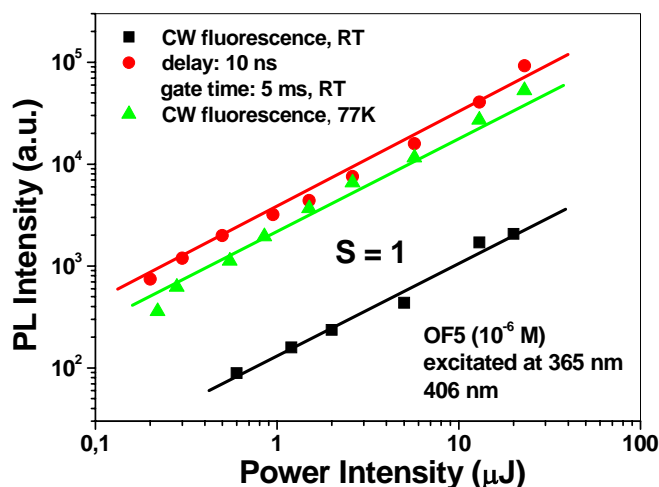
*Figure 5. 6. 2. The dependence of fluorescence, and delayed fluorescence intensity of **OF5** in m-THF on pump intensity at room temperature and 77K. The time delay for measurements of DF was 10 ns; Excitation wavelength is 365 nm.*

The delayed emission spectra of a dilute solid solution of **OF5** at 77K are shown in Figure 5. 6. 3. The delayed emission was detected 1 μs after optical excitation at 380 nm. In the delayed emission spectra of **OF5** in dilute solid solution, two different contributions can be distinguished. The spectral position of the high energy part of the spectra is coincident with the prompt fluorescence at 3.05 eV (406 nm) and shows the same vibronic splitting of about 170 meV. This emission is due to delayed fluorescence (DF) from the S_1 state of **OF5**. At lower energy the delayed emission band at 2.25 eV (552 nm) can be assigned to the $S_0 \leftarrow T_1$ transition bearing a vibronic splitting of 170 meV, identical to the prompt fluorescence. This is also similar with that of PF2/6.[21] The singlet-triplet energy gap in **OF5** amounts to $\Delta E_{ST} \approx 0.80$ eV. Except for the spectral position of the DF and the phosphorescence, the signatures of the delayed emissions are very similar to the spectra of polyfluorenes (**PF2/6**) as shown in Figure 5. 6. 4.[22] The energy level of the T_1 state of the **PF2/6** in *m*-THF solution is at 2.18 eV. The delayed fluorescence spectra at high-energy part peak at 2.39 eV and shows the same vibronic splitting of about 170 meV. In dilute solution the singlet-triplet gap of **PF2/6** with $\Delta E_{ST} \approx 0.75$ eV is smaller than that of **OF5** ($\Delta E_{ST} \approx 0.80$ eV).

(a)

(b)

(c)

(d)
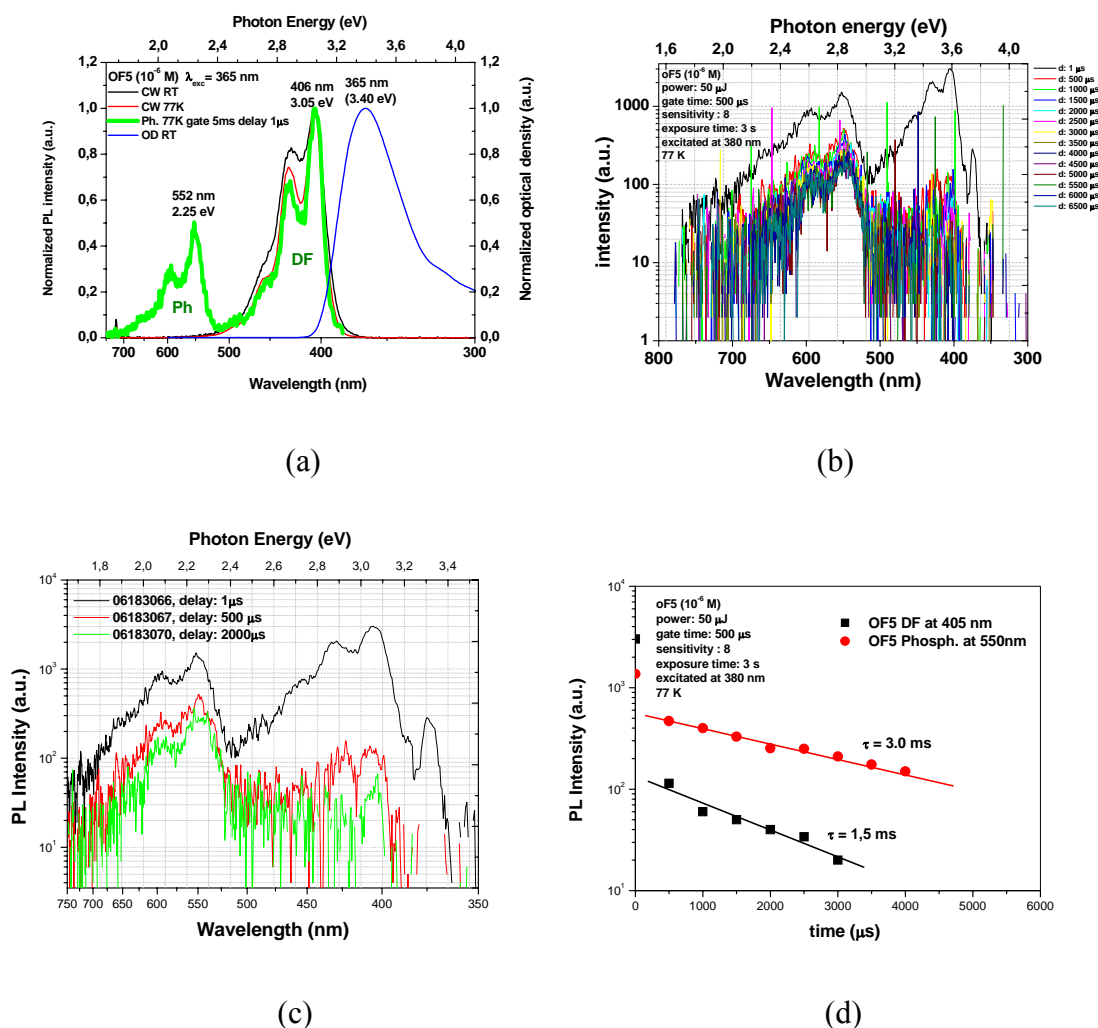
*Figure 5. 6. 3. a) Delayed emission spectra (green line) and CW fluorescence spectra (black line at RT and red line at 77K) and absorption spectra (blue line) of **OF5** in m-THF at 77K. The delay time is 1μs after laser excitation and gate time is 5 ms, exposure time: 3s, sensitivity: 8; b) and c) Delayed emission spectra of **OF5** in m-THF at 77K with different delay time on semi-logarithmic scales; d) dependence of phosphorescence and DF intensity upon time (**OF5** in m-THF solution at 77K). The **OF5** solution was excited at 380 nm.*

The delayed fluorescence of **OF5** in *m*-THF frozen solution probably has a similar origin as DF of PF2/6 in *m*-THF frozen solution, i. e., triplet-triplet annihilation (TTA).[21,22]

Figure 5. 6. 3 (b) and (c) show the delayed fluorescence at different delay time. The emission intensity decreases very fast from 1μs to 500 μs, then decays slowly. The dependence of DF and phosphorescence (Ph) intensity upon the time for **OF5** in dilute solid solution is shown in Figure 5. 6. 3 (d). The phosphorescence in dilute solution decays

monoexponentially over the entire time range from 500 –5000 µs , as expected when the decay of the triplet reflects the intrinsic lifetime, and the lifetime is about $\tau_{Ph} \sim 3$ ms. The DF decays also monoexponentially over the time range studied starting from 500 µs, and the lifetime is about $\tau_{DF} \sim 1.5$ ms, just half the value of the Phosphorescence lifetime.
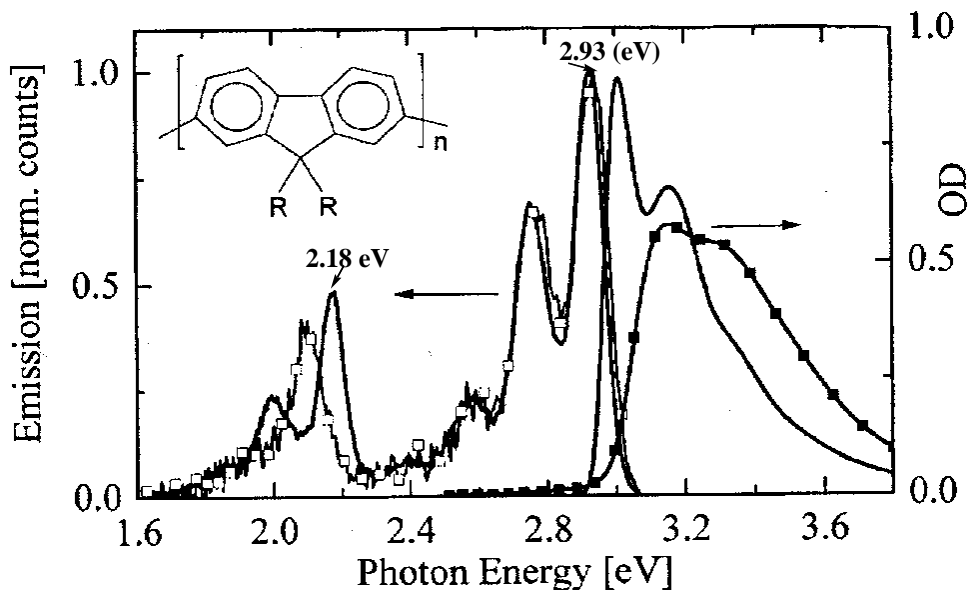
*Figure 5. 6. 4. The absorption spectra of **PF2/6** in m-THF (solid line) and a **PF2/6** film (solid line with ■) at 80 K. Delayed emission of **PF2/6** in m-THF (solid line) and a **PF2/6** film (solid line with □) at 80 K detected after 5 ms delay following excitation[22].*

The spectra of delayed emission of **OF5** in dilute solid solution at 77K under different laser excitation intensities are shown in Figure 5. 5. 10 (a), and the DF intensity decreases faster than that of phosphorescence as the laser excitation intensity decreases. The variation of the phosphorescence intensity with pump intensity is illustrated in Figure 5. 6. 5 (b). For recording Phosphorescence, the detection is delayed to 1µs after optical excitation. At the detection range, the phosphorescence intensity increases linearly with light flux with a slope of 0.85 on a double logarithmic scale.

| (a) | (b) |
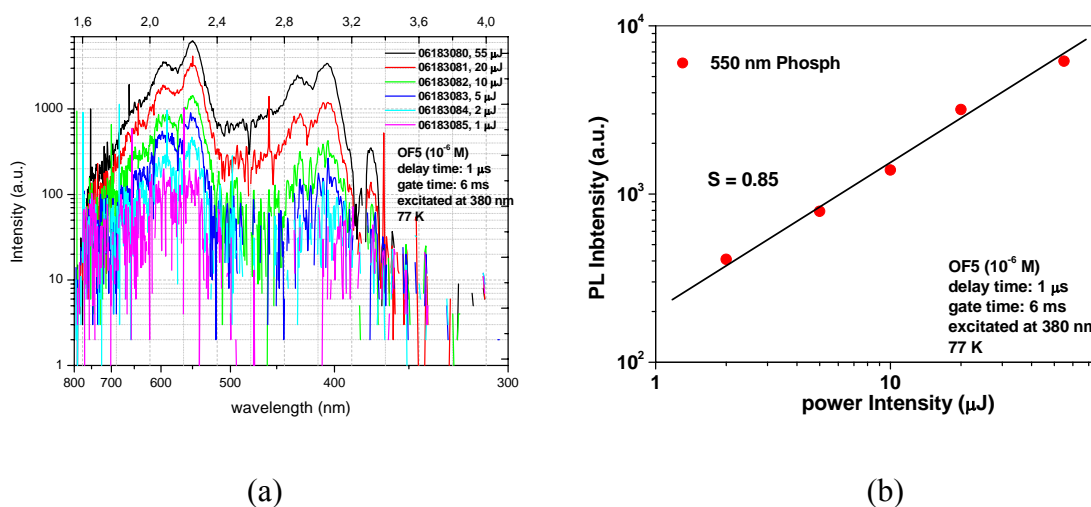
*Figure 5. 6. 5. a) The delayed emission spectra of **OF5** at different laser intensity in m-THF at 77K; b) dependence of phosphorescence intensity of **OF5** in dilute solid solution on pump intensity at 77K. The time delay for measurements of DF and Ph was 1 μs, and the photon energy for optical excitation was 380 nm (3.26 eV).*

In Figure 5. 6. 6 (a) the low temperature (77K) delayed emission spectra of a dilute solid solution of **OF3** are also presented. The delayed emission was detected 1 μs after optical excitation at 3.49 eV (355 nm). Similar to **OF5**, the delayed emission spectra of **OF3** in dilute solid solution display two different contributions. The spectral position of the high energy part of the spectra is coincident with the prompt fluorescence at 3.21 eV (386 nm) and shows the same vibronic splitting of about 160 meV. This emission is due to delayed fluorescence (DF) from the S_1 state of **OF3**. At lower energy the delayed emission at 2.31 eV (537 nm) can be assigned to the $S_0 \leftarrow T_1$ (0-0) transition bearing a vibronic splitting of 160 meV, identical to the prompt fluorescence. This is also similar with that of PF2/6.[21,22] The singlet-triplet energy gap in **OF3** amounts to $\Delta E_{ST} \approx 0.90$ eV.

<div align="center">(a)   (b)</div>
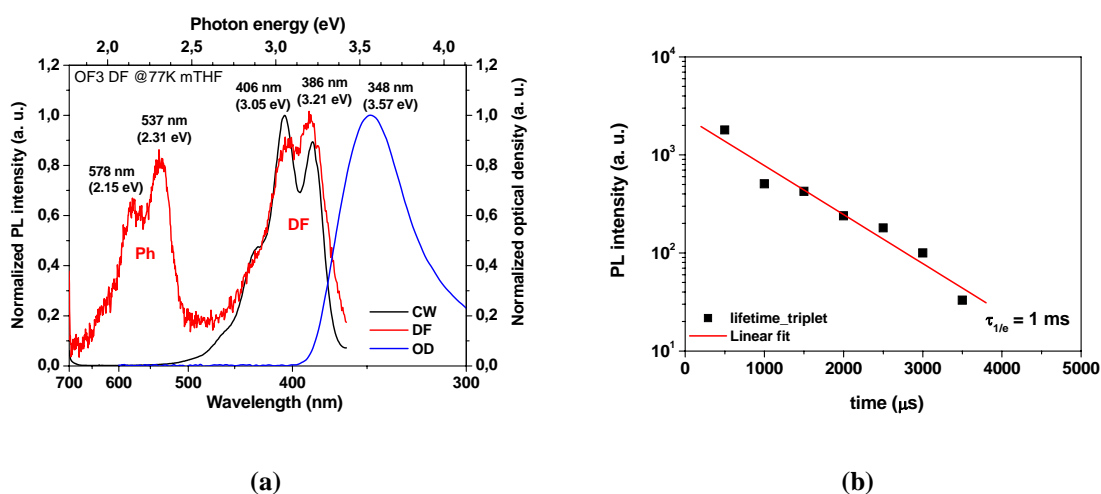
*Figure 5. 6. 6. a) Delayed emission spectra (red line) of **OF3** in m-THF at 77K, CW fluorescence (black line) and absorption spectra (blue line); b) dependence of phosphorescence upon time of the **OF3** in m-THF solution at 77K. The **OF3** solution was excited at 3.49 eV (355 nm).*

The dependence of phosphorescence intensity upon time for OF3 in dilute solid solution is shown in Figure 5. 6. 6 (b). The phosphorescence decays exponentially over the time range studied starting from 500 μs. The lifetime is about $\tau_{Ph} \sim 1$ ms, which is less than the 3 ms found for **OF5**, and much less than the 1.0s for **PF2/6** in dilute solid solution at 80 K (*m*-THF solvent).[22] The lifetime of the phosphorescence in the series of the homo-oligofluorenes increases with the molecular size, in contrast to the fluorescence life-time. This behavior can be explained by increased probabilities of intersystem crossing with the increase of chain-length.

In table 5. 6. 1 a compilation of the energy gaps, such as S_0-S_1, S_0-T_1, S_1-T_1 for **OF1**, **OF3**, **OF5** and **PF2/6** are listed. The energy of S_1-S_0, T_1-S_0 transitions decreases with the molecular length, i.e. the emission maximum of fluorescence and phosphorescence are red shifted with the molecular size. A linear relation is observed between the emission maximum wavenumber of fluorescence and phosphorescence and the reciprocal number of fluorene units in Figure 5. 6. 7. Apparently the S_1[23] and T_1[24] energies of the oligomers can be expressed as $\Delta E(n) = \Delta E_\infty + const./n$, the basic spectral features upon increasing the molecular length[25], where n is the number of fluorene units. The data has allowed the extrapolation to PF2/6 (n = ∞) and the evaluation of its singlet energy (2.80 eV) and triplet energy (2.05 eV). These values are lower than that of experimental PF2/6 which has singlet

energy of 2.93 eV and triplet energy of 2.18 eV. The slope (1.23) of the plot is bigger for fluorescence than that (0.89) for phosphorescence. This means that the decrease of energy gap of S_1-S_0 is faster than that of T_1-S_0 with molecular length, i.e. the spectra of fluorescence are red shifted faster than those of the phosphorescence, resulting in the convergence of the singlet-triplet energy gap with the molecular length. The singlet-triplet energy gap (ΔE_{ST}) in **OF1**, **OF3**, **OF5**, **PF2/6** is 1.09, 0.9, 0.8, 0.75 eV respectively.

This smaller slope of the straight line as compared to the singlet data indicates that T_1 is less extended, as has also been shown by semi-empirical calculations.[26] The singlet-triplet gap of the PPP-type polymers decreases with increasing conjugation along the polymer backbone in accord with observations in thiophene oligomers.[27]

*Table 5. 6. 1 the compilation of the energy gap, such as S_0-S_1, S_0-T_1, S_1-T_1 for **OF1**, **OF3**, **OF5**, and **PF2/6**. (**OF1**: the fluorene monomer)*

	N (FL)	S_1-S_0 (eV)	T_1-S_0 (eV)	S_1-T_1 (eV)	
OF1	1	4.03 (308 nm)	2.94 (422 nm)	1.09	77K hydroc. solv.[a]
OF3	3	3.21	2.31	0.90	77K m-THF
OF5	5	3.05	2.25	0.80	77K m-THF
PF2/6	314	2.93	2.18	0.75	77K m-THF[b]

[a] Herkstroeter et. al. JACS; [b] Hertel et. al. JCP (2002), the molecular weight of PF2/6 was M_n = 122000 g/mol; M_w = 244000 g/mol)
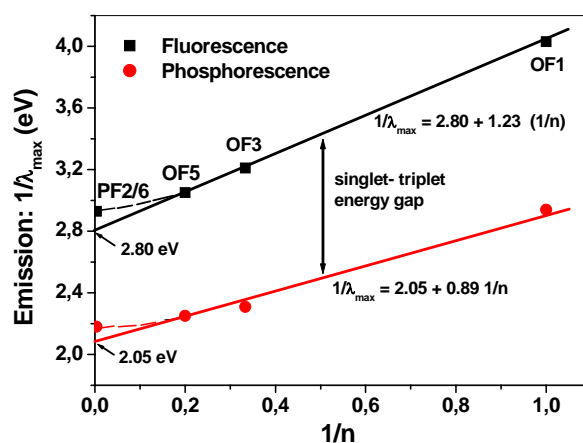
Figure 5. 6. 7. The maximum wavenumber versus the reciprocal degree of polymerization.

*(**OF1**: the fluorene monomer)*

The energy level diagram can be obtained from the Table 5. 6. 1 and the Table 3. 2. 2 (**Chapter 3**) for the series of oligofluorenes and polyfluorenes. For example, the energy level diagram of **OF5** is shown in Figure 5. 6. 8. The value of energy level for the S_0, S_1, and T_1 are the 5.5, 2.45, 3.25 eV, respectively. The energy level diagram illustrates the relative position of absorption, fluorescence and phosphorescence spectra. The triplet state is populated by intersystem crossing (ISC) from optically excited singlet states.
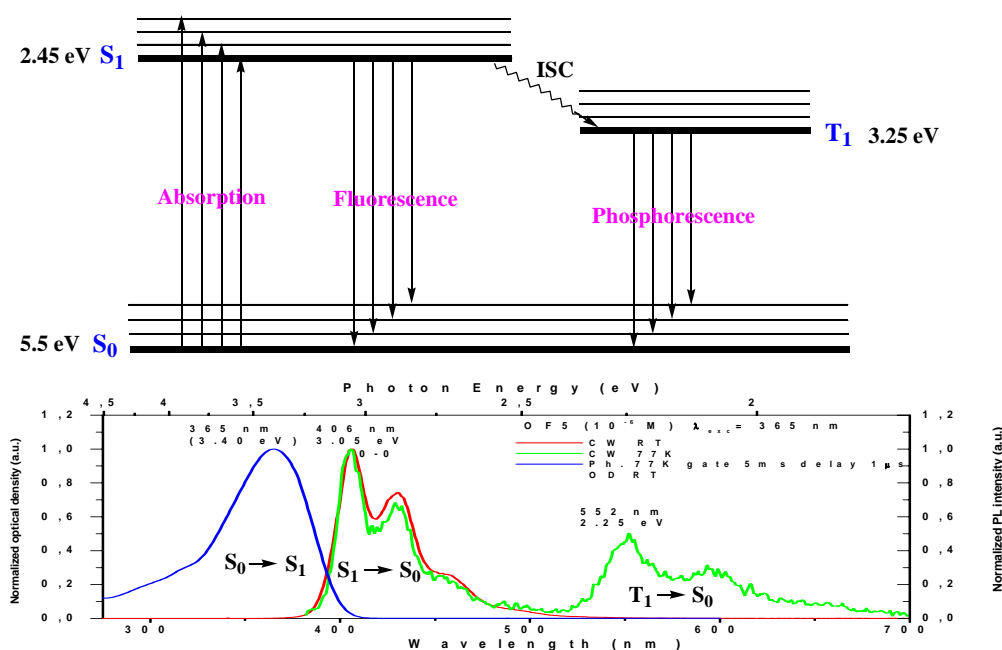
*Figure 5. 6. 8. The energy level diagram of **OF5** and illustration of the relative position of absorption, fluorescence and phosphorescence specra.*

5. 7 Summary

In this chapter, the basic theory of energy level diagrams of molecules was used to explain the mechanism of the photophysical properties. The time-resolved photoluminescence methods and further experimental principles are explained (streak camera and the gate detection technique). The steady state spectra (UV-vis absorption and fluorescence spectra) of oligofluorenes (**OF-n**) and polyfluorenes (**PF2/6**) both in solution and thin film are presented. The time-resolved fluorescence spectra of the oligofluorenes

were measured making use of streak camera and gate detection technique in *m*-THF solution and films at both RT and 77K. The lifetime of the oligofluorenes decreases as the the chain-length grows. Green emission was not observed in CW, or in prompt or delayed fluorescence for oligofluorenes in *m*-THF and film at RT and 77K. Concentration and laser excitation intensity dependence of oligofluorenes were also investigated. Phosphorescence was observed for oligofluorenes in frozen dilute *m*-THF solution at 77K and its lifetime increased with length of the oligofluorenes. Finally, the photophysical processes were rationalized by singlet and triplet states of oligofluorenes and the energy level diagram was derived. A linear relation was obtained for triplet energy and singlet energy as a function of the reciprocal degree of polymerization, and the singlet-triplet energy gap (S_1-T_1) was found to decrease with the increase of degree of polymerization.

5. 8 Experiment

5. 8. 1 Ultrafast time-resolved PL (TRPL) experiments

For TRPL experiments a frequency doubled Ti: Sapphire laser producing 130 fs pulses at a repetition rate of 80 MHz with laser Pulse duration 12 ns, followed by a frequency doubling BBO crystal, was used to obtain a suitable excitation line for the studies of the oligofluorenes. The detection system for the ultrafast TRPL measurements consisted of a streak camera system with a maximal time resolution of 4 ps, combined with a 0.25 m monochromator. The TRPL measurements were carried out mainly at room temperature either under vacuum ($<10^{-5}$ mbar) with films or under ambient condition with solutions.

5. 8. 2 Experimental setup of gate detection technique:

Time-resolved PL spectroscopy was carried out with an Nd:YAG-laser system (10 Hz repetition rate, 7 ns pulse width). The pulse energies could be tuned between 0.5 μJ and 50 μJ, using a rotatable neutral density filter. The excitation photon energy was also tunable with a combination of an optical parametric oscillator(OPO, GWU GmbH, Germany) and frequency doubler (GWU GmbH, Germany). Photoluminescence emission was detected by a gatable optical multichannel analyzer (OMA EG&G), which consisted of a

monochromator in conjunction with a electrically cooled intensified CCD array. Smallest gate 50 ns. The measurements were performed in a cold finger cryostat ($< 10^{-5}$ mbar) at approximately 80 K and 295 K.

Thin films of all materials were made by spin-coating of solution in chloroform onto quartz substrate. The thickness of all of the films was approximately 50 nm, which was estimated by Tencor P-10 Surface Profiler.

5. 9 References and Notes

[1] (a) Anémian, R.; Mulatier, J.-C.; Andraud, C.; Stéphan, O.; Vial, J.-C. *Chem. Commun.* **2002**, 1608-1609; (b) Geng, Y.; Trajkovska, A.; Katsis, D.; Ou, J. J.; Culligan, S. W.; Chen, S. H. *J. Am. Chem. Soc.* **2002**, *124*, 8337-8347.

[2] (a) Rothe, C.; Hintschich, S. I.; Pålsson, L.-O.; Monkman, A. P.; Guentner, R.; Scherf, U. *Chem. Phys. Lett.* **2002**, *360*, 111-116; (b) Franco, I.; Tretiak, S. *Chem. Phys. Lett.* **2003**, *372*, 403-408.

[3] Zojer, E.; Pogantsch, A.; Hennebicq, E.; Beljonne, D.; Brédas, J.-L.; de Freitas, P. S.; Scherf, U.; List, E. J. W. *J. Chem. Phys.* **2002,** *117*, 6794-6802.

[4] Valeur, B. *'Molecular Fluorescence'* **2001**, *31*, WILEY-VCH.

[5] Pope, M.; Swenberg, C. E. "*Electronic Processes in Organic Crystals and Polymers"*, Oxford University Press, New York, 1999.

[6] (a) O'Connor, D. V.; Phillips, D. "*Time~correlated Single Photon Counting"* **1984**, The Royal Institute, London, UK; (b) Lakowicz, J. R. *"Principle of Fluorescence Spectroscopy"* **1999**, Kluwer Academic/Plenum Publishers, New York.

[7] Bennett, R. G., *'Instrument to measure fluorescence lifetimes in the millimicrosecond region' Rev. Sci. instrum.* **1960,** *31,* 1275-1279.

[8] (a) Bhaumik, M. L.; Clark, G. L.; Snell, J.; Ferder, L. *Rev. Sci. Instrum.* **1965**, *36*, 37-40; (b) Barisas, B. G.; Leuther, M. D.; *Rev. Sci. Instrum.* **1980**, *51*, 74-78.

[9] Steingraber, O. J.; Berlman, I. B. *Rev. Sci. Instrum.* **1963**, *34*, 524-529; Hundley, L.; Coburn, T.; Garwin, E.; Stryer, L. *Rev. Sci. Instrum.* **1967**, *38*, 488-492

[10] James, D. R.; Siemiarczuk, A.; Ware, W. R. *Rev. Sci. Instrum.* **1992**, *63*, 1710-1716.

[11] Neher, D. *Macromol. Rapid Commun.* **2001**, *22*, 1365-1385.

[12] (a) Davidov, A. S.; *Zh. Eksp. Teor. Fiz.,* **1948**, *18*, 515; (b) *Theory and Application of Ultraviolet Spectroscopy*, eds. Jaffé, H. H.; Orchin, M. Wiley, NY, **1964,** p 274.

[13] Fukuda, M.; Sawada, K.; Yoshino, K. *J. Polym. Sci. Part A: Polym. Chem.* **1993**, *31*, 2465-2471.

[14] Gamerith, S.; Gadermaier, C.; Scherf, U.; List, E. J. W. *Phys. Stat. Sol.* **2004**, *201*, 1132-1151

[15] (a) Scherf, U.; List, E. J. W. *Adv. Mater.* **2002**, *14*, 477-487; (b) Lee, J.-I.; Klaerner, G.; Miller, R. D. *Chem. Mater.* **1999**, *11*, 1083-1088; (c) Gamerith, S.; Gadermaier, C.; Scherf, U.; List, E. J. W. *Phys. Stat. Sol.* **2004**, *201*, 1132-1151.

[16] Jo, J.; Chi, C.; Höger, S.; Wegner, G.; Yoon, Do Y.. *Chem. Eur. J.* **2004**, *10*, 2681-2688.

[17] Anémian, R.; Mulatier, J.-C.; Andraud, C.; Stéphan, O.; Vial, J.-C. *Chem. Commun.*, **2002**, 1608-1609.

[18] *Spectroscopy with Polarized Light*, Michl, J.; Thulstrup, E. W. VCH, New York, **1986**, p34.

[19] McRae, E. G.; Kasha, M. *J. Chem. Phys.*, **1958**, *28*, 721.

[20] (a) Zojer, E.; Pogantsch, A.; Hennebicq, E.; Beljonne, D.; Brédas, J.-L.; de Freitas, P. S.; Scherf, U.; List, E. J. W. *J. Chem. Phys.* **2002**, *117*, 6794-6802; (b) Gamerith, S.; Gadermaier, C.; Scherf, U.; List, E. J. W. *phys. Stat. Sol.* **2004**, *201*, 1132-1151; (c) List, E. J. W.; Guentner, R.; de Freitas, P. S.; Scherf, U. *Adv. Mater.* **2002**, *14*, 374-378.

[21] Hertel, D.; Bässler, H.; Guentner, R.; Scherf, U. *J. Chem. Phys.*, **2001**, *115*, 10007-10013

[22] Hertel, D.; Setayesh, S.; Nothofer, H.-G.; Scherf, U.; Müllen, K.; Bässler, H. *Adv. Mater.* **2001**, *13*, 65-70

[23] (a) Grimme, J.; Kreyenschmidt, M.; Uckert, F.; Müllen, K.; Scherf, U. *Adv. Mater.* **1995**, *7*, 292; (b) Chosrovian, H.; Rentsch, S.; Grebner, D.; Dahm, D. U.; Birckner, E. *Synth. Met.* **1993**, *60*, 23; (c) Janssen, R. A. J.; Smilowitz, L.; Sariciftci, N. S.; Moses, D. *J. Chem. Phys.* **1994**, *101*, 1787; (d) Janssen, R. A. J.; Moses, D.; Sariciftci, N. S. *J. Chem. Phys.* **1994**, *101*, 9519; (e) Horowitz, G.; Yassar, A.; von Bardeleben, H. J. *Synth. Met.* **1994**, *62*, 245.

[24] (a) de Melo, J. S.; Silva, L. M.; Arnaut, L. G.; Becker, R. S. *J. Chem. Phys.* **1999**, *111*, 5427; (b) Scaiano, J. C.; Redmond, R. W.; Mehta, B.; Arnason, J. T. *Photochem. Photobiol*, **1990**, *52*, 655.

[25] *"Electronic Materials: The Oligomer Approach"* Müllen, K.; Wegner, G. Wiley-VCH, **1998,** Chapter7.

[26] Beljonne, D.; Shuai, Z.; Friend, R. H.; Brédas, J. L. *J. Chem. Phys.* **1995**, *102*, 2042.

[27] de Melo, J. S.; Silva, L. M.; Arnaut, L. G.; Becker, R. S. *J. Chem. Phys.* **1999**, *111*, 5427.

6   **Synthesis and characterization of oligofluorenes with one fluorenone group**

Oligofluorenes (trimer, pentamer and heptamer) with one fluorenone unit at the center were synthesized and are used as model compounds to understand the origin of the low-energy emission band in the photoluminescence and electroluminescence spectra of polyfluorenes. The thermal properties and the steady-state UV-vis and fluorescence spectroscopic properties were investigated.

6.1 Introduction

In the development of polymer light-emitting diodes (LEDs), blue light emission is of particular importance. Although a number of fully conjugated and partially conjugated polymers have been designed and synthesized in an attempt to realize efficient blue photoluminescence (PL) and electroluminescence (EL),[1] only a limited number of these polymers appear promising for use in blue polymer LEDs. The 9,9-disubstituted poly(2,7-fluorene)s (PFs)[2] are among the most promising candidates. The PFs exhibit high PL and EL quantum efficiencies, high EL brightness[1c,1d], high charge transport, thermal stability, and attainability of physical parameters through chemical modification and copolymerization. The high-efficiency blue PL emission from the PF structure is attractive for use in displays.[3] Moreover, as a host material, the PFs can enable full color (blue, green, and red) via energy transfer to longer wavelength emitters in blends with other conjugated polymers and with phosphorescent dyes.[4] Because the PFs homopolymers exhibit thermotropic liquid crystallinity, they can be oriented on rubbed polyimide layers.[5] Although there have been significant advances toward stability of polymer light-emitting diodes (PLEDs),[6] the lifetime and color purity need improvement for commercialization of full-color displays. Photo-oxidation plays an important role in the lifetime of PLEDs fabricated from phenylene vinylene derivatives.[7] Yet, despite the remarkable improvements in terms of stability and color purity of OLEDs based on PFs-type emitters, most of these OLEDs suffer from a degradation of the device and a loss of efficiency under operation, which is most visibly documented in the formation of a low energy emission band at 2.2-

2.4 eV (520-560 nm). As a result, the color of the emission shifts from desired blue to blue-green (and even yellow). This undesired long wavelength emission is observed in the photoluminescence (PL)[8] after photooxidation of the polymer and the electroluminescence (EL) spectra, but it is typically more intense in the EL spectrum.[9] At the beginning, the long wavelength emission (and associated problems) has been mostly attributed to aggregates and /or excimer formation in the material.[10]

Several attempts have been made to stabilize the blue color of PFs via chemical modification, including incorporation of benzothiadiazole, perylene, and anthracene moieties into the PF main chain and via end-capping, but the green EL was not completely eliminated.[11] Pure blue emission was obtained from PF-based PLEDs by doping with a dilute concentration of hole-transporting (HT) molecules.[3, 12] However, slow phase-separation in this blend limits device stability. Thus, the achievement of stabilized blue EL from PF-based PLEDs continues to be a challenge.

However, as shown recently[13] by two groups of List, E. J. W. et al., the more or less intense low-energy emission band at 2.2-2.3 eV can be identified as the emission from exciton and /or charge trapping keto defect sites (9-fluorenone sites), which in fact can be regarded as emission of a guest (defect) accidentally incorporated into the π-conjugated PF backbone. As shown below, such keto defects, leading to the unwanted low energy emission band in polyfluorenes, can be formed already during synthesis (in the case of 9-monoalkylated polyfluorenes, MA-PF), or as result of a photo- (or electro-) oxidative degradation process of almost any PFs, for example, a 9,9-dialkylated polyfluorene (DA-PF).[13a]

The 9-monoalkylated polyfluorene (MA-PF) and the 9,9-dialkylated derivative DA-PF discussed here (alkyl = 3,7,11-trimethyldodecyl) can be synthesized from the corresponding 2,7-dibromofluorene monomers in a reductive aryl-aryl coupling according to Yamamoto. The long and branched side groups hereby allow a simple liquid chromatographic separation of mono- and dialkylated dibromofluorene monomers to be carried out, which is more difficult for PFs bearing smaller side-chains. The pristine 9-monoalkylated MA-PF was already found to contain 9-fluorenone defect sites after polymer synthesis. An explanation for the ongoing mechanism of defect-site generation is the following (Scheme 1): The highly active Ni^0 species used in the reductive coupling of the dibromo monomers reduce a certain amount of the 9-monoalkylated fluorene building blocks (I) to (aromatic) fluorenyl anions (II) under formation of hydrogen. These anions can form hydroperoxide

anions (III) with atmospheric oxygen during the work-up of the reaction mixture. The hydroperoxide anions then undergo a final rearrangement to fluorenone moieties (IV).
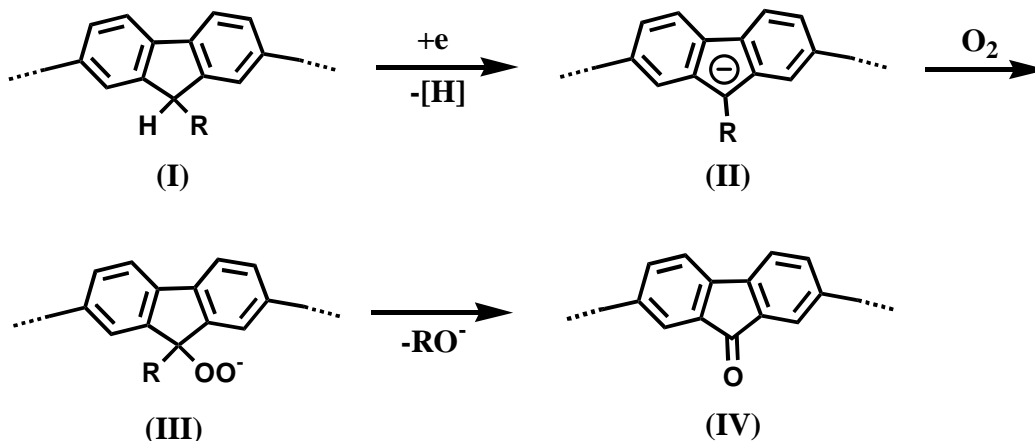
Scheme 1. Proposed mechanism for the generation of keto defect sites in MA-PF

The incorporation of the fluorenone defect sites in MA-PF dramatically changes the emission properties of the polymer and the low energy emission band is dominant in emission spectra. The energetic position of the low-energy emission band at ca. 2.3 eV in MA-PF is very similar to the low-energy emission band of the fluorenone building block in statistical dialkylfluorene/fluorenone copolymers.[14] It is also similar to the emission band of photooxidized (photodegradated) fluorene-endcapped poly(9,9-dihexylfluorene-2,7-diyl) (PF6) as demonstrated by the IBM Almaden group,[15] where, terminal, unsubstituted fluorene moieties were photooxidized to fluorenone units. In this light, the often favored interpretation that the low-energy emission bands in PF are associated with ongoing aggregate or excimer formation is at the very least questionable.

The keto defect sites present in MA-PF are formed already during the synthesis of the polymer. However, such keto defect sites can not only be formed as side reaction during polymer synthesis, as shown for MA-PF, but can also be formed as result of a photo- or (electro-) oxidative degradation of DA-PF.[13] Moreover, the emission contribution of keto defect sites is more pronounced in EL devices when compared to that of PL experiment. The reason for this behavior is the presence of two parallel processes that give a low-energy EL contribution due to the presence of fluorenone defect sites: a) energy transfer of singlet excitons from the PF main chain to keto defect sites and b) trapping of charges at the

fluorenone defect sites and their subsequent emissive recombination. The second process cannot proceed in PL experiments and increases the contribution of the defect-site-related low-energy EL band. Therefore, in contrast to the PL process, in EL devices a much lower concentration of fluorenone defects results in a dominating low-energy emission band.[16]

Gong and Moses et.al. have also studied both the PL and EL from PFs and found that the low-energy emission band originates from fluorenone defects.[13b] They show that fluorenone defects are generated by photo-oxidization and thermal oxidation. It is well known that the low-energy emission band from PF is typically more intense in EL than in PL, implying that such defects are also generated during device fabrication. Using X-ray photo-emission spectroscopy (XPS), they have shown that the oxidation of PF is catalyzed by calcium, thereby explaining why the low-energy band is more intense in the EL spectra. By inserting a specific buffer layer between the PF and Ca/Ag (Ba/Ag) electrode to block the diffusion of calcium into PFs, fluorenone defects are inhibited, and the blue emission is stabilized.

Although a number of possible mechanisms [2,9, 11] has been suggested that the longer wavelength emission band origins from aggregates and /or excimer formation or fluorenone defects in backbone of PFs, but it remains unclear. The mechanisms of 'fluorenone defects' is more convincing. In order to improve the performance and lifetime of PF based PLEDs, it is important to identify the origin of the long wavelength emission band and to understand the mechanism of the color degradation.[2,17] So in this work, the oligofluorenes (trimer, pentamer, heptamer) with one fluorenone group were synthesized, and they can serve as model compounds for understanding the long wavelength emission of PFs by investigating their electronic and photophysical properties.

In this chapter, the synthesis of the oligofluorenes (trimer, pentamer, heptamer) with one fluorenone group is first introduced. Their thermal, electrochemical properties was studied by DSC, POM, WXRD and CV techniques. Their photophysical properties especially the transition fluorescence spectroscopic characterizations will be discussed in next chapter.

6. 2 Synthesis and characterization of oligofluorenes with one fluorenone group

The synthetic strategy of oligofluorenes with one fluorenone unit is shown in Scheme 6.2.1. The synthesis of compound **41, 44** and **48** were introduced in chapter 2. The trimer (**OF3K**) **55** was prepared by Suzuki coupling reaction between the mono-boronate substituted fluorene **41** and 2,7-dibromofluorenone (**54**). The syntheses of higher fluorenyl oligomers with one fluorenone unit such as pentamer (**OF5K**, **53**) and heptamer (**OF7K**, **58**)
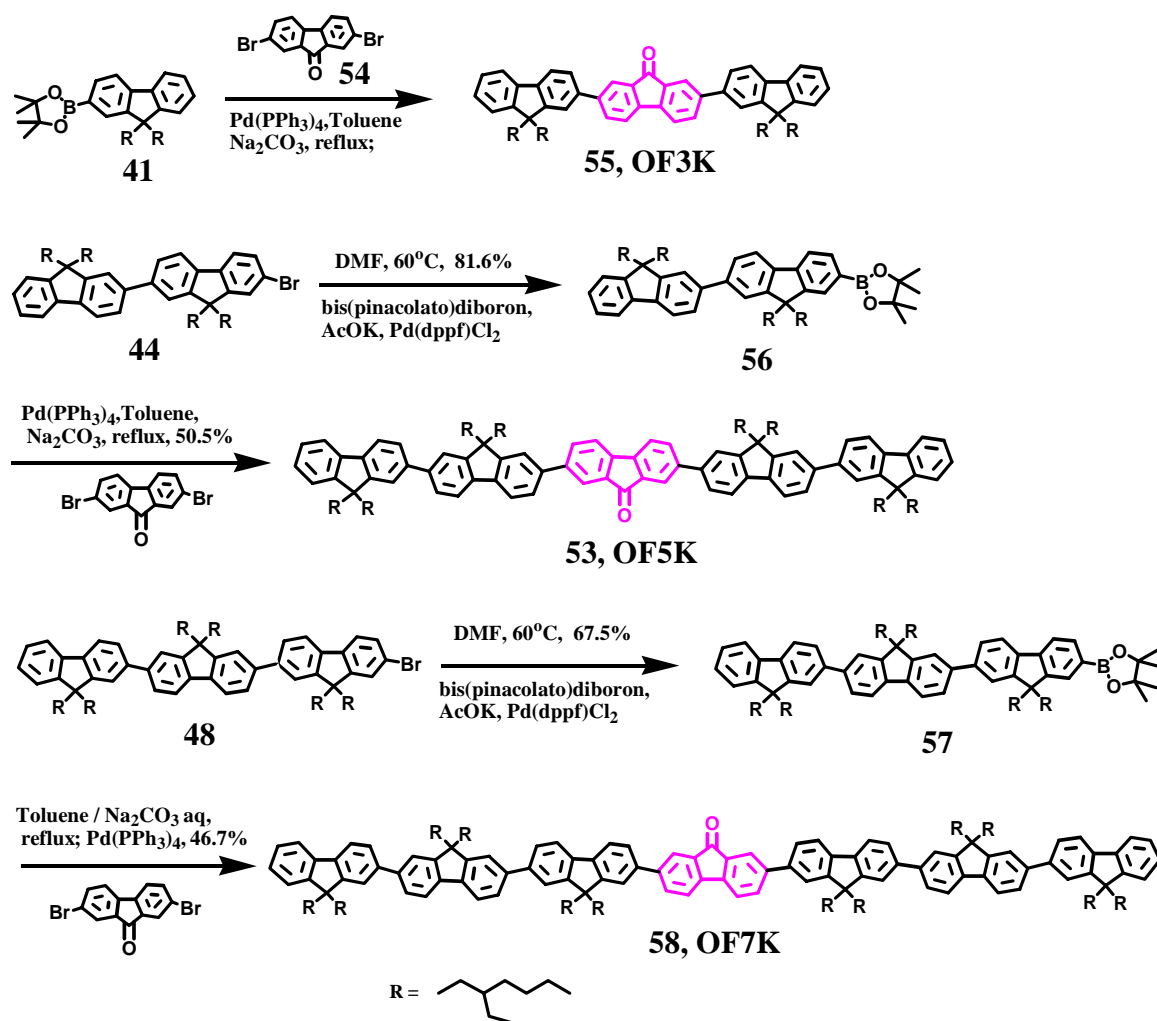
Scheme 6.2.1. The synthetic strategy of oligofluorenes with one fluorenone group.

were based on two important syntons, the monobromides of the fluorenyl-dimer (**44**) and trimer (**48**). The palladium-catalyzed Miyaura reaction [18] was used to transform the bromides to the boronates and the corresponding boronates (**56** and **57**) were obtained in 80% and 70% high yield, respectively, under mild conditions after standard column

chromatography work-up. The target products **OF5K** (**53**) and **OF7K** (**58**) were then prepared by Suzuki coupling reactions between the mono-boronate fluorene **56** (and **57**) with compound 2,7-dibromofluorenone, respectively.

During the synthesis, all compounds were purified by standard column chromatography and confirmed by field desorption mass spectroscopy (FD-MS) and ^{1}H or ^{13}C-NMR techniques.

The combined ^{1}H NMR spectra of all the oligomers OF3K-OF7K are shown in Figure 6.2.1. In the ^{1}H NMR spectra of **OF3K** (Figure 6.2.2), well resolved peaks related to the alkyl and aromatic protons were observed, however the signals became broad due to overlap of the resonances with increasing of the chain-length, and the peaks assigned to aromatic protons also slightly shift downfield. The integration ratio of aliphatic/aromatic protons observed for the **OF3K** (**55**), **OF5K** (**53**), **OF7K** (**58**) are 3.40, 4.25, 4.64, respectively, which are in good agreement with the calculated values: 3.38, 4.27 and 4.62. ^{13}C NMR spectra of the oligomers (Figure 6.2.3) were also analyzed and further supported the high purity.
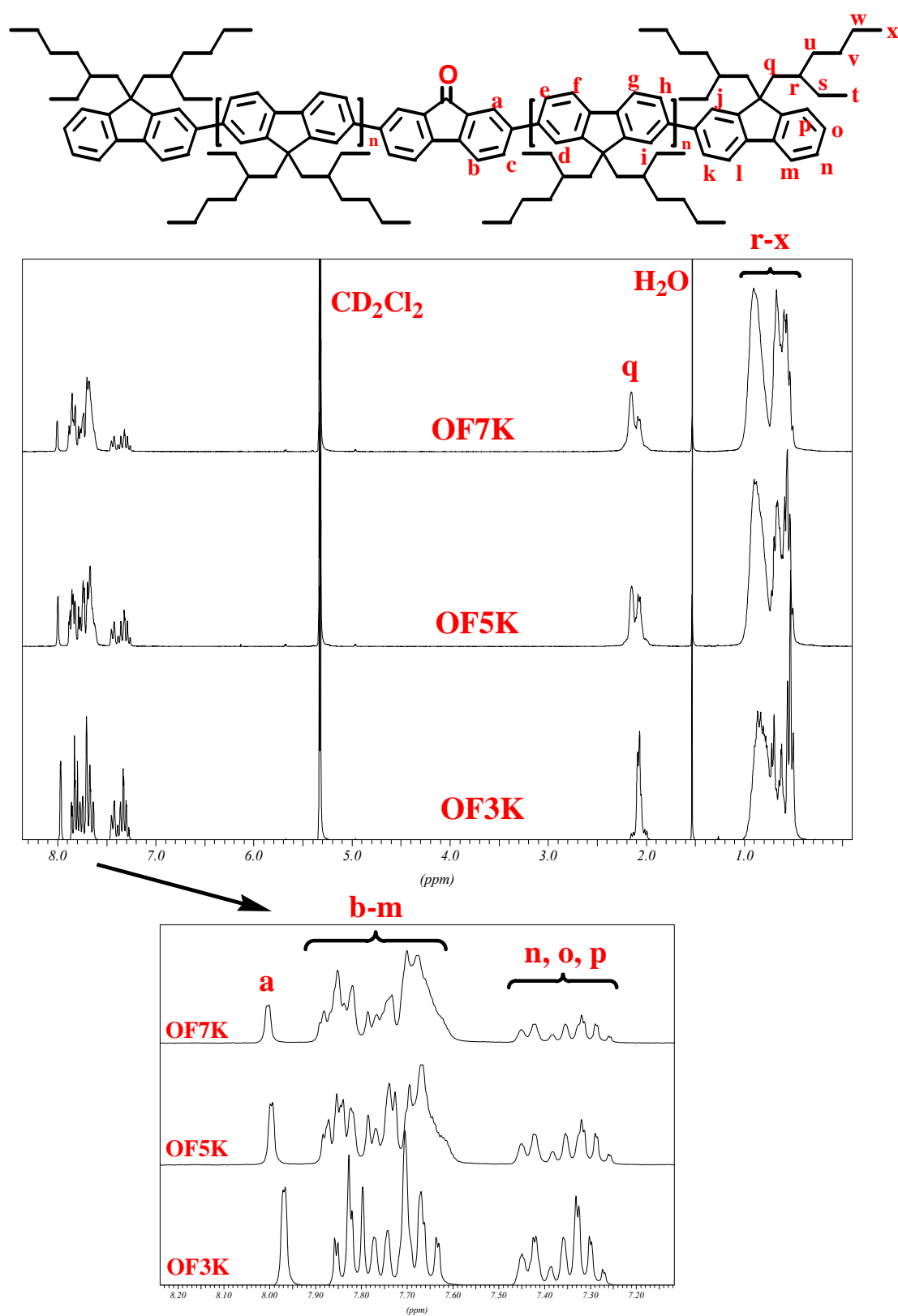
*Figure 6.2.1. Combined ^1H NMR spectra of **OF3K**, **OF5K** and **OF7K** in dichloromethane-d^2.*

OF3K	Aliphatic Protons/Aromatics Protons
Calculated	68/20 = 3.40
Observed	34.1/10.1 = 3.38
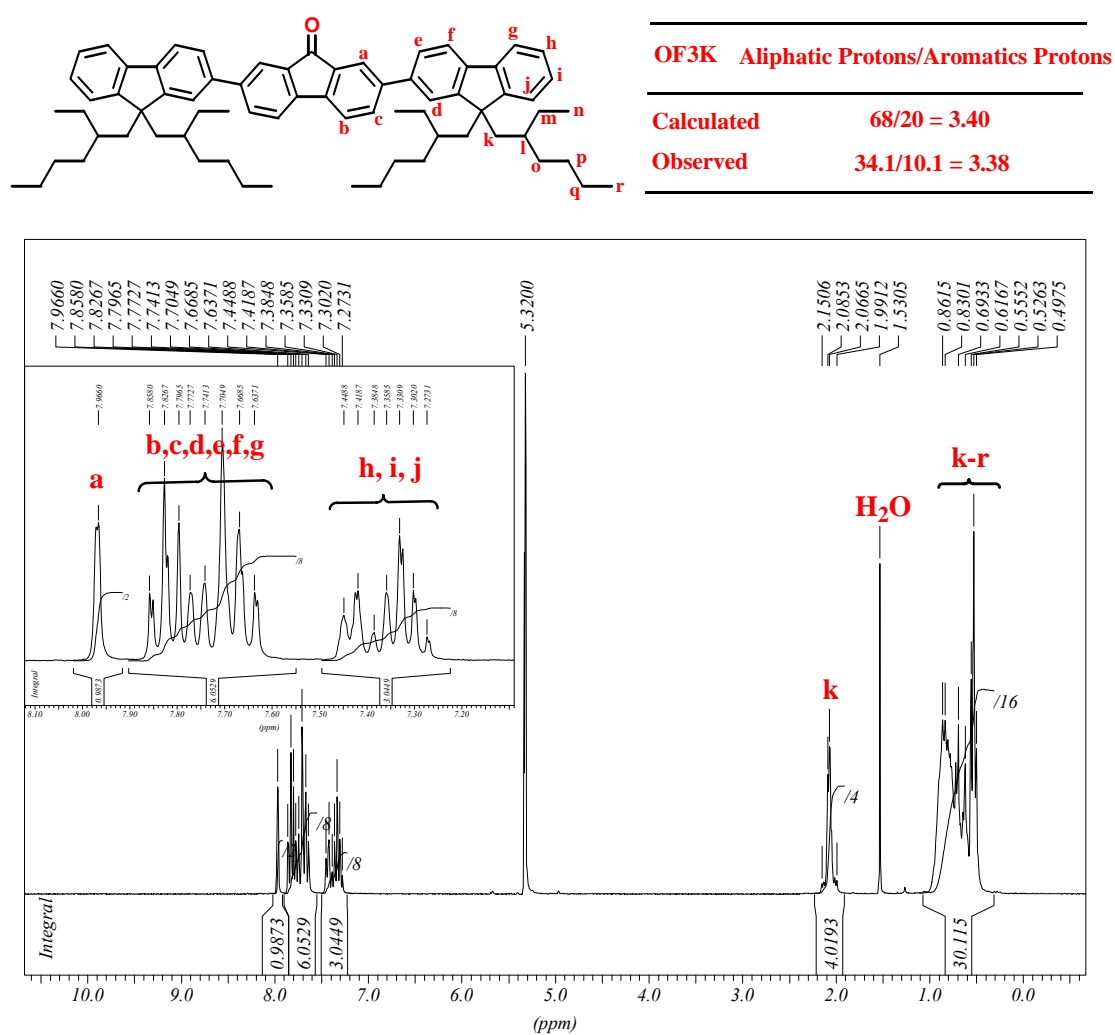
*Figure 6. 2. 2.   Detailed assignment of the ^1H NMR spectrum of **OF3K** (**55**) in dichloromethane-d^2.*
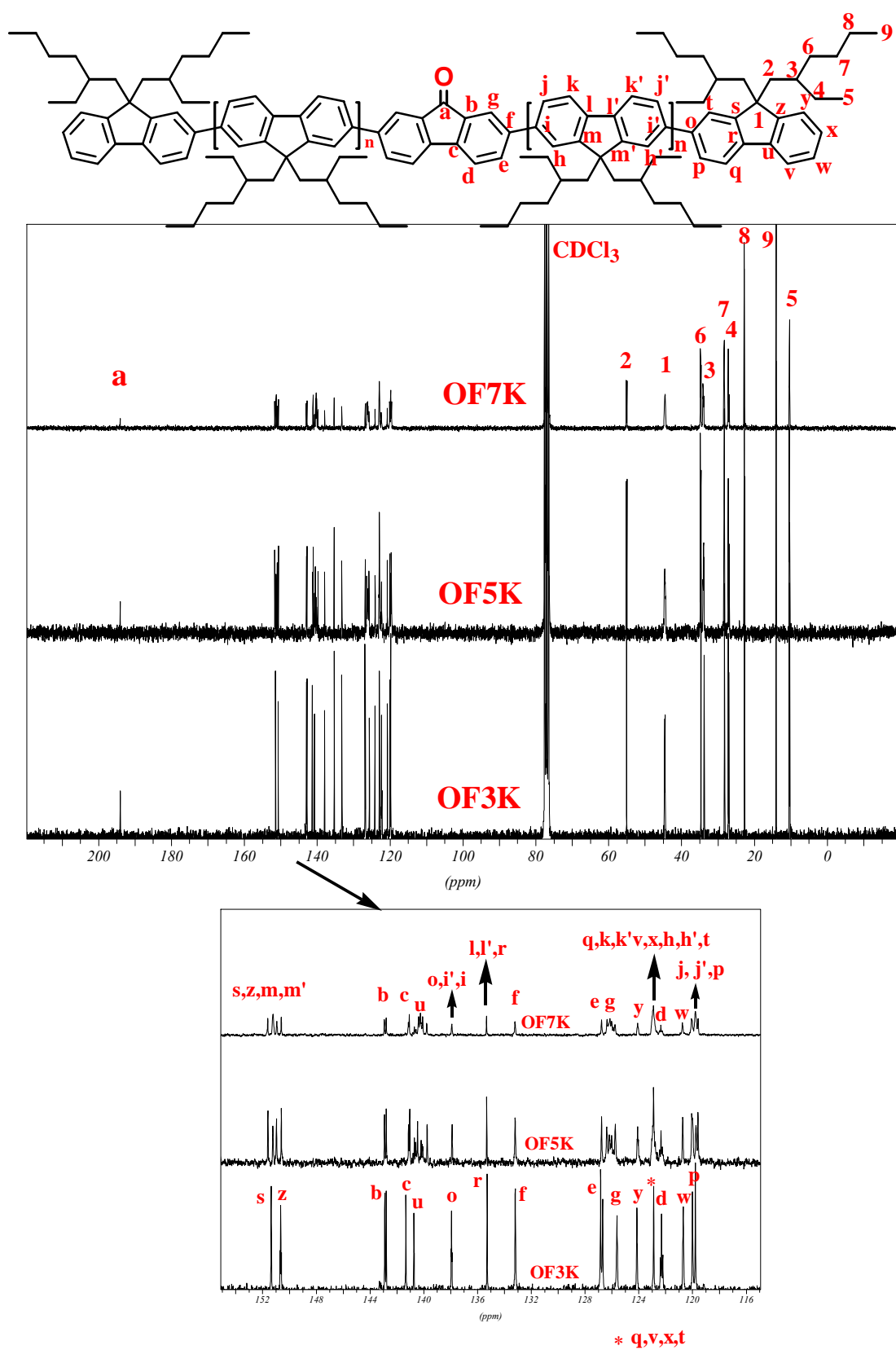
*Figure 6. 2. 3. Combined ^{13}C NMR spectra of the **OF3K**, **OF5K** and **OF7K** in dichlroromethane-d^2.*

Field-desorption (FD) mass spectra of the **OF3K**, **OF5K** and **OF7K** are shown in Figure 6. 2. 4 a-c. In all case, the molecular ionic peaks correlated to the molecular weight of the compounds were observed. Some peaks assigned to multi-charged species (M^{2+} and M^{3+}) were also found. For heptamer with one fluorenone group (OF7K), the peak at 2510.7 is assigned to M^+ of OF7K, while the peaks at 1255.2, 836.8, and 627.7 are related to the M^{2+}, M^{3+}, M^{4+} respectively.
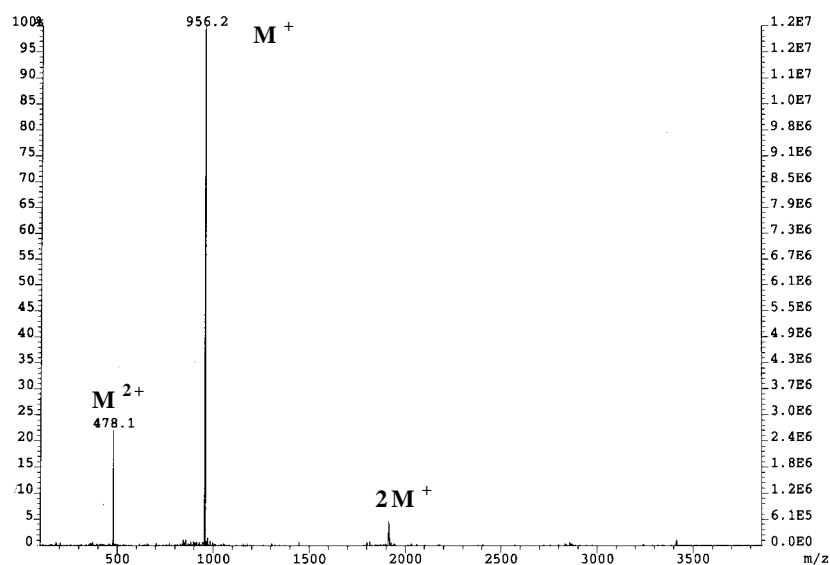
*Figure 6. 2. 4a. FD-MS for OF3K (**55**) (m/z: 956.2 [M^+]).*
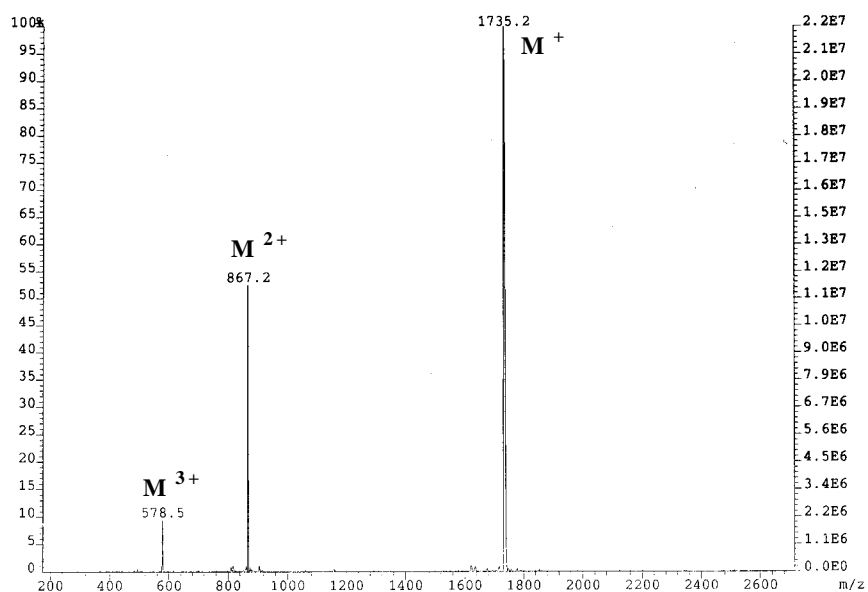
*Figure 6. 2. 4b. FD-MS for OF5K (**53**) (m/z:1735.2 [M^+]).*
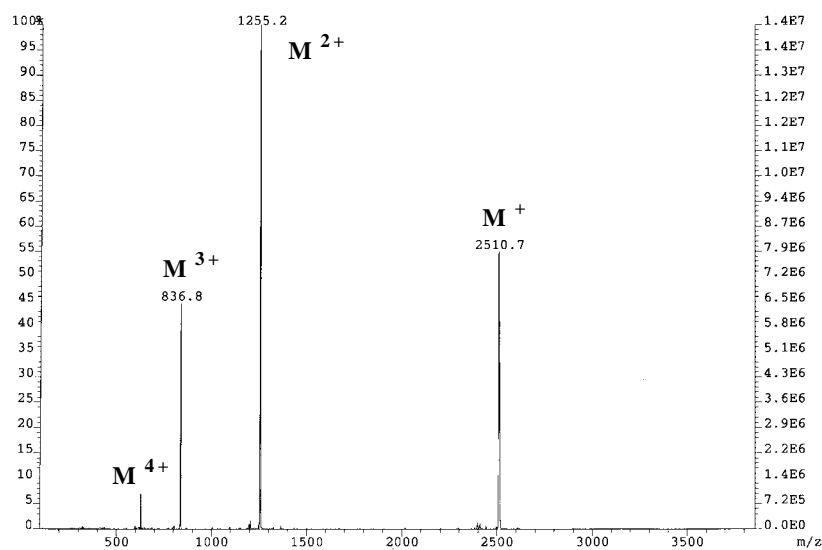
*Figure 6. 2. 4c. FD-MS for OF7K (**58**) (m/z: 2510.7 [M⁺]).*

6. 3 Thermotropic characterization

The thermotropic properties of the oligofluorenes with one fluorenone group are similar like that of homo-oligofluorenes. The Thermal Gravimetric Analysis (TGA) of **OF3K (55)**, **OF5K (53)**, **OF7K (58)** in a nitrogen atmosphere shows no change in mass until above $370^{o}C$ (figure 6. 3. 1.). The DSC traces shown in figure 6. 3. 2 clearly exhibit the glass transitions for all of the oligomers with one fluorenone units **OF3K**, **OF5K** and **OF7K** at the low temperature, followed by an endothermic transition for the **OF5K** and **OF7K** as the temperature is increased (Table 6. 3. 1). The latter transition is identified as the liquid crystalline phase to isotropic phase transition based on the polarized optical microscopic study. For a thin film of **OF5K** and **OF7K**, typical Schlieren texture shown in figure 6. 3. 3, was observed during slow cooling from the isotropic phase between crossed polarizers. The Schlieren texture as well as the very small enthalpy of the transition, indicate the liquid crystalline structure to be probably of nematic character, but a smectic liquid crystalline phase was proved by a further study in the single crystal structure of **OF5K** and X-ray diffraction of **OF5K**, as has been discussed in chapter 4.
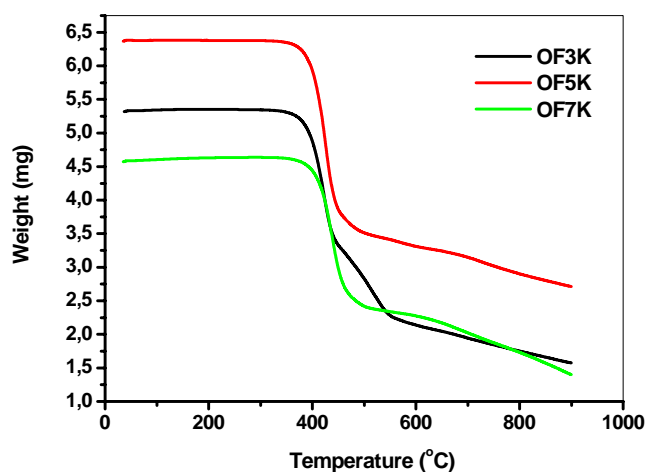
Figure 6. 3. 1 TGA traces of OF3K, OF5K, OF7K measured in a nitrogen atmosphere (heating at 10 K/min).
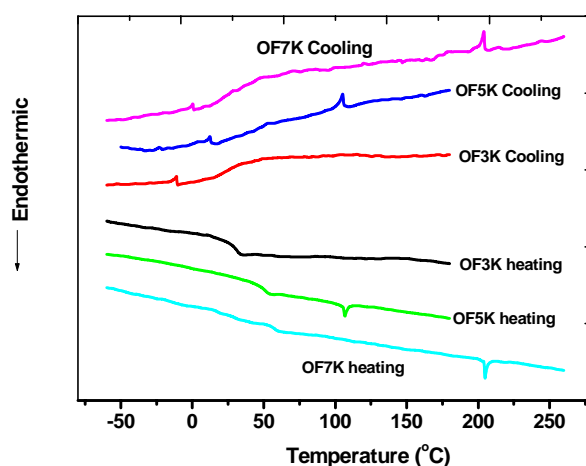
Figure 6. 3. 2. DSC traces of OF3K, OF5K, OF7K measured in a nitrogen atmosphere second heating and cooling at 10 K/min).

Table 6. 3. 1. A summary of glass transition temperature (T_g), isotropization temperature (T_{iso}), and enthalpy change during the isoptropization transition (ΔH_{iso}) for the oligofluorenes with one fluorenenone unit.

	OF3K	OF5K	OF7K
T_g (°C)	29.8	49.8	57.1
T_m (°C)		106.8	204.6
ΔH_{iso} (Jg^{-1})		-0.74	-0.77
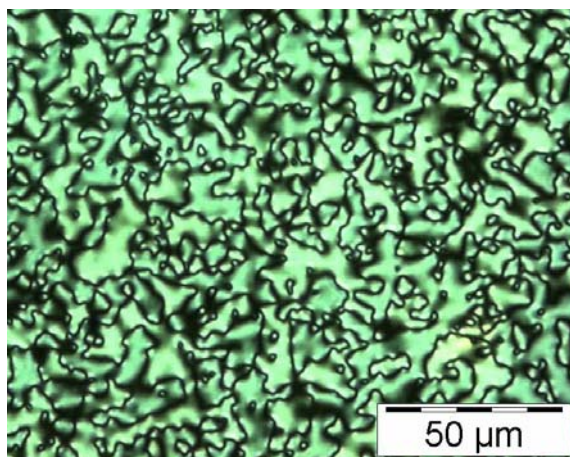
*Figure 6. 3. 3. Typical Schlieren texture obtained at 80 °C during slow cooling from the isotropic phase for **OF5K (53)** between two crossed polarizers.*

6. 4 Electronic and Electrochemical Properties

6.4.1 Electrochemical measurements

The results of the cyclic voltammetry (CV) measurements in solutions of the oligofluorenes with one fluorenone group (**OF3K**, **OF5K** and **OF7K**) are presented in Figure 6. 4. 1, and the data are collected in Table 6. 4. 1. In all cases, two or multiple reversible oxidation waves and one reduction wave were observed. With the extension of the chain-length, the $E_{1/2}^{1-2}$ for the related oxidation wave displayed a negative shift. For example, for trimer (**OF3K**), two reversible oxidation waves with $E_{1/2}^{1}$ and $E_{1/2}^{2}$ ($E_{1/2}$: half wave potential) at 1.20 and 1.38 V were observed, which are assigned to the successive generation of the radical mono-cation and dication. With chain-length extension to the pentamer (**OF5K**), two reversible oxidation waves with $E_{1/2}^{1}$ and $E_{1/2}^{2}$ at 1.08 and 1.37 V were observed. However, for all of compound (**OF3K**, **OF5K** and **OF7K**), the reduction wave with $E_{1/2}^{-1}$ around −1.53 V is almost not changed with the extension of the chain length. The plots of the current of all peaks (i_p) *versus* the square root of the scan rate ($v^{1/2}$) show a linear relationship, indicating the electrochemical process was controlled by diffusion for these oligomers (For example, for OF3K, shown in figure 6. 4. 2.).
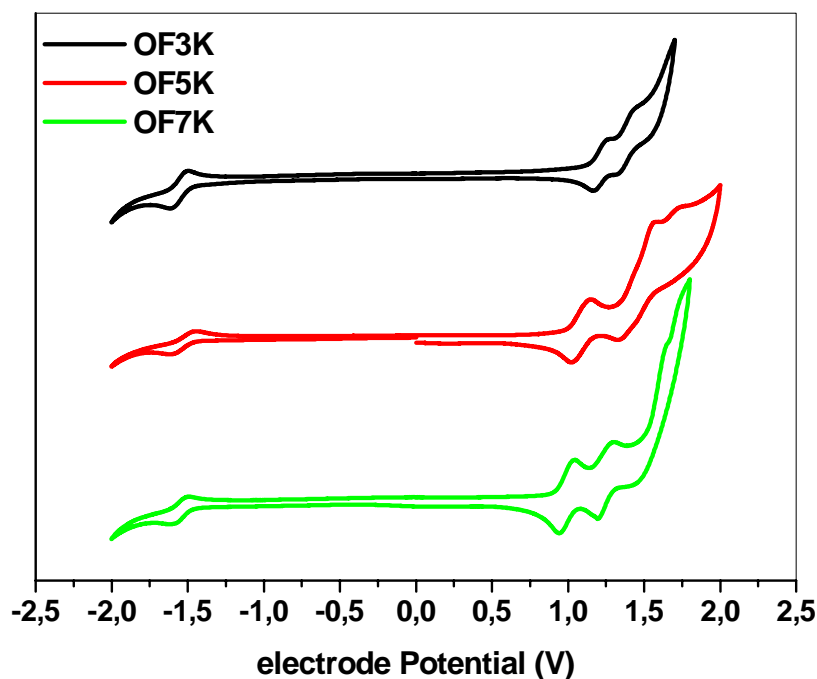
*Figure 6. 4. 1 Cyclic voltammetry of oligofluorenes with one fluorenone group (**OF3K** to **OF7K**).*

*Table 6.4. 1. Cyclic voltammetric Data for **OF3K-OF7K**, 5 × 10^{-4} M substrate and 0.1 M Bu_4NPF_6 in CH_2Cl_2. [a] I_p and E_a value relative to the vacuum level. ΔE is calculated from ΔE= Ip-Ea.*

Compound	$E_{1/2}^1$ (V)	$E_{1/2}^2$ (V)	$E_{1/2}^2$- $E_{1/2}^1$ (V)	$E_{1/2}^{-1}$Red. (V)	I_p (eV)	E_a (eV)	ΔE (eV)
OF3K	1.20	1.38	0.18	-1.54	5.73	3.13	2.60
OF5K	1.08	1.37	0.29	-1.52	5.61	3.14	2.47
OF7K	1.02	1.26	0.24	-1.53	5.52	3.13	2.39

[a] *Pt disc electrode as working electrode, $AgNO_3$/Ag electrode as reference electrode and a Pt wire as counter electrode. Scan rate: 100 mv/s, for Fc^+/Fc, $E_{1/2}$ = 0.232 V under the condition.*
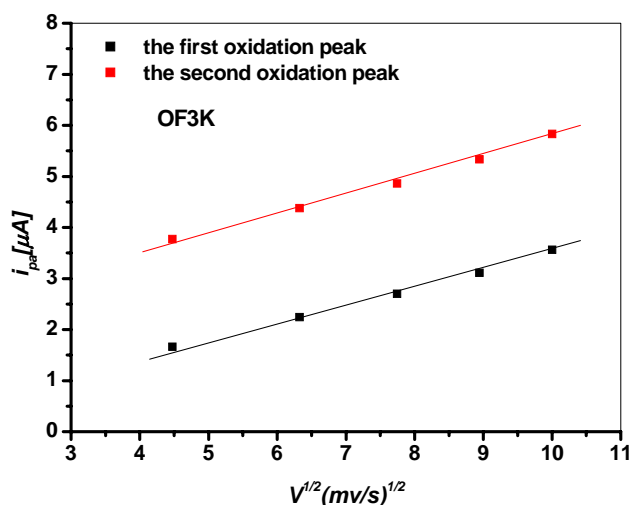
*Figure 6. 4. 2. The plot of the current of all peaks versus the square root of the scan rate for trimer of fluorene with one fluorenone group (**OF3K**).*

6. 4. 2 Determination of ionization potential (Ip) and electron affinity (Ea)

The redox potentials in all the measurements were internally calibrated by adding ferrocene(Fc) during the measurements and in the case of using $AgNO_3/Ag$ as reference electrode the $E_{1/2}(Fc^+/Fc) = 0.232$ V. Thus, ionization potential (Ip) and electron affinity (Ea) relative to the vacuum level of OF3K to OF7k can be written according to the same method used for OF2-OF7 by formula:

$$Ip= (E_{ox} + 4.4 + 0.435-0.232) \text{ eV}$$
$$Ea= (E_{red} + 4.4 +0.435 –0.232) \text{ eV}$$

where E_{ox} and E_{red} are, respectively, the onset potentials for oxidation and reduction relative to $AgNO_3/Ag$ reference electrode. Differently, for **OF3K-OF7K**, the onset potentials for reduction E_{red} and oxidation E_{ox} could be easily drawn out from the CV curves because of experimentally accessible stable anionic and cationic state. So Ip and Ea were obtained only from CV, not from absorption spectra, from which the onset of absorption energy was gained difficultly with an exact value because of the broad keto absorption band. The band gaps (ΔE) were calculated by equation:

$$\Delta E = Ip - Ea,$$

where the ΔE is the HOMO-LUMO gap. With the extension of the chain-length, the Ip values (table 6. 4. 1) decreased from 5.73 eV for **OF3K** down to 5.52 eV for **OF7K**, whereas the Ea values are almost not changed, resulting in a convergence of the HOMO-LUMO gap.

6. 4. 3 Optical Properties of Oligofluorenes with one fluorenone group

6. 4. 3. 1 Steady-state absorption and fluorescence spectra

Electronic absorption and emission spectra of monodisperse oligofluorenone with one fluorenone group in dilute chloroform solution with the same fluorene unit concentration of 1.0×10^{-5} M are shown in figure 6. 4. 3 and the data are collected in table 6. 4. 2.

The oligofluorenes with one fluorenone group (including fluorenone monomer) exhibit structured absorption bands. Comparing to homo-oligofluorenes, except for the maximun absorption peak related the π-π^* transition, the fluorenone band can be also observed as a broad long-wave absorption (n-π^*) and a shoulder closed to the maxium absorption peak (Figure 6. 4. 3). Moreover, if the absorption spectra of **OF3K**-**OF7K** are normalized at the
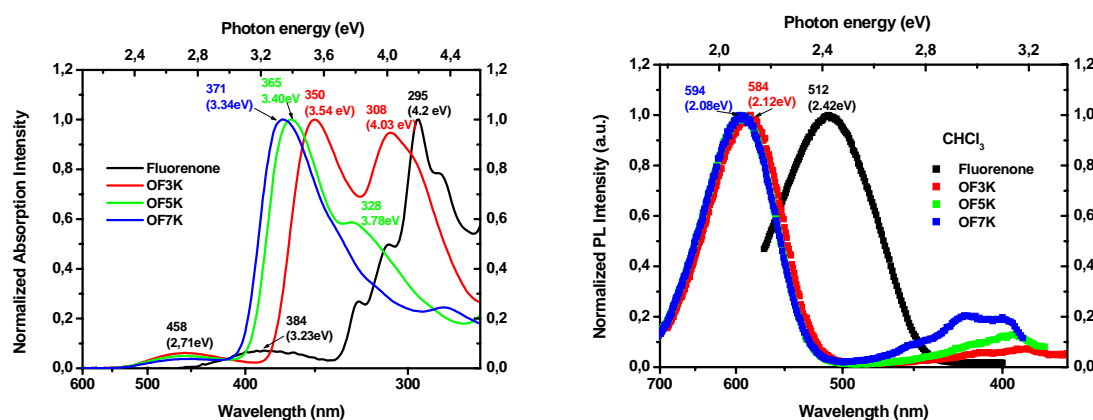

Figure 6. 4. 3. UV-vis absorption(left) and fluorescence(right) spectra of fluorenone **OF3K**, **OF5K** *and* **OF7K** *measured from the solution (1x10^{-5}M fluorene unit concentration) in chloroform at room temperature.*

wavelengths of their absorption maxima, the intensities of the fluorenone absorption band decrease with the molecular size from **OF3K** to **OF7K** because the amount of fluorenone component in the molecule decreases with the chain-length. The absorption spectra (including all of absorption bands) are red-shifted with increasing number (*n*) of fluorene units from **OF3K** ($\lambda_{max\ (abs)}$ = 350 nm, 3.54 eV) to **OF7K** ($\lambda_{max\ (abs)}$ = 371 nm, 3.34 eV).

*Table 6. 4. 2. A summary of UV-Vis absorption ($\lambda_{max\ (abs)}$), fluorescence ($\lambda_{max\ (emi)}$) data for oligofluorenes with one fluorenone group (**OF3K-OF7K**), in various solutions and solid film on quartz plate.*

		OF3K	OF5K	OF7K	OF7
UV (nm) (eV)	**CHCl₃**	**350 (3.54eV)**	**366 (3.39)**	**371 (3.34)**	**372 (3.33)**
	Toluene	**349 (3.55)**	**365 (3.40)**	**371 (3.34)**	**372 (3.33)**
	m-THF	**348(3.56)**	**364 (3.41)**	**370 (3.35)**	**371 (3.34)**
	m-Cyclohexane	**346 (3.58)**	**362 (3.43)**	**368(3.37)**	**369 (3.36)**
	film	**348 (3.56)**	**365 (3.40)**	**370 (3.35)**	**373 (3.32)**
PL (nm) (eV)	**CHCl₃**	**584 (2.12)**	**594 (2.09)**	**596 (2.08)**	**412 (3.01)**
	Toluene	**532 (2.33)**	**535 (2.32)**	**535 (2.32)**	**412 (3.01)**
	m-THF	**532 (2.33)**	**537 (2.31)**	**536 (2.31)**	**411 (3.02)**
	m-Cyclohexane	**507 (2.45)**	**512 (2.42)**	**512 (2.42)**	**410 (3.02)**
	film	**543 (2.28)**	**541 (2.29)**	**548 (2.26)**	**422 (2.94)**
Stokes shifts[a] (nm) (eV)	**CHCl₃**	**127 (0.59)**	**133 (0.60)**	**133 (0.60)**	**40 (0.32)**
	Toluene	**87 (0.46)**	**89 (0.46)**	**85 (0.44)**	**40 (0.32)**
	m-THF	**85 (0.44)**	**91 (0.47)**	**84 (0.43)**	**40 (0.32)**
	m-Cyclohexane	**66 (0.37)**	**69 (0.38)**	**70 (0.38)**	**41 (0.34)**

[a] the stokes shifts was calculated with ($n \leftrightarrow \pi^*$) transitions. m-THF: 2-methyl tetrahydrofuran; m-Cyclohexane: methyl-cyclohexane.

The fluorescence spectra of **OF3K** to **OF7K** (also including fluorenone monomer) in chloroform are shown in figure 6.4.3, excited at the corresponding energy of maximum absorption. A very strong yellow-green emission band accompanied by a weak blue emission can be observed from **OF3K-OF7K**. The very weak blue band with three well-resolved fluorescence bands can be assigned to the 0-0, 0-1 and 0-2 singlet excitation to ground state transitions.[19] The yellow-green emission bands are unstructured and broad.

This is very similar to the green emission band in the photoluminescence and electroluminescence spectra of PF. The emission maximum wavelengths are red-shifted with increasing number (*n*) of fluorene units from **OF3K** ($\lambda_{max\ (emi)}$ = 584 nm, 2.12 eV) to **OF7K** ($\lambda_{max\ (emi)}$ = 371 nm, 2.08 eV). For fluorenone monomer (**OF1K**), the emission maximum wavelength is in 512 nm (2.42 eV), a more higer energy than that of **OF3K**-**OF7K**.

The UV-Vis absorption spectra of thin films (see Figure 6. 4. 4) of the **OF3K-OF7K** on quartz substrates are practically identical to the solution data except slight blue-shifts (1 or 2 nm) in absorption maxima, as listed in Table 6. 4. 2. However, their solid state PL spectra from thin films (around 540 nm) is much more blue-shift than that in chloroform (580-590 nm) (Figure 6. 4. 4 a-c) and the data are also listed in Table 6. 4. 2. For example, for **OF3K**, the maximum emission wavelength of thin film is at 543 nm, which is large blue-shifted from 584 in chloroform. This can be explained with the polarity of chloroform, and will be discussed in detail in the next section.
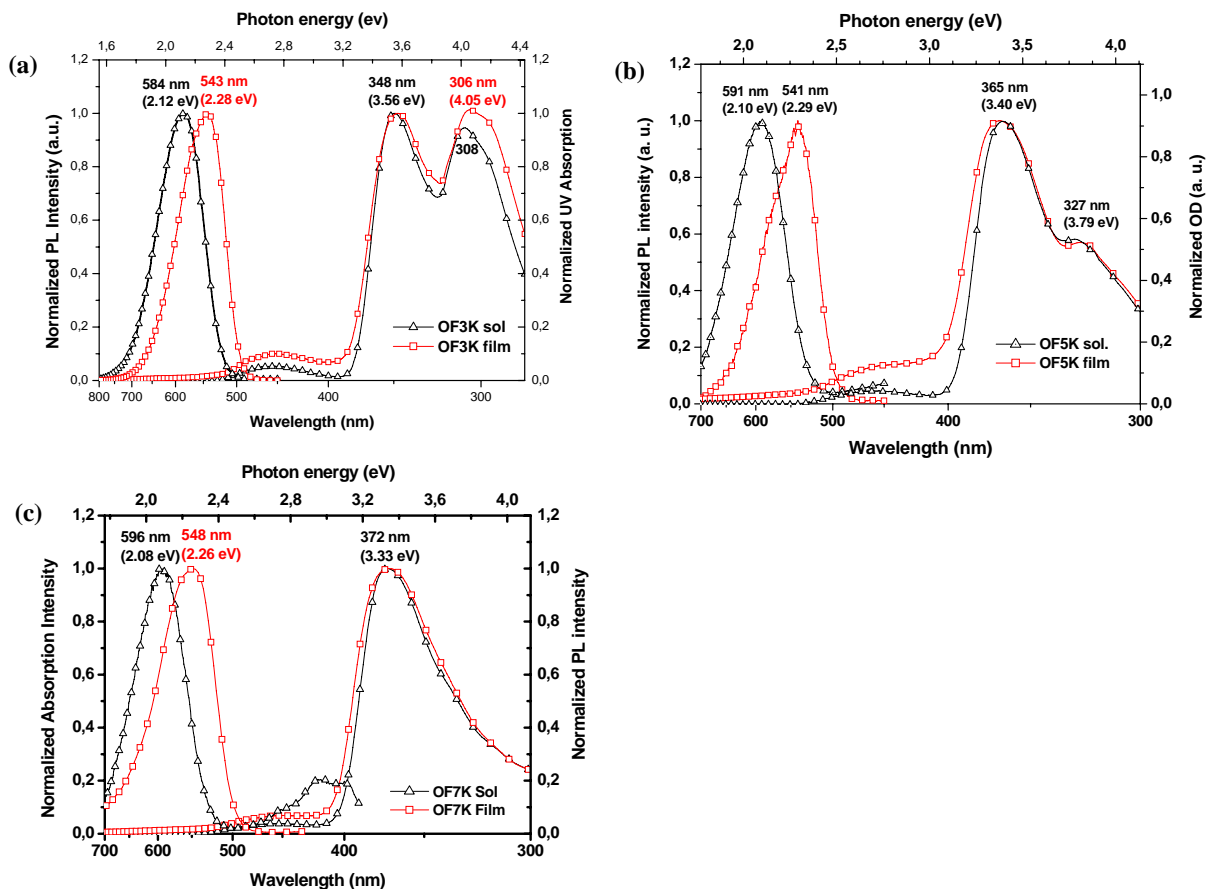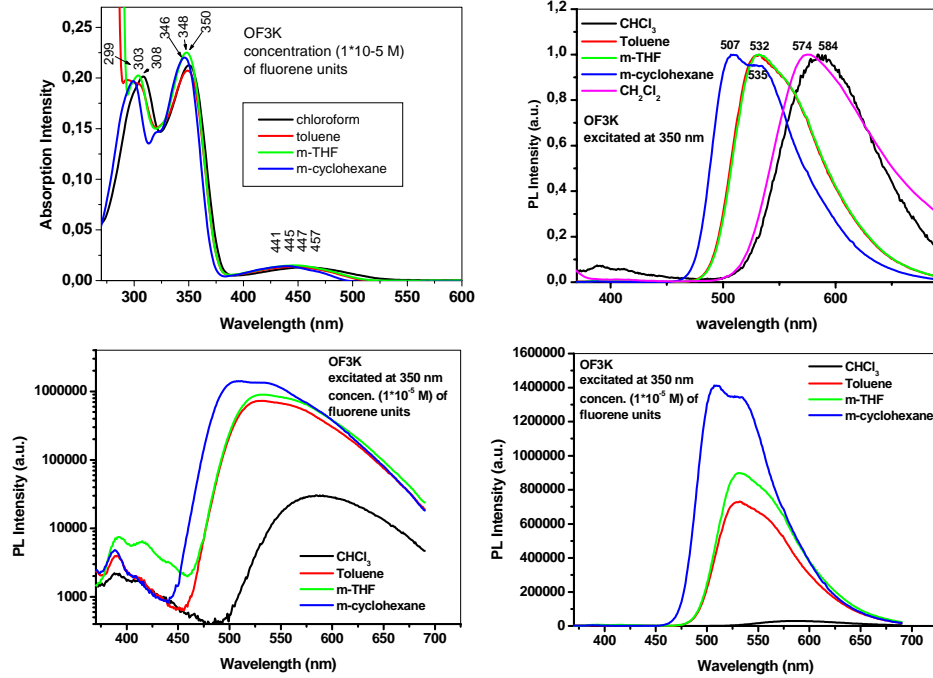
*Figure 6. 4. 4. The UV and fluorescence spectra of **OF3K** to **OF7K** in chloroform solution (black) and film on quartz plate (red).*

## 6. 4. 3. 2 Solvatochromic effect

All oligofluorenes with one fluorenone group are highly soluble in chloroform, methylene chloride, toluene, hexane, and tetrahydrofuran. It is known that solvent polarity affects the energy levels of the excited states in the oligomers containing both electron-donating and –withdrawing groups. [20] Therefore, both the peak position and the fluorescence spectral shape of the polymers can be expected to be affected. Figure 6. 4. 5 shows the normalized UV-vis and fluorescence spectra for **OF3K-OF7K** dissolved in solvents of different polarities, which are m-cyclohexane, toluene, m-THF and chloroform, respectively and the corresponding data are listed in Table 6. 4. 2. The effect of the solvent on the electronic absorption transition for the oligomers is very weak. For example, the highest energy transition ($\lambda_{max (abs)}$ = 346 nm, 3.58 eV) of **OF3K** are found with nonpolar solvent such as m-cyclohexane and the more polar solvents such as chloroform resulted in a slightly lower energy transitions ($\lambda_{max (abs)}$ = 350 nm, 3.54 eV). This behavior has been defined as a positive solvatochromic response ($\Delta\nu$ = + 330 cm^{-1})[21] that is related to a greater stabilization of the excited state relative to the ground state with increasing polarity of the solvent. Similar behavior has been observed for donor-acceptor molecules of terthiophene where the trend was rationalized as a consequence of an intramolecular charge transfer.[22] In addition, the effect of the solvent on the intensity and shape of UV absorption spectra is also not obvious (figure 6. 4. 5). The molar extinction coefficient (ε) of the oligofluorenes (see Table 6. 4. 3) shows very small changes.

If the oligomer contains both donor and acceptor groups, its fluorescence spectrum is more sensitive to the polarity of the environment. At equal concentration (1×10^{-6} M) as the solvent polarity increase, e.g., from m-cyclohexane to chloroform, the emission spectra are red-shifted. For example, the emission maximum is around 507 nm for **OF3K** in m-cyclohexane, 532 nm in toluene and *m*-THF, 584 nm in chloroform. That means the stoke shifts is also solvent dependence. As the solvent polarity increases, the Stokes shift increases, for example, the stoke shift *(n$\leftrightarrow$ π*)* of **OF5K** is 133 nm (0.60 eV) in chloroform, 91 nm (0.47eV) in m-THF, 89 nm (0.46 eV) in toluene, 69 nm (0.38 eV) in *m*-cyclohexane. This indicates the excited–state dipole moment is larger than that of the

ground state.[23]The shape of emission spectra is observed slight differently in these solvent, for example, in *m*-cyclohexane a maximum emission peak with a shoulder was observed

(a) OF3K
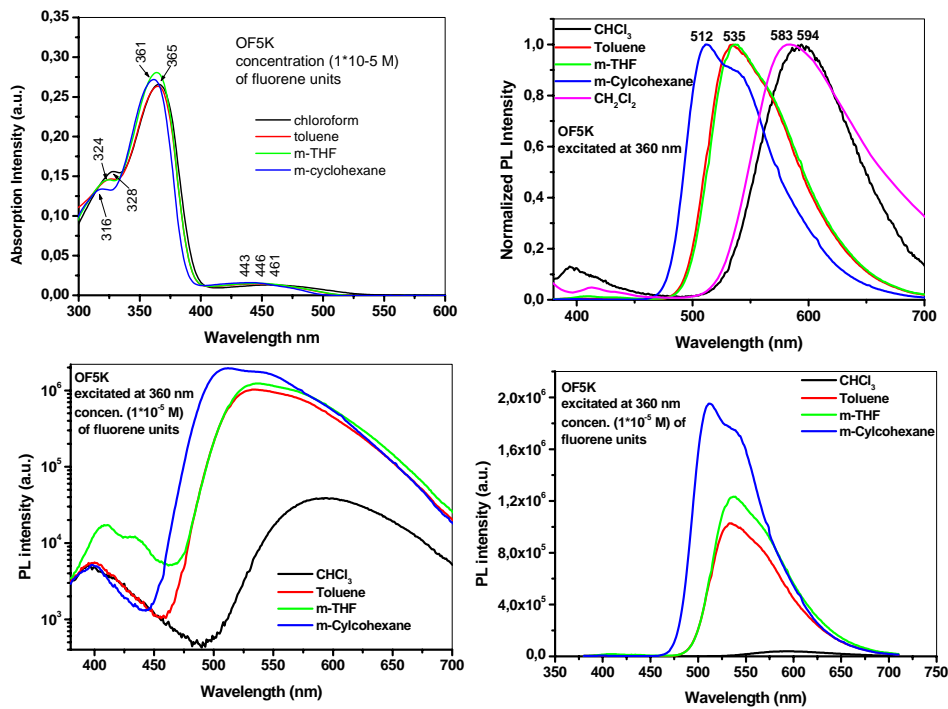
(b) OF5K
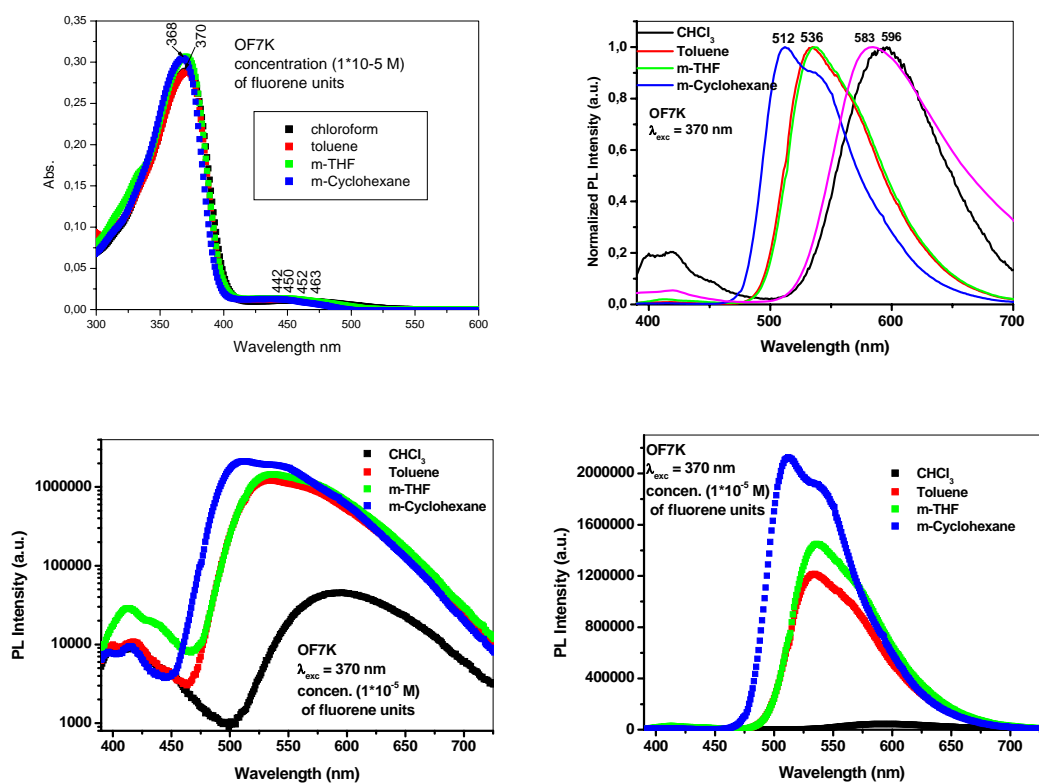
(c) OF7K

*Figure 6. 4. 5. TheUV-vis and fluorescence spectra of **OF3K** to **OF7K** in different polar solution. (concentration: 1×10^{-5} M fluorene units including the fluorenone unit)*

but in toluene, m-THF and chloroform only a broad emission band was found. At the same time, the full width at half-maximum (fwhm) of the emission for **OF3K-OF7K** increase from 82 (in m-cyclohexane, toluene, m-THF) to 100 nm (in chloroform). This is a solvent effect which results from the variations of the local environment of solute molecules, variations which are due to the statistical motions of the surrounding solvent.[23] Thus at any instant of time the surroundings of an assembly of solute molecules are inhomogeneous: some solute molecules are better solvated than others. This effect is more important with polar solvents and highly dipolar solutes. The general observation is that the bandwidth increases with solvent polarity. These phenomena indicate an intramolecular charge transfer within the excited state.[24]

In addtion, the fluorescence intensities of the oligomers decrease from non-polar solvents to polar solvents (figure 6. 4. 5). If the intensity in chloroform is defined 1, the values of around 25 in toluene, 30 for in m-THF and 50 in cyclohexane were observed.

This quenching action should be linked possibly to the energy gap law which controls the rates of non-radiative deactivations. As the energy of the excited state (e.g. S_1) is lowered by solvation in polar solvents, so the radiationless transitions $S_1 \rightarrow S_0$ generally become faster, and at the same time the corresponding radiative transition which depend on the frequency as ν^3 will be slower. This provides a general mechanism for the quenching action of polar solvents only if the excited state is more polar than the ground state, so that the effective transition energy $M^* \rightarrow M$ (radiative and non-radiative) diminishes with increasing solvent polarity.

Table 6. 4. 3 . Summary of ε_{max} and relative PL Intensity of fluorene oligomers with one fluorenone group, from various solutions. The PL Intensity is a relative value, and it is defined as 1 in choroform solution.

	ε_{max}(L mol^{-1} cm^{-1})				PL Intensity			
	CHCl$_3$	Toluene	m-THF	m-CyH	CHCl$_3$	Toluene	m-THF	m-CyH
OF3K	63813	63214	67553	66071	1	24	30	47
OF5K	132938	131827	140438	136022	1	26	32	50
OF7K	202557	201637	212834	213052	1	26	32	47

6. 5 Summary

Oligofluorenes (trimer, pentamer and heptamer) with one fluorenone unit at the center were synthesized and were used as model compounds to understand the origin of the low-energy emission band in the photoluminescence and electroluminescence spectra of polyfluorenes. Oligofluorenes with one fluorenone unit (OF3K, OF5K, OF7K) were prepared by Suzuki coupling reaction between the mono-boronate monomer, dimer, trimer and 2,7-dibromofluorenone. All of compounds were purified by standard column chromatography and confirmed by FD-MS, ^{1}H and ^{13}C-NMR techniques. The thermal properties and structure analysis (Chapter 4) were investigated by TGA, DSC, POM and WAXS. A smectic liquid crystalline phase was found between the glass transition and isotropic transition. Electrochemical properties were investigated by CV technique, and the ionization potential (I_p) and electron affinity (E_a) were calculated from the onset of

oxidation and reduction of **OFnK**. Finally, the steady-state UV-vis and fluorescence spectroscopic properties were studied. A strong absorption of π-π* transition accompanied with a weak long-wave absorption (n-π*) were observed. A strong green emission accompanied with a weak blue emission were obtained both in solution and on film, and the green emission was very similar with the low-energy emission of photo- or electro-oxidized PFs. The fluorescence of **OFnK** also displayed obvious solvatochromic effect. The wavelength of emission maximum was red-shifted and the fluorescence intensity decrease with the increasing of the polarity of solvent.

6. 6 Experimental

General Remarks.

Reactions requiring an inert gas atmosphere were conducted under argon, and the glassware was oven-dried by heating gun. THF was distilled from potassium prior to use. Commercially available chemicals were used as received. ^{1}H NMR and ^{13}C NMR spectra were recorded on a Bruker DPX 250 or AC 300 spectrometer (250 and 300 MHz for ^{1}H, 62.5 and 75.48 MHz for ^{13}C). Chemical shifts are given in ppm, referenced to residual proton resonances of the solvents. Thin-layer chromatography was performed on aluminum plates precoated with Merck 5735 silica gel 60 F_{254}. Column chromatography was performed with Merck silica gel 60 (230 ± 400 mesh). Field desorption spectra were recorded on a VG ZAB 2-SE FPD machine. Differential Scanning Calorimetry (DSC) was measured on a Mettler DSC 30 with heating or cooling rate of 10 K min^{-1}. Polarization microscopy was performed on a Zeiss Axiophot with a nitrogen flushed Linkam THM 600 hot stage. UV-vis spectra were recorded at room temperature with a Perkin-Elmer, Lambda 9, UV/Vis/NIR, spectrophotometer. Photoluminescence spectra were obtained on a Spex Fluorolog II (212). Optical properties of solid thin films were normally obtained for the samples spin-coated on quartz substrate from dilute chloroform solutions and dried in vacuum. Elemental analysis were performed by the University of Mainz.

2,7-Bis(2'-9',9'-di(2-ethylhexyl)fluorenyl)-9-fluorenone (55, OF3K):

A mixture of monobronate monomer **41** (2.0 g, 3.9 mmol) and 2,7-dibromofluorenone (0.59 g, 1.75 mmol) in toluene (30 mL) and 2M aqueous Na_2CO_3 solution (10 mL, 20 mmol) was degassed by "freeze-pump-thaw" cycles (3 ×) and $Pd(PPh_3)_4$ (204 mg, 0.177

mmol) was added under argon. The solution was heated to reflux with vigorous stirring for 20 h. After the reaction mixture was cooled to room temperature, diethyl ether and water were added. The organic layer was separated and washed with diluted HCl and brine, then dried over $MgSO_4$. The solvent was removed under vacuum and the residue was purified by column chromatography over silica gel with petroleum ether/dichloromethane (5:1) as the eluent (R_f = 0.24) to give the title compound (0.90 g, 56%): ^{1}H NMR (250 MHz, CD_2Cl_2): δ = 7.97 (s, 2H), 7.86-7.64 (m, 12 H), 7.45-7.27 (m, 6 H), 2.15-1.99 (m, 8 H), 0.86-0.50 (m, 60 H) ppm; ^{13}C NMR (62.5 MHz, $CDCl_3$): δ = 194.0, 151.4, 150.7, 142.9, 142.8, 141.3, 140.7, 137.9, 135.3, 133.2, 126.8, 126.7, 125.6, 124.1, 122.9, 122.3, 120.7, 120.0, 119.8, 55.0, 44.6 (two peaks), 34.7, 33.8, 28.2, 27.1, 26.9, 22.7, 14.0, 10.4 ppm; MS (FD): *m/z*: 957.49 [M^+]; 478.1 [M^{2+}].

7-(4,4,5,5-Tetramethyl[1.3.2]dioxaborolan-2-yl)-9,9,9´,9´-tetrakis-(2-ethylhexyl)-2,2´-bifluorene (56)

Under an argon atmosphere, 7-Bromo-9,9,9´,9´-tetrakis-(2-ethylhexyl)-2,2´-bifluorene (**44**) (6.70 g, 7.82 mmol), bis(pinacolato)diboron (2.98 g, 11.73 mmol), KOAc (3.83 g, 39.1 mmol) and Pd(dppf)Cl$_2$ (0.319 g, 0.319 mmol) were dissolved in DMF (70 mL) and heated to 60°C overnight. After the reaction mixture was cooled to room temperature, water and diethyl ether were added. The aqueous phase was extracted with diethyl ether and the combined organic layers were dried over $MgSO_4$. The solvent was removed under vacuum and the residue was purified by column chromatography over silica gel with petroleum ether/dichloromethane (5:1) as the eluent (R_f = 0.29), and afforded the monoboronic dimer **56** as an colorless oily product (5.77 g, 81.6 %): ^{1}H NMR (250 MHz, CD_2Cl_2): δ = 7.86-7.59 (m, 10 H), 7.44-7.25 (m, 3 H), 2.09-2.04 (m, 8 H), 1.35 (s, 12 H), 0.88-0.49 (m, 60 H) ppm; ^{13}C NMR (62.5 MHz, CD_2Cl_2): δ = 152.0, 151.4, 151.1, 150.2, 144.4, 141.5, 140.9, 140.5, 133.8, 130.7, 127.1, 126.8, 126.3, 124.6, 123.3, 120.5, 120.0,119.2, 84.0, 55.3, 44.8, 35.2, 34.1, 28.6, 27.6, 25.1, 23.1, 14.1, 10.4 ppm; MS (FD): *m/z*: 904.5 [M^+].

2,7-Bis(9',9',9'',9''- Tetrakis(2-ethylhexyl)-2'-7',2''bifluorenyl)-9-fluorenone (53, OF5K):

A mixture of monoboronic dimer **56** (2.89 g, 3.2 mmol) and 2,7-dibromofluorenone (0.27 g, 0.8 mmol) in toluene (16 mL) and 1M aqueous K$_2$CO$_3$ solution (8 mL, 8 mmol) was degassed by "freeze-pump-thaw" cycles (3 ×) and Pd(PPh$_3$)$_4$ (92.4 mg, 0.08 mmol)

was added under argon. The solution was heated to reflux with vigorous stirring for 20 h. After the reaction mixture was cooled to room temperature, diethyl ether and water were added. The organic layer was separated and washed with diluted HCl and brine, then dried over $MgSO_4$. The solvent was removed under vacuum and the residue was purified by column chromatograpy over silica gel with petroleum ether/dichloromethane (5:1) as the eluent (R_f = 0.22) to give **OF5K** (0.7 g, 50.5%): ^{1}H NMR (250 MHz, CD_2Cl_2): δ = 7.99 (s, 2H), 7.87-7.66 (m, 24 H), 7.45-7.26 (m, 6 H), 2.15-2.06 (m, 16 H), 0.90-0.53 (m, 120 H) ppm; ^{13}C NMR (62.5 MHz, $CDCl_3$): δ = 194.0, 151.6, 151.2, 151.0, 150.6, 142.8, 141.0, 140.4, 139.7, 137.9, 135.3, 133.2, 126.8, 126.4, 125.7, 124.1, 122.9, 122.3, 120.7, 120.1, 119.6, 55.0 (two peaks), 44.6, 34.8, 33.9, 28.2, 27.2, 22.7, 14.0, 10.4 ppm; MS (FD): m/z: 1735.2 [M^+], 867.2 [M^{2+}], 578.5 [M^{3+}].

7-(4,4,5,5-Tetramethyl[1.3.2]dioxaborolan-2-yl)-9,9,9',9',9'',9''-hexakis(2-ethylhexyl)-2,2'-7',2''-terfluorene (57)

The monoboronic trimer **57** was prepared according to the method used for monoboronic dimer **56** by using monobromo-fluorenyl-trimer **48** (2.93g, 2.35 mmol), bis(pinacolato)diboron (1.2 g, 4.7 mmol), KOAc (1.15 g, 11.75 mmol) and Pd(dppf)Cl$_2$ (96.0 mg, 0.117 mmol) in DMF (20 mL). Column chromatography over silica gel with Hexane/dichloromethane (4:1) as the eluent (R_f = 0.33) afforded the desired compound as a very stick gum (1.98 g, 67.5%): ^{1}H NMR (250 MHz, CD_2Cl_2): δ = 7.87-7.62 (m, 16 H), 7.44-7.26 (m, 3 H), 2.10-2.08 (m, 12 H), 1.36 (s, 12 H), 0.89-0.50 (m, 90 H) ppm; ^{13}C NMR (62.5 MHz, $CDCl_3$): δ = 151.6, 151.2, 150.6, 149.8, 144.0, 141.1, 140.2, 133.6, 130.4, 126.8, 126.0, 124.1, 123.0, 120.2, 119.7,118.9, 83.6, 54.9, 44.6, 34.7, 33.8, 28.2, 27.1, 24.9, 22.7, 14.0, 10.3 ppm; MS (FD): *m/z*: 1294 [M^+].

2,7-Bis(9',9',9'',9'',9''',9'''- Hexakis(2-ethylhexyl)-2'-7',2''-7'',2'''-terfluorenyl)-9-fluorenone OF7K (58):

Compound **OF7K** was prepared according to the procedure for **OF5K** by using 2,7-dibromofluorenone (76 mg, 0.225 mmol), monoboronic trimer **57** (1.5 g, 1.16 mmol) and Pd(PPh$_3$)$_4$ (34.7 mg, 0.03 mmol) in toluene (8 mL) and 1M aqueous Na$_2$CO$_3$ (4.0 mL, 4.0 mmol). The reaction took 24 h. After cooling to room temperature, the mixture was diluted with diethyl ether and the organic layer was washed with diluted aqueous HCl and brine, then dried over MgSO$_4$. The solvent was removed under vacuum and the residue was

purified by column chromatography over silica gel with hexane/dichloromethan (3:1) as the eluent (R_f = 0.48) to afford **58** as a yellow powder (264 mg, 46.7 %): ^{1}H NMR (250 MHz, CD_2Cl_2): δ = 8.00 (s, 2H), 7.88-7.68 (m, 36 H), 7.45-7.26 (m, 6 H), 2.14-2.06 (m, 24 H), 0.90-0.53 (m, 180 H) ppm; ^{13}C NMR (62.5 MHz, $CDCl_3$): δ = 194.1, 151.6, 151.2, 151.0, 150.6, 142.8, 141.1, 140.3, 139.8, 137.9, 135.3, 133.2, 126.8, 126.1 (multi-peaks), 124.1, 122.9, 122.3, 120.7, 119.8 (three peaks), 55.0 (two peaks), 44.5, 34.8, 34.0, 28.2, 27.1, 22.7, 14.0, 10.3 ppm; MS (FD): m/z: 2510.7 $[M^+]$, 1255.2 $[M^{2+}]$; 836.8 $[M^{3+}]$; 627.7 $[M^{4+}]$.

6. 7 References and Notes

[1] a) Grem, G.; Leditzky, G.; Ullrich, B.; Leising, G. *Adv. Mater.* **1992**, *4*, 36; b) Yang, Y.; Pei, Q.; Heeger, A. J. *J. Appl. Phys.* **1996**, *79*, 934; c) Pei, Q.; Yang, Y. *J. Am. Chem. Soc.* **1996**, *79*, 934; d) Grice, A. W.; Bradley, D. D. C.; Bernius, M. T.; Inbasekaran, M., Wu, W. W.; Woo, E. P. *Appl. Phys. Lett.* **1998**, *73*, 629; e) Berggren, M.; Inganäs, O.; Gustafsson, G.; Rasmusson, J.; Andersson, M. R.; Hjertberg, T.; wennerström, O. *Nature* **1994**, *372*, 444; f) Hilberer, A.; Brouwer, H.-J.; van der Scheer, B.-J.; Wildeman, J.; Hadziioannou, G.; *Macromolecules* **1995**, *28*, 4525; g) Garten, F.; Hilberer, A.; Cacialli, F.; Esselink, E.; van Dam, Y.; Schlatmann, B.; Friend, R. H.; Klapwijk, T. M.; Hadziioannou, G. *Adv. Mater.* **1997**, *9*, 127; h) Yu, W.-L.; Pei, J.; Cao, Y.; Huang, W.; Heeger, A. J. *Chem. Commun.* **1999**, 1837; i) Yu, W.-L.; Cao, Y.; Pei, J.; Huang, W.; Heeger, A. J. *Appl. Phys. Lett.* **1999**, *75*, 3270.

[2] Scherf, U.; List, E. J. W. *Adv. Mater.* **2002**, *14*, 477.

[3] Sainova, D.; Miteva, T.; Nothofer, H. G.; Scherf, U.; Glowacki, I.; Ulanski, J.; Fujikawa, H.; Neher, D. *Appl. Phys. Lett.* **2000**, *76*, 1810.

[4] a) Buckley, A. R.; Rahn, M. D.; Hill, J.; Cabanillas-Gonzalez, J.; Fox, A. M.; Bradley, D. D. C. *Chem. Phys. Lett.* **2001**, *339*, 331; b) O'Brien, D. F.; Giebeler, C.; Fletcher, R. B.; Cadby, A. J.; Palilis, L. C.; Lidzey, D. G.; Lane, P. A.; Bradley, D. D.; Blau, W. *Synth. Met.* **2001**, *116*, 379; c) Gong, X.; Ostrowski, J. C.; Bazan, G. C.; Moses, D.; Heeger, A. J.; Liu, M. S.; Jen, A. K-Y. *Adv. Mater.* **2003**, *15*, 45.

[5] Grell, M.; Bradley, D. D. C.; Inbasekarkan, M.; Woo, E. P. *Adv. Mater.* **1997**, *9*, 798.

[6] Sheats, J. R.; Antoniadis, H.; Hueschen, M.; Leonard, W.; Miller, J.; Moon, R.; Roitman, D.; Stocking, A. *Science* **1996**, *273*, 884.

[7] Scurlock, R. D.; Wang, B.; Ogilby, P. R.; Sheats, J. R.; Goitia, R. J. *J. Am. Chem. Soc.* **1995**, *117*, 10194.

[8] Bliznyuk, V. N.; Carter, S. A.; Scott, J. C.; Klärner, G.; Miller, R. D.; Miller, D. C. *Macromolecules* **1999**, *32*, 361.

[9] a) Uckert, F.; Tak, Y. H.; Müllen, K.; Bässler, H. *Adv. Mater.* **2000**, *12*, 905; b) Weinfurtner, K. H.; Fujikawa, H.; Tokito, S.; Taga, Y. *Appl. Phys. Lett.* **2000**, *76*, 2502.

[10] a) Lemmer, Heun, S.; Mahrt, R. F.; Scherf, U.; Hopmeier, M.; Siegner, U.; Göbel, E. O.; Müllen, K.; Bässler, H.; *Chem. Phys. Lett.* **1995**, *240*, 373. b) Cimrová, V.; Scherf, U.; Neher, D. *Appl. Phys. Lett.* **1996**, *69*, 608; c) Conwell, E. *Trends Polym. Sci.* **1997**, *5*, 218; d) Grell, M., Bradley, D. D. C.; Ungar, G.; Hill, J.; Whitehead, K. S. *Macromolecules* **1999**, *32*, 5810; d) Jenekhe, S. A.; Osaheni, J. A. *Science* **1994**, *265*, 765.; e) Yu, W. L.; Pei, J.; Huang, W.; Heeger, A. J. *Adv. Mater.* **2000**, *12*, 828, f) Kreyenschmidt, M.; Klaerner, G.; Fuhrer, T.; Ashenhurst, J.; Karg, S.; Chen, W. D.; Lee, V. Y.; Scott, J. C.; Miller, R. D. *Macromolecules* **1998**, *31*, 1099; g) Klärner, G.; Lee, J.-I.; Davey, M. H.; Miller, R. D.; *Chem. Mater.* **1999**, *11*, 1083; h) Teetsov, J.; Fox, M. A. *J. Mater. Chem.* **1999**, *9*, 2117.

[11] a) Yu, W. L.; Cao, Y.; Pei, J.; Huang, W.; Heeger, A. J.; *Appl. Phys. Lett.* **1999**, *75*, 3270. b) He, Y.; Gong, S.; Hattori, R.; Kanicki, J. *Appl. Phys. Lett.* **1999**, *74*, 2265; c) Klaerner, G.; Davey, M. H.; Chen, W. D.; Scott, J. C.; Miller, R. D. *Adv. Mater.* **1998**, *10*, 993; d) Setayesh, S.; Grimsdale, A. C.; Weil, T.; enkelmann, V.; Müllen, K.; Meghdadi, F.; List, E. J. W.; Leising, G. *J. Am. Chem. Soc.* **2001**, *123*, 946; e) Xiao, S.; Nguyen, M.; Gong, X.; Cao, Y.; Wu, H. B.; Moses, D.; Heeger, A. J. *Adv. Funct. Mater.* **2003**, *13*, 25.

[12] Campbell, A. J.; Bradley, D. D. C.; Virgili, T.; Lidzey, D. G.; Antoniadis, H. *Appl. Phys. Lett.* **2001**, *79*, 3872.

[13] a) List, E. J. W.; Güntner, R.; Scandiucci de Freitas, P.; Scherf, U.; *Adv. Mater.* **2002**, *14*, 374; b) Gong, X.; Iyer, P. K.; Moses, D.; Bazan, G.; Heeger, A. J.; Xiao, S. S. *Adv. Funct. Mater.* **2003**, *13*, 325.

[14] Nothofer, H.-G. *Ph.D. Thesis*, Universität Potsdam, Germany **2001**.

[15] a) Bliznyuk, V. N.; Carter, S.; Scott, J. C.; Klärner, G.; Miller, R. D.; Miller, D. C. *Macromolecules* **1999**, *32*, 361; b) Lee, J. I.; Klärner, G.; Miller, R. D. *Chem. Mater.* **1999**, *11*, 1083.

[16] a) List, E. J. W.; Leising, G.; Schulte, N.; Schlüter, A. D.; Scherf, U.; Graupner, W. *Jpn. J. Appl. Phys.* **2000**, *39*, L760; b) Tasch, S.; List, E. J. W.; Hochfilzer, C.; Leising, G.; Schlichting, P.; Rohr, U.; Geerts, Y.; Scherf, U.; Müllen, K. *Phys. Rev. B* **1997**, *56*, 4479.

[17] Prieto, I.; Teetsov, J.; Fox, M. A.; Vanden Bout, D. A.; Bard, A. J. *J. Phys. Chem. A* **2001**, *105*, 520.

[18] (a) Ishiyama, T.; Murata, M.; Miyaura, N. *J. Org. Chem.* **1995**, *60*, 7508-7510; (b) Read, M. W.; Escobedo, J. O.; Willis, D. M.; Beck, P. A.; Strongin, R. M. *Org. Lett.* **2000**, *2*, 3201-3204; (c) Giroux, A.; Han, Y.; Prasit, P. *Tetrahedron Lett.* **1997**, *38*, 3841-3844.

[19] Neher, D. *Macromol. Rapid Commun.* **2001**, *22*, 1365-1385.

[20] a) Oelkrug, D.; Tompert, A. S.; Gierschner, J.; Egelhaaf, H.-J.; Hanack, M.; Hohloch, M.; Steinhuber, E. *J. Phys. Chem. B* **1998**, *102*, 1902; b) Strehmel, B.; Sarker, A. M.; Malpert, J. H.; Strehmel, V.; Seifert, H.; Neckers, D. C. *J. Am. Chem. Soc.* **1999**, *121*, 1226.

[21] a) Effenberger, F.; Wurthner, F.; Steybe, F. *J. Org. Chem.* **1995**, *60*, 2082-2091; b) Reichardt, C. *Chem. Rev.* **1994**, *94*, 2319-2358.

[22] Garcia, P.; Pernaut, J. M.; Hapiot, P.; Wintgens, V.; Valat, P.; Garnier, F.; Delabouglise, D. *J. Phys. Chem.* **1993**, *97*, 513-516.

[23] *Solvatochromism;* Suppan, P.; Ghoneim, N. The Royal Society of Chemistry **1997**.

[24] a) Sarker, A. M.; Strehmel, B.; Neckers, D. C. *Macromolecules* **1999**, *32*, 7409; b) Schulte, R. D.; Kauffman, J. F. *Appl. Spectrosc.* **1995**, *49*, 31.

7 Photophysical properties of oligofluorenes with one fluorenone group

*One of the objectives of the photophysical investigations on the oligofluorenes with one fluorenone group (**OFnK**) is to determine whether the undesirable green emission in polyfluorenes arises from intermolecular aggregates or from fluorenone-type defects on the main chains. The steady state spectra of **OFnK**, such as UV-vis absorption, fluorescence and solvatochromic effects have been presented in Chapter 6. In this chapter, the time resolved fluorescence spectra of **OFnK**, a comparison between **OFn** and **OFnK**, and the photophysical properties of blend systems of **PF2/6** with **OFnK** will be presented and discussed.*

7.1 Time resolved fluorescence (TRF) spectra

The time-resolved fluorescence spectra of **OFn** and **OFnK** were investigated by the streak camera and gated detection technique at both RT and 77K.

7. 1. 1 An overview of TRF of OFnK

In this part, an overview of TRF of **OFnK** in dilute solution and as films will be described with the excitation wavelength at 450 nm for the n→π* transition band and at 365 nm for S_0-S_1 transition.

7.1.1.1 Fast time-resolved fluorescence spectroscopy (FTRF)

The fast time-resolved PL spectra of **OFnK** were measured both in toluene : methyl-cyclohexane (1 : 1) (TOL-MCH) and in *m*-THF solutions. The streak camera photos of **OF5K** in TOL-MCH (left) and in *m*-THF (right) excited at 370 nm are shown in Figure 7. 1. 1. Only one green emission band was observed for **OF5K** in TOL-MCH, whereas a

strong green emission accompanied with weak a blue emission band was observed in *m*-THF solution.
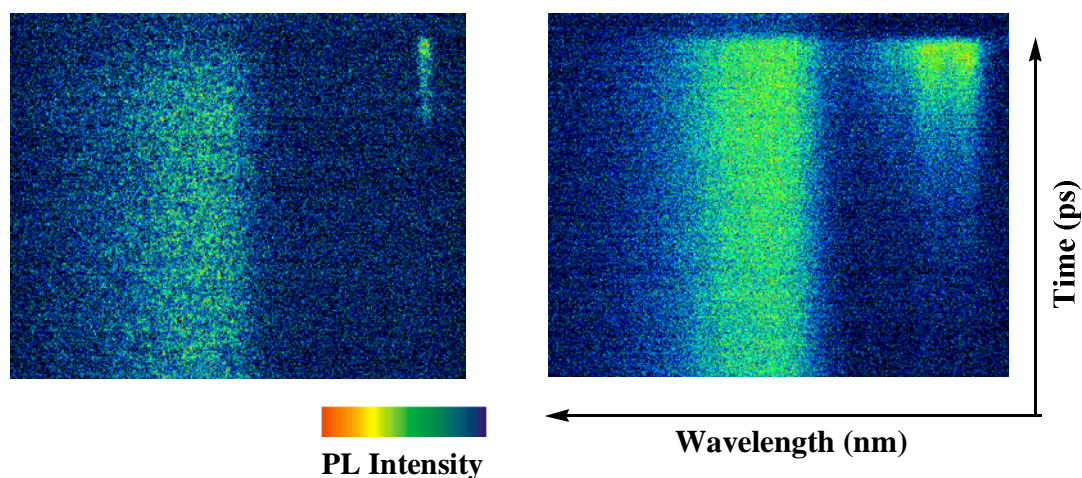

*Figure 7. 1. 1. The streak camera photos of **OF5K** in solutions: 1x 10^{-6} M in TOL-MCH (left) and 1x 10^{-6} M in m-THF (right) at room temperature (excitation at 370 nm).*

The fluorescence spectra of **OF5K** as film and in solution (TOL-MCH and *m*-THF) at 77K and RT are shown in Figure 7. 1. 2. Only a broad green emission band with maximum emission approximately at 2.30 eV (540 nm) was detected both in TOL-MCH solution and film (Figure 7. 1. 2a) at RT. This 2.30 eV (540 nm) emission band matches exactly with the previously reported troublesome green PL and EL band in blue-emitting polyfluorenes.[1] The strong green emission band was accompanied with a weak blue emission band when excited at 370 nm (Figure 7. 1. 2b). The weak blue emission band became weaker at 77K than that at RT. When the **OF5K** was excited at 430 nm, the green emission band was almost identical to that excited at 370 nm (Figure 7. 1. 2b).

At 77K, the green emission band with well-resolved structure at approximate (2.25 eV) 550 nm and (2.10 eV) 590 nm was observed in both solution and film of **OF5K** (Figure 7. 1. 2 (a) and (b)). The shape of the spectra was very similar to the fluorescence spectra of **OF5**, and showed the similar vibronic splitting of about 160 meV.

The fluorescence spectra of **OF5K** in *m*-THF at 77K excited at 370 nm with different power intensity are shown in Figure 7. 1. 3a. The position and shape of the spectra was independent of laser excitation intensity except for the fluorescence intensity, either excited at 370 nm or 430 nm (not shown). The dependence of the fluorescence intensity of **OF5K** in *m*-THF on pump intensity at 77K is shown in Figure 7. 1. 3b. The fluorescence intensity

varies approximately linear with the laser power (with slope S = 1), and a similar behaviour was obtained at RT.

(a)   (b)
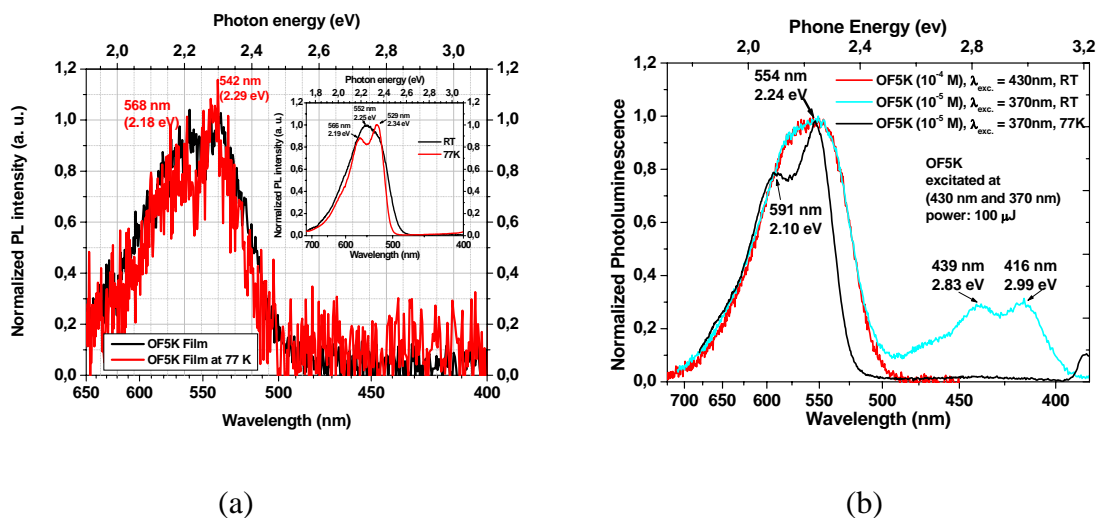
*Figure 7. 1. 2. a) The fluorescence spectra of the **OF5K** as film at both RT and 77K, the inserted figure shows the fluorescence spectra of **OF5K** in dilute TOL-MCH solution; b) the fluorescence spectra of **OF5K** in m-THF solution at both RT and 77K (the excitation wavelengths are at 430 nm and 370 nm, respectively).*

(a)   (b)

*Figure 7. 1. 3. a) The fluorescence spectra of **OF5K** (10^{-5} M in m-THF) under different power intensities; b) the dependence of the fluorescence intensity of **OF5K** in m-THF on pump intensity at 77K (excitation at 370 nm).*

The oligomers **OFnK** maybe considered as internally doped structures; e. g. for **OF5K**, efficient excitation transfer takes place by a doping concentration of 20 mol %, i.e.,

$$\frac{\text{FO}}{\text{FL-FL-FO-FL-FL}} = 20 \text{ mol \%}$$

(7. 1. 1)

(FO: fluorenone unit; FL: Fluorene units with the 2-ethylhexyl side chain)

The presence of the low optical gap chemical structure in the oligofluorene chain results in rapid energy transfer from higher energy sites (fluorene segments) to lower energy sites (fluorenone units) prior to the radiative decay of the excited species (Scheme 7. 1. 1).

Scheme 7. 1. 1. Energy migration by hopping of excitations along a single oligo- or polymer chain.

The fluorescence spectra of **OF3K** at RT and 77K are shown in Figure 7. 1. 4. The green emission band with well-resolved structures at 2.16 eV (574 nm) and 2.32 eV (534 nm) with similar vibronic splitting of 160 meV was observed in *m*-THF solution at 77K. At room temperature, only one broad emission centered at 2.27 eV (547 nm) was observed. In addition, a similar linear dependence of fluorescence intensity on the laser power was observed (Figure 7. 1. 4b).

The decay of the green fluorescence of **OFnK** is similar in solution (TOL-MCH and *m*-THF) and film at different excitation wavelengths (370 nm or 430 nm) (Figure 7. 1. 5 (a)), and different laser excitation intensities (Figure 7. 1. 5 (b)). Moreover, the decay of fluorescence at RT is faster than that at 77K. The decay of the green emission is slower than that of the blue emission, and the blue emission had a similar decay behaviour as that of the **OF5** (Figure 7. 1. 5 (a)). This suggests that the blue emission band arises from the fluorenyl species. The lifetime of the **OFnK** emission can not be obtained from the streak camera measurements, so longer time range fluorescence measurements were performed.

(a)   (b)

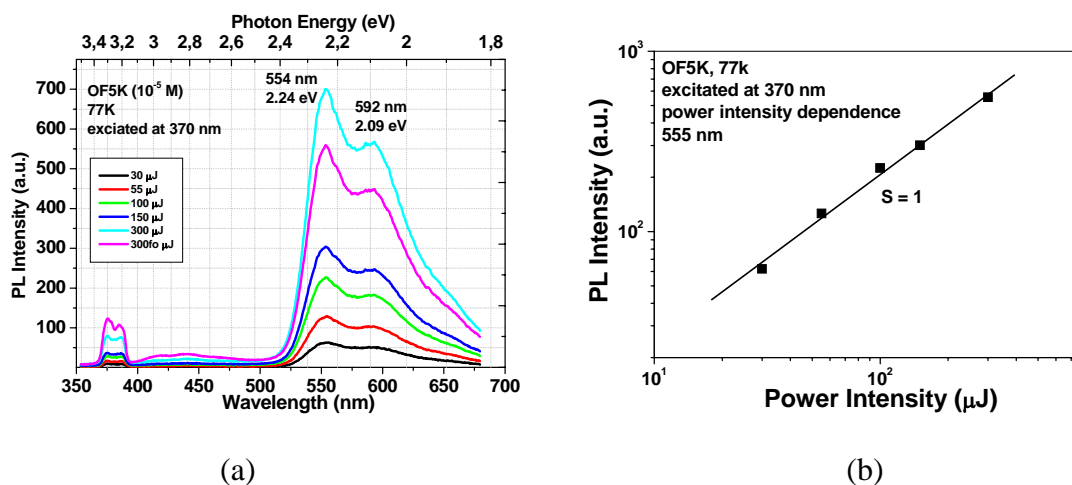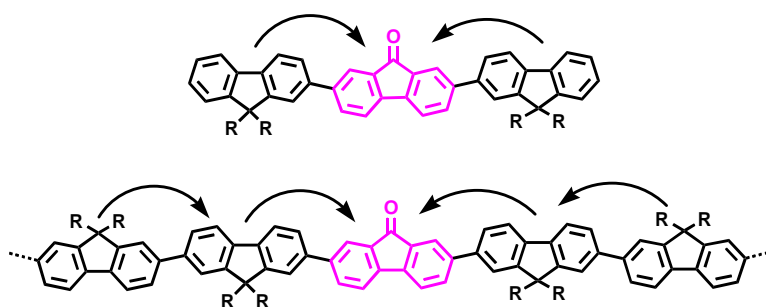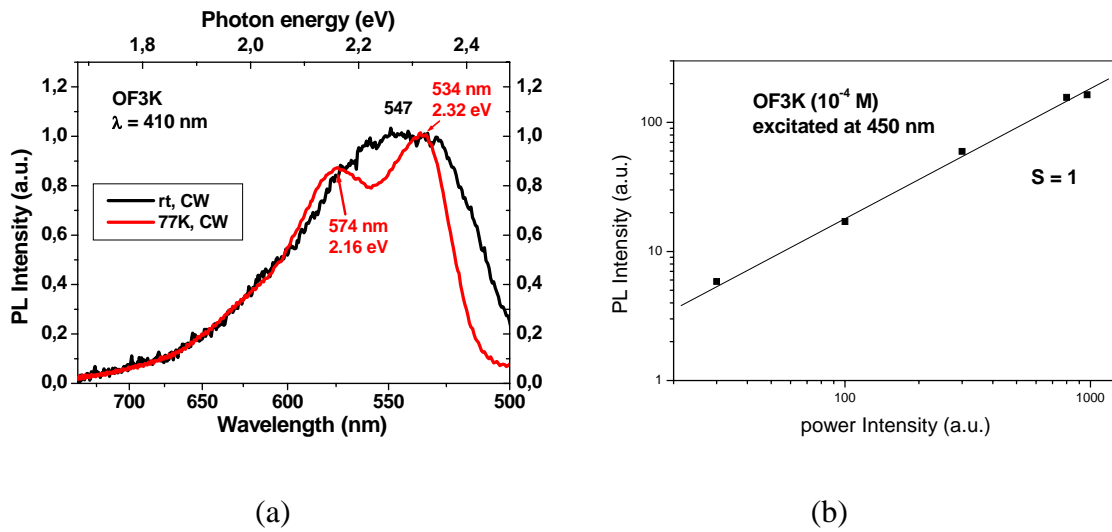*Figure 7. 1. 4. a)The fluorescence spectra of **OF3K** at RT and 77K; b) dependence of fluorescence intensity of **OF3K** in m-THF on laser excitation intensity at RT (excited at 430 nm).*
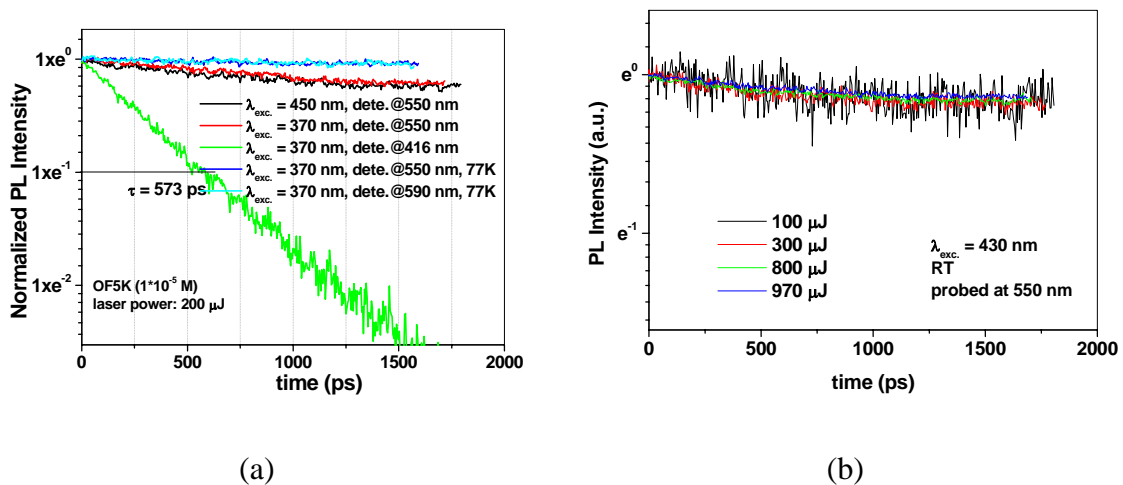

(a)   (b)

*Figure 7. 1. 5. a) The decay of fluorescence in m-THF solution both at RT and 77K; b) decay of the fluorescence of **OF3K** at different laser power intensities.*

7.1.1.2 Long range delayed time-resolved PL spectroscopy

The CW fluorescence spectra and DF of **OF5K** (10^{-6} M) at 77 K in *m*-THF as a dilute frozen matrix are shown in Figure 7. 1. 6. To verify the difference between absorption bands, namely, n→π* and π→π* transition, **OF5K** was excited both at 365 nm as well as 453nm. As shown in Figure 7. 1. 6 (a), a strong green emission band ("A" band) accompanied with the weak blue emission band (range from 411nm to 494 nm) was observed when the excitation wavelength was fixed at 365 nm. The wavelength of the maximum of the blue emission band ranges from 3.02 eV (411 nm) to 2.85 eV (435 nm) ("B" band) and arises from the excited singlet state of the fluorene unit, and the emission bands at 2.67 eV (466 nm) and 2.51 eV (494 nm) ("C" band) originates from an occasional photochemical reaction and it consequences for PL property. In fact, the "C" band did not exist when the sample was exposed to the excitating laser beam for a short time. Only **OF5K** with a fluorenone unit can also undergo a photochemical reaction at longer exposure to the excitating laser beam and subsequently a new emission band appears. This new band displays a similar spectral shape as the low-energy band with a similar vibronic splitting (ca.150 meV).

As shown in Figure 7. 1. 6 (b), the delayed fluorescence of **OF5K** was observed at different delay times when excited at 365 nm. The emission bands from 3.02 eV (411 nm) to 2.52 eV (493 nm) ("B" and "C" bands) nearly vanish when the delay time increases to 20 ns, and the green emission band intensity decreases with increasing delay time. The CW fluorescence spectra of **OF5K** excited at 453 nm are shown in Figure 7. 1. 6 (c) and a similar strong green emission band accompanied with a weak "C" band are observed. The delayed fluorescence spectra excited at 453 nm (Figure 7. 1. 6 (d)) discloses that the "C" band also vanishes when the delay time increases to 20 ns.
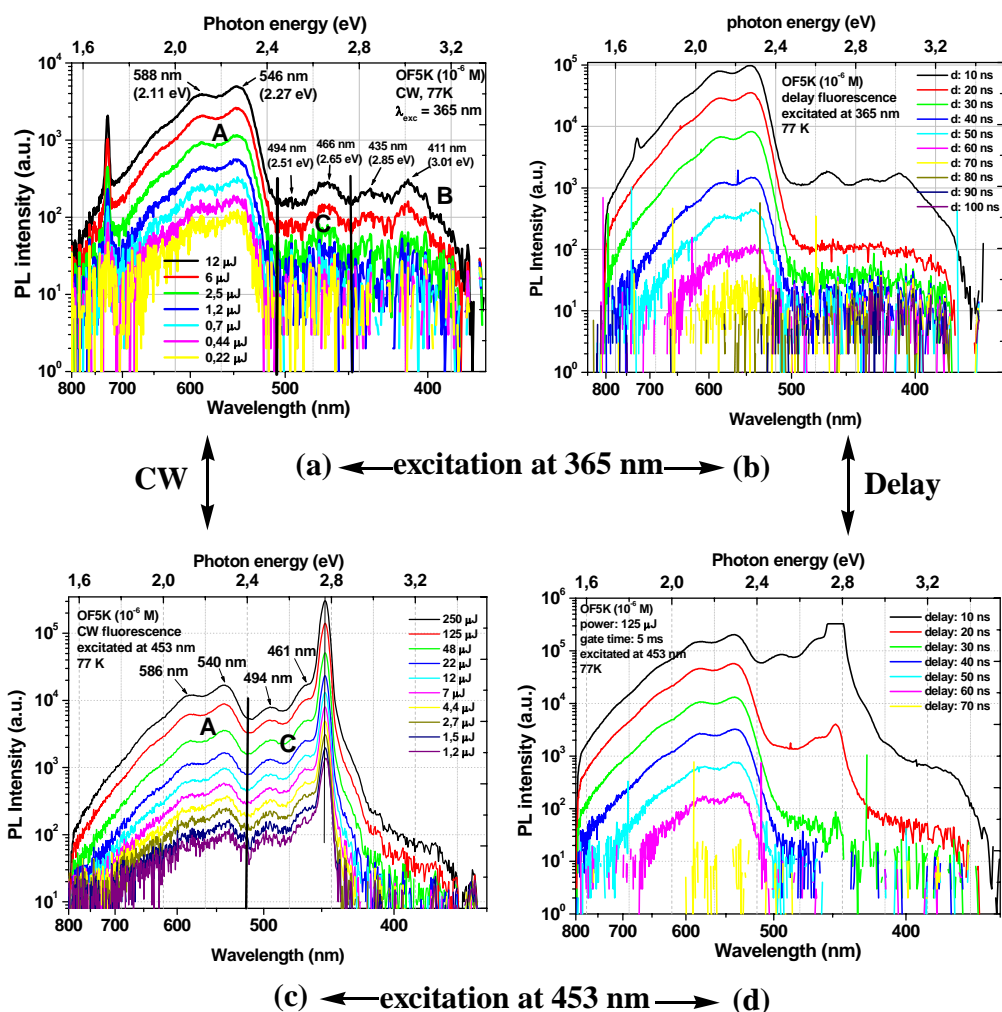
*Figure 7. 1. 6. The CW fluorescence spectra ((a) and (c)) and DF spectra ((b) and (d)) of **OF5K** at 77 K in m-THF as a dilute frozen matrix. Excitation was at 365 nm for (a) and (b), at 453 nm for (c) and (d).*

The kinetics of the green emission of **OFnK** at 77 K in *m*-THF was studied. The dependence of DF intensity upon time (t>10 ns) is shown in Figure 7. 1. 7. The **OF5K** frozen solution showed similar monoexponential decay kinetics under excitation at 453 nm (n → π* transition) and at 365 nm (S$_0$ → S$_1$ 0-0 transition) as shown in Figure 7. 1. 7 (left). The fluorescence lifetime of **OF5K** is approximately 8 ns with excitation wavelength at either 365 nm or 453 nm. Similar decay behaviour and the lifetimes (8.3 ns) were also obtained for **OF3K** (Figure 7. 1. 7 (right)) at 77K in *m*-THF frozen matrix.
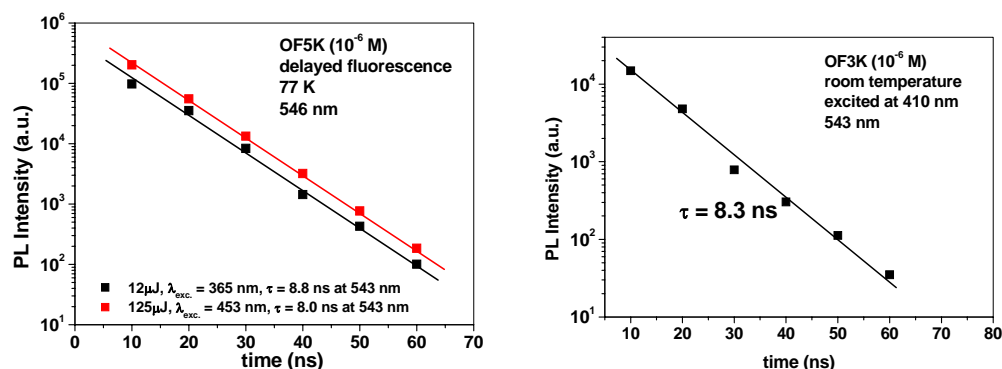
*Figure 7. 1. 7. The dependence of DF intensity upon time (t>10 ns) for **OFnK** probed at 543 nm at 77 K in m-THF. Left: The **OF5K** frozen solution was excited at 365 nm and 453 nm; Right: The **OF3K** frozen solution was excited at 410 nm.*

In Figure 7. 1. 8 the dependence of CW fluorescence, prompt fluorescence and delayed fluorescence intensity upon laser excitation intensity for **OF5K** in a dilute frozen solution at 77K is depicted. The delayed emission was recorded with a time delay of 20 ns after excitation at 363 nm and 453 nm. The CW, prompt fluorescence and DF intensity varies approximately linear with laser excitation intensity probed at 546 nm (Figure 7. 1. 8).

*Figure 7. 1. 8. The dependence of CW, prompt and DF intensity of **OF5K** on laser excitation intensity at 77 K in m-THF probed at 546 nm. The **OF5K** frozen solution was excited at both 365 nm and 453 nm.*

7. 1. 2. Site-selective excitation

Site-selective excitation PL experiments were carried out in order to clarify the origin of the low-energy emissions bands.

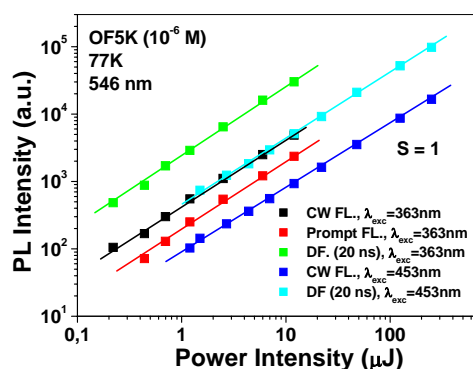   The CW fluorescence spectra of **OF5K** at 77K in *m*-THF at different excitation wavelengths from 510 nm to 420 nm are shown in Figure 7. 1. 9 (a). The green emission ("A" band) is observed and the emission maximum is slightly red-shifted (about 5 nm) with the excitation wavelength going from 510 nm to 420 nm (Figure 7. 1. 9 a). The green emission ("A" band) accompanied with a strong "C" band was observed at the same time when the excitation wavelengths were varied between 450 and 420 nm. The CW fluorescence spectra of **OF5K** excited at 420 nm at different laser excitation intensities at 77K in *m*-THF dilute frozen matrix are shown in Figure 7. 1. 9 (b). The PL intensity at 463 nm ("C" band) and 540 nm ("A" band) increases with the increasing of power intensity approximately linearly as depicted in Figure 7. 1. 10.

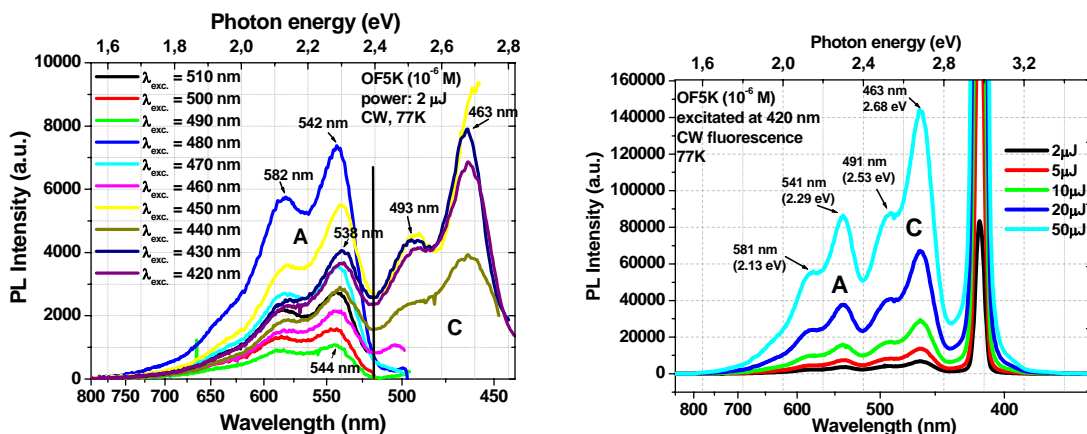*Figure 7. 1. 9. (a)The CW fluorescence spectra of **OF5K** at 77K in m-THF at different excitation wavelengths; (b) the CW fluorescence spectra of **OF5K** excited at 420 nm under different laser excitation intensities.*
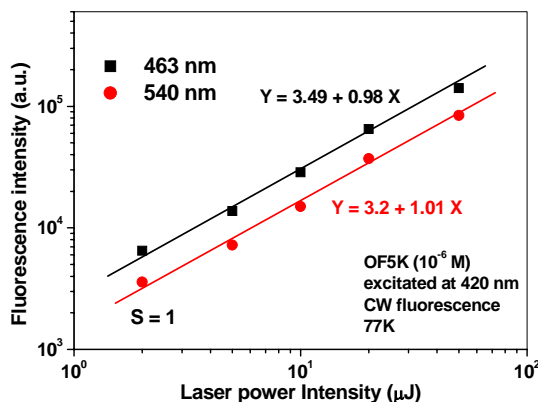

*Figure 7. 1. 10. Dependence of CW fluorescence intensity of **OF5K** in m-THF on laser excitation intensity at 77K probed at 463 nm and 540 nm (excitation at 420 nm).*

7. 1. 3 Concentration dependence

The fact that the green emission was observed in such dilute **OFnK** solution (10^{-6} M) suggests that the green emission does not originate from intermolecular aggregates or excimer formation, but is obviously related to the fluorenone defect sites in the main chain. On the other hand, from the structural point of view, the fluorenone moieties are more planar than the 9,9-dialkylfluorene units and thus the fluorenone-containing oligofluorenes may be more prone to from aggregates with increasing concentration as compared to the defect-free oligofluorene chains. So the green emission from **OFnK** in concentrated solution or solid films may originate from the fluorenone defects and/or excimers formation. We thus investigated the PL emission of **OFnK** as model compounds for fluorenone-containing polyfluorenes in *m*-THF solution under different concentrations such as 10^{-6}, 10^{-5}, 10^{-4} and 10^{-3} M.

7. 1. 3. 1 Fluorescence spectra and decay of fluorescence

The photophysical properties of **OF5K** at different concentrations (10^{-3}-10^{-6} M) were studied with a streak camera and gated detection technique at RT with the excitation wavelength at both 450 nm and 365 nm.

7. 1. 3. 1. 1 Fast time-resolved fluorescence spectra (FTRF)

The fluorescence spectra of **OF5K** (left) and the decay of the fluorescence (right) at RT at different concentrations in *m*-THF are shown in Figure 7. 1. 11(excited at 450 nm). The spectra are identical at different concentrations except for the emission intensity. The same mono-exponential decay behaviour was observed, except that the decay rate was slightly faster with increasing concentration.
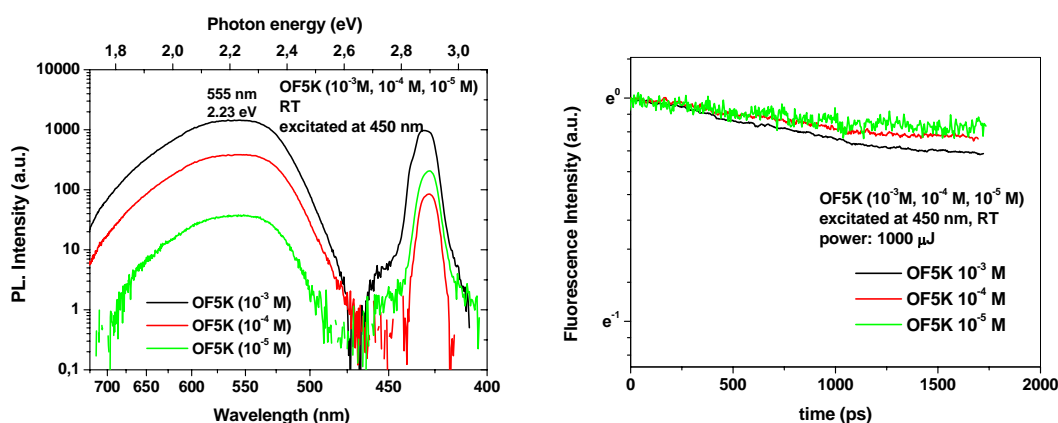
*Figure 7. 1. 11.The fluorescence spectra of **OF5K** (left) and decay of fluorescence (right) in m-THF solutions at different concentrations at RT (excited at 450 nm).*

The fluorescence spectra of **OF5K** (left) and normalized fluorescence spectra excited at 365 nm (right) in *m*-THF solutions with different concentrations at RT are shown in Figure 7. 1. 12. The strong green emission ("A" band) accompanied with the weak blue emission ("B" band) is observed. When the spectra are normalized at 414 nm, the PL spectra of **OF5K** (Figure 7. 1. 12 (right)) show a steady growth of the 550 nm band as the concentration increases. The ratios of green and blue emission intensity are 1.7, 3.1, 4.5, 7.2 with the concentrations of 10^{-6}, 10^{-5}, 10^{-4} and 10^{-3} M, respectively. These results suggest that as the concentration increases the intermolecular interactions became obvious, leading to enhanced green emission. It is worthy to note that Romaner et al. did not observe such a concentration dependence of the green emission band in toluene solutions of polyfluorenes containing fluorenone defects[2], and that this difference can be explained by the relatively low concentrations of the solutions they studied (~10^{-8}-10^{-7} M).

The dependence of the PL intensity on the concentration for **OF5K** (left) is shown in Figure 7. 1. 13. The PL intensity at 550 nm and 417 nm increases with increasing concentration from 10^{-6} M to 10^{-4} M, and approximately reaches a plateau in the region of 10^{-4} M to 10^{-3} M. To further understand the nature of the green emission of **OFnK**, we have investigated the fluorescence decays of the PL emission bands in *m*-THF solutions at different concentrations. Single exponential fits to the decay would indicate that these is only one emitting species, whereas multiexponential decay would imply complex kinetics involving several species, formation of excimers or clusters[3]. The decay behaviour of **OF5K** at different concentrations at 419 nm and 550 nm is shown in Figure 7. 1. 13 (right,

excitation at 365 nm). A monoexponential decay behaviour independent on concentration is observed. We thus rule out the possibility that the green emission band originates from aggregates or excimer formation in solution. The observed strong concentration dependence of the green emission band in solution can be explained by enhanced interchain hopping processes.
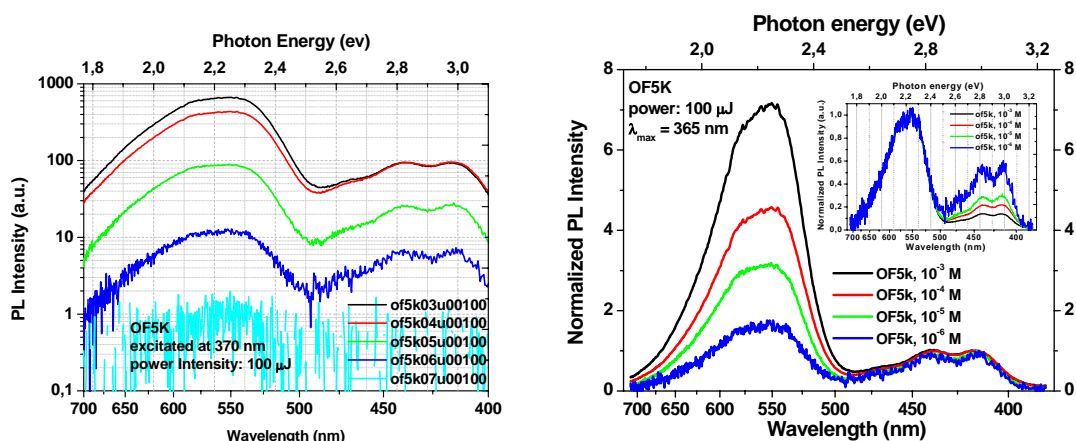
*Figure 7. 1. 12. The spectra of **OF5K** (left) and normalized fluorescence spectra (right) in m-THF solutions with different concentrations at RT (excited at 365 nm). The inserted figure shows the spectra normalized to 550 nm.*
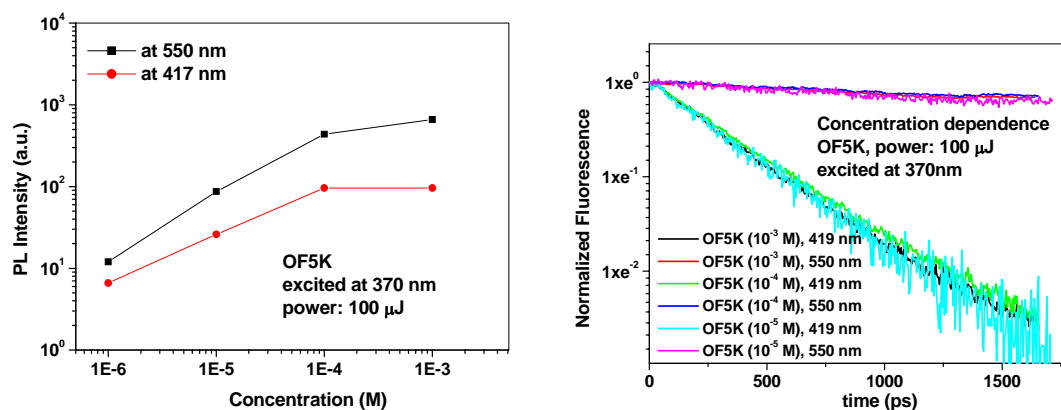

*Figure 7. 1. 13. The dependence of the PL intensity on concentration for **OF5K** (left) and the decay behaviour of **OF5K** at different concentrations probed at 419 nm and 550 nm (right). The excitation was at 365 nm.*

7. 1. 3. 1. 2 Long range delayed time-resolved fluorescence

The long range delayed fluorescence spectra (normalized) of **OF5K** in *m*-THF with different concentration (10^{-3} M to 10^{-6} M) at RT are shown in Figure 7. 1. 14.. The shape and position of the spectra did not show any change with concentrations except for that the fluorescence intensity increased with increasing concentration. Dependence of CW, prompt fluorescence and DF intensity on concentration at 540 nm was similar to that shown in Figure 7. 1. 13 (red line). The PL intensity reached saturation for concentrations around 10^{-4} to 10^{-3} M. The dependence of fluorescence intensity of **OF5K** (excited at 450 nm) upon time for t > 10 ns is shown in Figure 7. 1. 14 (b). Similar mono-exponential decay behaviour is observed and the lifetime decreases slightly with increasing of concentration, in agreement with the results based on the fast time-resolved fluorescence spectra shown in Figure 7. 1. 11 (right).

(a)   (b)

(b)
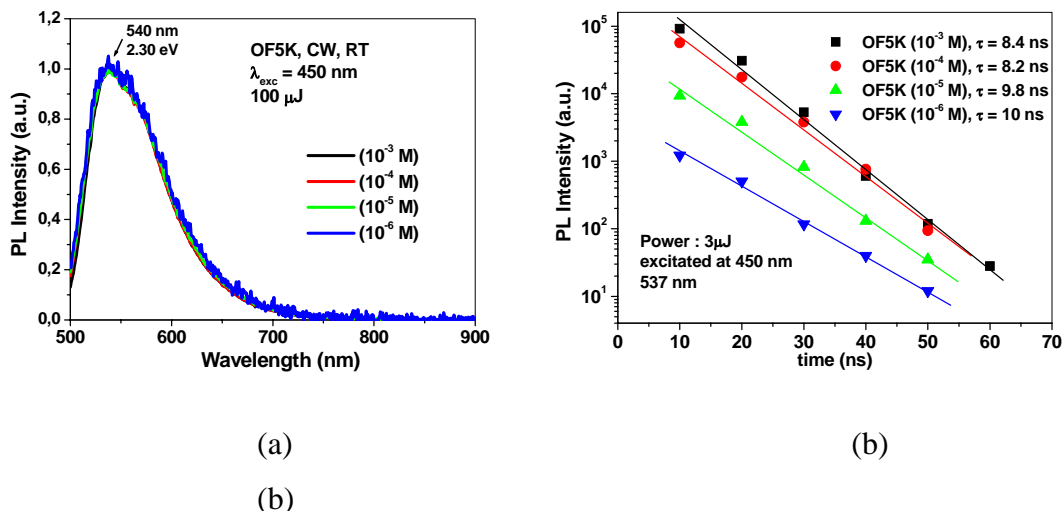
*Figure 7. 1. 14. a) The normalized fluorescence spectra of **OF5K** in m-THF with different concentrations at RT; b) Dependence of fluorescence intensity of OF5K upon time for t > 10 ns probed at 537 nm. Excitation was at 450 nm.*

The dependence of fluorescence intensity of **OF5K** upon time for t > 10 ns in *m*-THF with different concentrations at RT is also shown for the excitation wavelength of 365 nm (Figure 7. 1. 15). The fluorescence decays mono-exponentially over the time range studied

starting from 10 ns. The lifetime is about 7-8.5 ns for the different concentrations (10^{-3} M to 10^{-7} M), and decreases slightly with the decrease of the concentration.

The monoexponential decay behaviour of **OF5K** and **OF7** (shown in Chapter 5 . 5. 2) at different concentrations further supports that the green emission does not originate from aggregates or excimer formation. The obvious concentration dependence of the green emission band in solution suggests that increased interchain interactions among **OFnK** enhance the emission from the fluorenone defects. In addition, the **OF5K** and **OF7** can be regarded as the model compounds of PFs with keto defects situated on the chain and pristine PFs. So we rule out the possibility that in the oxidized or annealed PFs the green emission originates from ground state aggregates or excimer formation.

In solution, the oligomer and polymer chains can adopt different conformations and possess rotational freedom.[4] In dilute solutions (10^{-7}-10^{-6} M), one can envisage isolated chains with very limited collisions between them, and thus the energy migration would be one-dimensional by means of "loop" transfer or "non-nearest neighbour" transfer[4] to the keto defects, with very little contribution from interchain energy transfer. In more concentrated solutions (10^{-3} M), the number of chain collisions would increase and interchain energy transfer would contribute to the number density of excitons localized on fluorenone defect sites. Hence, we see a steady increase in the green emission at 535 nm with increasing concentration for all **OFnK**.

The observed long lifetimes of the green emission in the **OFnK** are similar to those previously reported for the 9-fluorenone molecules[5] and poly-(9,9-dihexylfluorene-co-fluorenone)s[6]. Based on the PL decay dynamics of **OFnK** in dilute solution, we thus concluded that the green emission in **OFnK** originates from the fluorenone units contained on individual chains. In addition, the fluorenone containing PFs exhibit a single mono-exponential decay of the green emission as films[6], implying the presence of only one type of emitting species, which would not be expected for typical excimer emission in thin films. These results are also consistent with the recent reports which claimed that one deals with a single-chain defect emission from the fluorenone moieties and not an aggregate or excimer emission[2,7].
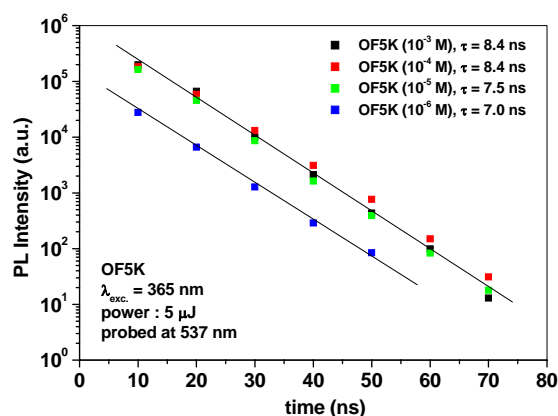
*Figure 7. 1. 15 Dependence of fluorescence intensity of **OF5K** upon time for t > 10 ns in m-THF at different concentrations at RT. The excitation was at 365 nm.*

7. 1. 3. 2 The dependence on laser excitation power

The delayed fluorescence spectra of **OF5K** (10^{-5} M, excited at 365 nm) at different laser excitation intensities (left) and the normalized spectra at 550 nm (right) are shown in Figure 7. 1. 16. The blue emission intensity increases slightly faster than that of the green emission upon increasing of the laser excitation intensity, i.e. the ratio of the green to blue emission band decreases. The decay behaviour of fluorescence is independent on the laser excitation intensity probed at both 419 nm and 552 nm (not shown).
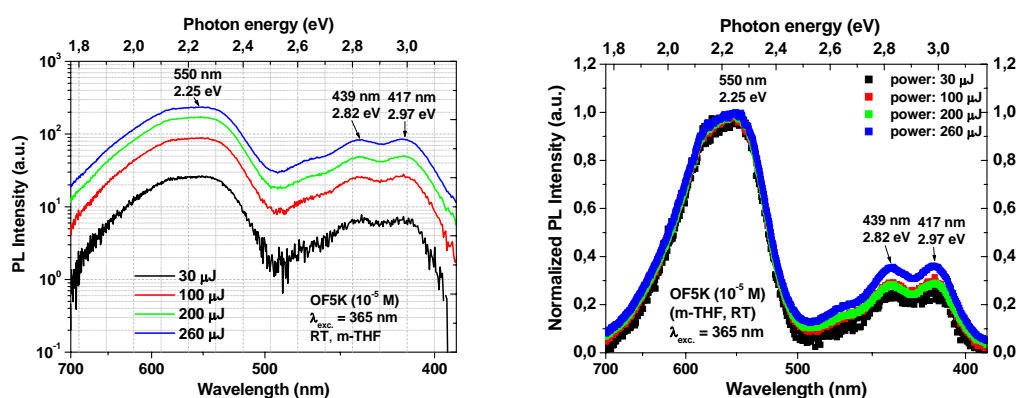
*Figure 7. 1. 16. The delayed fluorescence spectra of **OF5K** (10^{-3} M) at different laser excitation intensities (left) and the normalized spectra at 550 nm (right). Excitation was at 365 nm.*

The dependence of fluorescence intensity of **OF5K** in *m*-THF with different concentrations on laser excitation intensity probed at 417 nm (left) and 550 nm (right) at RT is shown in Figure 7. 1. 17 (excited at 365 nm and 450 nm by streak camera technique). In all of the cases, the fluorescence intensity varies approximately linear with laser excitation intensity. The dependence of laser excitation power was also investigated by gated detection technique. The CW fluorescence, DF, prompt fluorescence intensity also varies approximately linear with laser excitation intensity for the sample concentration from 10^{-7} M to 10^{-3} M both excited at 450nm and 365 nm (not shown).
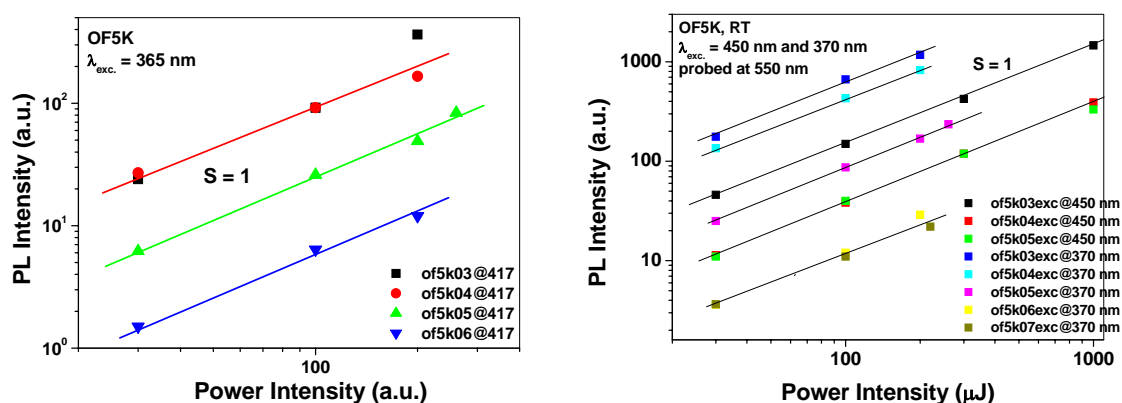
Figure 7. 1. 17. the dependence of fluorescence intensity of OF5K at 417 nm (left) and 550 nm (right) in m-THF on laser excitation intensity at RT. Excitation was at 365 nm and 450 nm.

7. 2 A comparison of the photophysical properties of OFn and OFnK

Table 7. 2. 1 presents a summary of the photophysical properties of **OF5** and **OF5K**. Here, we discuss both the steady-state spectra and time-resolved fluorescence spectra and try to draw conclusions on the origin of each emission.

*Table 7. 2. 1. Comparison of photophysical properties between **OF5** and **OF5K**.*

		OF5	OF5K
Absorption	shape and position	absorption peak (300-400 nm)	328 (shoulder) 365 (strongest) π-π* broad band (400-500 nm) n-π*
	λ_{max}(abs) (nm)	365 (π-π*)	365 (π-π*)
Emission	shape and position	structured blue band (400-500 nm)	weak blue (400-500 nm) strong broad green band (500-600 nm)
	λ_{max}(em) (nm)	409	591
	power dependence [a]	S = 1	S = 1
	decay behaviour	monoexponential	monoexponential
	Lifetime	549 ps	9 ns (green emission)
	phosphorescence	observed	not observed

[a]S = 1: Fluorescence intensity varies approximately linear with laser excitation intensity.

7. 2. 1 Comparison of the steady spectra of OFn and OFnK

Figure 7. 2. 1 (a-c) shows a comparison of normalized steady absorption and emission spectra of **OF3** and **OF3K**, **OF5** and **OF5K**, **OF7** and **OF7K** both in chloroform solution and in thin film. The absorption maximum (π-π*) of **OFnK** is very similar to the corresponding homo-oligofluorenes (**OFn**), but the emission maximum is significantly different. For example, the absorption maximum is seen at 3.40 eV (365 nm, $\pi \rightarrow \pi^*$ transition) for both **OF5** and **OF5K** in chloroform solution. A shoulder at 3.78 eV (328 nm) and a broad long-wave absorption band at 2.76 eV (450 nm, $n \rightarrow \pi^*$ transition) are also observed in the UV-vis absorption spectra of **OF5K**. For all **OFnK**, a yellow-green emission band at 2.07-2.34 eV (530-600 nm) is observed both in solution and for thin films. The absorption spectra of **OF5** and **OF5K** in form of films are almost identical with those in solution with only 1-2 nm shift.

The fluorescence spectra of **OF5** and **OF5K** are dramatically different. Upon increasing of wavelength three well-resolved blue emission bands with maximum at 3.04 eV (408 nm) are observed for **OF5** in dilute chloroform solution, which are correlated to the 0-0, 0-1, 0-2 transitions, whereas a broad green emission band with maximum at 2.10 eV (591 nm) accompanied with a weak blue band was observed for **OF5K** in dilute chloroform solution.

The emission spectra of **OF5** film are similar to those in solution with only a slight red-shift (8 nm), while for **OF5K**, the green emission band displays solvotachromism and is significantly red-shifted going from non-polar to polar solvents (see Chapter 6. 4. 3. 2). The emission spectra of **OF5K** film with emission maximum at 2.29 eV (541 nm) is blue-shifted around 0.19 eV (50 nm) compared to that in chloroform solution. As the magnitude of intermolecular interactions increases upon going from dilute solution to thin films, the green emission became dominant. As shown in Figure 7. 1. 12, Figure 7. 1. 14, and Figure 7. 2. 1, the green emission band is always accompanied by a weak blue emission band in solutions of **OFnK**, but in the thin film, only the green emission is observed (Figure 7. 1. 2a and Figure 7. 2. 1). In the solid state, interchain interactions are obvious. On the other hand, mainly intrachain energy transfer is predominant in dilute solutions. Such dominant green emission has been reported for fluorenone-containing polyfluorenes[2] and was explained as being due to strong intermolecular interactions in the thin films, but this should not be interpreted as evidence of excimer emission. The enhancement can be understood in terms of the more efficient excitation energy transfer from fluorene segments to the lower-energy fluorenone moieties in the solid state[6].

(a)

(b)

(c)
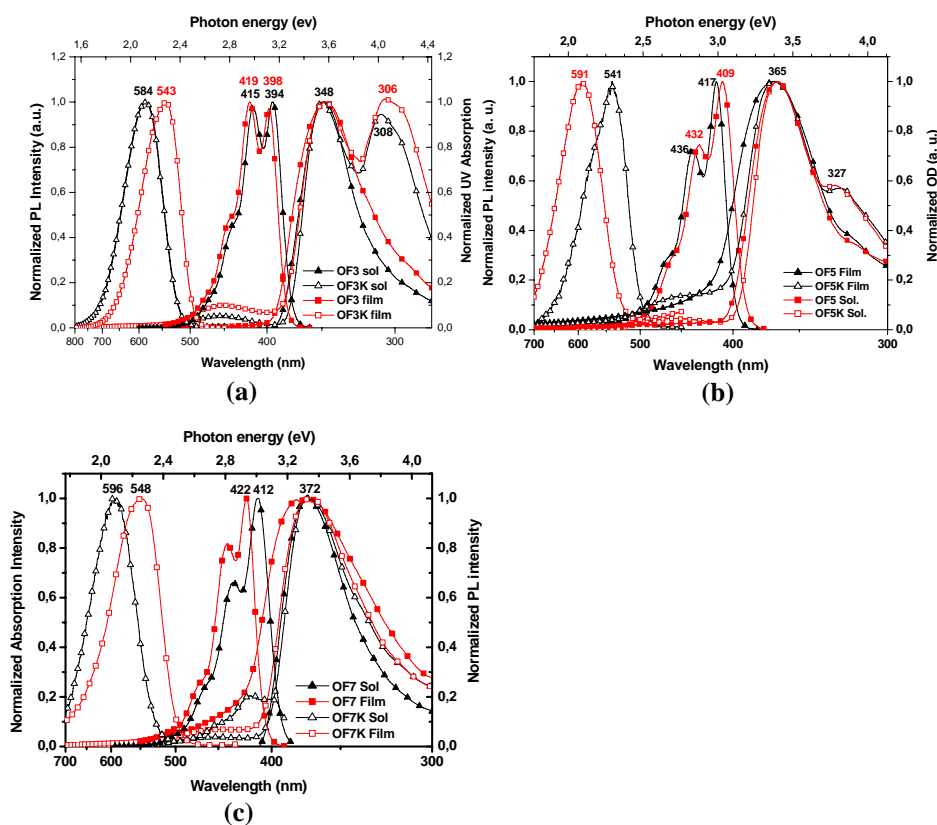
*Figure 7. 2. 1. The steady state UV-vis and fluorescence spectra of **OFn** and **OFnK** in solution (chloroform) and thin film: a) **OF3** and **OF3K**; b) **OF5** and **OF5K**; c) **OF7** and **OF7K**.*

The UV-vis absorption and fluorescence spectra of **OF5** and **OF5K** were measured at fixed concentration in chloroform as shown in Figure 7. 2. 2. The fluorene unit concentration of **OF5** and **OF5K** for UV-vis absorption spectra was 1×10^{-5}M and 1×10^{-6} M for the fluorescence spectra. The absorption intensity of the two solutions are similar, but the PL intensity of **OF5K** is approximately twice lower than that of **OF5** solution. This can be explained by the polarity of the solvent. In fact, a very strong yellow-green emission can be observed in nonpolar solvents such as *m*-cyclohexane.
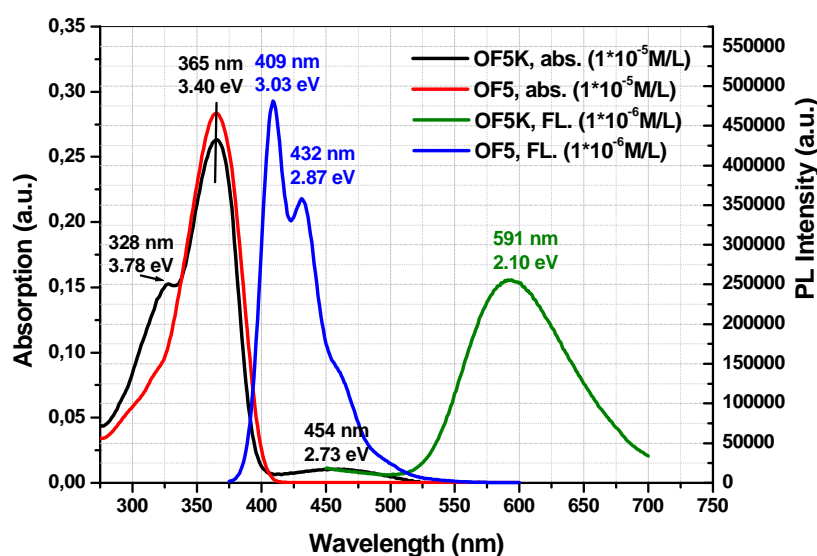
*Figure 7. 2. 2. UV-vis absorption spectra and fluorescence spectra of **OF5** and **OF5K** were measured at a fixed concentration in chloroform at RT. The UV-vis absorption spectra of **OF5** and **OF5K** were recorded at 1×10^{-5}M of fluorene units, and the fluorescence spectra were recorded at 1×10^{-6} M of fluorene units.*

7. 2. 2. Comparison of the time resolved fluorescence spectra of OFn and OFnK

The combined time-resolved fluorescence spectra of **OF5K** and **OF5** in *m*-THF at RT are shown in Figure 7. 2. 3 (left, excited at 365 nm). Only a blue emission band with

maximum at 417 nm is observed for **OF5**, which is identical with the blue emission band of **OF5K**. The dependence of the PL intensity of **OF5** and **OF5K** at 417 nm on time is also shown in Figure 7. 2. 3 (right). A very similar monoexponential decay behaviour is observed, suggesting that the blue emission bands originate from the same species, i.e. the fluorene units in both compounds. The lifetime of the blue emission of **OF5K** is slightly longer than that of **OF5**, and this could arise from the different environments of fluorene units in **OF5K** and **OF5**.
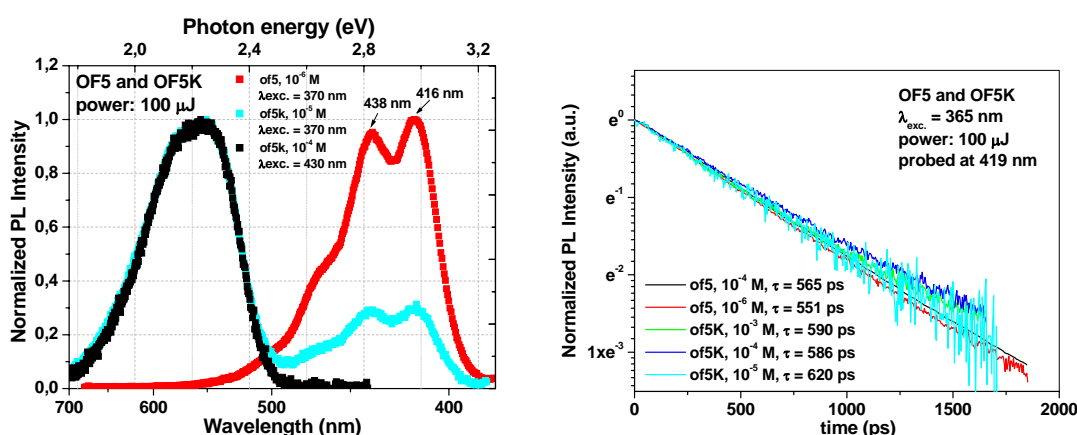
*Figure 7. 2. 3. The combined fluorescence spectra of **OF5K** and **OF5** in m-THF at RT (left) and the dependence of PL intensity of the **OF5K** and **OF5** on time at 417 nm (right). Excitation was at 365 nm.*

The green emission bands of **OF5K** are identical when excited either at 365 nm or 450 nm. The lifetime of the green emission band is approximately 8 ns, that is much longer than that of the blue emission of **OF5** (Table 7. 2. 1).

The CW fluorescence, DF, and prompt fluorescence intensity of **OF5** and **OF5K** varies approximately linear with the laser excitation intensity in dilute frozen *m*-THF matrix at 77K (Table 7. 2. 1), suggesting that possible subsequent bimolecular reactions of the excited species such as singlet-singlet annihilation or triplet-triplet annihilation do not take place.

The combined UV-vis absorption, CW fluorescence, DF or phosphorescence spectra of **OF5** and **OF5K** are shown in Figure 7. 2. 4. Interestingly, a structured phosphorescence (green line) band with identical vibronic splitting as the fluorescence band is observed for

OF5 in frozen *m*-THF matrix at 77K. Such phosphorescence was not observed for **OF5K**. In the delayed fluorescence of OF5K in frozen m-THF matrix at 77K (delay: 20 ns), the

*Figure 7. 2. 4 The combined UV-vis absorption, CW fluorescence, DF or phosphorescence spectra of **OF5** and **OF5K**. The UV-vis absorption spectra were recorded at 10^{-5} M in chloroform, and the CW fluorescence, DF and phosphorescence were recorded at 10^{-6} M in m-THF.*

blue emission band is very weak and its position and shape is the same as that in the CW fluorescence. The shape and position of the phosphorescence band of **OF5** is similar to that of the fluorescence of **OF5K** at 77K with the same vibronic splitting of about 160 meV. This will be explained by an energy diagram in the subsequent part (Chapter 7. 2. 3). The

lifetime of the green emission of **OF5K** is around 8 ns, but the lifetime of the related phosphorescence of **OF5** is as long as 3ms, indicating that these two similar emission bands do originate from different mechanisms. Similar phenomena are also observed for **OF3K** and **OF3** (Figure 7. 2. 5).
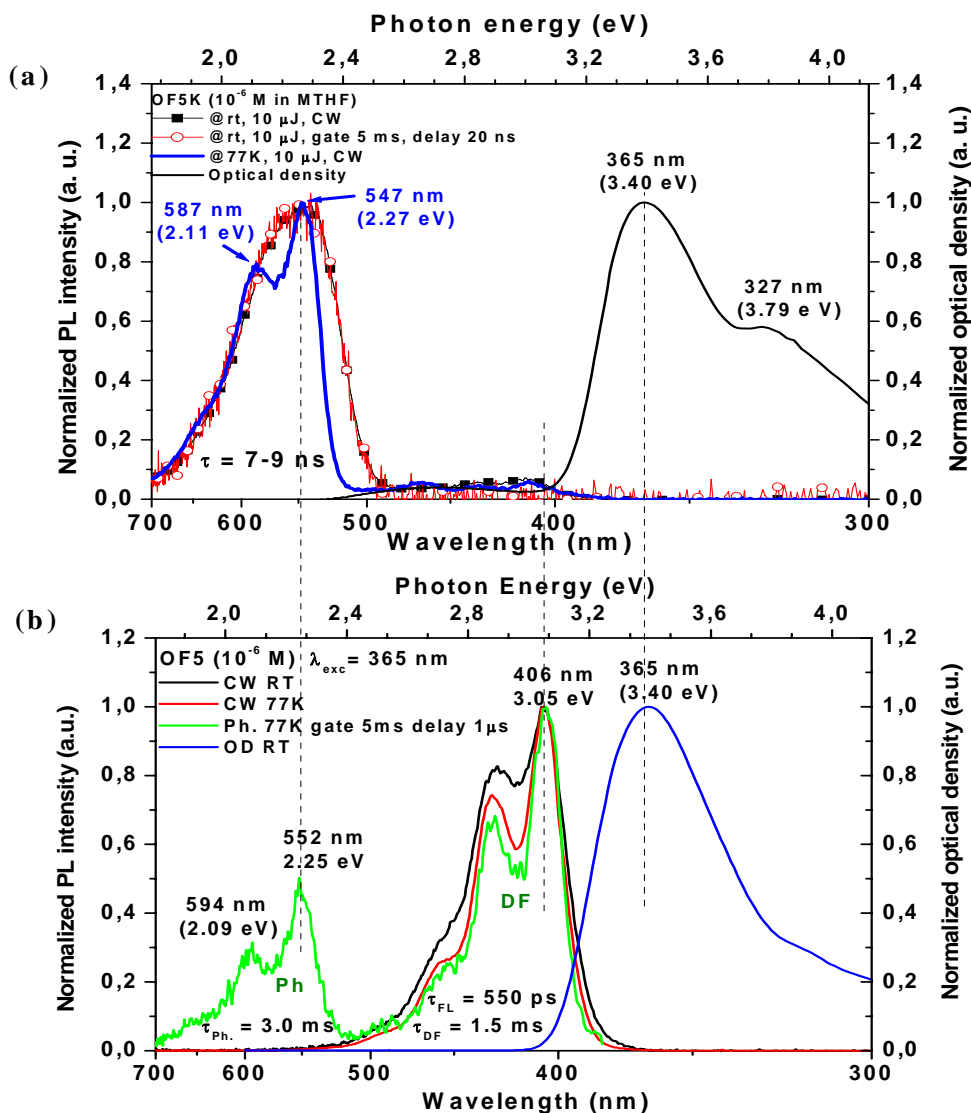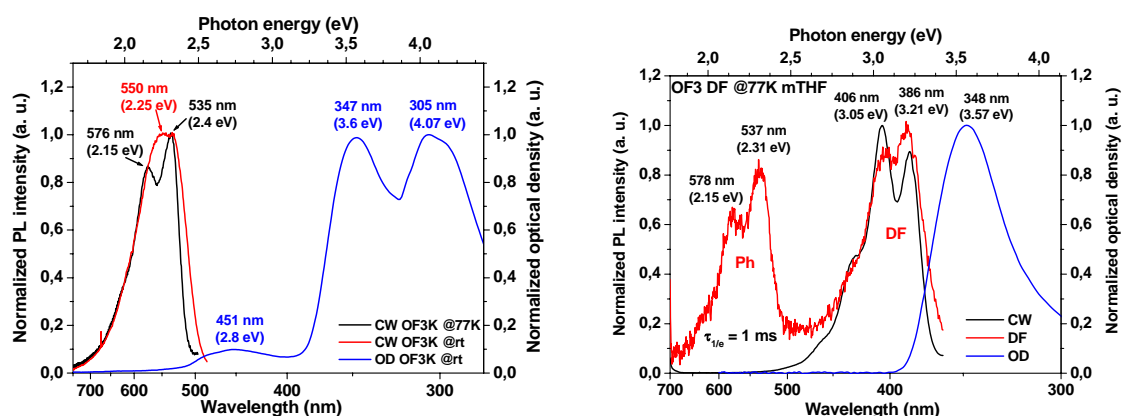

Figure 7. 2. 5 The combined UV-vis absorption, CW fluorescence, DF or phosphorescence spectra of **OF3K** *(left) and* **OF3** *(right). The UV-vis absorption spectra were recorded at 10^{-5} M in chloroform, and the CW fluorescence, DF and phosphorescence were recorded at 10^{-6} M in m-THF.*

7. 2. 3 Discussion

In this part, we combine our experimental results with quantum-chemical calculations[8] reported by Egbert Zojer and coworkers to gain a better understanding of the photophysical properties of oligofluorenes and oligofluorenes containing keton defects. It has also been shown that the emissive properties of fluorenone are strongly influenced by chemical substitution.[9] Therefore, we will discuss the influence of the length of the oligofluorene chain in **OFnK**. Special emphasis was devoted to excited-state localization effects induced by fluorenone units and their influence on the photophysical properties of fluorene-based materials. Some questions raised by the above experiments will be discussed. For example, why are similar absorption maxima observed for **OFn** and **OFnK**, while a strong blue emission is observed for **OFn** and a green emission for **OFnK**; why the long-wave absorption band (450 nm) of **OFnK** is so weak; why the emission maximum of **OF5K** at 77K is almost same as the phosphorescence of **OF5** at 77K. Comparing with the reports on

the green emission of polyfluorenes in the literature, our results will give a powerful support to the conclusion that the green emission in polyfluorenes originates from the keto defects especially when the samples have been subject to photo- or electro- oxidation.

7. 2. 3. 1 An energy level analysis

The calculated transition energies and oscillator strengths reported by Egbert Zojer etc[8]. for the most relevant excited states of the two model molecules **OF5** and **OF5K** in their ground-state equilibrium geometry are listed in Table 7. 2. 2. In the **OF5**, the lowest lying singlet excited state S_1 is strongly optically allowed and is dominated by a configuration in which an electron is excited from the highest occupied molecular orbital (HOMO) to the lowest unoccupied molecular orbital (LUMO) (see Figure 7. 2. 6). The energetic position of that excited state, 3.6 eV, is about 0.2 eV higher than the experimental value of the absorption maximum; this discrepancy is in part due to the relatively small size of the studied model system and the reciprocal dependence of the energy gap on the number of repeat units usually observed in organic systems[10].

*Table 7. 2. 2. Calculated singlet transition energies and oscillator strengths for the molecules of **OF5** and **OF5K** in their ground-state conformations.*

State		E (eV)	Osc.str
OF5			
$S_{1,OF5}$	π-π*	3.58	4.27
OF5K			
$S_{1,OF5K}$	n-π*	2.77	0.00
$S_{2,OF5K}$	CT π-π*	3.05	0.42
$S_{3,OF5K}$	π-π*	3.68	3.82

For **OF5K**, S_0-S_1 corresponds to an optically forbidden transition and possesses a n→π* character (as will become evident from the discussion of the nature of the excited states in part 7. 2. 3. 2).

OF5K

OF5
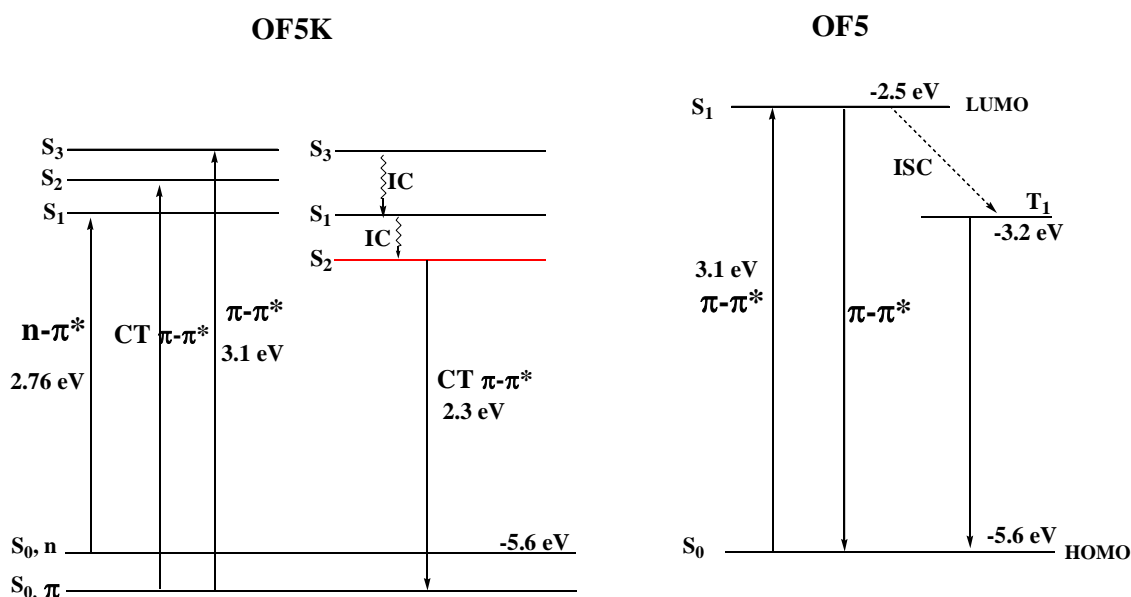
*Figure 7. 2. 6. Energy level diagram–using data from cyclic voltametry, spectroscopic and quantum-chemical techniques[8] reported by Egbert Zojer etal. S_3 in **OF5K** has the same energy as the lowest singlet excited state in the **OF5**.*

This means that the description of the lowest level excited state is dominated by determinants in which an electron has been excited from a σ-orbital localized on the C=O moiety of the molecule to the lowest unoccupied π* orbital. Such low-lying n-π* states are common in aromatic ketones. The next excited state (S_2) is also only weakly optically allowed in **OF5K**. As all these orbitals display a π-electronic character and an excitation to the S_2 state is associated with a significant charge redistribution in the fluorenone unit, S_2 can be classified as a π-π* charge transfer (CT) state. The first state with high oscillator strength in **OF5K** is the third singlet excited state S_3, and it is actually located at about the same energy as the lowest singlet excited state in the **OF5** (see Table 7. 2. 2).

The keto moiety does not destroy the conjugation along the oligo- or poly(fluorene) backbone, i.e., the most strongly optically allowed excited state in the low energy region is hardly affected by the presence of the keto group. This conclusion actually also holds for the similar absorption maximum of **OFn** and **OFnK**, in agreement with our experimental results.

In the low energy range of the absorption spectra, the absorption is very weak (Figure 7. 2. 1.) because the low lying states in fluorenone-containing chains (S_1 and S_2) possess very

low oscillator strength and they can hardly be observed in the absorption spectra of materials with low fluorenone concentration. This is also consistent with the lack of absorption in the low energy region observed in photodegradation experiments on polyfluorenes[6,8,11]. Consequently, the products of photo- and/or electro-oxidation will become accessible via absorption spectroscopy only in strongly degraded materials[7a,12].

7. 2. 3. 2. The nature of the excited states

We now discuss why an efficient green emission can be obtained from **OFnK**. For the compound **OF5K**, lattice relaxation phenomena take place from the lowest lying excited state that have been also explored by Egbert Zojer etal[8]. They found that if one included geometric relaxation phenomena in the excited state, a reversal in the ordering of the lowest two excited states is predicted, with the first excited state becoming the CT π-π* excitation (see Figure 7. 2. 6). The energies and oscillator strengths calculated for the lowest excited states of **OF5K** in the relaxed S_1 conformation are summarized in Table 7. 2. 3. For **OF5K**, the vertical transition energy from the first relaxed singlet excited state to the ground state is *very close to the experimentally observed yellow-green emission* (2.1-2.4 eV), and the vertical transition energy is also close to the vertical transition energy (2.1-2.4 eV) from the triplet state to the ground state of **OF5**. *This is the reason why the yellow-green emission is observed for **OF5K**, and the emission has a similar spectral position as the phosphorescence emission of **OF5***. In addition, the small, but nonvanishing, calculated oscillator strength associated with the CT π-π* excited state is in agreement with the experimental observations: (i) the fluorenone defect *is emissive*; but (ii) the quantum efficiencies of fluorenone-containing materials will usually be very low. In fact, the quantum efficiency of **OF5K** drops significantly compared with **OF5**. Similarly the fluorescence of the photo-oxidized films is also significantly decreased compared to pristine polyfluorenes.[12a]

The LUMOs of **OF5K**, which are rather strongly confined to the fluorenone unit (with large electron densities on the C $=$ O bond), have no counterparts in keto-free oligofluorenes. Therefore, one can not find the equivalent to the CT π-π* state in "pristine" oligo- or poly(fluorene)s.

This simple analysis based on molecular orbitals (electron-hole two particle wave functions) implies that the two lowest lying excited states (S_1 (n-π*) and S_2 (CT π-π*)) in the fluorenone-containing materials should supply the dominant contributions on the fluorenone unit (or even on the C $=$ O part of the molecule)[8]. The CT π-π* excited state becomes strongly localized on the central fluorenone unit. This localization can be simply explained on the basis of the Coulomb interaction between the electron (confined in the localized LUMO orbital) and the hole. At the same time a nonvanishing electron–hole density is also distributed on the neighboring fluorene units. The probability of finding the electron and/or the hole on fluorene segments at larger-distance, however, decreases drastically. This indicates that at least the fluorene segments that are directly attached to the fluorenone unit affect to a certain extent the electronic structure of the S_2 state. The localization is even more pronounced for the $n–π^*$ state, where the electron–hole pair is confined to the oxygen and the neighboring carbon atom[8]. In contrast to that, for the S_3 (π–π*) state, the electron–hole two-particle wave function in **OF5K** is delocalized along the whole chain and is strongly reminiscent of the lowest excited state in the OF5 ($S_{1,(OF5)}$)[8].

Table 7. 2. 3. Singlet transition energies and osillator strengths for the compound OF5K in the relaxed geometry of the lowest lying excited state.[8]

State	OF5K	
	E (eV)	Osc.
CT π-π*	2.45	0.48
n-π*	2.65	0.00
π-π*	3.44	3.02

Quantum-chemical calculations for the fluorenone monomer **OF1K** were also performed by Egbert Zojer et al.[8]. The energies of the $n–π^*$ states are virtually identical in **OF1K** and **OF5K**. The shift between the CT $π–π^*$ states of **OF1K** and the longer model systems is relatively small (0.19 and 0.33 eV, respectively), whereas the energy difference between the $π–π^*$ states in **OF1K** and **OF5K** is quite large (around 1.4 eV). To study that in more detail, we have calculated the dependence of the excited state energies on the number of repeat units, both for **OF5** and **OF5K** from Table 3. 2. 2, Table 5. 6. 1 and Table 6. 4. 2. The results are summarized in Fig. 7. 2. 7. **OF5** displays a linear dependence of the S_1 energy on

the inverse number of repeat units, as is common for the delocalized $\pi–\pi^*$ excited states in conjugated organic materials[13]. The S_3 (S_5 for $n = 1$) states in the fluorenone-containing materials show a similar trend. In contrast, the energy of the S_1 state ($n–\pi^*$) in all fluorenone-containing materials is chain-length independent[8]. As we described above, the absorption maximum wavelength (π-π^*) S_3 (S_5 $n = 1$) is red-shifted with the molecular length of **OFnK**, while the long-wave absorption maximum (S_1, $n–\pi^*$) is almost constant from **OF3K** to **OF7K** (Figure 7. 2. 8). This is in agreement with the quantum chemical calculations. For compounds **OFnK**, the calculated energy of the S_2 (CT π-π^*) state decreases by 0.32 eV when going from **OF1K** to the **OF3K** and then remains constant upon further increasing the chain length[8]. This is further confirmed by our experimental results (Figure 7. 2. 8).

   As shown in Figure 7. 2. 8 (C), when the fluorescence spectra are normalized for the green emission maximum, the blue emission intensity increases with increasing chain length. This is due to the increasing fraction of fluorene units in the higher oligomers. In addition, the blue emission band is also red-shifted with the molecular length due to the delocalized π-π^* state.
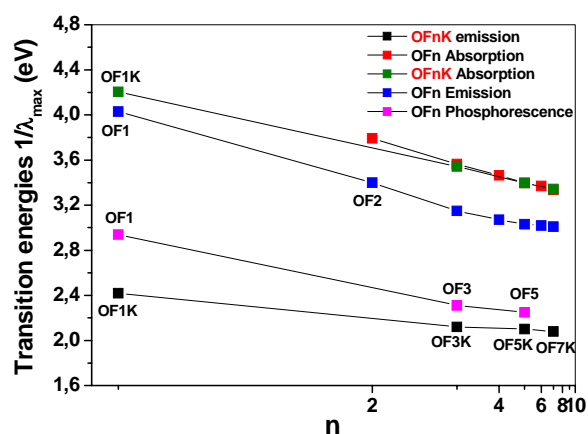
*Figure 7. 2. 7. The dependence of transition energies on number of fluorene units (reciprocal scale) for **OFn** and **OFnK** (for **OFnK**; the n is the number of fluorene+fluorenone units. All the data used here were selected from Table 3. 2. 2, Table 5. 6. 1 and Table 6. 4. 2. The data of absorption and emission of **OF5** and **OF5K** were*

*recorded from chloroform, and the data of phosphorescence of **OF5** were recorded from a frozen m-THF matrix at 77K.*
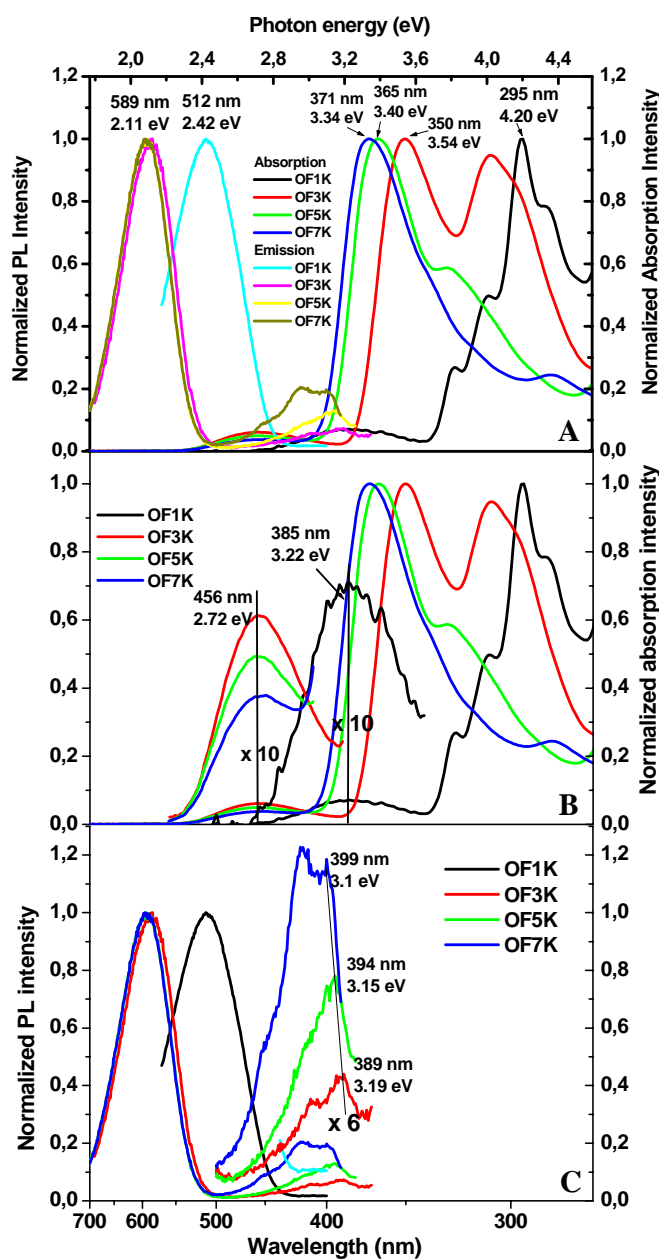
*Figure 7. 2. 8. A) The normalized UV-vis absorption and emission spectra of **OF1K**, **OF3K**, **OF5K** and **OF7K** in dilute chloroform solution (10^{-5} M fluorene units for the absorption spectra, and 10^{-6} M fluorene units for emission spectra); B) the UV-vis absorption spectra of **OFnK** with the magnified long-wave absorption band; C) the emission spectra of **OFnK** with the magnified weak blue emission band.*

A series of studies of fluorenone-containing oligofluorenes proposed efficient Förster energy transfer to the fluorenone defects and strong exciton confinement on the fluorenone moieties, because of their lower-lying energy levels, compared to fluorene segments.[3] Efficient funneling of the excitation energy from the high lying energy levels of the fluorene segments to the low lying energy level of the fluorenone defects results from energy migration by hopping of excitations along a single polymer chain until they are trapped on the fluorenone defects on that chain or transferred onto neighboring chains by Förster-type interchain energy transfer process (will be discussed in Chapter 7. 3).

7.3 Energy transfer in PFs/OFnK blend system

7. 3. 1 Introduction

The low energy emission bands in PF-type polymers were identified as the emission from a keto defect based on our own experimental results and literature[1b,7,14]. It was shown that by incorporating keto defects into the polymer backbone the emissive characteristics of oxidatively degraded polyfluorenes, especially the appearance of the 530 nm band (ca. 2.3 eV) could be faithfully reproduced. From the discussions in the last part (Chapter 7. 2), we know that efficient funneling of excitation energy takes place from the high energy (fluorene segments) to low energy sites (fluorenone units) by hopping along a single polymer chain until they are trapped on the fluorenone defects on that chain and then give a main yellow-green emission. In addition, the green emission may also arise from Förster-type interchain excitation energy transfer from fluorene segments of one chain to fluorenone units in neighboring chains. If only a small fraction of PFs samples is oxidized to have keto defects, what will change in their photophysical properties? Can energy transfer take place from the defect-free PFs molecules to keto-defect containing molecules? In this part, energy transfer was investigated using a model system consisting of polyfluorenes doped by the **OFnK** molecules.

The CW PL spectroscopy of the spin-coated films of **OF5**, **OF5K**, and a **PF2/6**:**OF5K**-blend system (10 wt. %) are shown in Figure 7. 3. 1. Only a blue emission band for **OF5** film and a green emission for **OF5K** in the films are observed. For the **PF2/6** and **OF5K**

blend system, the blue emission band is slightly red-shifted and the green emission band is blue-shifted, comparing with **OF5** and **OF5K**, respectively.
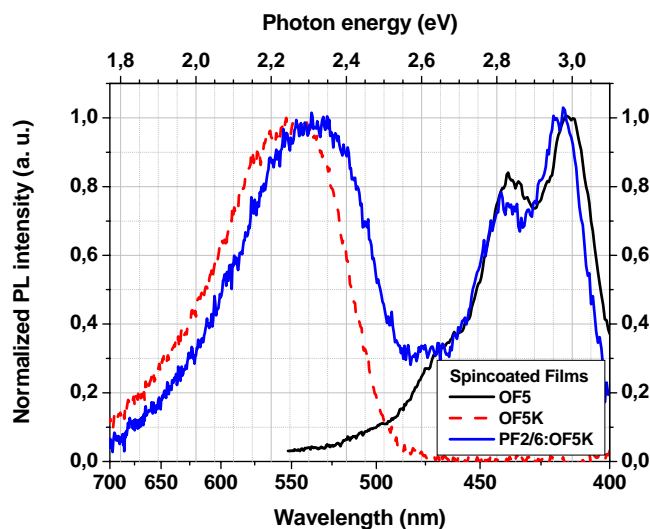

*Figure 7. 3. 1. The CW fluorescence spectra of the spin-coated films of **OF5**, **OF5K**, and a **PF2/6**:**OF5K** blend system (the film thickness is about 50 nm).*

7.3.2 Photophysical properties of the blend system

The UV-vis absorption (left) and steady state fluorescence spectra (right, excited at 383 nm) of **PF2/6** doped with different concentrations of **OF3K** at RT are shown in Figure 7. 3. 2. All of the absorption spectra of the blends doped with 0.1, 0.3, 1, 3, 10 wt. % **OF3K** are almost the same as that of pure **PF2/6**. Comparing with the absorption spectra of **OF3K** as film (Figure 6. 4. 4), the keto band ($n \rightarrow \pi^*$) with a broad long-wave absorption band and a shoulder was not resolved in the blend system. This is, however, not suprising as the amount of keto defects is relatively low in our doping experiments which makes them undetectable in the optical absorption measurement. This phenomena is similar to that of poly(fluorene-co-fluorenone)s with different fluorenone content in toluene solution[2].

In all of the emission spectra (Figure 7. 3. 2b), the typical spectral features of polyfluorenes are observed, namely a maximum at 2.94 eV (422 nm) with a vibronic shoulder at 2.80 eV (443 nm). Upon increasing of the **OF3K** doping concentration from 0.3 % - 10 %, an additional green emission band with maximum at 2.35 eV (527 nm) similar to

that of OF3K thin film (Figure 6. 4. 4) is observed. All of the emission spectra were normalized at 490 nm, and we found that the green emission intensity increases while the blue emission intensity decreases with the **OF3K** doping concentration. Similar phenomena were also observed for the non-normalized emission spectra of **OF5K** and **PF2/6** blend
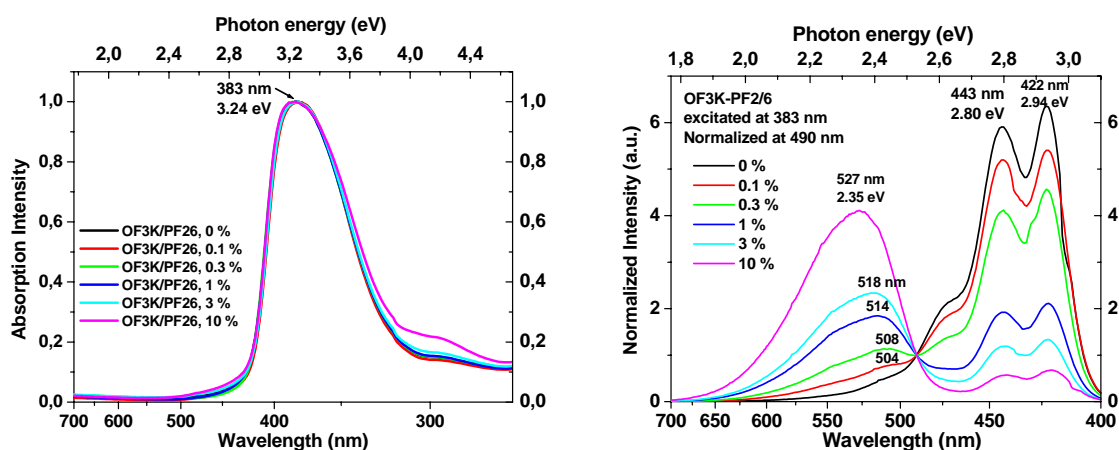
Figure 7. 3. 2. The UV-vis absorption (left) and steady state fluorescence spectra (right) of ***PF2/6*** *doped with different concentrations of **OF3K** at RT ($\lambda_{exc.}$ = 383 nm).*

system (Figure 7. 3. 3). The ratio of the green emission intensity at maximum to the blue emission intensity at maximum listed in Table 7. 3. 1. This ratio in **OF3K** & **PF2/6** blend system increases with the **OFnK** doping concentration with the values being 0.1, 0.3, 0.9, 1.7 and 6.2 for 0.1, 0.3, 1, 3, 10 wt. % doping concentration, respectively. This implies that the emission is related to the fluorenone moieties.[15] Although the concentrations of **OFnK** are low, energy transfer can be expected from the photoexcited polyfluorenes or fluorene species of **OFnK** to segments containing the fluorenone sites emitting at 2.35 eV in a solid-state sample where efficient three-dimensional excited-state migration is highly probable.
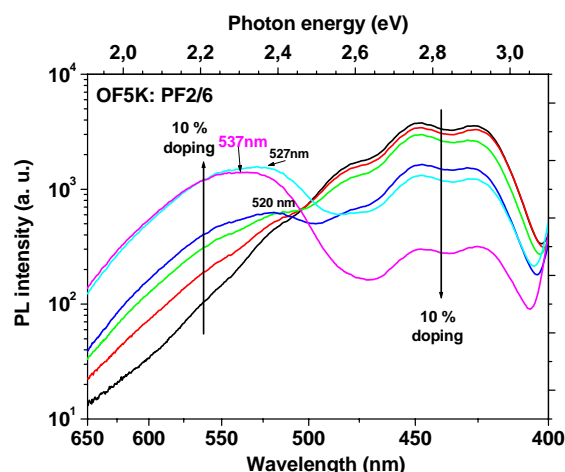
*Figure 7. 3. 3. The fluorescence spectra (left) of **PF2/6** doped with different concentrations of **OF5K** at RT ($\lambda_{exc.}$ = 383 nm).*

*Table 7. 3. 1. A compilation of the ratio of green to blue emission intensity, and the lifetimes of blue emission from **OF3K** & **PF2/6** and **OF5K** & **PF2/6** blend systems with different doping concentrations.*

Doping[a]	ratio[b]			τ_{blue} (ps)[c]		
Conc.	**OF3K**-RT	**OF5K**-RT	**OF5K**-77K	**OF3K**-RT	**OF5K**-RT	**OF5K**-77K
0 %				273	274	395
0.1 %	0.1	weak	weak	255	257	376
0.3 %	0.3	0.2	weak	186	201	254
1 %	0.9	0.4	0.15	84	112	237
3 %	1.7	1.2	0.5	52	63	117
10 %	6.2	4.4	1.8	33	36	58

[a] *Doping concentration (wt. %), representing the weight content of **OFnK** in the blend systems;* [b] *The values listed are the ratios of green emission maximum intensity / blue emission maximum intensity.* [c] *the values listed are lifetimes of the blue emission.*

    The dependence of the ratio of green to blue fluorescence intensity on the doping concentration for **OF3K & PF2/6** and **OF5K & PF2/6** blend systems is shown in Figure 7. 3. 4. This ratio increase slightly faster for **OF5K** as dopant as for **OF3K**, and the blue emission intensity at 448 nm decreases faster for **OF5K** than for **OF3K** as dopant (inserted figure), suggesting that the **OF5K** is slightly more effective than **OF3K** in the blend

system. In addition, the ratio of the green to blue emission intensity for **OF5K** as dopant increases faster at RT than at 77K, indicating that the energy transfer is more effective at RT.
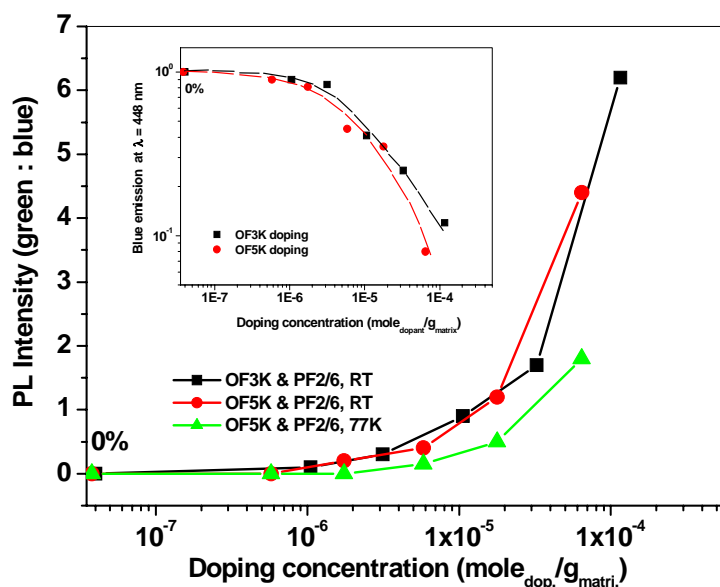
Figure 7. 3. 4. The dependence of the ratio of green to blue fluorescence intensity on the doping concentration (excited at 383 nm and the unit of doping in concentration is mol_{dop}/g_{matrix}).

The green emission band is red-shifted with the **OF3K** doping concentration from 508 nm (0.3 % doping concentration) to 527 nm (10 % dopping concentration, Figure 7. 3. 2). Similar phenomena are also observed for the **OF5K & PF2/6** blend (Figure 7. 3. 3). A possible explanation is: at low doping concentration, the fluorenone moieties give rise to a weak emission peaking at about 500 nm (2.48 eV). With the increase of dopant, more fluorenone groups are added to the system. The energy of the CT π-π* state is lower when the fluorenone units are contained within the macromolecule as discussed in the last section. Consequently, an increasing fraction of the fluorenone units in the blend system leads to a shift of the greenish emission to longer wavelengths.

Similar phenomena have been noted in the photodegradation process of the system of poly(9,9-di-n-hexyl-fluorene) end-capped with fluorene units. In the PL spectra, the weak greenish part of the emission spectrum that peaks at around 490 nm (2.53 eV) became noticeable and shifted to longer-wavelengths after photodegradation in air[11]. This scenario

is also consistent with the results of an investigation on the thermal treatment of different types of polyfluorenes.[16] In poly(9,9-di-*n*-hexyl-fluorene)s end-capped with unsubstituted fluorenes, the maximum of the greenish emission was originally found at about 490 nm and gradually shifted to longer wavelengths with longer annealing times (annealing at 200°C). The tertiary hydrogen atoms at the 9 and 9' positions of the terminal fluorene units are chemically significantly less stable than the sites where the di-*n*-hexyl side chains are attached to the other fluorene units in the polymer. As a first step (possibly already prior to the intentional photo-oxidation), the chemically less stable end groups are oxidized and give rise to the weak emission peaking at about 490 nm (2.53 eV). During the UV irradiation in air, an increasing fraction of the "inner" 9,9-di-n-hexyl-fluorene units is converted into fluorenone defects, as proved by the high intensity of the IR band associated with the C=O stretching vibration measured for the photooxidized sample[11]. According to the results from Zojer [8], the energy of the CT π-π* state is lower when the fluorenone units are contained within the chain. Consequently, an increasing fraction of fluorenone units within the polymer chains is expected to lead to a shift of the greenish emission to longer wavelengths, as observed experimentally.

The red-shift results from the fluorenone group concentration in the system, but not from excimer formation in variation with the number of interaction PF chains. As shown in the literature and by our experiments, with the increase of **OFnK** doping concentration in **PFs** or the content of fluorenone in PFs backbone, the green emission band is red-shifted from 490 nm to 520 nm, i.e. the intra- and intermolecular energy transfer becomes more efficient with increasing keto defect concentration.

The dependence of the fluorescence intensity upon laser excitation intensity at different doping concentrations at RT is shown in Figure 7. 3. 5 (excited at 383 nm). The fluorescence intensity varies approximately linear with the laser excitation intensity in all cases, i.e., the dependence of fluorescence intensity upon laser excitation intensity is independent of the doping content **OFnK** in the blends.
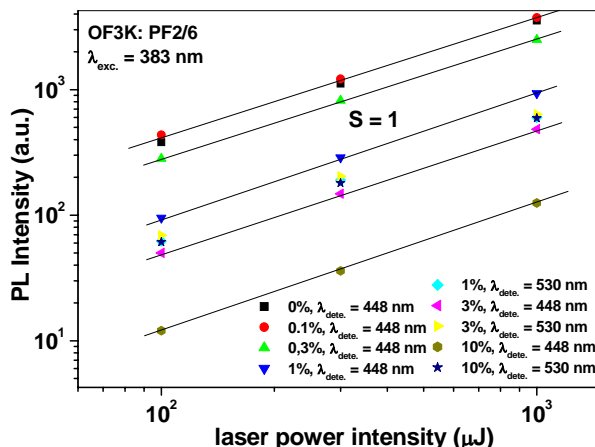
Figure 7. 3. 5. The dependence of the fluorescence intensity on the laser power intensity (excited at 383 nm at RT).

The decay of the fluorescence of **OF3K & PF2/6** (left) and **OF5K & PF2/6** (right) blends probed at 422 nm at different doping concentration at RT is shown in Figure 7. 3. 6. In all cases, a monoexponential decay is observed for the blue emission. The decay becomes faster upon increasing of the concentration of **OFnK**, i.e., the lifetime of the blue emission of the **OFnK & PF2/6** blends decreases with the doping concentration (see Table 7. 3. 1). For **OF5K & PF2/6** blends at RT, the lifetime decreases from 274 ps to 36 ps when the doping concentration increases from 0 to 10 wt. %, indicating a systematical increase of the quenching rate with increasing concentration of **OFnK**. The decay of the fluorescence of **OF5K & PF2/6** with different doping concentrations probed at 537 nm (green emission) is shown in Figure 7. 3. 7. The decay of the green emission band is slowed down, i.e., the lifetime increases with the **OFnK** concentration in the blend. In addition, the energy transfer process is thermally activated. The decay of the blue emission for **OF5K & PF2/6** (0 % and 10 % doping) at 77K is also shown in Figure 7. 3. 6 (right), and all data for different doping concentrations at 77K are listed in Table 7. 3. 1. The lifetime of the blue emission at 77K is higher than that at RT at the same doping concentration, indicating that the energy transfer from **PF2/6** to **OFnK** is easier at higher temperature.The operationally simplest way to quantify the doping effect on the fluorescence in **PF2/6** is to plot experimentally determined decay times as a function of concentration (Figure 7. 3. 8). The decrease of the lifetime with increasing of doping concentration is slightly faster for **OF5K**

than **OF3K** as dopant. This means that the energy transfer is more effective for **OF5**K &
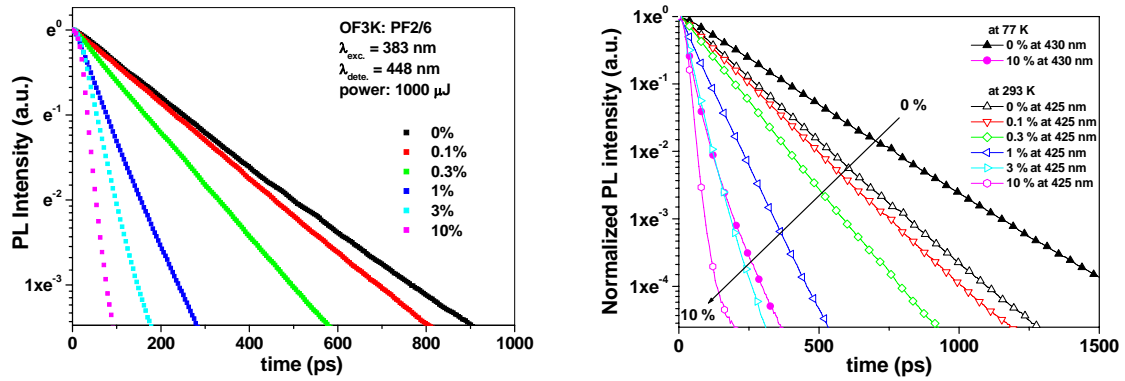PF2/6 blends.

*Figure 7. 3. 6. The decay of fluorescence of **OF3K & PF2/6** (left), **OF5K & PF2/6** (right)
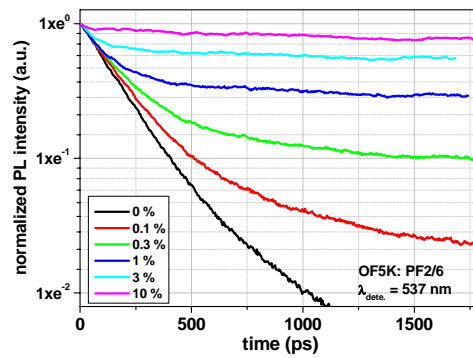blends probed at 422 nm.*

*Figure 7. 3. 7. The decay of fluorescence of **OF5K & PF2/6** at different doping
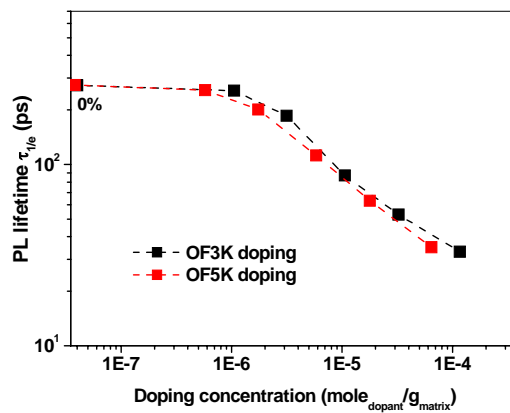concentrations probed at 537 nm (green emission).*

*Figure 7. 3. 8. The dependence of PL lifetime (1/e) on the **OFnK** concentration.*

7. 3. 3. Energy transfer mechanism

7. 3. 3. 1. A general introduction to the energy transfer

Energy transfer from an excited molecule (donor) to another that is chemically different (acceptor) according to $D^* + A \rightarrow D + A^*$ is called heterotransfer. This process is possible provided that the emission spectrum of the donor partially overlaps the absorption spectrum of the acceptor.

If the donor and acceptor are identical, we have homotransfer $D^* + D \rightarrow D + D^*$. When the process can repeat itself so that the excitation migrates over several molecules, it is called excitation transport or energy migration.

It is important to distinguish between radiative and non-radiative transfer. Radiative transfer corresponds to the absorption of a photon by a molecule A (or D) emitted by a molecule D and is observed when the average distance between D and A (or D) is larger than the wavelength. Such a transfer does not require any interaction between the partners, but it depends on the spectral overlap and on the concentration. In contrast, non-radiative transfer occurs without emission of photons at distances less than the wavelength and results from short- or long-range interactions between molecules. For instance, non-radiative transfer by dipole-dipole interaction is possible at distances up to 80-100Å.

Non-radiative energy transfer can result from different interaction mechanisms. The interactions may be Coulombic and/or due to intermolecular orbital overlap. The Coulomobic interactions consist of long-range dipole-dipole interactions (Förster's mechanism) and short-range multi-polar interactions. The interactions due to intermolecular orbital overlap include electron exchange (Dexter's mechanism) and charge resonance interactions.

For allowed transitions on D and A the Coulombic interaction is predominant, even at short distances. For forbidden transitions on D and A (e.g. in the case of transfer between triplet states ($3D^* + 1A \rightarrow 1D + 3A^*$), in which the transitions $T_1 \rightarrow S_0$ in D^* and $S_0 \rightarrow T_1$ in A are forbidden), the Coulombic interaction is negligible and the exchange mechanism is found, but is operative only at short distances (< 10 Å) because it requires overlap of the molecular orbitals. In contrast, the Coulombic mechanism can still be effective at large distances (up to 80-100 Å).

For **OFnK & PF2/6** blend system, the Förster transfer as a main energy transfer mechanism was investigated herein. Although the excitation transport (or energy migration)

can also be happen in **OFnK** itself from fluorene to fluorenone group (see Scheme 7. 1. 1), the main energy transfer discussed here is from **PF2/6** to **OFnK** in the blends. The molecules **OF3K** or **OF5K** can be regarded as an acceptor, and the **PF2/6** or a segment of **PF2/6** as a donor.

7. 3. 3. 2. Energy transfer mechanism in OFnK & PF2/6 blends

The absorption spectra of **OF3K**, **OF5K**, **OF7K** and the fluorescence spectra of **PF2/6** in film are shown in Figure 7. 3. 9. The spectral overlap in the range of 400-550 nm can be seen between the long-wavelength absorption band of **OFnK** and the fluorescence spectra of **PF2/6**. A simplified Jablonski-type diagram of **OF5K** and **PF2/6** illustrates the case in Figure 7. 3. 10. The radiative transfer is possible with the absorption by the molecule **OFnK** (acceprtor) of a photon emitted by the molecule **PF2/6** (donor).
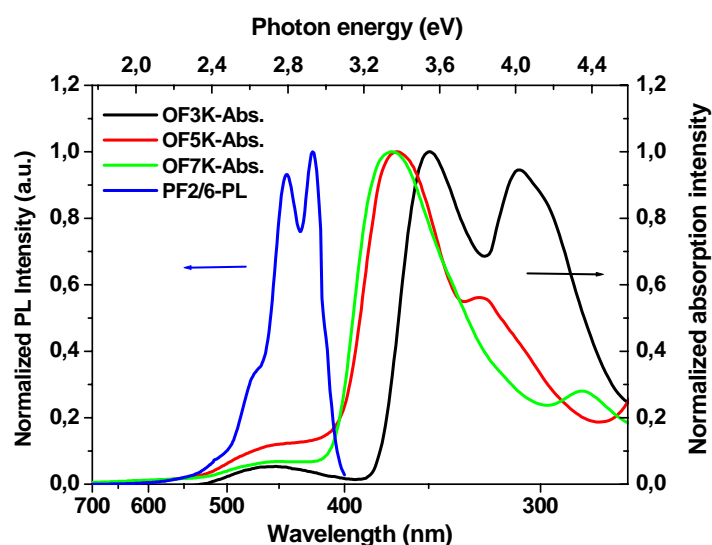

*Figure 7. 3. 9. The UV-vis absorption spectra of **OF3K**, **OF5K**, **OF7K** in film and the fluorescence spectra of **PF2/6** in film.*

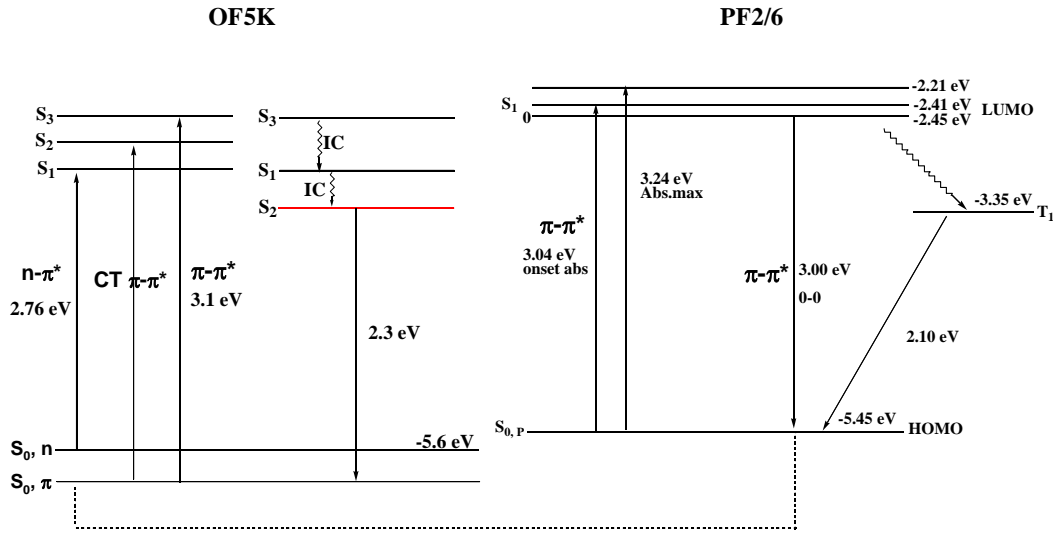**OF5K**   **PF2/6**

Figure 7. 3. 10. Simplified Jablonski-type diagram of OF5K and PF2/6 illustrating the overlap of spectra.

In a classical molecular crystal the rate limiting process for excitation quenching is the exciton migration within the host matrix. In a random medium like a conjugated polymer this is a dispersive process because the energy levels of the molecules/subunits of the polymer are distributed in energy. This gives rise to energetic relaxation of an exciton and, concomitantly, to a temporal decrease of the exciton mobility[17]. For Förster type energy transfer, dipole-dipole interactions control a single step transfer from an excited donor to an acceptor. In order to assess the importance of this mechanism one has to calculate the relevant rate constant $k_{D^* \to A}$ according to Förster theory[18]

$$k_{D^* \to A} = \frac{9000(\ln 10)\kappa^2 \phi_D^0}{128\pi^5 n^4 N_A \tau_D^0 R^6} \int_0^\infty F_D(\lambda)\varepsilon_A(\lambda)\lambda^4 d\lambda \qquad (7.3.1)$$

where τ_D^0 is the intrinsic lifetime of the donor, ϕ_D^0 is quantum yield of the donor fluorescence, n is the refractive index of medium, N_A is the Avogadro's number, κ is the molecular orientation factor ($\kappa^2 = 2/3$ for random orientation), λ is the wavelength, $F_D(\lambda)$ is the corrected fluorescence intensity of the donor with the total intensity normalized to unity, $\varepsilon_A(\lambda)$ is the extinction coefficient of the acceptor at λ, and R is the mutual distance between donor and acceptor molecules. Eq. (7. 3. 1) can be expressed more conveniently as

$$k_{D^* \to A} = \frac{1}{\tau_D^0}\left(\frac{R_0}{R}\right)^6, \qquad (7.3.2)$$

where R_0 is the critical distance at which excitation transfer and fluorescence decay of donor contribute equally and can be expressed as

$$R_0^6 = \frac{9000(\ln 10)\kappa^2\phi_D^0}{128\pi^5 n^4 N_A}\int_0^\infty F_D(\lambda)\varepsilon_A(\lambda)\lambda^4 d\lambda = \frac{9000(\ln 10)\kappa^2\phi_D^0}{128\pi^5 n^4 N_A}J \qquad (7.3.3)$$

where ϕ_D is the fluorescence quantum yield of the donor and J is the spectral overlap integral between donor fluorescence and acceptor absorption spectra.

If the wavelength is expressed in nanometers, then $J(\lambda)$ is in units of $M^{-1}cm^{-1}(nm)^4$ and Föster distance, in angstroms, is given by

$$R = 0.211\left[\kappa^2 n^{-4}Q_D J(\lambda)\right]^{1/6} \qquad (7.3.4)$$

Calculations based on the absorption spectrum of **OF3K** or **OF5K** in toluene assuming the fluorescence quantum yield of 0.73[1a] for **PF2/6** and a refractive index of 2[19] afforded a $R_0 = 25.6$ Å and 28.3 Å for **OF3K & PF2/6** and **OF5K & PF2/6**, respectively.

If the fluorescence decay of the donor following pulsed excitation is a single exponential, the measurement of the decay time in the presence (τ_D) and absence (τ_D^0) of transfer is a straightforward method of determining the transfer rate constant, the transfer efficiency and the donor-acceptor distance, by using the following relations:[3c]

$$\frac{1}{\tau_D} = \frac{1}{\tau_D^0} + k_T \quad \text{or} \quad k_T = \frac{1}{\tau_D} - \frac{1}{\tau_D^0} \qquad (7.3.4)$$

$$\Phi_T = 1 - \frac{\tau_D}{\tau_D^0} \qquad (7.3.5)$$

$$r = \frac{R_0}{(\tau_D^0/\tau_D - 1)^{1/6}} \qquad (7.3.6)$$

The transfer rate constant k_T and the transfer efficiency ϕ_T listed in Table 7.3.2 were calculated according to Eq. 7.3.4 , 7.3.5 , in which the lifetimes in the presence (τ_D) and absence (τ_D^0) of acceptor were taken from Table 7.3.1. In all of the cases, the transfer rate constant k_T and the transfer efficiency ϕ_T increases with increasing doping concentration (Figure 7.3.11). k_T and ϕ_T increase faster for **OF5K & PF2/6** blends at RT than at 77K, and the energy transfer is faster for **OF5K & PF2/6** than **OF3K & PF2/6** blends at RT. The energy transfer efficiency becomes almost saturated when the **OFnK** concentration increases up to 3% (wt. %).

The donor-acceptor distance of the two blend systems (**OF3K & PF2/6, OF5K & PF2/6**) decreases with the increasing doping concentration (Table 7.3.2), i.e., the donor

and acceptor are more close under higher doping concentration, and energy transfer is also more effective.

*Table 7. 3. 2. A list of the energy transfer rate constants, energy transfer efficiencies and donor-acceptor distances of **OF3K & PF2/6** and **OF5K & PF2/6** blends with different doping concentrations.*

Dopping[a] Conce. Wt. %	k_T [b] (ns^{-1})			ϕ_T [c]			r [d] (Å)	
	OF3K RT	OF5K RT	OF5K 77K	OF3K RT	OF5K RT	OF5K 77K	OF3K- RT	OF5K- RT
0 %	0	0	0	0	0	0	-	-
0.1 %	0.26	0.24	0.13	0.07	0.06	0.05	39.8	44.5
0.3 %	1.72	1.33	1.41	0.32	0.27	0.35	29.1	33.5
1 %	8.24	5.28	1.69	0.69	0.59	0.40	22.4	26.6
3 %	15.57	12.22	6.02	0.81	0.77	0.70	20.1	23.1
10 %	26.64	24.13	14.71	0.88	0.87	0.85	18.4	20.7

[a] *Dopping concentration, representing the weight content of **OFnK** in the blends;* [b] *the energy transfer rate constant (k_T).* [c] *energy transfer efficiency (ϕ_T).* [d] *the donor-acceptor distance (r).*
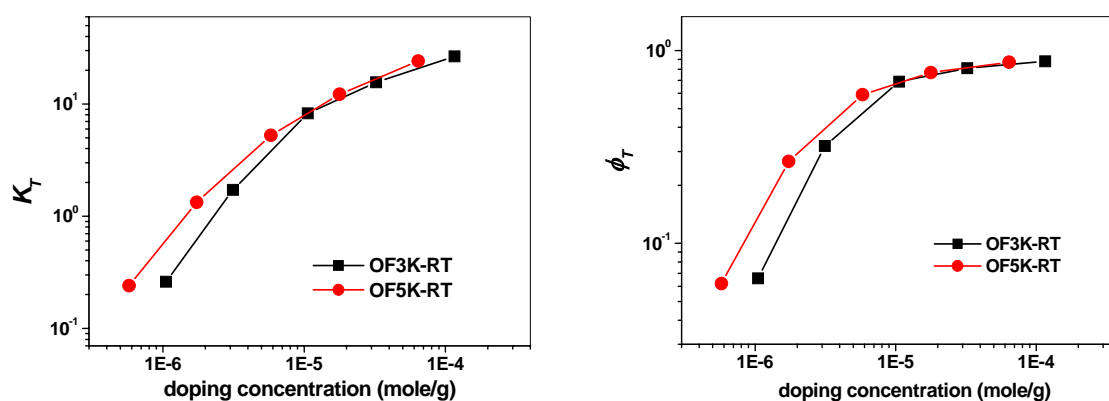

*Figure 7. 3. 11. The dependence of k_T and ϕ_T on the doping concentration for **OF3K & PF2/6** and **OF5K & PF2/6** blends.*

7.4. Summary

A series of oligofluorenes with one fluorenone group in the center of the chain (**OFnK**) were used as the model compounds to investigate the origin of the green emission of PFs. The photophysical properties of OFnK were studied in dilute solution and thin film. Only a broad green emission band with maximum emission approximately at 540 nm was detected both in TOL-MCH solution and film at RT for **OF5K**. The strong green emission was accompanied with a weak blue emission when excited at 370 nm. The strong green emission of **OFnK** suggested that rapid energy transfer from higher energy sites (fluorene segments) to lower energy sites (fluorenone unit) prior to the radiative decay of the excited species. At 77K, the green emission band with well-resolved structure appeared at approximately 550 nm with a vibronic splitting of about 160 meV. The fluorescence intensity varies approximately linearly with laser excitation intensity when excitation wavelength is 365 nm and 450 nm. Monoexponential decay behaviour was observed and the lifetime of the green band is about 8 ns for **OF3K** and **OF5K**, which is longer than that of blue emission from **OF5**. In addition, site-selective excitation and concentration dependence of the fluorescence spectra were also investigated. The ratio of green and blue emission intensity increases with the increase of the concentration. The observed strong concentration dependence of the green emission band in solution suggests that increased interchain interactions among the fluorenone-containing oligofluorene chains enhances the emission from the fluorenone defects at higher concentration. The mono-exponential decay behaviour and power dependence were not influenced significantly by the concentration. We have ruled out the possibility that the green emission band originates from aggregates or excimer formation.

By comparing of the photophysical properties of **OF5** and **OF5K** with experimental results and reported quantum-chemical calculations[8], some important conclusions were drawn:

The low lying states S_1 (n-π^*) and S_2 (CT π-π^*) in fluorenone-containing chains possess very low oscillator strength, so the absorption in the low energy range of OFnK (2.2-2.4 eV) is very weak. The first state with high osillator strength in OF5K is the third singlet excited state S_3. It is actually located at about the same energy as the lowest singlet excited

state in the OF5, so similar absorption maximum wavelength is observed for OFnK and OFn.

   i) The energy of the CT π-π* state is below that of the n-π* state due to excited-state geometry relaxation. The green emission arises from the radiative decay of the excited species from the first relaxed singlet excited state to the ground state. The LUMOs of **OF5K**, which are rather strongly confined to the fluorenone unit (with large electron densities on the C = O bridge), have no counterparts in keto-free oligo(fluorene)s. Therefore, one finds no equivalent to the CT π-π* state in "pristine" oligo- or poly(fluorene)s.

   ii) The wavelength of the absorption maximum is red-shifted with the chain-length increasing for both **OFnK** and **OFn**. This is a consequence that the π-π* excited state is delocalized in the whole molecules. The position of low-energy absorption and the green emission is independent of the chain-length of **OFnK** except for **OF1K**. This is explained for the reason that the n-π* state and CT π-π* are localized dominantly on the central fluorenone unit of **OFnK**.

   Energy transfer was investigated using a model system of a polyfluorene doped by **OFnK**. Förster-type energy transfer takes place from **PF2/6** to **OFnK**, and the energy transfer efficiency increases with increasing doping concentration of **OFnK**.

   A series of studies on the blends suggests an efficient Förster energy transfer to the fluorenone defects and strong exciton confinement on the fluorenone moieties, because of their lower-lying energy levels, compared to fluorene segments.[10] Efficient funneling of excitation energy from the high-energy fluorene segments to the low-energy fluorenone defects results from energy migration by hopping of excitations along a single polymer chain until they are trapped on the fluorenone defects on that chain or transferred onto neighbouring chains by Förster-type interchain energy transfer processes.

   These results imply that the red-shifted emission in polyfluorenes can originate from (usually undesirable) keto groups at the bridging carbon atoms-especially if the samples have been subject to photo- or electro-oxidation or if fluorenone units are present due to an improper purification of the monomers prior to polymerization.

7. 5 Experimental part

PF2/6 blended with 0.1, 0.3, 1, 3, 10 wt. % **OFnK** was spin coated onto quartz substrates from toluene solution (10 mg/ml) at 2000 rpm, resulting in homogenous films with thickness of 50 nm. **OF5K** was added as part of the total weight, for example, 1% doped polymer films were spin coated from a 0.495 wt.% **PF2/6** /0.005 wt.% OFnK solution in toluene. The film thickness was measured with a Tencor P-10 Surface Profiler. Experimental setup for the fast TRF (streak camera technique) and long range delayed fluorescence measurement (gate-detection technique) was alrealy described in Chapter 5. 7.

UV-vis spectra were recorded at room temperature with a Perkin-Elmer Lambda 9 UV/Vis/NIR spectrophotometer. Steady state photoluminescence spectra were obtained on a Spex Fluorolog II (212). Thin films of all materials were made by spin-coating of solution in chloroform onto quartz substrate except for the films of blend system. The thickness of all of film is approximately 50 nm.

7. 6 References and Notes

[1] Recent reviews on polyfluorenes: (a) Neher, D. *Macromol. Rapid Commun.* **2001**, *22*, 1365; (b) Scherf, U.; List, E. J. W. *Adv. Mater.* **2002**, *14*, 477.

[2] Romaner, L.; Pogantsch, A.; Scandiucci, de Freitas, P.; Scherf, U.; Gaal, M.; Zojer, E.; List, E. J. W. *Adv. Funct. Mater.* **2003**, *13*, 597.

[3] (a) Jenekhe, S. A.; Osaheni, J. A. *Science* **1994**, *265*, 765; (b) Osaheni, J. A.; Jenekhe, S. A.; *Macromolecules* **1994**, *27*, 739; (c) Valeur, B.; *Molecular Fluorescence: Principles and Application;* Wiley-VCH: Weinheim, Germany, **2002**; (d) Förster, T. *Angew. Chem. Int. Ed. Engl.* **1969**, *8*, 333.

[4] Guillet, J. Polymer Photophysics and photochemistry, Cambrige University Press: Cambridge, U. K., 1985.

[5] (a) Andrew, L. J.; Deroulede, A.; Linschitz, H. *J. Phys. Chem.* **1978**, *82*, 2304; (b) Biczók, L.; Bérces, T. *J. Phys. Chem.* **1988**, *92*, 3842; (c) Biczók, L.; Bérces, T.; Márta, F. *J. Phys. Chem.* **1993**, *97*, 8895; (d) Murphy, R. S.; Moorlay, C. P.; Green, W. H.; Bohne, C. *J. Photochem. Photobiol. A: Chem.* **1997**, *110*, 123. (e) Rani, S. A.; Sobhanadri, J.; Rao, T. A. P. *J. Photochem. Photobiol. A: Chem.* **1996**, *94*, 1-5. (f) Rani, S. A.; Sobhanadri, J.; Rao, T. A. P. *Spectrochim. Acta A* **1995**, *51*, 2473.

[6] Kulkarni, A. P.; Kong, X. Jenekhe, S. A. *J. Phys. Chem. B* **2004**, *108*, 8689.

[7] (a) List, E. J. W.; Guentner, R.; Scandiucci de Freitas, P.; Scherf, U. *Adv. Mater.* **2002**, *14*, 374; (b) Lupton, J. M.; Craig, M. R.; Meijer, E. W. *Appl. Phys. Lett.* **2002**, *80*, 4489.

[8] Zojer, E.; Pogantsch, A.; Hennebicq, E.; Beljonne, D.; Brédas, J.-L.; de Freitas, P. S.; Scherf, U.; List, E. J. W. *J. Chem. Phys.* **2002,** *117*, 6794-6802.

[9] Biczók, L.; Bérces, T.; Inoue, H.; *J. Phys. Chem.* **1999**, *103*, 3837.

[10] (a) Grimme, J.; Kreyenschmidt, M.; Uckert, F.; Müllen, K.; Scherf, U. *Adv. Mater.* **1995**, *7*, 292; (b) Chosrovian, H.; Rentsch, S.; Grebner, D.; Dahm, D. U.; Birckner, E. *Synth. Met.* **1993**, *60*, 23; (c) Janssen, R. A. J.; Smilowitz, L.; Sariciftci, N. S.; Moses, D. *J. Chem. Phys.* **1994**, *101*, 1787; (d) Janssen, R. A. J.; Moses, D.; Sariciftci, N. S. *J. Chem. Phys.* **1994**, *101*, 9519; (e) Horowitz, G.; Yassar, A.; von Bardeleben, H. J. *Synth. Met.* **1994**, *62*, 245.

[11] Bliznyuk, V. N.; Carter, S. A.; Scott, J. C.; Klärner, G.; Miller, R. D.; Miller, D. C. *Macromolecules* **1999**, *32*, 361.

[12] Gamerith, S.; Gadermaier, C.; Scherf, U.; List, E. J. W. *Phys. Stat. Sol. (a)* **2004**, *201*, 1132.

[13] Bredas, J. L.; Silbey, R.; Boudreaux, D. S.; Chance, R. R. *J. Am. Chem. Soc.* **1983**, *105*, 6555.

[14] (a) Sainova, D.; Neher, D.; Dobruchowska, E.; Luszczynska, B.; Glowacki, I.; Ulanski, J.; Nothofer, H.-G.; Scherf, U. *Chem. Phys. Lett.* **2003**, *15*, 371; (b) Gaal, M.; List, E. J. W.; Scherf, U. Macromolecules **2003**, *36*, 4236.

[15] In this context it is interesting to mention that the experimental emission spectrum of poly(fluorenone) peaks at 2.12 eV. [see: Uckert, F.; Tak, Y.-H.; Müllen, K.; Bässler, H. *Adv. Mater.* **2000**, *12*, 905.

[16] Lee, J.-I.; Klaerner, G.; Miller, R. D. *Chem. Mater.* **1999**, *11*, 1083.

[17] (a) Elschner, A.; Mahrt, R. F.; Pautmeier, L.; Bässler, H. Stolka, M.; McGrane, K. *Chem. Phys.* **1991**, *150*, 81; (b) Meskers, S. C. J.; Hübner, J.; Oestreich, M.; Bässler, H. *Chem. Phys. Lett.* **2001**, *339*, 223.

[18] (a) Förster, T. *Discuss. Faraday Soc.* **1957**, *27*, 7; (b) Lakowicz, J. R. *Principles of Fluorescence Spectroscopy*, Plenum Press, New York, **1999**.

[19] Geng, Y.; Trajkovska, A.; Culligan, S. W.; Ou, J. J.; Chen, H. M. P.; Katsis, D.; Chen, S. H. *J. Am. Chem. Soc.* **2003**, *125*, 14032.

8 Summary

Homo-oligofluorenes (**OFn**), polyfluorenes (**PF2/6**) and oligofluorenes with one fluorenenone group in the center (**OFnK**) were synthesized in this Ph.D. work. They were used as model compounds to understand of the structure-property relationships of polyfluorenes and the origin of the green emission in the photoluminescence (after photooxidation of the PFs) and the electroluminescence (EL) spectra. The electronic, electrochemical properties, thermal behavior, supramolecular self-assembly, and photophysical properties of **OFn**, **PF2/6** and **OFnK** were investigated.

Oligofluorenes with 2-ethylhexyl side chain (**OF2-OF7**) from the dimer up to the heptamer were prepared by a series of stepwise transition metal mediated Suzuki and Yamamoto reactions. Unsymmetrical monobromides of monomer, dimer and trimer of fluorenes are important intermediate compounds for higher oligomers. Polyfluorenes was synthesized by Yamamoto coupling of 2,7-dibromo-9,9-bis(2-ethylhexyl)fluorene. Oligofluorenes with one fluorenone group in center (**OF3K, OF5K, OF7K**) were prepared by Suzuki coupling between the monoboronic fluorenyl monomer, dimer, trimer and 2, 7-dibromofluorenone. Hundred of milligrams pure compounds were obtained.

The electrochemical and electronic properties of homo-oligofluorenes (**OFn**) were systematically studied by several combined techniques such as cyclic voltammetry, differential pulse voltammetry, UV-vis absorption spectroscopy, steady- and transition state fluorescence spectroscopy. It was found that the oligofluorenes behave like classical conjugated oligomers, i.e., with the increase of the chain-length, the corresponding oxidation potential, the absorption and emission maximum, ionization potential, electron affinity, band gap and the photoluminescence lifetime displayed a very good linear relation with the reciprocal number of the fluorene units (1/n). The extrapolation of these linear relations to infinite polymers predicted the electrochemical and electronic properties of the corresponding polyfluorenes.

The thermal behavior, single-crystal structure and supramolecular packing, alignment properties, and molecular dynamics of the homo-oligofluorenes (**OFn**) up to the polymer were studied using techniques such as TGA, DSC, WAXS, POM and DS. The **OFn** from tetramer to heptamer show a smectic liquid crystalline phase with clearly defined isotropization temperatures; and this allows extrapolation to the expected isotropization

temperature of the polymer at around 475 °C. Unlike the polymer, the oligomers do show a glass transition which exhibits n^{-1} dependence and allows extrapolation to a hypothetical glass transition of the polymer at around 64 °C. This glass transition refers to a freezing of a liquid-crystal phase not seen for the polymer. A smectic packing and helix-like conformation for the oligofluorenes from tetramer to heptamer was supported by WAXD experiment, simulation, and single-crystal structure of some oligofluorene derivatives. The twist angle between the two neighboring fluorene units was approximately 144 °, and was in agreement with the torsional angle between neighboring monomers for polyfluorenes in the case of a 5/2 helix. Oligofluorenes were aligned more easily than the corresponding polymer, and the alignability increased with the molecular length from tetramer to heptamer. The molecular dynamics in a series of oligofluorenes up to the polymer was studied using dielectric spectroscopy. Two dielectrically active processes were found, one below T_g (β-process) and one above (α-process) associated with the DSC T_g. The latter bears many polymeric features.

In addition, structural and supramolecular packing, alignment properties, and molecular dynamics of **OF5K** were also studied in a similar way. The **OF5K** can be also aligned on rubbed **PI** and the alignability was weak slightly comparing to that of the homo-**OF5**. The single crystal of **OF5K** was obtained and the smectic liquid crystalline phase was confirmed, further supporting the smectic liquid crystal phase for the high homo-oligofluorenes. Dielectric spectroscopy is very sensitive to the presence of keto defects that drastically influence the optical and electronic properties and it revealed that the effect of the keto defects on the molecular dynamics was mainly to stiffen the backbone and increased the T_g by about 15 K.

The photophysical properties of **OFn** and **PF2/6** were investigated by the steady-state spectra (UV-vis absorption and fluorescence spectra) and time-resolved fluorescence spectra. The steady state spectra of oligofluorenes (**OF-n**) and polyfluorenes (**PF2/6**) both in solution and thin film were presented. The time-resolved fluorescence spectra of the oligofluorenes were measured by streak camera and gate detection technique in *m*-THF solution and film at both RT and 77K. The lifetime of the oligofluorenes decreased with the extension of the chain-length. No green emission was observed in CW, prompt and delayed fluorescence for oligofluorenes in *m*-THF and film at RT and 77K. Concentration and laser excitation intensity dependence of oligofluorenes were also investigated. Phosphorescence was observed for oligofluorenes in frozen dilute *m*-THF solution at 77K and its lifetime

increased with length of oligofluorenes. A linear relation was obtained for triplet energy and singlet energy as a function of the reciprocal of n (the number of fluorene units in oligofluorenes), and the singlet-triplet energy gap (S_1-T_1) was found to decrease with the increase of n.

Oligofluorenes with one fluorenone unit at the center were used as model compounds to understand the origin of the low-energy emission band in the photoluminescence and electroluminescence spectra of polyfluorenes. Their electrochemical properties were investigated by CV technique, and the ionization potential (I_p) and electron affinity (E_a) were calculated from the onset of oxidation and reduction of **OFnK**. The photophysical properties of **OFnK** were studied in dilute solution and thin film by steady-state spectra and time-resolved fluorescence spectra. A strong absorption of π-π* transition accompanied with a weak long-wavelength absorption (n-π*) were observed in the steady-state UV-vis spectra. A strong green emission accompanied with a weak blue emission were obtained in solution and only green emission was observed from the film; the green emission was very similar with the low-energy emission of photo- or electro-oxidized **PFs**. The strong green emission of **OFnK** suggested that rapid energy transfer from higher energy sites (fluorene segments) to lower energy sites (fluorenone unit) prior to the radiative decay of the excited species. The fluorescence spectra of **OFnK** also showed solvatochromism. At 77K, the green emission band with well-resolved structure appeared at approximately 550 nm with a vibronic splitting of about 160 meV. Monoexponential decay behaviour was observed by time-resolved fluorescence measurements and the lifetime of the green band is about 8 ns for **OF3K** and **OF5K**, which is longer than that of blue emission from **OF5**. In addition, the site-selective excitation and concentration dependence of the fluorescence spectra were also investigated. The ratio of green and blue emission band intensity increases with the increase of the concentration. The observed strong concentration dependence of the green emission band in solution suggests that increased interchain interactions among the fluorenone-containing oligofluorene chain enhanced the emission from the fluorenone defects at higher concentration. On the other hand the mono-exponential decay behaviour and power dependence were not influenced significantly by the concentration. We have ruled out the possibility that the green emission band originates from aggregates or excimer formation.

By comparing of the photophysical properties of **OF5** and **OF5K** from experimental results and reported quantum-chemical calculations, some important conclusions were

drawn: i) the low lying states S_1 (n-π*) and S_2 (CT π-π*) in fluorenone-containing chains possess very low oscillator strength, so the absorption in the low energy range of **OFnK** (2.2-2.4 eV) is very weak. The first state with high osillator strength in **OF5K** is the third singlet excited state S_3, and it is actually located at about the same energy as the lowest singlet excited state in the **OF5**, so similar absorption maximum wavelength is observed for **OFnK** and **OFn**; ii) the energy of the CT π-π* state is below that of the n-π* state due to the excited-state geometry relaxations. The green emission arises from the radiative decay of the excited species from the first relaxed singlet excited state to the ground state. iii) The wavelength of absorption maximum is red-shifted with the increasing of chain-length for both **OFnK** and **OFn**. This is due to the π-π* excited state that is delocalized in the whole molecules. The position of low-energy absorption and the green emission spectra is independent with the chain-length of **OFnK** except for **OF1K**. This is due to the n-π* state and CT π-π* is localized dominantly on the central fluorenone unit of **OFnK**.

Energy transfer was investigated using a model system of a polyfluorenes doped by **OFnK**. Förster-type energy transfer took place from **PF2/6** to **OFnK**, and the energy transfer efficiency increases with the increasing of the doping concentration of **OFnK**. A series of studies on the photophysical properties of **OFnK** and blend systems proposed an efficient Förster energy transfer to the fluorenone defects and strong exciton confinement on the fluorenone moieties. Efficient funneling of excitation energy from the high-energy fluorene segments to the low-energy fluorenone defects results from energy migration by hopping of excitations along a single polymer chain until they are trapped on the fluorenone defects on that chain or transferred onto neighbouring chains by Förster-type interchain energy transfer process. These results imply that the red-shifted emission in polyfluorenes can originate from (usually undesirable) keto groups at the bridging carbon atoms-especially if the samples have been subject to photo- or electro-oxidation or if fluorenone units are present due to an improper purification of the monomers prior to polymerization.

Based on the present research, the homo-oligofluorenes are as a defect-free material for blue LED and a material with high alignability for polarized light-emitting diodes (**PLED**). In addition, although the fluorenone defects in the oligo- and polyfluorenes completely destroy the normal blue emission, they can instead be used as efficient green electroluminescent materials in LEDs.

List of symbols and abbreviations

A   Acceptor

COD   Cycloocta-1,5-diene

CT   Charge transfer

CV   Cyclic Voltametry

CW   Continuous wavelength

D   Dichroic ratios

DF   Delayed fluorescence

DMF   N,N-dimethylformamide

DMSO   Dimethylsulfoxide

DPV   Different pulse voltammetry

DS   Dielectric spectroscopy

DSC   Differential scanning calorimetry

$E_{1/2}$ Half wave potential

E_a Electron affinity

ECL   Effective conjugation length

E_g Energy of band gap

EL   Electroluminescence

FETs   Field-effect transitions

FD-MS   Field desorption mass spectroscopy

FTRF   Fast time-resolved fluorescence

h.   hour

I_p Ionization potential

GPC   Gel permeation chromatography

HOMO   The highest occupied molecular orbital

HPLC   High pressure liquid chromatography

ISC   Intersystem crossing

ITO   Indium tin oxide

LB   Langmuir-Blodgett

LCs   Liquid crystal

LCOs   Linear π-conjugated oligomers

LCPs   Liquid crystalline polymers

LECs	Light-emitting electrochemical cells
LEDs	Light-emitting diodes; Light-emitting devices
LPPP	Ladder poly(*p*-phenylene)
LUMO	The lowest unoccupied molecular orbital
MCP	Micro-channel plate
MEH-PPV	Poly(2-methoxy-5-[2'-ethylhexyloxyl]-*p*-phenylene-vinylene)
m.p.	Melting point
NMR	Nuclear magnetic resonance
OFn	Oligofluorenes
OLED	Organic blue-light-emitting diode
OMA	Optical multichannel analyzer
OPO	Optical parametric oscillator
P	Polarization ratio
PA	Polyactylene
PD	Polydispersities
PDA	Poly(diacetylene)s
PF2/6	Poly(9,9-bis(2-ethylhexyl)fluorene-2,7-diyl)
PF3/5	Poly(9,9-bis(2-propylpentyl)fluorene)
PF4C12	Poly(2,7-(9,9-bis(2-butyl)co-(9,9-bis(dodecyl))fluorene)
PF8/1/1C2/6	Poly(2,7-(9,9-bis(2-ethylhexyl))co-(9,9-bis((3S)-3,7-dimethyloctyl))fluorene)
PFL	Prompt fluorescence
PFO	Poly(9,9-bis(2-octyl)fluorene
PFs	Polyfluorenes
Ph	Phosphorescence
PI	Polyimide
PL	Photoluminescence
PLEDs	Polymer light-emitting diodes
POM	Polarizing Optical Microscopy
PPE	Poly(*p*-phenyleneethynylene)
PPP	Poly(*p*-phenylene)
PPV	Poly(para-phenylenevinylene)
PS	Polystyrene

PT	Poly- (α-thiophene)s
PTFE	Poly(tetrafluoroethylene)
RT	Room temperature
SEC	Size-exclusion chromatography
SPT	Single-photon timing technique
TBAPF$_6$	Tetrabutylammonium hexafluorophosphorate
TD	Time-domain
TEM	Transition electron microscopy
T$_g$	Glass transition
TGA	Thermal gravimetric analysis
T$_{iso}$	Isotropic transition
THF	Tetrahydrofuran
m-THF	2-methyl tetrahydrofuran
TOL-MCH	Toluene: methyl-cyclohexane
TRF	Time resolved fluorescence
TRPL	Time-resolved photoluminescence
TTA	Triplet-triplet annihilation
VFT	Vogel-Flulcher-Tammann
WAXS	Wide angle X-ray scattering
XPS	X-ray photo-emission spectroscopy
XRD	X-ray diffraction

Publication List:

[1] Jungho Jo, Chunyan Chi, Sigurd Höger, Gerhard Wegner*, and Do Y. Yoon, "Synthesis and Characterizytion of Monodisperse Oligofluorenes." *Chem. Eur. J.* **2004**, *10*, 2681-2688.

[2] P. Papadopoulos, G. Floudas*, Chunyan Chi, G. Wegner* "Molecular Dynamics of Oligofluorenes: A Dielectric Spectroscopy Investigation." *J. Chem. Phys.* **2004**, *120*, 2368-2374.

[3] Chunyan Chi, Gerhard Wegner* "Chain-Length Dependence of the Electrochemical and spectral Properties of Conjugated Oligofluorenes." *Chem. Eur. J.* to be submitted.

[4] Chunyan Chi, Günter Lieser, Volker Enkelmann, Gerhard Wegner* "Chain-Length Dependence of the Liquid Crystalline Properties of Conjugated Oligofluorenes." manuscript in preparation

[5] Chunyan Chi, Volker Enkelmann, Günter Lieser, Gerhard Wegner* "The Single Crystal Structure of the Oligofluorenes with One Fluorenone Group." *Adv. Mater* to be submitted.

[6] Chunyan Chi, Chan Im, Gerhard Wegner* "Time-resolved Fluorescence Spectra of Oligofluorenes" manuscript in preparation.

[7] Chunyan Chi, Chan Im, Gerhard Wegner* "Oligofluorenes with Fluorenone as Model Compounds to Investigate the Original Green-emission of Polyfluorenes" manuscript in preparation.

[8] E. Somma, B. Loppinet, C. Chi, G. Fytas, G. Wegner "Static and dynamic solution properties of monodisperse oligofluorenes" submitted to *J. Phys. Chem. B.*

Curriculum Vitae

Personal Details:

Name: Chunyan Chi

Sex: female

Date of birth: September 16th, 1975

Nationality: Chinese

Hometown: Harbin city, Heilongjiang Province, P. R. China

Education:

1982.9-1988.7 Nanfang Elemental School, China

1988.9-1991.7 Yanglin Primary Middle School, China

1991.9-1994.7 The first Senior Middle School in Hulan, China

1994.9-1998.7 Qiqihaer University, Department of Chemistry, China

1998.9-2001.7 Master thesis under Prof. Fosong Wang and Prof. Xianhong Wang, Changchun Institute of Applied Chemistry, Chinese Academy of Sciences, topic: *"Synthesis, Self-assembly and Electronic Properties of Conjugated Phenylethynylene Dendrimers"*.

2001.7-2004.11 Ph.D. thesis under Prof. Dr. Gerhard Wegner, Max-Planck Institute for Polymer Research, Mainz, Germany, topic: *"Liquid Crystalline Oligofluorenes and their Derivatives: Synthesis, Characterization and Physical Properties"*.

Acknowledgements